

AD-A246 903

SECURITY CLASSIFICATION



PAGE

Form Approved
OMB No. 0704-0188


1a. REPORT SECURITY CLASSIFICATION Unclassified			1b. RESTRICTIVE MARKINGS		
2a. SECURITY CLASSIFICATION AUTHORITY DTIC ELECTE			3. DISTRIBUTION/AVAILABILITY OF REPORT Approved for Public Release, distribution Unlimited.		
2b. DECLASSIFICATION/DOWNGRADING SCHEDULE MAR 05 1992			4. PERFORMING ORGANIZATION REPORT NUMBER(S) AFOSR-TR 02 0013		
6a. NAME OF PERFORMING ORGANIZATION Professor Jack Feinberg		6b. OFFICE SYMBOL (if applicable)	7a. NAME OF MONITORING ORGANIZATION Dr. Howard Schlossberg Air Force Office of Scientific Research		
6c. ADDRESS (City, State, and ZIP Code) University of Southern California Los Angeles, CA 90089-0484			7b. ADDRESS (City, State, and ZIP Code) Building 410, Bolling AFB D.C. 20332-6448		
8a. NAME OF FUNDING/SPONSORING ORGANIZATION Same as 7a		8b. OFFICE SYMBOL (if applicable)	9. PROCUREMENT INSTRUMENT IDENTIFICATION NUMBER F-49620-88-C-0095		
8c. ADDRESS (City, State, and ZIP Code) Same as 7B			10. SOURCE OF FUNDING NUMBERS		
			PROGRAM ELEMENT NO. 101102F	PROJECT NO. 2301	TASK NO. AS
11. TITLE (Include Security Classification) Stimulated Scattering and Phase conjugation in photorefractive materials					
12. PERSONAL AUTHOR(S) Professor Feinberg					
13a. TYPE OF REPORT Final		13b. TIME COVERED FROM 8/1/88 TO 9/30/91		14. DATE OF REPORT (Year, Month, Day) 92/1/31	
15. PAGE COUNT 128					
16. SUPPLEMENTARY NOTATION					
17. COSATI CODES			18. SUBJECT TERMS (Continue on reverse if necessary and identify by block number)		
FIELD	GROUP	SUB-GROUP	Phase Conjugation, Photo Refractives, Barium Titanate, Stimulated Scattering		
19. ABSTRACT (Continue on reverse if necessary and identify by block number)					
<p>Applications and properties of nonlinear optical materials were studied, especially photorefractive crystals. A summary includes: (1) Demonstration of a new technique for seeing an object buried in or behind a scattering medium using time-resolved holography in a spectral hole-burning material. (2) Demonstration of an all-optical switchboard using stimulated, mutually-pumped phase conjugation in a photorefractive crystal. (3) Use of optical novelty filters to detect small changes in an optical scene. (4) Invention of an electric field correlator to measure the coherence length of picosecond laser pulses, using two-wave mixing in a photorefractive crystal. (5) Derivation of a theory of beam coupling and pulse shaping picosecond light pulses in photorefractive crystals. (6) Development of a new, multiple level model to explain the nonlinear photoconductivity of barium titanate crystals. (7) Investigation of the role of absorption gratings in beam coupling in barium titanate crystals and showing how these gratings can conveniently be used to determine the density of charge in these crystals. (8) Explanation of how stimulated processes cause the curved beam paths observed in mutually-pumped and self-pumped phase conjugators.</p>					
20. DISTRIBUTION/AVAILABILITY OF ABSTRACT <input type="checkbox"/> UNCLASSIFIED/UNLIMITED <input type="checkbox"/> SAME AS RPT. <input type="checkbox"/> DTIC USERS			21. ABSTRACT SECURITY CLASSIFICATION Unclassified		
22a. NAME OF RESPONSIBLE INDIVIDUAL Schlossberg			22b. TELEPHONE (Include Area Code) 202-767-4906		22c. OFFICE SYMBOL NE

UNCLASSIFIED
APPROVED FOR PUBLIC RELEASE
DISTRIBUTION UNLIMITED

Final Technical Report:
Period Covered: August 1, 1988 to September 30, 1991
"Stimulated Scattering and Phase Conjugation in
Photorefractive Materials"
Contract #F49620-88-C-0095
United States Air Force Office of Scientific Research

submitted by:
J. Feinberg, Principal Investigator
Department of Physics
University of Southern California
Los Angeles, CA
(213) 740-1134

92 3 03 065

92-05592


(I) INTRODUCTION

This final report describes the results of our research on stimulated processes and phase conjugation in photorefractive crystals. The research supported by this 3-year AFOSR contract resulted in the publication of 11 papers (in addition to conference proceedings). Some highlights are: We demonstrated a new technique for seeing an object buried in or behind a scattering medium using time-resolved holography. We demonstrated an all-optical switchboard using stimulated, mutually-pumped phase conjugation in a photorefractive crystal. We explored the use of optical novelty filters to detect small changes in an optical scene. We invented an electric field correlator to measure the coherence length of picosecond laser pulses, using two-wave mixing in a photorefractive crystal. We derived a theory of beam coupling and pulse shaping of picosecond light pulses in photorefractive crystals. We developed a new, multiple level model to explain the nonlinear photoconductivity of BaTiO₃ crystals. We investigated the role of absorption gratings in beam coupling in BaTiO₃ and showed how these gratings can conveniently be used to determine the density of charge in these crystals. We showed that stimulated processes explain the curved beam paths observed in mutually-pumped and self-pumped phase conjugators.



Accession For	
NTIS CRA&I	<input checked="" type="checkbox"/>
DTIC TAB	<input type="checkbox"/>
Unannounced	<input type="checkbox"/>
Justification	
By	
Distribution	
Availability Codes	
Dist	Avail and/or Special
A-1	

(2) RESEARCH OBJECTIVES

The original project goals included:

- 1) Study of real-time holographic interconnections.
- 2) Study of nonlinear optical devices for position sensing with sensitivity in the sub-Angstrom range.
- 3) Study of light-pulse transformation techniques.
- 4) Study of the photorefractive, piezoelectric, and ferroelectric properties of important nonlinear optical crystals.
- 5) Modeling and experimental observations of the dynamics of stimulated processes responsible for nonlinear optical phase conjugation phenomena in crystals.

All of these goals have been met.

In addition to the above projects, we were also able to:

- 6) Demonstrate a new technique for seeing through a scattering medium using temporal holography.
- 7) Complete a review article on photorefractive materials and phase-conjugate optics for the journal Scientific American.

We describe our results in more detail in the following section, and we also include reprints of the publications that resulted from this research contract.

(III) RESULTS

1) REAL-TIME OPTICAL INTERCONNECTIONS.

We developed and demonstrated an optical switchboard for interconnecting an array of optical channels. The switchboard will connect any one of N input channels to any subset of M output channels. The device uses a photorefractive crystal of BaTiO_3 as a mutually-pumped phase conjugator in a "bird-wing" geometry, as shown in Fig. 1. The conjugator connects two beams incident from opposite sides of the crystal. The two incident beams need not be coherent with each other, or even be present in the crystal at the same instant. The device works fine as a 1 to M or as an N to 1 coupler, so one can broadcast a single channel into many output ports, or feed many channels into a single output port. However, the device has the following drawback when used as a full N to M coupler: it broadcasts everyone's signal to everyone else. Consequently, the different signal would have to be encoded, probably in the time domain, to make a true N by M crossbar without crosstalk.

Our first-generation device used a 1-mm diameter bundle of single mode fibers. Light was sent into any one of the fibers in bundle A, and light was also

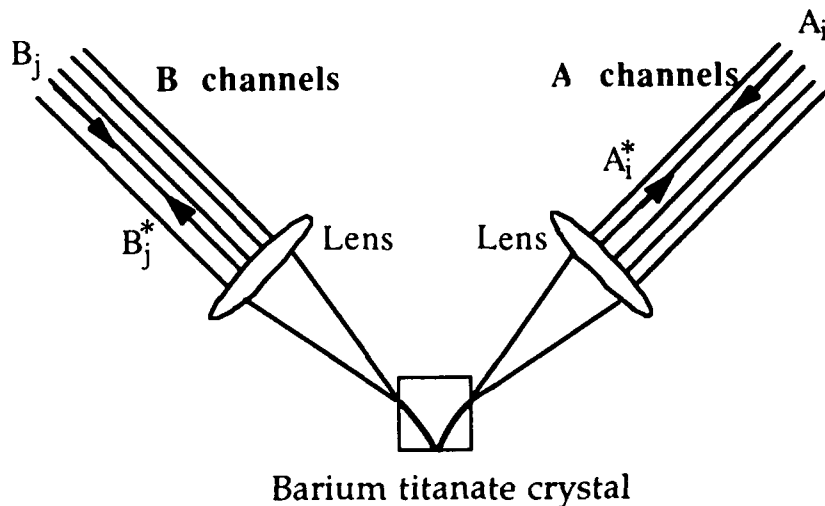


Figure 1: Schematic of interconnection device using a BaTiO_3 crystal as a mutually-pumped phase conjugator to connect elements of channels A and B.

sent into any one of the fibers in the other bundle B. The two light beams were not coherent with each other, although they were at the same nominal wavelength of 514.5 nm. The BaTiO_3 crystal connected the two beams using a stimulated hologram that grew from noise inside the crystal. A typical interconnection throughput was a few percent, but could be as high as 50%.

Our second-generation device used a tapered, multimode fiber to scramble the beams and thereby make the spatial profiles of the two bundles more uniform. Because the multimode fiber also scrambled the polarization of the light beams, we needed to construct a mutually-pumped phase conjugator that would work equally well for light of any polarization. This device is shown in Fig. 2. The specially fabricated tapered fiber mixed the signals from all of the A channels just before they entered the crystal, thereby ensuring a uniform spatial overlap between all of the various channels in the two fibers. Upon readout, the phase conjugator unscrambled the beams and directed each beam into its proper output channel. With this

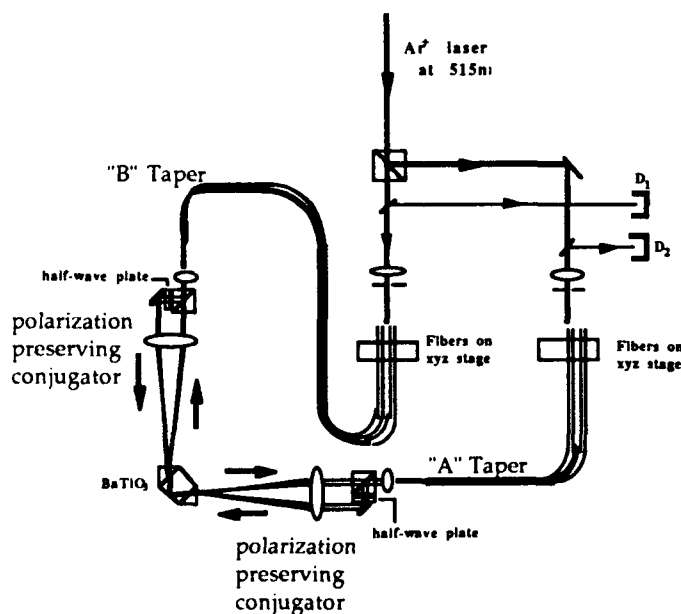


Figure 2. Optical set-up to demonstrate interconnection of different channels using a polarization-preserving mutually-pumped phase conjugator. Different channels are selected by moving the xyz stages to select different fibers, whose optical signals are mixed in the tapered regions of the bundles.

arrangement, the transmission of any channel to any other channel had the same uniform throughput (about 12%), regardless of which channel was chosen.

These results have been submitted for publication.¹

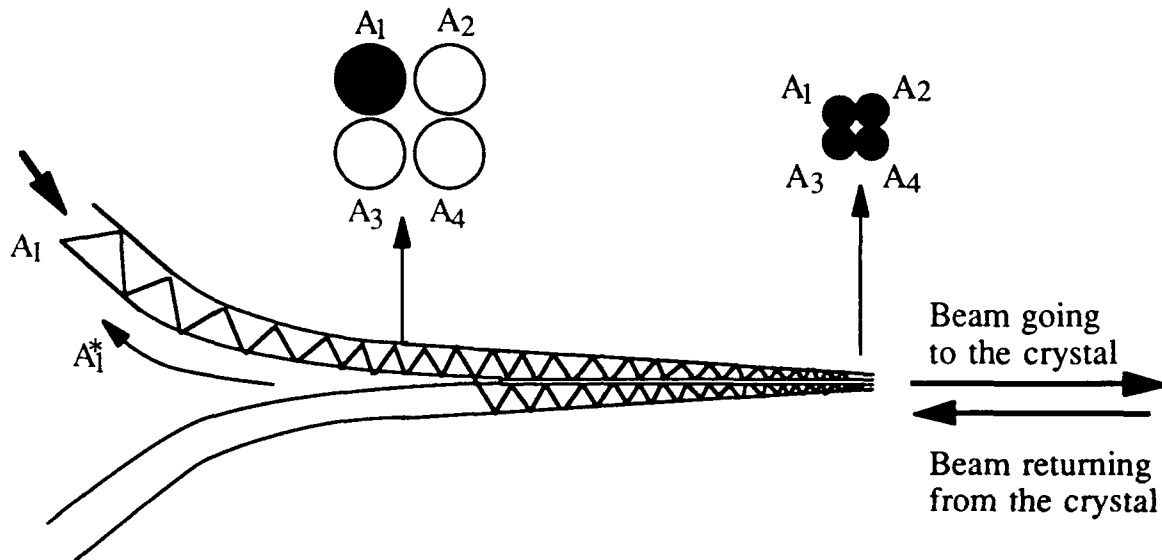


Figure 3: Each input channel enters the tapered fiber A, where it mixes with all of the other A channels. In the drawing above, only one channel A_1 is input, but it has mixed with the other three channels just before entering the crystal. The crystal, acting as a mutually-pumped phase conjugator, keeps track of the relative phases of all (four) A channels, and directs light from the B channel into only channel A_1 .

2) STUDIES OF NONLINEAR OPTICAL DEVICES FOR POSITION SENSING WITH SENSITIVITY IN THE SUB-ANGSTROM RANGE.

In this work we concentrated on novelty filters, which show what is new, or novel, in an input image compared with the input's recent history. Novelty filters are an essential ingredient to the front-end visual system of many animals. Frogs, for example, use novelty filtering to detect flying insects, while humans use novelty detection to rid our visual field of the image of the cells located in front of the retina. Airport controllers use digital novelty filters to rid their radar displays of everything that is not moving.

At present most novelty filtering uses digital electronics: the current scene from a video camera is subtracted (in a serial fashion) from a scene stored in memory, (and at the same time the current scene is also serially stored into memory). The difference between the live scene and the stored scene is serially computed and fed into a video memory for display.

In contrast to a digital novelty filter, the optical novelty filters we studied use a real-time holographic medium for the memory. The hologram inherently records the time-exponential average of the input scene. At the same time, interference subtracts the stored scene from the live scene essentially instantaneously, with the entire scene processed in parallel. These optical novelty filters are simple and work remarkably well. An important measure of their performance is the output contrast when the input changes completely, say, from light to dark. Demonstrations have so far yielded peak contrasts of approximately 30:1.

We have investigated the use of photorefractive crystals in various geometries to make optical novelty filters. (Some of these devices were invented previously by the P. I.). We analyzed their filter characteristics using Laplace transform techniques, and compared the relative advantages and disadvantages of the various geometries.

This review paper has been published in the IEEE Journal of Quantum Electronics.²

3) STUDIES OF LIGHT-PULSE TRANSFORMATION TECHNIQUES.

(a) Measuring the coherence length of mode-locked laser pulses in real time.

At the end of our previous AFOSR contract we had just invented a new device to measure the field autocorrelation of a picosecond laser pulse. In this present contract we pursued the applications of this device, and also analyzed the theory of the device in detail.

Our new device differs from a conventional second-harmonic generation correlator, in that it measures the coherence length of the pulse's optical electrical field, as opposed to the duration of the pulse's intensity envelope. For example, the pulses from our sync-pumped dye laser have a duration of ~4 picoseconds, but a coherence length of only ~1 psec. The field autocorrelator works by splitting an incident pulsed laser beam into two beams. The reference beam travels to a BaTiO₃ crystal. The probe beam hits a diffraction grating at grazing incidence, and the beam diffracted approximately normal to the grating surface is collected by a lens to

intersect the reference beam inside the crystal, as shown in Fig. 4. Different portions of the probe beam now have suffered different temporal delays. The probe beam from the grating will experience photorefractive coupling gain with the reference beam only if it is temporally coherent with the reference beam in the crystal. Observing the profile of the probe beam with a one-dimensional detector array then gives a real-time measure of the electric field autocorrelation of the incident laser beam. This field autocorrelator was used to measure the coherence length of pulses from a mode-locked Nd:Yag laser, as shown in Fig. 5. This device is described in Applied Physics Letters.³

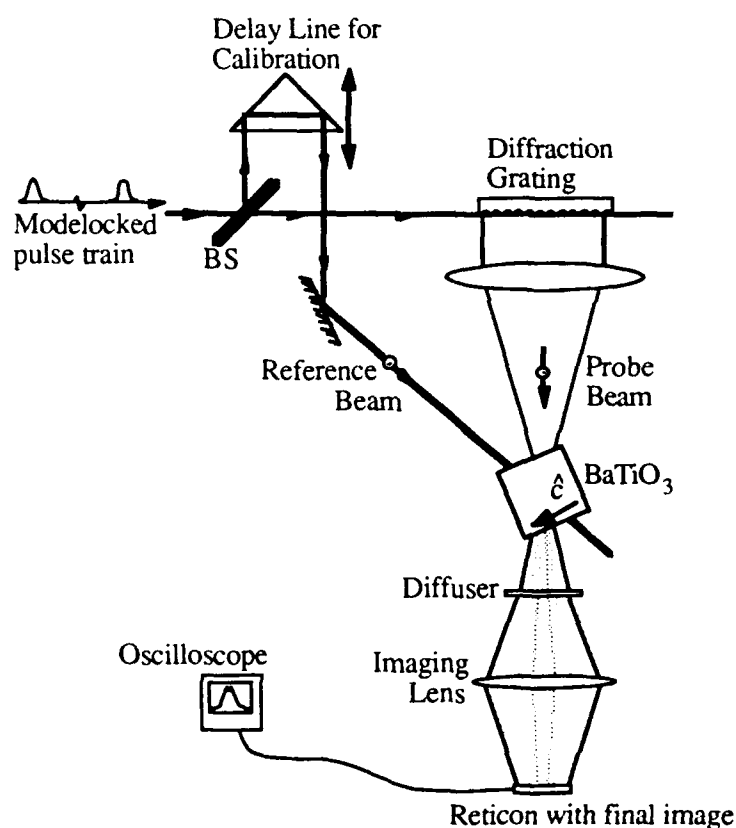


Fig. 4. Optical field correlator using two-wave mixing in a BaTiO₃ crystal. The diffraction grating encodes different delays onto different portions of the probe beam.

(b) Theory of beam coupling and pulse shaping of mode-locked laser pulses in a photorefractive crystal.

We produced an analytic theory of how laser pulses couple and alter their shapes when traversing photorefractive crystals. We find that the time-average intensity gain (or loss) of each beam is proportional to the magnitude squared of the electric-field correlation of the interfering beams at the entrance face of the crystal. We use this theory to analyze, in detail, the operation of the laser-beam coherence analyzer described above. Figure 5 compares the measured output from our field autocorrelator compared to that predicted by our theory; the fit is so precise that it is almost indistinguishable from the data!

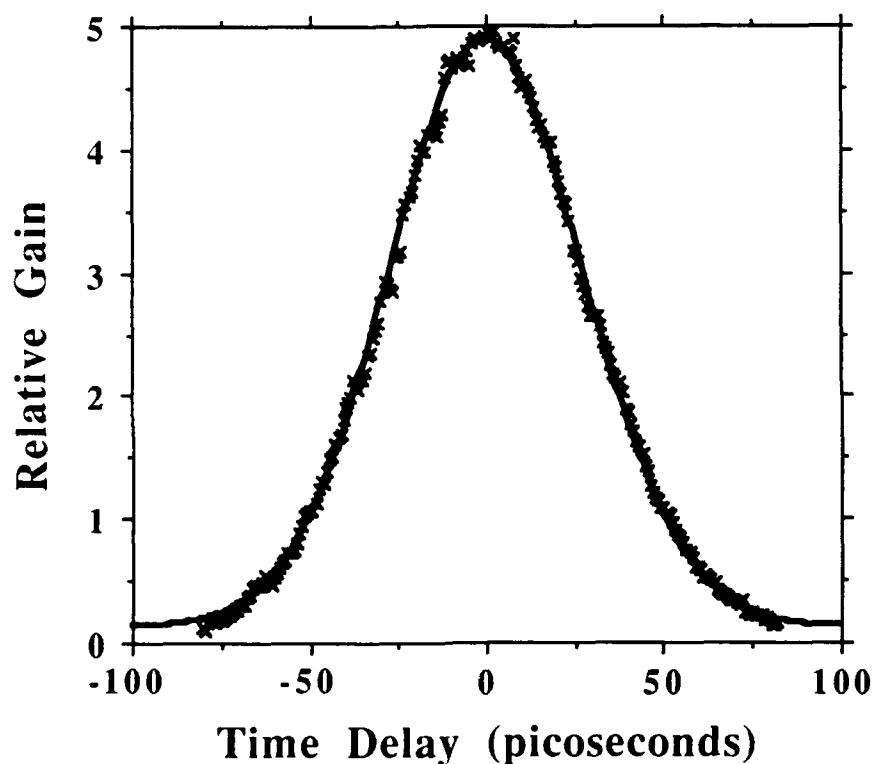


Fig. 5. Comparison of our theory (solid line) and our experimental data (crosses) for the field autocorrelation of a picosecond laser pulse.

We also showed that one can alter the temporal shapes of trains of picosecond pulses by mixing them with other pulses in a photorefractive crystal. The basic principle is shown in Fig. 6, where two temporally square-shaped pulses intersect in a BaTiO_3 crystal. The crystal transfers energy from one of the pulses to the other (depending on the direction of the crystal's c axis). The transmitted pulses will have spikes or notches added to their shapes.

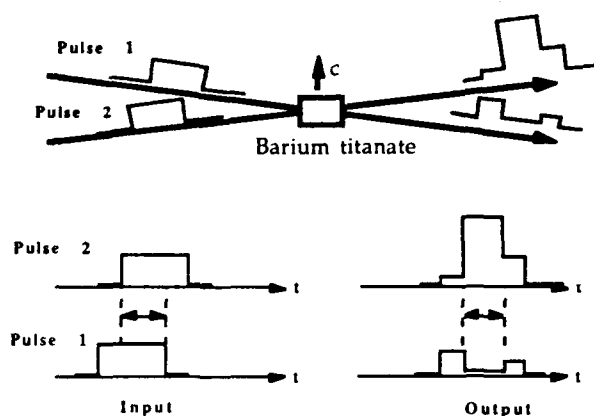


Fig. 6. Schematic showing pulse shaping by two-wave mixing in a BaTiO_3 crystal. Energy is transferred from one pulse to the other, depending on the direction of the crystal's c-axis.

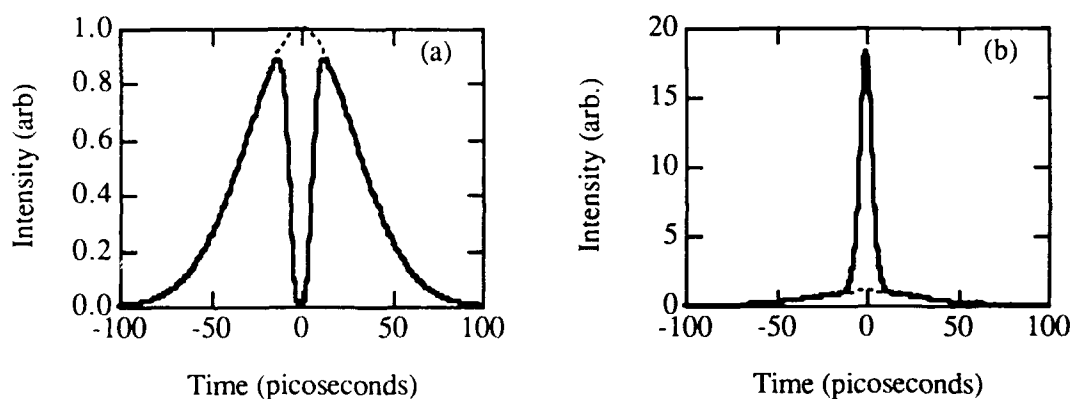


Fig. 7. Pulse shaping using Gaussian pulses with the same spectral width. The peaks of both beams reach the entrance face of the crystal at the same time, but the duration of one beam is 10 times greater than that of the other. The dotted curve is the beam shape before the crystal, the solid line is after the crystal. In (a) the crystal is oriented to transfer energy out of the detected beam. In (b) the crystal has been oriented to transfer energy into the detected beam.

Our detailed theory predicts the temporal shapes of the output pulses for a variety of initial pulse durations and temporal offsets. For example, Fig. 7 shows the pulse shaping that results from two initially Gaussian beams with the same spectral

width but with very different durations (so that the longer pulse is not transform limited). A sharp temporal spike can be either carved out of (see Fig. 7a) or grafted onto (see Fig. 7b) the incident beam, depending on the orientation of the crystal. Such beam shaping may prove useful for soliton generation in optical fibers.

This work has been published in the Journal of the Optical Society of America.⁴

4) STUDIES OF THE PHOTOREFRACTIVE, PIEZOELECTRIC, AND FERROELECTRIC PROPERTIES OF IMPORTANT NONLINEAR OPTICAL CRYSTALS. THIS SUBJECT FORMED THE HEART OF THIS RESEARCH CONTRACT, AND RESULTED IN FOUR PUBLICATIONS:

(a) Multiple trapping levels in photorefractive crystals:

We show that much of the complicated behavior of photorefractive crystals can be explained by the presence of more than one level of trapping centers in the crystal. We show that multiple levels causes the speed of the photorefractive effect to scale less-than-linearly with the light intensity, thereby solving the decade-old mystery of the nonlinear photoconductivity of BaTiO_3 . We also explain why seemingly identical BaTiO_3 crystals can have such markedly different photorefractive behavior. We show that BaTiO_3 crystals can be divided into two classes (which we call type A and type B), which determines their degree of optical linearity, their dark-storage time, and the dependence of their photorefractive coupling strength on optical intensity. We also explain why these properties are correlated.

This work was published in Physical Review Letters,⁵ and a longer, more detailed article published in the Journal of the Optical Society of America.⁶

(b) Absorption gratings

A photorefractive crystal having multiple trapping levels will have additional beam-coupling terms that are independent of the electrooptic effect, including a term caused by the rearrangement of charges among the different trapping sites at the same spatial location. These "absorption gratings" prove to be useful for accurately determining the effective number density of trapping sites in the crystal. Absorption gratings also complicate the interpretation of beam-coupling experiments, and, if are not taken into account, can lead to spurious values for crystal parameters.

An Optics Letter⁷ discussed the use of absorption gratings for measuring transmittance, and a longer article in Journal of the Optical Society of America⁸ discussed the detailed effects of absorption gratings, and compared our theory and experiments.

5) MODELING STUDIES AND EXPERIMENTAL OBSERVATIONS OF THE DYNAMICS OF STIMULATED PROCESSES AND NONLINEAR OPTICAL PHASE CONJUGATION IN CRYSTALS.

Stimulated scattering lies at the heart of self-pumped and mutually-pumped phase conjugators; it provides the small seeding beam that is amplified to become the phase-conjugate signal. These stimulated light beams often follow complicated paths in the crystal. In this work we show why, under some conditions, the stimulated light beams appear to follow a curved path in the crystal. In particular, we show that in a mutually-pumped phase conjugator the beam path will consist of a multitude of short line segments that approximate a curve. These line segments result from the successive bifurcations of the path of the stimulated beams. An example is shown in Fig. 8, where two input beams are shown to lead to a bridging beam between them, which then bifurcates again, so as to approximate a curved final path.

This work will be published in the Journal of the Optical Society of America.⁹

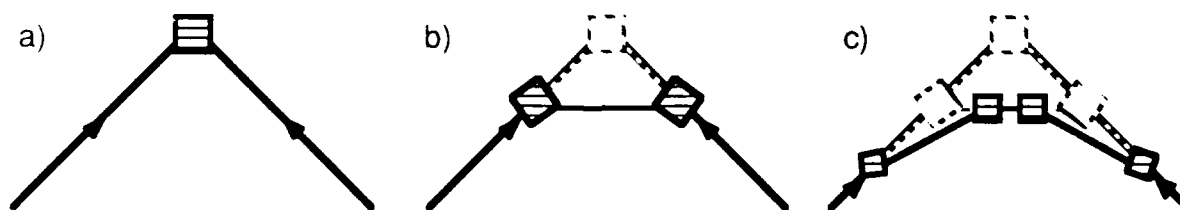


Fig. 8. Beam paths inside a mutually-pumped phase conjugator. The two input beams come from the bottom left and bottom right. In (a) the beams meet and interact in the top region. In (b) the system has spontaneously bifurcated to form a new beam path connected by two new interaction regions. In (c) the system has bifurcated again. The final beam path consists of many straight-line segments resembling a curve.

(6) DEMONSTRATION OF A NEW TECHNIQUE FOR SEEING THROUGH A SCATTERING MEDIUM USING TEMPORAL HOLOGRAPHY.

Probably the most dramatic (and unexpected) achievement of this research contract has been the demonstration of a new method for imaging an object through a scattering material. A patent application for this new process is being prepared by the University of Southern California. Articles describing this new technique appeared last spring in the New York Times and the London Economist. The technique would, in principle, allow one to use visible laser light to look into the human body, so as to visualize small tumors. It would also let one see through clouds and fog.

The technique is based on the principle that when light travels through a scattering medium, a very small fraction of the light may traverse the medium without scattering. This so-called "ballistic light" travels the shortest path and therefore emerges from the medium first, before the light that has suffered multiple scattering. If one could selectively view this ballistic light and exclude the multiply scattered light, then one could see an object through the scattering medium.

Our device uses the information storage properties of spectral hole-burning materials to selectively view either the early, ballistic light or, if desired, the later, multiply-scattered light. The technique requires a laser having a short coherence length to illuminate the object. Light travels from the object through the scattering medium and strikes the sample of hole-burning material. A separate reference beam also strikes the hole-burning material. The two light beams record a "temporal hologram" inside the material. By directing a reading beam onto the material, a movie of object beam is recreated. Depending on the direction of the reading beam, the movie can show only those parts of the object beam that arrived before the reference beam, thereby preferentially displaying the light that travelled through the object with a ballistic path.

This Paper was published in Nature,¹⁰ and was picked up by the popular press, including the Wall Street Journal, the New York Times, and the Economist (London).

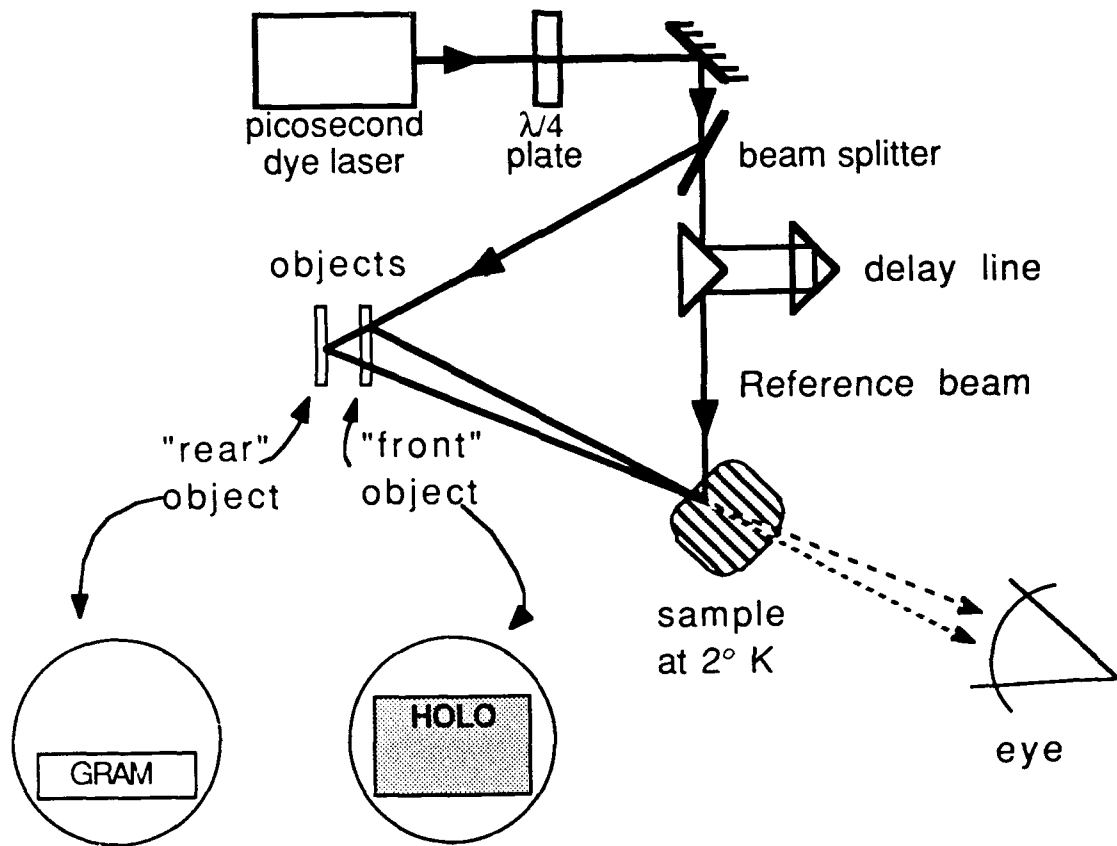


Fig. 9. Set-up for demonstrating temporal holography. Light from a picosecond laser is reflected off of two objects, with the front object painted with a strongly scattering material, so as to obscure the image of the back object. The light from both objects is holographically recorded in a spectral hole-burning medium at 2° K. When the hologram is viewed with another reference beam pulse, only light from the rear object is displayed.

IV) PUBLICATIONS

Papers published under this contract:

1. X.S. Yao and J. Feinberg, "Photorefractive optical switchboard," submitted to **Optics Letters**.
2. D.Z. Anderson and J. Feinberg, "Optical Novelty Filters," **IEEE J. of Quantum Electronics** 25, 635-647 (1989).
3. V. Dominic, X.S. Yao, R.M. Pierce, and J. Feinberg, "Real-Time Measurement of the Coherence Length of a Modelocked Laser," **Applied Physics Letters**, 56, 521-523 (1990).
4. X. S. Yao, V. Dominic, and J. Feinberg, "Theory of beam coupling and pulse shaping of short optical pulses in a photorefractive crystal," **Journal of the Optical Society of America-B** 7, 2347-2355, (1990).
5. D. Mahgerefteh and J. Feinberg, "Explanation of the apparent sublinear photoconductivity of photorefractive barium titanate," **Physical Review Letters** 64, 2195-2198 (1990).
6. P. Tayebati and D. Mahgerefteh, "Theory of the photorefractive effect for $\text{Bi}_{12}\text{SiO}_{20}$ and BaTiO_3 with shallow traps," **Journal of the Optical Society of America B** 8, 1053-1064 (1991).
7. R. M. Pierce, R. S. Cudney, G. D. Bacher, and J. Feinberg, "Measuring photorefractive trap density without the electrooptic effect," **Optics Letters** 15, 414-416 (1990).
8. R. S. Cudney, R. M. Pierce, G. D. Bacher, and J. Feinberg, "Absorption gratings in photorefractive crystals having multiple levels," **Journal of the Optical Society of America-B** 8, 1326-1332 (1991).

9. V. V. Eliseev, A. A. Zozulya, G. D. Bacher, and J. Feinberg, "Self-bending of light beams in photorefractive phase conjugators," to appear in **Journal of the Optical Society of America-B**, February, 1992.
10. A. Rebane and J. Feinberg, "Time-Resolved Holography," **Nature** 351, 378-380 (1991).
11. D. M. Pepper, J. Feinberg, and N. V. Kukhtarev, "The Photorefractive Effect," **Scientific American**, October (1990).

Articles in the popular press about this work:

- a) **The New York Times**, June 4, 1991, "SCIENCE WATCH: Beyond X-rays."
- b) **The Economist (London)**, July 13, 1990, "Seeing through people".
- c) **The Wall Street Journal**, October 26, 1988, "Physicists Who Play with Crystals see Serious Applications."
- d) **The New York Times**, February 20, 1990, "SCIENCE TIMES: Magic crystals: Key to New Technologies?"
- e) "Phase conjugation with photorefractive crystals," an interview with Jack Feinberg in **Lasers and Optronics**, June 1990

(V) PROFESSIONAL PERSONNEL:

Principal Investigator:

Jack Feinberg

Post-doctoral Research Associates:

Robert M. Pierce

Graduate Students:

G. David Bacher

Roger Cudney

Vince Dominic

Daniel Mahgerefteh

Jien-Ping Jiang

X. Steve Yao

Undergraduate students:

Jeff Nuttall

Kimberly Ludwig

(VI) ADVANCED DEGREES AWARDED:

Two students received Ph.D. degrees:

1) Daniel Mahgerefteh, May 1990, "The speed of the photorefractive effect, shallow traps, photogalvanic currents, and light-induced surface damage in BaTiO_3 ."

2) Jien-Ping Jiang, December 1990, "Four-wave mixing in photorefractive and polymeric materials: ring phase conjugator and time-resolved measurement of third-order optical nonlinearity."

(VII) CONFERENCES

1. Contributed talk (with X. S Yao) "Spectral pulse distortion from two-beam coupling of sub-picosecond pulses in a photorefractive crystal," Photorefractive Materials and Devices Topical Meeting, July 29-31, 1991, Beverly, Massachusetts.
2. Contributed talk (with R.S. Cudney, G.D. Bacher, R.M. Pierce) "Origins of the photorefractive phase shift," Photorefractive Materials and Devices Topical Meeting, July 29-31, 1991, Beverly, Massachusetts.
3. Contributed talk (with R.S. Cudney, R.M. Pierce, G.D. Bacher) "Absorption gratings with multiple levels," Photorefractive Materials and Devices Topical Meeting, July 29-31, 1991, Beverly, Massachusetts.
4. Contributed talk (with V.V. Eliseev, A.A. Zozulya, G.D. Bacher) "Why light beams follow curved paths in photorefractive phase conjugators," Photorefractive Materials and Devices Topical Meeting, July 29-31, 1991, Beverly, Massachusetts.
5. Seminar speaker at Stanford University, December 3, 1991.
6. Seminar speaker for the Optical Society of America-Ann Arbor, April 23, 1991.
7. Invited talk, "Photorefractive nonlinear optics," at the Material Research Society, April 27-May 3, 1991, in Anaheim, California.
8. Invited talk, "Photorefractive materials and devices," at the Nonlinear Optics: Materials, Phenomena, and Devices meeting, July 16-20, 1990, in Kauai, Hawaii.
9. Invited plenary lecture, "Unravelling and using the photorefractive effect," French-Israeli Symposium on Nonlinear Optics, April 22-27, 1990, in Rehovot, Israel.

10. Contributed talk (with R.M. Pierce, R.S. Cudney, and G.D. Bacher), "Absorption gratings in BaTiO₃ crystals," at the Conference on Lasers and Electro-Optics (CLEO), May 21-26, 1990, in Anaheim, California.
11. Contributed talk (with X.S. Yao and V. Dominic), "Optical pulse shaping using a photorefractive crystal," at the Conference on Lasers and Electro-Optics (CLEO), May 21-26, 1990, in Anaheim, California.
12. Contributed talk (with V. Dominic, X.S. Yao, and R.M. Pierce), "Measuring the coherence length of modelocked laser pulses in real time," at the Conference on Lasers and Electro-Optics (CLEO), May 21-26, 1990, in Anaheim, California.
13. Contributed talk (with D. Mahgerefteh), "Shallow traps resolve the I^x mystery in photorefractive BaTiO₃," at the Conference on Lasers and Electro-Optics (CLEO), May 21-26, 1990, in Anaheim, California.
14. Contributed talk (with R.M. Pierce, R.S. Cudney, G.D. Bacher) "Photorefraction without the electrooptic effect," OSA topical meeting on the Photorefractive Materials, Effects, and Devices, Jan, 1990, in Aussois, France.
15. Contributed Talk (with D. Mahgerefteh), "Shallow traps resolve the I^x mystery in photorefractive BaTiO₃," OSA topical meeting on the Photorefractive Materials, Effects, and Devices, Jan, 1990, in Aussois, France.
16. Colloquium speaker at IBM Almaden Research Center, November 17, 1989.
17. **Chairman**, Gordon Research Conference on Nonlinear Optics and Lasers, July 24-28, 1989.
18. Colloquium speaker at Sandia National Laboratories, July 31, 1989.
19. Colloquium speaker at Stanford Linear Accelerator Center (SLAC), April 1, 1989.

20. Invited talk "Optical Phase Conjugation," Optcon '88, November 3, 1988, Santa Clara, California.

21. Contributed talk (with D. Mahgerefteh and R.M. Pierce) "On the photovoltaic effect in barium titanate," Optical Society of America Annual Meeting, Oct. 31 - Nov. 4, 1988, Santa Clara, California.

22. Contributed talk (with R.S. Cudney, G.D. Bacher, and R.M. Pierce) "Measuring the photorefractive phase shift using two-beam coupling," Optical Society of America Annual Meeting, Oct. 31 - Nov. 4, 1988, Santa Clara, California.

23. Contributed talk (with G.D. Bacher and R.S. Cudney) "Detecting sub-Angstrom vibration of a rough surface using real-time holography," Optical Society of America Annual Meeting, Oct. 31 - Nov. 4, 1988, Santa Clara, California.

24. Invited talk "Photorefractive Nonlinear Optics," Ontario Laser and Lightwave Research Centre Workshop, September 23, 1988, Toronto, Canada.

25. Invited talk "Transient Detection Microscope," Seventh Annual Symposium on Advances in Microscopy," September 23-25, 1988, Pine Knoll Shores, North Carolina.

(VIII) INTERACTIONS WITH OTHER U.S. LABORATORIES:

University of Colorado:

Prof. Dana Z. Anderson - Photorefractive devices

Rockwell International Science Center:

Dr. Monte Khoshnevisan - Characterization of photorefractive materials

Dr. Ratnakar R. Neurgaonkar - Photorefractive crystal growth

(IX) PATENTS OR INVENTIONS STEMMING FROM THIS RESEARCH EFFORT:

1) "Method of Imaging Through a Scattering Medium using Coherent Light,"
pending.

2) "Nonlinear Optical Microscope," United States Patent No. 5,005,927 granted
April 9, 1991, assigned to the U.S Government.

Optical Novelty Filters

DANA Z. ANDERSON AND JACK FEINBERG, MEMBER, IEEE,

(Invited Paper)

Abstract—A novelty filter detects what is new in a scene and may be likened to a temporal high-pass filter. We review the current status of optical novelty filters (and related devices) that use four-wave mixing or two-beam coupling in photorefractive media. A detector that shows only what is not new (which we call) a monotony filter may be likened to a temporal low-pass filter. Demonstrations of high- and low-pass and bandpass temporal image filters are discussed. An analytical treatment of the two-beam coupling devices is given in a Laplace transform framework in the undepleted pump approximation assuming plane wave inputs. This allows a unified treatment of the various filter characteristics.

I. INTRODUCTION

A NOVELTY filter shows what is new in an input image compared with the input's recent history [1]. Novelty filters are an essential ingredient to the front-end visual system of many animals. Frogs, for example, use novelty filtering to detect flying insects. Humans also use novelty detection to rid our visual field of the image of the blood vessels located in front of the retina: we constantly move our eyes in small tremors and in rapid, jerky movements (saccades), and then automatically remove from the image everything that does not change [2].

Novelty detection using an optical system is similar to temporal high-pass filtering. However, the final output sensor (our eyes or a TV camera) detects the optical field intensity rather than amplitude, and as a result a novelty filter can produce seemingly peculiar results. For example, imagine a quiet lily pond viewed through a novelty filter. At first the filter displays the pond. In time, however, the filter adapts to its input and removes the image of the stationary pond from the output. On the other hand, a flying bug is a constant stream of newness, so the bug remains visible. The peculiar feature is that if a frog should leap from one lily pad to another, the frog would instantly appear in *two* places: where it is, because it was not there before, and where it was, because its sudden absence is just as novel as its sudden presence.

Although the detection of change in a scene is impor-

tant when it is change that is special, when nearly everything in the scene is undergoing change, then it may be what is static (or nearly so) that is more interesting. For example, consider tracking a moving object: we constantly move our attention in the visual scene in order to keep the object fixed, to keep it *un-novel*, to keep it *monotonous*. We call the complement of a novelty filter a monotony filter. The most celebrated use of the monotony filter is the detection of the modes of vibrating objects (even the eardrum). The application of holography to this purpose using photographic plates long preceded the invention of the optical novelty filter.

A monotony filter behaves like a low-pass filter. Together, novelty and monotony filters are fundamental building blocks for more general linear processing systems. Having these functions in hand makes optics a more attractive potential competitor to electronics for processing images.

Consider how we might detect change in a scene using digital electronics: the current scene from a video camera is digitally subtracted (in a serial fashion) from a scene stored in memory and fed into a video memory for display (and at the same time the current scene is also serially stored into memory).

In contrast, an optical novelty filter uses a real-time holographic medium for the memory. The hologram inherently records the time-exponential average of the input scene. At the same time, interference subtracts the stored scene from the live scene essentially instantaneously, with the entire scene processed in parallel. These optical novelty filters are simple and work remarkably well. An important measure of their performance is the output contrast when the input changes completely, say, from light to dark. Demonstrations have so far yielded peak contrasts of approximately thirty to one.

In order to encode a visual scene onto a laser beam, several of the optical novelty filters use a modified liquid crystal television. These televisions currently have 52 500 pixels in a rectangle measuring two inches diagonally, and the televisions are the limiting element for both the subtraction speed and the picture resolution in the novelty filters.

Our main purpose for presenting this review is to stimulate interest in these simple but effective optical novelty and monotony filters. We believe that they can be made practical, and we hope to see them incorporated as components in larger systems.

The following section gives a brief review of the photorefractive effect, which has been used in all demonstrations of optical novelty and monotony filters to date. In

Manuscript received July 12, 1988; revised September 7, 1988. J. Feinberg was supported in part by the Visiting Fellow Program, Joint Institute for Laboratory Astrophysics and by the National Science Foundation. The work of D. Z. Anderson was supported in part by the Air Force Office of Scientific Research, and in part by the ERC program of the National Science Foundation through the Optoelectronic Computing Systems Center.

D. Z. Anderson is with the Department of Physics and the Joint Institute for Laboratory Astrophysics, University of Colorado, Boulder, CO 80309.

J. Feinberg is with the Department of Physics, University of Southern California, University Park, Los Angeles, CA 90089, on leave at the Department of Physics and the Joint Institute for Laboratory Astrophysics, University of Colorado, Boulder, CO 80309.

IEEE Log Number 8825904.

the second part of that section we investigate the time response of two-beam coupling using Laplace transform techniques in order to bring out the filter characteristics. (The reader may wish to skip Section II at first reading and go directly to following sections.)

Our review of novelty filters begins in Section III: the various systems are taken in more or less the chronological order as they appeared in the conference or journal literature. These devices include: the ring novelty filter [3], the four-wave mixing interferometer [3]–[5], the two-beam coupling novelty filter [6], [7], the transient energy coupling or bandpass filter [8], the beam fanning filter [6], [9], and the image velocity filter [10].

In Section IV we briefly discuss photorefractive materials for monotony detection (perhaps better known as time-averaging interferometry). Much of the formalism presented in Section II-B on filter characteristics carries directly over to this section by simply changing the sign of the two-beam coupling coefficient. We close in Section V with some comments regarding applications.

II. THE PHOTOREFRACTIVE EFFECT

All of the devices described here use a photorefractive crystal as the active element, and all but one of the devices rely principally on two-beam coupling in the photorefractive material. (The exception is the four-wave mixing interferometer.) In this section we present first a brief review of the theory of the photorefractive effect, and then a treatment of the temporal response of the two-beam coupling phenomena in the undepleted pump regime, which is particularly amenable to linear systems analysis of the medium as a filter. Our review of the photorefractive effect is not a complete one: it is intended to provide the reader with the general principles so that some insight into the behavior of the photorefractive filters can be gained. For more detail, we refer the reader to some of the excellent work that may be found in the literature. Glass has written one of the early reviews of the photorefractive effect [11]. Much of the current work on the theory of photorefractive effects attributes its roots to the work of Kukhtarev and collaborators [12], [13]. A review of some of the recent applications, materials, and devices employing photorefractive media has been written by Günter [14]. Optical phase-conjugation and two-beam coupling in photorefractive media is reviewed by Feinberg [15]. A very recent collection of works edited by Günter and Huinard is a superb resource [16].

A. Two-Beam Coupling: Steady State

Photorefractive two-beam coupling is a result of a remarkable synergism among several effects. An image-bearing beam and a reference beam interfere in a photorefractive crystal, and the resulting spatially-periodic intensity pattern from these "writing" beams redistributes mobile charges in the crystal. The static electric field from the spatially-periodic charge pattern distorts the crystal lattice, making a phase "grating" or hologram in the

crystal. One of the interesting properties of photorefractive crystals is that the stored phase grating is, in general, spatially shifted from the intensity interference pattern. In this case, the grating will couple the amplitudes of the two writing beams, so that one beam will emerge amplified and the other depleted, with the direction of energy coupling determined by the positive direction of the c axis of the crystal.

The usual approach to photorefractive coupling is to assume that the optical fields are plane waves of frequency ω and having amplitudes that vary slowly as the waves propagate through the crystal:

$$E_1(r, t) = \frac{1}{2} \varepsilon_1(z) \exp \{ i(k_1 \cdot r - \omega t) \} + \text{c.c.} \quad (1a)$$

$$E_2(r, t) = \frac{1}{2} \varepsilon_2(z) \exp \{ i(k_2 \cdot r - \omega t) \} + \text{c.c.} \quad (1b)$$

where c.c. means complex conjugate and where we have assumed scalar optical fields. The input beams are also assumed to propagate such that the bisector of the angle between them is defined to be the z axis, and we choose their plane of intersection as the xz plane. In response to the interference pattern of the optical waves, the medium evolves a space-charge field that, in turn, gives rise to a refractive-index grating that mimics the interference pattern except, in general, for a spatial phase-shift. For convenience we define a scalar "grating field" $G(z, t)$ whose amplitude is proportional to the amplitude $\Delta n(z, t)$ of the refractive index grating [17]:

$$G = -i\omega\Delta n/(2c). \quad (2a)$$

The time evolution of the slowly-varying amplitude of G is governed by the interference of the optical fields [12], [16]:

$$\frac{\partial G(z, t)}{\partial t} = \gamma \left\{ -G(z, t) + \frac{\Gamma}{2} \frac{\varepsilon_1(z) \varepsilon_2^*(z)}{I(z)} \right\} \quad (2b)$$

where γ is a decay constant that is approximately proportional to the intensity and Γ is a coupling constant. The quantities γ and Γ may both be complex, but in a diffusion dominated crystal, such as barium titanate with no applied dc field, they are both real. Expressions for the coupling and decay constants in terms of the material parameters, possible applied electric field, and optical geometry may be found in [16]. In (2b), $I(z) = |\varepsilon_1(z)|^2 + |\varepsilon_2(z)|^2$ is the total intensity, which may vary along z due to absorption in the crystal.

In a medium having a large coupling constant Γ , the grating changes the optical field distribution, which then affects the grating again. This mutual interaction between grating and fields in both time and space is what makes an analytical treatment so difficult. However, in steady state, the grating field amplitude clearly becomes

$$G(z) = \frac{\Gamma}{2} \frac{\varepsilon_1(z) \varepsilon_2^*(z)}{I(z)}. \quad (3)$$

The spatial evolution of the fields may be approached using the coupled-wave theory of Kogelnik [18]. In a medium with loss constant α the coupled wave equations take the simple form

$$\frac{d\mathcal{E}_1}{dz} = g\mathcal{E}_2 - \frac{\alpha}{2}\mathcal{E}_1 \quad (4a)$$

$$\frac{d\mathcal{E}_2}{dz} = -g^*\mathcal{E}_1 - \frac{\alpha}{2}\mathcal{E}_2 \quad (4b)$$

These can be rewritten in terms of the field intensity and phase by writing $\mathcal{E} = I^{1/2}e^{i\phi}$ and by recognizing that $dI/dz = \mathcal{E}^* d\mathcal{E}/dz + \text{c.c.}$ Then the rate of change of the intensities I_1 and I_2 and phases ϕ_1 and ϕ_2 of the two beams with distance in the crystal is:

$$\frac{dI_1}{dz} = \text{Re}\{\Gamma\} \frac{I_1 I_2}{I_1 + I_2} - \alpha I_1;$$

$$\frac{dI_2}{dz} = -\text{Re}\{\Gamma\} \frac{I_1 I_2}{I_1 + I_2} - \alpha I_2 \quad (5a)$$

$$\frac{d\phi_1}{dz} = 1/2 \text{Im}\{\Gamma\} \frac{I_2}{I_1 + I_2};$$

$$\frac{d\phi_2}{dz} = 1/2 \text{Im}\{\Gamma\} \frac{I_1}{I_1 + I_2}. \quad (5b)$$

The coupling strength Γ is determined primarily by the Pockels coefficient and the dielectric constant of the crystal, and is taken to be real if the refractive index grating is shifted by 90° from the intensity pattern. Note that for $\text{Re}\{\Gamma\} > 0$, beam 1 will grow in intensity with distance, and that for $I_1 \ll I_2$, its growth is exponential and is independent of the intensity of the strong beam I_2 . Note also that even for the case $I_1 > I_2$, the strong beam will still rob the weaker beam of its energy.

Equations (5) were derived assuming the beams are both plane waves, which is not true if the beams carry images. Nevertheless, in order to derive some insight into the novelty filter behavior we can solve the above equations retaining the plane wave assumption. We shall also assume that Γ is purely real and positive, and that there are no absorption or reflection losses ($\alpha = 0$). With purely real Γ , according to (5b), the phases do not change at all. The intensities are found by solving (5a):

$$I_1(\ell) = I_1(0) \frac{1+r}{1+r/g} \quad (6a)$$

$$I_2(\ell) = I_2(0) \frac{1+1/r}{1+g/r} \quad (6b)$$

where ℓ is the length of the beam interaction region, $g = \exp[\text{Re}(\Gamma)\ell]$ is the coupling gain, and r is the intensity ratio of the input beams,

$$r = \frac{I_2(0)}{I_1(0)}. \quad (7)$$

Suppose that beam 2 carries the image. As the coupling gain g approaches infinity, beam 2 becomes more depleted and its intensity I_2 approaches zero. What happens if the image changes? We will look at this in more detail in the next section, but one can see important features here. For simplicity, let us assume that $r = 1$ (equal incident beam intensities). Suppose the phase of the input beam 2 suddenly changes by 180° , so that the instantaneous intensity interference pattern suddenly shifts by half a wavelength. Before the grating has had a chance to respond, the output from the photorefractive crystal will behave as though Γ had suddenly changed sign. From (6), the instantaneous change in output intensity, which we call the contrast ratio C , will be

$$C \equiv \frac{I_{\text{novel}}}{I_{\text{old}}} = \frac{1+g}{1+1/g}. \quad (8)$$

In the limit of large gain, $C = g$. Two-wave mixing gain in barium titanate can easily exceed 100, and therefore, so can the contrast C . Note that after a while a new photorefractive grating will be written; the steady-state intensities will once again succumb to (5a), making beam 2 fade. In the next section we take a closer look at the temporal behavior of two-beam coupling.

B. Filter Characteristics

We have been saying that the novelty filter is something like a high-pass filter and the monotony filter is like a low-pass filter. What do they actually do? To answer this question we need to work with a theory that can treat time and space simultaneously for the medium. Solymar and Heaton [19] and Heaton and Solymar [20] described transient energy transfer in the holographic writing process in photorefractive crystals. Cronin-Golomb [21] extended their work by allowing one input signal to vary in time to show the time-differentiating behavior of the two-beam coupling process. His solution is derived in the undepleted pump approximation assuming plane wave beams; unfortunately, a novelty filter that employs a high-gain photorefractive element typically violates both of these assumptions. There are many obstacles in the way of compiling a complete analytical theory. As an example, consider that in the depleted pump case with nonplane optical beams, the intensity within the crystal varies spatially and therefore so does the photorefractive time constant. To treat the problem fully one would need to include these spatial variations.

Since the emphasis here is on filter characteristics, we take a somewhat different approach from Cronin-Golomb to solving the problem of time-dependent coupling in the undepleted pump regime. In linear systems theory, Laplace transform techniques are often employed [22]. Here we introduce the temporal Laplace transform of an input

field $\mathcal{E}(t)$:

$$\mathcal{E}(t) = \frac{1}{2\pi i} \int_{\sigma-i\infty}^{\sigma+i\infty} \epsilon(s) e^{st} ds \quad (9a)$$

with

$$\epsilon(s) = \int_0^\infty \mathcal{E}(t) e^{-st} dt \quad (9b)$$

where s is a complex frequency $s = \sigma + i\omega$. In this case, the signal is presumed to commence at $t = 0$. The beauty of this technique is that a filter can be simply described by a transfer function $h(s)$ such that the output $\epsilon'(s)$ from the filter is given by a product:

$$\epsilon'(s) = h(s) \epsilon(s) \quad (10)$$

so that the output signal $\mathcal{E}(t)$ is given by

$$\mathcal{E}(t) = \frac{1}{2\pi i} \int_{\sigma-i\infty}^{\sigma+i\infty} h(s) \epsilon(s) e^{st} ds. \quad (11)$$

High- and low-pass filter characteristics correspond to the location of the various zeros and poles in the transfer function.

We wish to find $h(s)$ for the two-beam coupling process. We start with the fields of (1) except that now beam 1, the image carrying beam, is allowed to have a spatially-varying amplitude that also varies slowly in time.

$$E_1(r, t) = \text{Re} \left\{ \mathcal{E}_1(z, t) \exp \{ i(k_1 \cdot r - \omega t) \} \right\}. \quad (12)$$

In the undepleted pump approximation the pump field \mathcal{E}_2 does not vary with distance. For the signal field, as in (4a) but now ignoring loss ($\alpha = 0$):

$$\frac{\partial \mathcal{E}_1}{\partial z} = g \mathcal{E}_2. \quad (13)$$

Now recall (2) for the evolution of the grating amplitude:

$$\frac{\partial \mathcal{G}(z, t)}{\partial t} = \gamma \left\{ -\mathcal{G}(z, t) + \frac{\Gamma}{2} \frac{\mathcal{E}_1(z) \mathcal{E}_2^*(z)}{I(z)} \right\}. \quad (14)$$

With $I_2 \gg I_1$, we may replace $I(z) \approx |\mathcal{E}_2|^2$. We may also use (13) to eliminate \mathcal{G} from (14):

$$\frac{\partial^2 \mathcal{E}_1(z, t)}{\partial t \partial z} = \gamma \left\{ -\frac{\partial \mathcal{E}_1(z, t)}{\partial z} + \frac{\Gamma}{2} \mathcal{E}_1(z, t) \right\}. \quad (15)$$

In the subsequent discussion, we shall drop the subscript from \mathcal{E} . In order to solve this mixed differential equation, we invoke our Laplace techniques and transform both sides of (15). With this transformation, time differentiation corresponds to multiplying by s in the transformed space. Thus (15) becomes

$$s \frac{\partial \epsilon(z, s)}{\partial z} = \gamma \left\{ -\frac{\partial \epsilon(z, s)}{\partial z} + \frac{\Gamma}{2} \epsilon(z, s) \right\} \quad (16)$$

or

$$\frac{\partial \epsilon(z, s)}{\partial z} = \frac{\gamma \Gamma}{2(s + \gamma)} \epsilon(z, s). \quad (17)$$

This has the solution

$$\epsilon(z, s) = \epsilon(0, s) \exp \left\{ \frac{\gamma \Gamma z}{2(s + \gamma)} \right\} \quad (18)$$

with $\epsilon(0, s)$ given by the transform of $\mathcal{E}(0, t)$:

$$\epsilon(0, s) = \int_0^\infty \mathcal{E}(0, t) e^{-st} dt. \quad (19)$$

The inverse Laplace transform evaluated at $z = \ell$ gives us the output of the filter:

$$\mathcal{E}(\ell, t) = \frac{1}{2\pi i} \int_{\sigma-i\infty}^{\sigma+i\infty} \epsilon(0, s) \exp \left\{ \frac{\gamma \Gamma \ell}{2(s + \gamma)} \right\} e^{st} ds. \quad (20)$$

For any particular $\epsilon(0, s)$ (20) can be integrated using the method of residues [23] after expanding the first exponential as a Taylor series. Here we are most interested in a filter function that represents the behavior of the device. Evidently, the photorefractive medium's transfer function $h(s)$ is

$$h(s) = \exp \left\{ \frac{\gamma \Gamma \ell}{2(s + \gamma)} \right\}. \quad (21)$$

Setting $s = i\omega$ we see that $h(i\omega)$ is in fact a high- or low-pass filter as $\text{Re} \{ \Gamma \}$ is greater than or less than zero, respectively. That is, the magnitude of the exponent is a maximum for $\omega = 0$ and tends to zero as $\omega \rightarrow \infty$. The interpretation of the transfer function is really quite simple. For real Γ we recognize $h(0) = \exp \{ \Gamma \ell / 2 \}$ as the steady-state (amplitude) gain for the signal. The exponent *itself*, not simply the signal amplitude, has a pole at a cutoff frequency given by the decay constant. Therefore, the signal gain changes very rapidly for frequencies near the cutoff frequency. For reasonably large $\Gamma \ell$ the filter rolloff is strong indeed. The magnitude and phase of the transfer function for $\Gamma \ell / 2 = -10$ and $\gamma = 1$ is shown in Fig. 1.

Having the transfer function in hand, the contrast is given by the ratio of the transfer function at as $\omega \rightarrow \infty$ to that at $\omega = 0$. For the novelty filter ($\text{Re} \{ \Gamma \} < 0$):

$$C = \frac{I_{\text{novel}}}{I_{\text{old}}} = \left| \frac{h(i\infty)}{h(i0)} \right|^2 = e^{\Gamma \ell} = g \quad (22)$$

which is the same result obtained earlier for two-beam coupling *including* pump depletion for equal input beam intensities and in the limit of large gain. Simply reversing the sign of the coupling coefficient gives the transfer function for the monotony filter.

III. OPTICAL NOVELTY FILTERS

As history would have it, the earliest demonstrations of adaptive optical novelty filters were the most complicated; the more recent demonstrations are considerably simpler. What distinguishes one novelty filter from another is the method used to read out the hologram stored in the crystal, and whether or not the device takes advan-

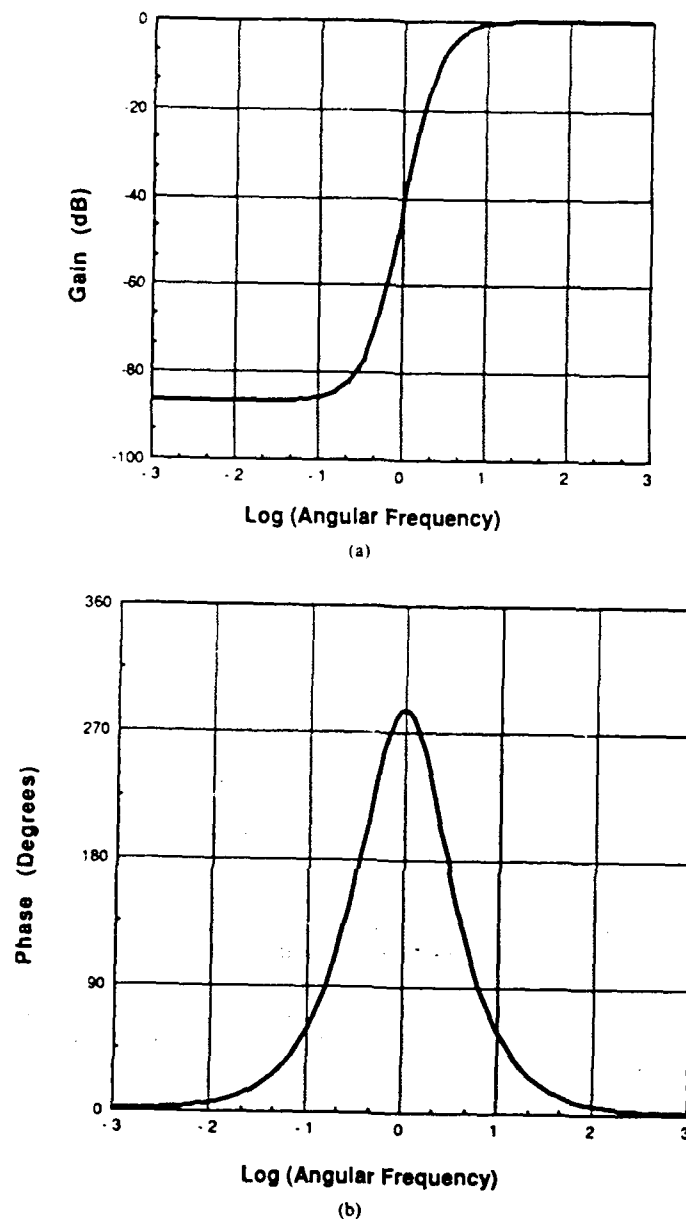


Fig. 1. Transfer function for two-beam coupling in undepleted pump approximation. The angular frequency is normalized to $|\gamma|$. (a) Gain (magnitude), (b) phase. These curves correspond to $\Gamma t/2 = -10$, $\gamma = 1$, showing a novelty detection characteristic. The monotony filter characteristic can be obtained by changing the sign of the ordinates.

tage of the two-beam energy coupling described above. Perhaps the first demonstration of the use of wave mixing in a photorefractive as a two-dimensional image filter was by Jahoda *et al.* [24], who made a Michelson interferometer having one phase-conjugating mirror [25]. A rapidly varying phase disturbance in the phase-conjugating arm of the interferometer would affect the pattern of output fringes of the device, while slowly-varying distortions would not. However, there was nothing to guarantee that the output would become a null in the absence of a time-varying signal. The novelty filters described produce a

relatively null output (defined by the contrast) when nothing is moving or changing in the scene.

A. The Ring Novelty Filter

The first optical novelty filter sprang from the observed behavior of a ring resonator that used a photorefractive medium in place of a conventional mirror [26]. The output from this ring tends to zero at steady state [3]. However, a sudden change in the resonator length was observed to produce an intense output. The ring resonator can be made into a novelty filter by placing a spatial light

modulator inside the resonator cavity [5] as shown in Fig. 2. The spatial light phase modulator is connected to a television camera, so that it encodes a live phase image onto the transmitted laser beam. The beam transmitted through the modulator is deflected by mirrors to reenter the crystal and intersect the original beam. These two beams create a volume phase hologram inside the photorefractive crystal, which in barium titanate is spatially shifted from the intensity pattern by 90° , and so couples the amplitudes of the two beams. The crystal's c axis direction is chosen so that energy is coupled from the incident beam into the ring resonator cavity. Energy then builds up inside the resonator. Because the ring resonator can store energy, the intensity inside the ring can be greater than the incident intensity. The two-beam coupled wave equations (5) can be solved for the ring by requiring, in steady state, the intensity after one round-trip in the ring to be the same as its initial value. The solution shows that the ratio of the intensity circulating in the ring to the incident intensity is given by the buildup parameter b [3]:

$$b = \frac{1}{2} L e^{\Gamma \ell} \left\{ \left[1 + 4 \frac{1-L}{L^2 e^{\Gamma \ell}} \right]^{1/2} - 1 \right\} \quad (23)$$

where L is the total round-trip intensity loss of the loop (including the crystal losses),

$$L = 1 - R \exp(-\alpha \ell). \quad (24)$$

R is the net round-trip effective reflectivity of the combined optical elements in the ring (including the spatial light phase modulator), and α is the intensity absorption coefficient of the photorefractive medium having length ℓ , as before. In the limit of large coupling, the buildup becomes independent of the coupling strength Γ :

$$b \approx \frac{1-L}{L}. \quad (25)$$

(Here the coupling is considered large when $\exp(\Gamma \ell) \gg (1-L)/L^2$.) On the other hand, the light at the output of the loop is

$$I_{\text{out}} = \frac{1}{R} (1-L) \left[1 - \frac{1+b}{1+be^{-\Gamma \ell}} L \right] I_{\text{incident}} \quad (26)$$

$$\approx \frac{(1-L)^2}{RL} e^{-\Gamma \ell} I_{\text{incident}} \quad (27)$$

which goes to zero for large coupling [3]. If a portion of the beam in the ring changes phase by 180° (giving the maximum possible signal), that portion will appear intensified at the output. The resulting contrast is the same as for the two-beam coupling case:

$$C = I_{\text{novel}}/I_{\text{old}} = e^{\Gamma \ell}.$$

In practice the ring is a rather awkward geometry because the incident light must be expanded after traversing

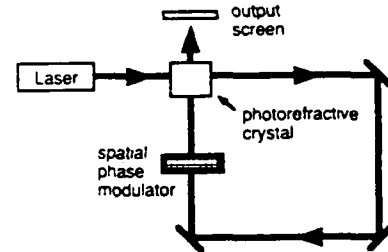


Fig. 2. Ring resonator with a holographic mirror used as a novelty filter.

the photorefractive crystal to the dimensions of the LCTV, then reduced to enter the crystal again.

B. Four-Wave Mixing Novelty Filter

A more practical geometry, demonstrated by Anderson *et al.* [4], uses four-wave mixing in an arrangement identical to that used to demonstrate optical phase conjugation. As shown in Figs. 3 and 4, two variations are possible. In one case an incident plane wave is divided by a beamsplitter. One resulting beam passes through an optical phase modulator that contains a picture of the live scene. Both beams are subsequently incident on the same phase-conjugating mirror [15], [16]. The conjugator generates the phase-conjugate beams, which propagate back towards the beamsplitter. Under steady-state conditions, the information on the one phase-conjugate wave is exactly cancelled by its return trip through the phase modulator, so that it emerges as a plane wave. In steady-state, the two phase-conjugated beams coherently recombine at the beamsplitter so as to travel back into the light source, with no light going into the "output port" of the beamsplitter. This can be explained by drawing upon the analogy between phase-conjugation and time reversal [27]: since no light came into the output port of the beamsplitter, no light should leave this port. However, if the image on the modulator changes in a time faster than the response time of the phase conjugator, the beam emerging from the modulator will not be a plane wave. In particular, the wavefront will be altered for those locations in the modulator that are changing in time, and there will be an instantaneous signal at the output port of the beamsplitter. After the medium has had time to respond, the output fades again.

A second implementation of the four-wave mixing novelty filter uses a polarization modulator instead of a phase modulator to impress a polarization-encoded image onto the beam. The liquid-crystal display from commercially available hand-held televisions is inherently a polarization modulator. (Liquid crystal televisions use two between sheet polarizers in order to make the display modulate the intensity of the light). The configuration shown in Fig. 4 uses the liquid crystal display's polarization characteristics [28]–[30]. An incident polarized plane wave is transmitted by the first polarizing beamsplitter. The beam traverses a liquid crystal display sandwiched between a pair of waveplates. The transmitted beam is then sent into a phase conjugator designed to accommo-

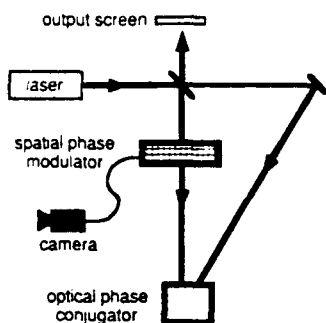


Fig. 3. A phase-conjugating novelty filter using a phase modulator in a self-aligning interferometer configuration.

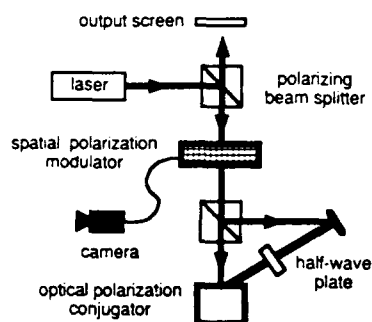


Fig. 4. A polarization-conjugating novelty filter using a polarization modulator and two polarizing beamsplitters.

date any polarization [31]. (The beam is first divided by a second polarizing beamsplitter into two linearly-polarized components. Since a photorefractive phase-conjugator will only conjugate one component, a half-wave plate is used in one arm to rotate the polarization 90° . The two beams are separately conjugated and then recombined at the polarizing beamsplitter). The conjugate beam passes back towards the modulator, and back to the first polarizing beamsplitter. In steady-state the light returning to the first polarizing beamsplitter will have its original polarization intact, and so the beam will be sent towards the laser. However, any sudden change in the image will alter the polarization of the beam returning to the first polarizing beamsplitter, and so that part of the image will be deflected into the output port.

It is interesting to note that in both systems, while the output from the beamsplitter or the polarizing beamsplitter shows the novelty of the scene, the light that propagates back toward the laser carries the monotonous information. This information can be observed with an additional beamsplitter placed directly in front of the plane wave source.

Anderson *et al.* used a barium titanate crystal as self-pumped phase conjugating mirror in the configuration of Fig. 4 [4], [33]. In order to obtain a quantitative measurement of the performance of the system, a Pockels cell was substituted for the spatial light modulator. The Pockels cell produced a uniform polarization change across the

entire beam, so the "image" only had one pixel. Fig. 5 shows an oscilloscope trace of the results. The lower trace is the Pockels cell voltage: it is simply stepped on, then stepped off. The step height is the half-wave voltage of the cell, which produces a 90° polarization rotation of the transmitted beam. The upper trace shows the output intensity from the interferometer (note that the intensity scale is inverted). The output intensity rises immediately with the voltage step, then decays as the phase-conjugator adapts. The output has essentially the same response to the step down of the Pockels cell voltage. The observed decay time constant of ~ 0.25 s was obtained using approximately 0.5 W/cm^2 total light intensity incident on the barium titanate crystal. The contrast indicated in the figure is about 15:1.

Fig. 6 shows experimental results in which a commercial LCTV is used as the spatial polarization modulator. In the figure, the input image is the phrase "NOVELTY FILTER," which was produced by a character generator driving a video camera. Fig. 6 shows that the image can be seen only when the character generator is turned on or off. Note that any change in the image will appear instantly, because the speed of the phase conjugator determines only the time required for an unchanging image to fade, but not for a changing image to appear.

The two-beam coupling treatment presented in Section II is inadequate to describe this interferometric novelty filter having a self-pumped phase-conjugating mirror. We can, however, make the following qualitative observation that this novelty filter acts like a bandpass filter. For simplicity, first consider what happens for a plane wave input (no image). The return beam relies on a grating generated in the photorefractive medium, which has a finite time response. If the input wave changes slowly, then the photorefractive medium tracks the change and there is no output from the novelty filter. If the input wave changes very rapidly, then no grating can form, and once again there is no output signal. Only if the input beam changes in a time comparable to the photorefractive response time will there be an output signal. (This is in contrast to the two-beam coupling novelty filter described below, in which a very-rapidly-varying input simply propagates undepleted through the crystal to the output port). For the general case of an arbitrary input image to a self-pumped phase conjugator, it is not simple to describe the behavior of the device. The gratings within the photorefractive medium are formed with many interacting parts of the image. If only a small part of the image is undergoing change, then the device seems to behave as a bandpass filter. However, if too much of the image is constantly undergoing large change, then self-pumping will cease, and the entire output will disappear.

The contrast of the four-wave mixing novelty filter does not depend upon the coupling constant of the crystal alone. Two signals are subtracted at the (polarizing) beamsplitter. If the phase-conjugation is perfect, the contrast is infinite. The interferometer configurations are therefore well

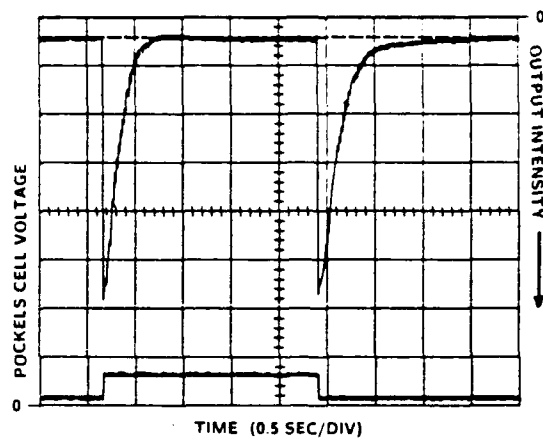


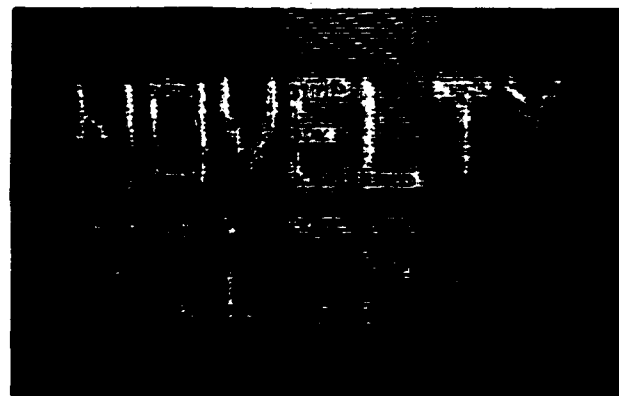
Fig. 5. Oscilloscope trace of the time response of the novelty filter of Fig. 4. Lower trace shows the voltage on a Pockels cell polarization modulator. The step corresponds to 90° polarization rotation. The upper trace is the output from the output beamsplitter showing approximately exponential decay after the initial response to the step change in polarization.



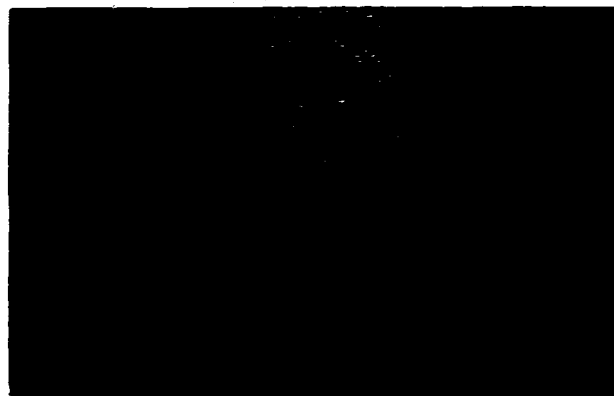
(a)



(b)



(c)



(d)

Fig. 6: Results using the novelty filter of Fig. 4. (a) The character generator inputs a new message, which appears instantly. (b) A few seconds have elapsed, and the image has faded because it is no longer novel. (c) The message is suddenly removed, and is therefore immediately seen. (d) A few seconds have elapsed, and the message's disappearance is no longer novel.

suited to perform novelty detection with any four-wave mixing medium. In particular, one is not limited to photorefractive materials, with their large gain but slow response, and instead could use other nonlinear optical media such as sodium vapor or laser dyes.

C. Two-Beam Coupling Novelty Filter

Cronin-Golomb *et al.* demonstrated an elegantly simple novelty filter that uses two-wave energy coupling [6]. Fig. 7 shows the image-bearing beam and a reference beam intersecting in a barium titanate crystal. Due to the 90° phase shift between the intensity interference pattern and the refractive index pattern in this crystal, in steady state the image-bearing beam transfers energy to the reference beam and emerges from the crystal severely depleted. If the image-bearing beam suddenly changes, the energy coupling is momentarily defeated, and the transmitted image becomes more intense by the factor derived in Section II:

$$C \equiv \frac{I_{\text{novel}}}{I_{\text{old}}} = e^{\Gamma \ell}.$$

Here again the coupling strength Γ is here taken to be real.

A physical explanation for the two-wave mixing depletion of the image beam is destructive interference: the transmitted image beam and the deflected reference beam destructively interfere on the output screen. The output screen, then, always contains two superimposed images: the real image transmitted through the crystal, and the holographically-reconstructed image produced by the deflected reference beam. In the steady state, these two images are of nearly equal amplitude and 180° out of phase with each other, so that they tend to cancel. If either of the beams is altered, the destructive interference is thwarted, and the screen becomes bright. Note that in contrast to the four-wave mixing novelty filter, the image can be in the form of either phase or amplitude modulation (or both). (However, any steady-state polarization change in the image-bearing beam will not be canceled in the output beam.)

D. Bandpass Filter

Our analysis in Section II-B of two-beam coupling in photorefractive media assumed real coupling coefficient Γ and decay constants γ . In this case the transfer function shows that at steady state the output is a minimum for the novelty filter or a maximum for the monotony filter. This same analysis can be extended to the case of complex coupling and decay constants, but the response of the medium to input signals can be substantially different from the case of real-valued coefficients. In particular, in a material having purely imaginary coupling Γ , in steady state there will be no energy coupling between beams. However, coupling can take place as a transient phenomena. Kwong *et al.* realized that a novelty filter could be based upon this effect and demonstrated the concept in a crystal of

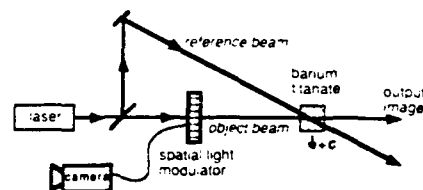


Fig. 7. A novelty filter that uses two-wave mixing to deplete energy from the image-bearing beam.

BSO ($\text{Bi}_{12}\text{SiO}_{20}$) [8]. Kwong *et al.*'s device has a bandpass characteristic, as we shall see. This is a significant addition to the very short list of photorefractive linear processing elements. Vachss and Hesselink used the bandpass characteristic to implement a velocity selecting novelty filter (discussed in Section III-G).

Recall the two-beam coupling transfer function:

$$k(s) = \exp \left\{ \frac{\gamma \Gamma \ell}{2(s + \gamma)} \right\}. \quad (28)$$

For purely imaginary coupling Γ , we see that for dc signals ($s = 0$) there will be no amplitude change of the input signal, only a phase change. It is also true that there will be no beam coupling, even in the transient regime, when the signal and pump intensities are equal [34], [35], [14]. However, there can be transient energy transfer if the signal and pump beams have unequal incident intensities, and energy will always flow from the stronger to a weaker beam. We will use the undepleted pump regime for the analysis of this problem.

To account for its complex nature let us write

$$\gamma \rightarrow \gamma_r + i\omega_\gamma.$$

With this notation the transfer function becomes

$$\begin{aligned} k(s) &= \exp \left\{ \frac{\Gamma \ell}{2} \frac{\gamma_r + i\omega_\gamma}{s + \gamma_r + i\omega_\gamma} \right\} \\ &= \exp \left\{ \frac{\Gamma \ell}{2} \frac{1}{1 + \frac{s}{\gamma_r + i\omega_\gamma}} \right\}. \end{aligned} \quad (29)$$

Setting $s = i\omega$, the transfer function has maximum gain when $\omega = |\gamma| \equiv (\gamma_r^2 + \omega_\gamma^2)^{1/2}$. Gain falls off on either side of this frequency. For drift dominated materials, we can set $\text{Re} \{ \Gamma \} \approx 0$. (This is essentially the case for a BSO crystal with a large applied dc field.) With Γ as purely imaginary, at dc and at high frequencies the medium simply passes the input signal. Fig. 8 shows the bandpass transfer function for $\Gamma \ell / 2 = 0 + i10$ and $\gamma_r = \omega_\gamma = 1/\sqrt{2}$. It is natural to define a contrast as the maximum intensity gain (since the gain at $\omega = 0$ and as $\omega \rightarrow \infty$ is unity):

$$C \equiv \left| \frac{k(i\omega_m)}{k(i0)} \right|^2 = \exp \left\{ \frac{\ell}{2} \frac{\gamma_r}{|\gamma| + \omega_\gamma} \text{Im} \{ \Gamma \} \right\}. \quad (30)$$

Kwong *et al.*'s optical arrangement is basically the same as for the two-beam coupling novelty filter. An electric

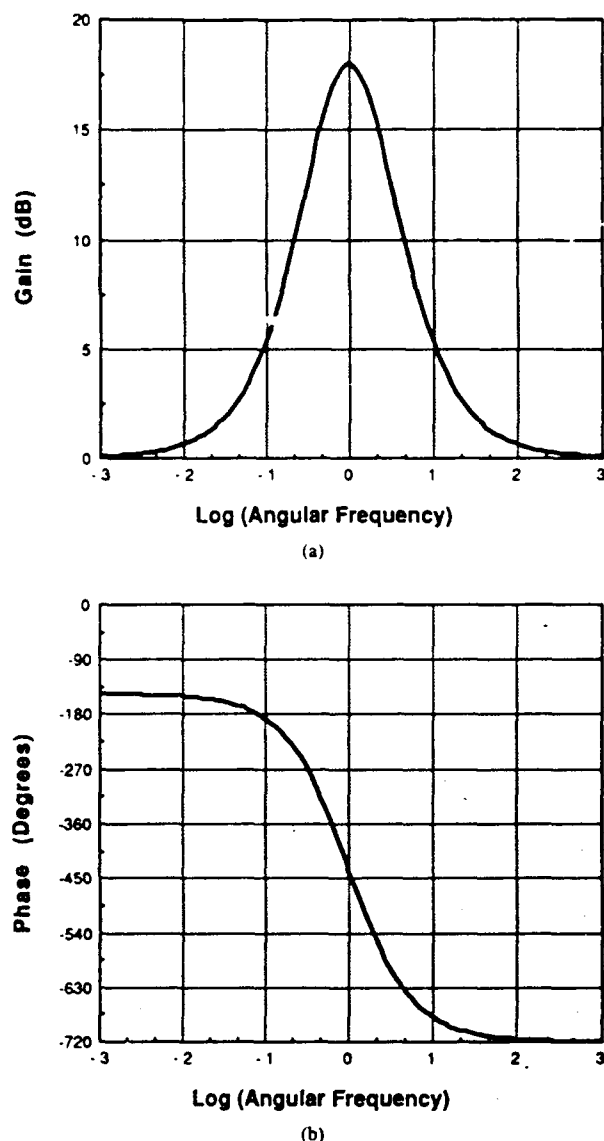


Fig. 8. Bandpass characteristic transfer function of transient energy coupling. The angular frequency is normalized to $|\gamma|$. (a) Gain (magnitude), (b) phase. Curves plotted for $\Gamma t/2 = 0 + i10$, $\gamma = (1 + i)/\sqrt{2}$.

field is applied along the c axis of the BSO crystal so that migration of charges is dominated by drift rather than by diffusion. A small beam crossing angle also enhances the effect.

E. Beam-Fanning Novelty Filter

Ford *et al.* [9] demonstrated what must be the world's simplest novelty filter (as suggested by Cronin-Golomb *et al.* [6]). It uses only one input beam into a barium titanate crystal. The device is similar to that of Fig. 7, except that the pumping beam is replaced by amplified scattered light (beam fanning) from the single incident beam. Two-wave mixing with this scattered light inside the crystal depletes the stationary portions of the transmitted beam, so that only the changing portions of the scene are transmitted.

This device requires a large two-beam coupling gain, which is obtained by using a crystal of barium titanate specially cut so that its input and exit faces are oriented at a 45° angle to the c axis of the crystal, thereby taking maximum advantage of the large r_{42} Pockels coefficient of barium titanate. Depending on how the input image is focused into the crystal, this device is sensitive to changes in the amplitude, phase, wavelength, or polarization of the incident beam.

F. Microscopic Novelty Filter

Cudney *et al.* used a two-wave mixing scheme to construct a novelty-filtering microscope [7]. Instead of using a spatial light modulator to encode an image onto a laser beam, the microscopic organisms themselves served as optical phase and amplitude modulators. Fig. 9 shows the optical setup, in which a pair of microscope objectives are used to focus and then image the incident laser onto the barium titanate crystal. The intensity of light on the sample can be made quite weak (less than the intensity of ordinary sunlight). The measured contrast ratio was 30:1, and the spatial resolution was a few microns. In Fig. 9 the images of the moving protozoa can be seen, while the image of the stationary algae are largely removed from the scene. (Note however, that any birefringent algae will not be blocked out, as can be seen in Fig. 10.)

G. Velocity Selecting Novelty Detection

Once the connection is made between novelty and monotony detection and high- and low-pass filtering, the challenge is to construct more interesting devices. Vachss and Hesselink used a BSO crystal as a bandpass filter to construct a velocity-selecting novelty filter [10]. Their device is more than just an extension of the two-beam coupling filters described here. They recognized that an image undergoing translational motion gives rise to moving grating components generated by effective frequency shifts between writing beams. In the previous section we saw that with purely imaginary coupling, the maximum signal response frequency occurs $\omega = |\gamma|$. Hence, motion in the image plane giving rise to frequency shifts in this range will yield an enhanced output. As with Kwong's work, Vachss and Hesselink's experiment was done using a BSO crystal with an applied electric field. However, for signal output they use a harmonic of the grating generated by the usual two-beam interaction in a photorefractive material. The harmonic gratings are due to nonlinear processes in the photorefractive medium and have grating wave vector magnitudes $k = nk_1$. A harmonic grating must be read out by a separate laser, since it will not be phase matched with either of the writing beams.

Vachss and Hesselink have shown that a higher order grating is more sensitive to the dynamical properties involved, that is, a sharper frequency response can be obtained than with the fundamental grating [36]. However, the enhanced sensitivity is at the expense of a decreased resolution permitted by the second-order gratings [10],

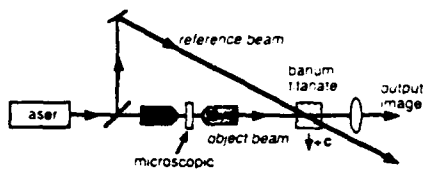


Fig. 9. A microscopic novelty filter using the organisms as living spatial light modulators.

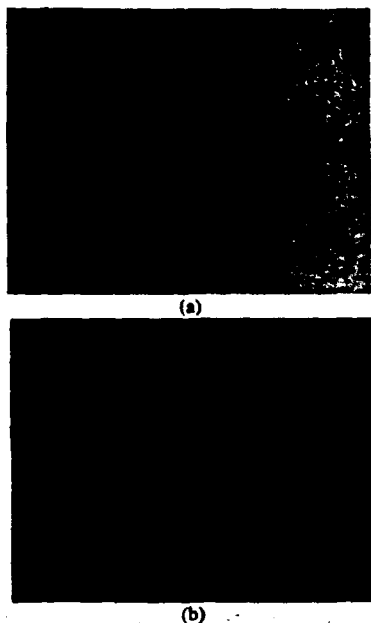


Fig. 10. Images of swimming protozoa viewed through the microscopic novelty filter of Fig. 9. (a) The novelty filter is off, and the protozoa and the stationary background are both visible. (b) The novelty filter is turned on, and the background is now removed.

[36]. The transfer function that we derived above for the two-beam coupling interaction will need to be modified to account for these altered properties and to account for the separate reading beam. Without having to actually know the equations of motion for the higher order grating, we can anticipate the qualitative features to be similar to the case of transient energy transfer from the fundamental grating. The signal frequency for maximum response, however, will no longer be for $\omega = |\gamma|$, but $\omega = \omega_\gamma/n^2$ for the n th harmonic grating [10]. In this geometry, the output signal maximum evidently occurs for a maximum grating amplitude, not for maximum energy transfer between the writing beams.

To see how the frequency shift comes about from a moving image, Vachss and Hesselink allow a plane wave with vector amplitude \mathcal{E}_1 and propagation direction k_1 to illuminate the object with two-dimensional transmittance $t(r)$. The resulting beam interferes with a second plane wave in the medium. The total field amplitude is thus

$$\mathcal{E}(r) = \mathcal{E}_1 t(r) \exp[i(k_1 \cdot r - \omega t)] + \mathcal{E}_2 \exp[i(k_2 \cdot r - \omega t)] \quad (31)$$

so that the intensity at the input is

$$I(r) = |\mathcal{E}_1|^2 |t(r)|^2 + |\mathcal{E}_2|^2 + (\mathcal{E}_1 \cdot \mathcal{E}_2^* t(r) \cdot \exp[i(k_1 - k_2) \cdot r] + \text{c.c.}) \quad (32)$$

This can be written in terms of the field intensities I_1 , I_2 , and the two-dimensional spatial Fourier transform $\mathcal{Q}(k)$ of $t(r)$:

$$I(r) = I_1 |t(r)|^2 + I_2 + 2\sqrt{I_1 I_2} \left\{ \mathcal{Q}(k) \cdot \exp[i(k + k_G) \cdot r] + \text{c.c.} \right\} \quad (33)$$

where $k_G \equiv k_1 - k_2$ is the grating wave vector. If the image is moving with velocity \mathcal{V} then $t(r)$ becomes replaced by $t(r - \mathcal{V}t)$. Now (33) becomes

$$I(r) = I_1 |t(r - \mathcal{V}t)|^2 + I_2 + 2\sqrt{I_1 I_2} \left\{ \mathcal{Q}(k) \cdot \exp[i(k + k_G) \cdot (r - \mathcal{V}t)] + \text{c.c.} \right\} \quad (34)$$

Vachss and Hesselink point out that this shows that the component of the image with spatial frequency k induces a grating component having frequency $|k + k_G|$ moving in the positive $(k + k_G)$ direction with velocity

$$v(k) = \frac{k \cdot \mathcal{V}}{|k + k_G|} \quad (35)$$

The motion may also be thought of as inducing a frequency shift, $\omega(k) = k \cdot \mathcal{V}$.

It is also true, however, that many combinations of k and \mathcal{V} give rise to the same frequency shift—there is no direction sensitivity to the velocity at this point. Furthermore, an amplitude modulated image has symmetrical sidebands in $\mathcal{Q}(k)$, one of which will be deenhanced by about as much as the other is enhanced by the transient coupling process. The two together will tend to cancel the desired effect. To avoid these problems, Vachss and Hesselink placed a knife-edge in the Fourier plane of the object. The knife-edge eliminates one set of sidebands in the spectrum and provides a degree of direction sensitivity to the system.

Fig. 11 shows the image of a resolution chart that is translated at three different speeds. The middle photograph shows enhanced response over the other two. Vachss and Hesselink also demonstrated the system's sensitivity to direction [10].

IV. MONOTONY FILTERS

One can also make an all-optical device that selectively displays only the stationary portions of an image. Such a device can be called a "monotony filter," because it highlights only objects that are motionless and unchanging. All the devices so far discussed except the beam-fanning one have a monotony port as well as a novelty port. In the two-beam coupling cases it is simply a matter of reversing the roles of the input beams, so that the two-wave interaction amplifies instead of depletes the image-bearing beam. In the development of Section II, one need

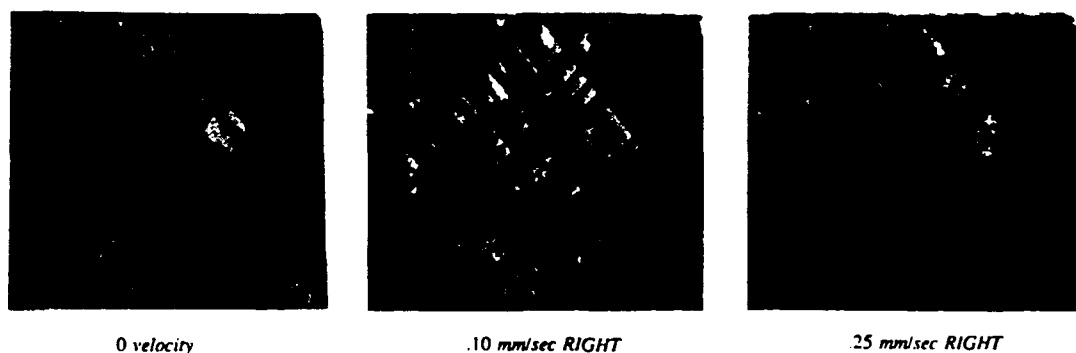


Fig. 11. Output from velocity selective novelty filter. An image is translated at three different velocities. The middle velocity gives rise to an enhanced output.

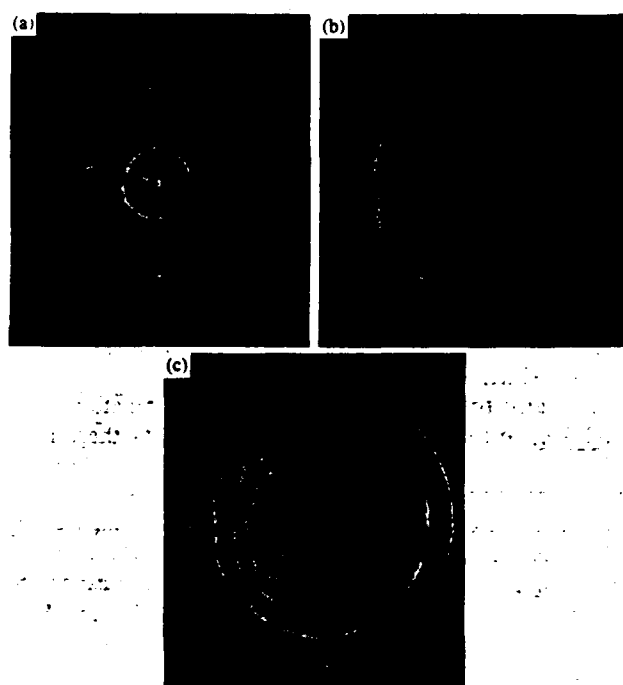


Fig. 12. Images of a vibrating loudspeaker seen through a monotony filter

only reverse the sign of $\text{Re}\{\Gamma\}$ to make a monotony filter. Now only the *stationary* parts of the image will be amplified, because the changing portions of the image do not form efficient holograms, and so do not become amplified. In the four-wave mixing interferometer versions, the monotonous portion of the filter is always present and propagates back toward the light source. Note that in the novelty filter any new features show up instantly, while in the monotony filter any monotonous features show up only after a photorefractive response time.

Marrakchi *et al.* used a four-wave mixing geometry to make a monotony filter [37]. The image-bearing beam was reflected off of a vibrating loudspeaker (whose cone had been sprayed with reflecting white paint) into a photorefractive crystal of BSO. A reference beam interfered with the reflected beam in the crystal, and formed a hologram

with only the stationary parts of the vibrating image. The hologram was read out by a third beam, counter-propagating to the reference beam. The images are shown in Fig. 12, where the standing wave patterns of the loudspeaker cone are clearly visible. This dynamic application of holography has also been demonstrated using a BTO crystal by Kamslulin *et al.* [38] and using a SBN crystal by Kukhtarev *et al.* [39].

V. CONCLUSION

We have described a number of all-optical devices that can process an entire image in parallel, and display either the novel or the monotonous portions of a scene. These devices use a photorefractive crystal as a holographic memory. We sum up the present optical novelty filters with the following practical observation: in any application for which the required adaptation time is on the order of many milliseconds to seconds, the two-beam coupling version is the best because of its simplicity and performance. In order to perform well, it requires a material with a high coupling constant, and such materials (e.g., barium titanate, strontium barium niobate) are available. However, these materials are always slow. Faster materials having lower coupling efficiency can be used in the four-wave mixing phase-conjugating geometry. It would be interesting to try this configuration using sodium vapor or another fast nonlinear medium.

The devices we have described are simple but effective all-optical processors that extract the temporal changes from a two-dimensional input. They are dedicated optical computers that can transform an entire scene in parallel. Because they are simple devices, we believe that they may be easily developed further. Vachss and Hesselink's work with the velocity-selecting novelty filter is a step in this direction. The filters discussed in this review have high-pass, low-pass, or bandpass filter characteristics. These are fundamental processing primitives that can be combined to perform complex operations. The other ingredient essential to processing is nonlinearity (although the filters use nonlinear elements they are performing linear operations). We anticipate that these linear functions will be united with the appropriate optical and/or electronic

nonlinearities to make more sophisticated optical processors.

REFERENCES

- [1] Our terminology for the novelty filter comes from T. Kohonen, *Self-Organization and Associative Memory*. New York: Springer, 1983, ch. 4.
- [2] See D. Falk, D. Bril, and D. Stork, *Seeing the Light*. New York: Harper and Row, 1986, pp. 192-193.
- [3] Discussed in D. Z. Anderson and M. C. Ene, "Resonator memories and optical novelty filters," *Opt. Eng.*, vol. 26, pp. 434-444, 1987. The actual demonstration remains unpublished.
- [4] D. Z. Anderson, D. M. Lininger, and J. Feinberg, "An optical tracking novelty filter," *Opt. Lett.*, vol. 12, pp. 123-125, 1987.
- [5] U.S. Patent 4 773 719, Sept. 27, 1988.
- [6] M. Cronin-Golomb, A. M. Biernacki, C. Lin, and H. Kong, "Photorefractive time differentiation of coherent optical images," *Opt. Lett.*, vol. 12, pp. 1029-1031, 1987.
- [7] R. Cudney, R. M. Pierce, and J. Feinberg, "The transient detection microscope," *Nature*, vol. 332, pp. 424-426, 1988.
- [8] N. S.-K. Kwong, Y. Tamita, and A. Yariv, "Optical tracking filter using transient energy coupling," *J. Opt. Soc. Amer. B*, vol. 5, pp. 1788-1791, 1988.
- [9] J. E. Ford, Y. Fainman, and S. H. Lee, "Time-integrating interferometry using photorefractive fanout," *Opt. Lett.*, vol. 13, pp. 856-858, 1988.
- [10] F. Vachss and L. Hesselink, "Synthesis of a holographic image velocity filter using the nonlinear photorefractive effect," *App. Opt.*, vol. 27, pp. 2887-2894, July 15, 1988.
- [11] A. M. Glass, "The photorefractive effect," *Opt. Eng.*, vol. 17, p. 470, 1978.
- [12] N. V. Kukhtarev, V. B. Markov, S. G. Odulov, M. S. Soskin, and V. L. Vinetskii, "Holographic storage in electrooptic crystals. I. Steady state," *Ferroelectrics*, vol. 22, pp. 949-960, 1979.
- [13] N. V. Kukhtarev, V. B. Markov, S. G. Odulov, M. S. Soskin, and V. L. Vinetskii, "Holographic storage in electrooptic crystals. II. Beam coupling—Light amplification," *Ferroelectrics*, vol. 22, pp. 961-964, 1979.
- [14] P. Günter, "Holography, coherent light amplification and optical phase conjugation," *Phys. Rep.*, vol. 93, pp. 200-299, 1982.
- [15] J. Feinberg, "Optical phase conjugation in photorefractive materials," in *Optical Phase Conjugation*, R. A. Fisher, Ed. New York: Academic, 1983, pp. 417-443.
- [16] *Photorefractive Materials and Their Applications I: Fundamental Phenomena*, P. Günter and J.-P. Huignard, Eds. New York: Springer, 1988.
- [17] For a discussion of the grating treated as a plane wave field, see D. Z. Anderson and R. Saxena, "Theory of multimode operation of a unidirectional ring oscillator having photorefractive gain: Weak-field limit," *J. Opt. Soc. Amer. B*, vol. 4, pp. 164-176, 1987.
- [18] H. Kogelnik, *Bell Syst. Tech. J.*, vol. 48, p. 2909, 1969.
- [19] L. Solymar and J. M. Heaton, "Transient energy transfer in photorefractive materials; an analytic solution," *Opt. Commun.*, vol. 51, pp. 76-78, 1984.
- [20] J. M. Heaton and L. Solymar, "Transient energy transfer during hologram formation in photorefractive crystals," *Opt. Acta*, vol. 32, pp. 397-408, 1985.
- [21] M. Cronin-Golomb, "Analytic solution for photorefractive two beam coupling with time varying signal," in *Dig. Top. Meet. Photorefractive Materials, Effects, Devices*. Washington, DC: Opt. Soc. Amer., 1987, pp. 142-145.
- [22] See, for example, B. P. Lathi, *Signal Systems and Communication*. New York: Wiley, 1965, ch. 5.
- [23] See, for example, G. Arfken, *Mathematical Methods for Physicists*, 3rd ed. New York: Academic, 1985, ch. 7.
- [24] F. C. Jahoda, B. T. Anderson, P. R. Forman, and P. G. Weber, "Application of optical phase conjugation to plasma diagnostics," *Rev. Sci. Instrum.*, vol. 56, pp. 953-957 (Invited), 1985.
- [25] J. Feinberg, "Interferometer with a self-pumped phase-conjugator mirror," *Opt. Lett.*, vol. 8, pp. 569-571, 1983.
- [26] D. Z. Anderson, "Optical resonators for associative memory," *SPIE*, vol. 613, *Nonlinear Optics and Applications*, pp. 85-89, 1986.
- [27] M. D. Ewbank, P. Yeh, M. Khoshnevisan, and J. Feinberg, "Time reversal by an interferometer with coupled phase-conjugate reflectors," *Opt. Lett.*, vol. 10, pp. 282-284, 1985.
- [28] H. Liu, J. Davis, and R. Lilly, "Optical data processing properties of a liquid crystal television spatial light modulator," *Opt. Lett.*, vol. 10, pp. 635-637, 1985.
- [29] L. M. Blinov, *Electro-Optical and Magneto-Optical Properties of Liquid Crystals*. New York: Wiley, 1983.
- [30] D. Casasent, "Performance evaluation of spatial light modulators," *Appl. Opt.*, vol. 18, p. 2445, 1979.
- [31] I. McMichael, M. Khoshnevisan, and P. Yeh, "Polarization preserving phase-conjugator," *Opt. Lett.*, vol. 11, pp. 525-527, 1986.
- [32] J. O. White, M. Cronin-Golomb, B. Fischer, and A. Yariv, "Coherent oscillation by self-induced gratings in the photorefractive crystal BaTiO₃," *Appl. Phys. Lett.*, vol. 40, p. 450, 1982.
- [33] J. Feinberg, "Self-pumped, continuous-wave phase-conjugator using internal reflection," *Opt. Lett.*, vol. 7, pp. 486-488, 1982.
- [34] V. L. Vinetskii, N. V. Kukhtarev, and M. S. Soskin, *Sov. J. Quantum Electron.*, vol. 7, p. 230, 1977.
- [35] N. Kukhtarev, V. Markov, and S. Odulov, *Opt. Commun.*, vol. 23, p. 338, 1977.
- [36] F. Vachss and L. Hesselink, "Selective enhancement of spatial harmonics of a photorefractive grating," *J. Opt. Soc. Amer. B*, vol. 5, p. 1814, 1988.
- [37] A. Marrakchi, J.-P. Huignard, and J. P. Herriau, "Application of phase conjugation in Bi₁₂SiO₂₀ crystals to mode pattern visualization of diffuse vibrating structures," *Opt. Commun.*, vol. 34, pp. 15-18, 1980.
- [38] A. Kamluln, E. Mokrushina, in *Symp. Optika '84*, Budapest, Hungary. SPIE, vol. 433, 1984, pp. 83-86.
- [39] N. V. Kukhtarev in *Photorefractive Materials and Their Applications I: Fundamental Phenomena*, P. Günter and J.-P. Huignard, Eds. New York: Springer, 1988, ch. 4.

Dana Z. Anderson received the B.S.E.E. degree from Cornell University, Ithaca, NY, in 1975 and the Ph.D. degree in physics from the University of Arizona, Tucson, in 1981.

He spent three years as a research associate at the California Institute of Technology, Pasadena, working on a prototype gravitational wave optical interferometer. He is now an Assistant Professor with the Department of Physics, University of Colorado, Boulder, and a Fellow of the Joint Institute for Laboratory Astrophysics of the University of Colorado and the National Institute of Standards and Technology. He is also a member of the Optoelectronic Computing Systems Center at the University of Colorado. His primary research interests are optical gyroscopes, nonlinear optics, and optical neural networks.

Dr. Anderson is an Alfred P. Sloan Research Fellow and a National Science Foundation Presidential Young Investigator.



Jack Feinberg was born and raised in New York, N.Y. He received the A.B. degree in physics with honors from Columbia University, New York, in 1972, and the Ph.D. from the University of California, Berkeley, in 1977, where he worked on molecular spectroscopy.

He joined the University of Southern California as a postdoctoral researcher, joined the Department of Physics in 1981, and became an Associate Professor in 1985. His interests include anything optical, especially optical phase conjugation, nonlinear optics, spectroscopy, applications of optics to medicine, and making movies.

Prof. Feinberg is a member of various professional and veterinary societies.

Measuring the coherence length of mode-locked laser pulses in real time

Vince Dominic, X. Steve Yao, R. M. Pierce, and Jack Feinberg

Departments of Physics and Electrical Engineering, University of Southern California, Los Angeles, California 90089-0484

(Received 11 September 1989; accepted for publication 25 November 1989)

We demonstrate a new technique for displaying the electric field autocorrelation function of a laser pulse in real time, using two-beam coupling in a photorefractive crystal. This technique can be used over the entire visible and near-infrared regions of the spectrum, even with weak laser beams, and is automatically self-phase matched.

The coherence length of a laser pulse can be measured by interfering the pulse with its own delayed replica.¹⁻⁴ Here we measure the coherence length¹⁰ of a pulse from a mode-locked laser, where we average over many pulses. As suggested by Johnson *et al.*,¹¹ we make each laser pulse interfere with itself in a photorefractive crystal. However, we improve upon their technique by encoding different time delays across a single laser beam,¹² so that the entire field autocorrelation function can be determined in essentially real time (a few milliseconds). Our technique works over a wide range of wavelengths (limited only by the spectral response of the photorefractive crystal) and with very weak laser pulses (\sim microwatt average power).

The technique is outlined in Fig. 1. The incident laser beam is split into two, with one beam (the reference beam) directed into a photorefractive crystal. The other beam (the probe beam) illuminates a diffraction grating at grazing incidence. The first-order diffracted beam has different time delays encoded onto its different portions.¹² Inspection of Fig. 1 shows that the left side of the diffracted probe beam travels a shorter distance to the photorefractive crystal than the right side of the diffracted probe beam, and so arrives at the crystal first. This diffracted probe beam is focused by a lens into the photorefractive crystal, where it intersects the reference beam and forms an intensity interference pattern, but only in those regions of the crystal where the two beams are coherent with each other.

The intensity pattern creates an index-of-refraction hologram in the photorefractive crystal. The strength of the hologram depends on the visibility of the intensity interference fringes, which depends on the relative coherence of the two interfering beams. Note that if the incident laser pulses are weak, it may take many pulses to build up the photorefractive hologram. This hologram couples the two beams, so that the probe beam experiences gain (or loss, depending on the orientation of the crystal). A one-dimensional array of detectors measures the profile of the amplified probe beam and stores it in a computer. *The probe beam gain will vary with distance x across the face of the beam, and will depend on the local degree of coherence of the probe beam with the reference beam. As we show below, the gain profile of the amplified probe beam is simply related to the electric field autocorrelation function of the incident laser beam.*

Our coherence length measurement technique can be applied to a train of (almost) arbitrarily weak laser pulses. The photorefractive hologram integrates the intensity interference pattern over time, and reaches a steady-state ampli-

tude that is independent of the total intensity of the incident beams. (However, the time required to reach the steady state will increase if the laser intensity is decreased.) For example, in the experiments reported here, the time-average intensity of the reference beam was 3.3 W/cm^2 (power, 74 mW; beam diameter, 1.7 mm). At this optical intensity, the response time of the crystal was about one-tenth of a second, enabling an essentially "real time" measurement of the coherence length. However, we also tried decreasing the incident laser intensity by a factor of 1000, so that the photorefractive crystal needed a minute or so to build up its hologram, and we still obtained the same value for the average coherence length of each laser pulse.

The device is calibrated as follows. The reference beam is delayed relative to the probe beam by an optical delay line consisting of a retroreflecting prism mounted on a calibrated translation stage. We repeatedly take data with different known time delays, and we measure the translation of the output beam's profile across the reticon array, as shown in Fig. 2. This plot is linear, as expected, and its slope yields the calibration factor of our apparatus.

Here are some experimental details: The photorefractive crystal is a single-domain crystal of BaTiO_3 , which we use at room temperature without an applied electric field. Both the reference beam and the probe beam are polarized

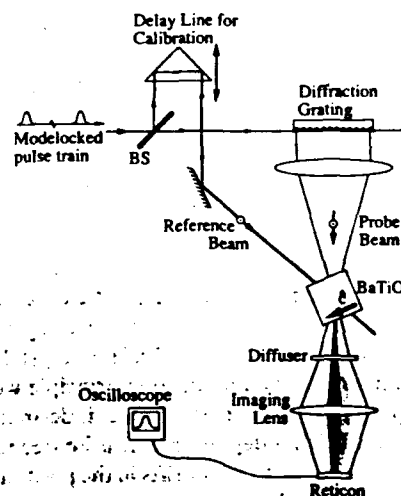


FIG. 1. Optical setup for measuring the average coherence length of a series of optical pulses. The diffraction grating encodes different time delays onto different portions of the probe beam.

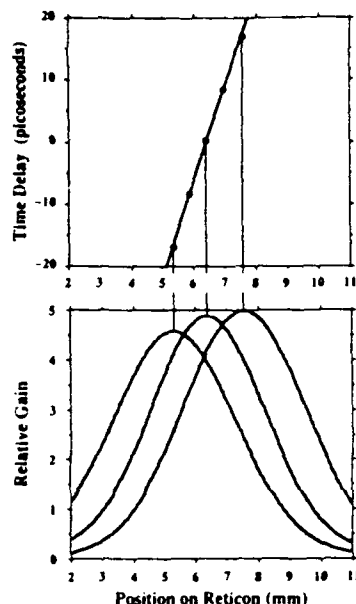


FIG. 2. Calibrating the apparatus. The bottom portion of the figure shows the output beam profile translation across the reticon as the time delay is changed. The top graph shows the linear relationship between the known time delay and the displacement of the beam profile.

perpendicular to the plane of incidence, and both beams are ordinary rays in the BaTiO₃ crystal. (Although this choice of polarization has the drawback of reducing the overall two-beam coupling gain of the probe beam, it has the advantage of minimizing two-beam self-coupling between the various angular components of the probe beam.) An $f = 25$ cm lens focuses light from the diffraction grating into the BaTiO₃ crystal, which is placed one focal length from the lens. The diffraction grating is 5.8 cm square with 1800 lines/mm. The focused probe beam has a full cone angle of 12° outside the crystal. The unfocused reference beam (intensity full width at half maximum = 1.7 mm) and the probe beam are symmetrically incident on the crystal at exterior angles of $\pm 19^\circ$. The BaTiO₃ crystal is oriented with its c axis parallel to the wave vector of the photorefractive hologram, with the crystal's positive c -axis direction chosen to amplify the probe beam. With this geometry the maximum intensity gain of the probe beam is 2–5, depending on which BaTiO₃ crystal we use. Depletion of the reference beam was minimized by using a weak probe beam (power = 3 μ W). We prevent scattered light from striking the detector array by inserting slits and apertures in both the reference and the probe beams. We reduce speckle noise by inserting a rotating plastic diffuser between the crystal and the detector array, and then imaging the diffuser onto the array. Some of our BaTiO₃ crystals have dark storage times of over an hour, so in principle we can integrate laser pulses for that length of time, if desired. However, in practice the useful integration time is limited to no more than a few minutes, due to slow drifts in the position of the mirrors on the optical table.

If the diffraction grating were replaced by a mirror, so that each portion x of the probe beam had the same delay τ with respect to the reference beam then the intensity

$I_{\text{out}}(x)$ of the amplified probe after two-wave mixing in a crystal of length L would be¹³

$$[I_{\text{out}}(x) - I_{\text{in}}(x)]/I_{\text{in}}(x) = |G(\tau)|^2 [e^{(\Gamma - \alpha)L} - 1], \quad (1)$$

where $G(\tau)$ is the normalized electric field autocorrelation function of the incident beam, Γ is the intensity two-wave mixing gain per cm for the case of perfectly coherent cw light beams, and α is the intensity absorption coefficient. However, unlike a mirror, the diffraction grating encodes different time delays τ on each portion x of the probe beam according to

$$\tau(x) = x(\sin \theta_{\text{in}} - \sin \theta_{\text{out}})/c \cos \theta_{\text{out}}, \quad (2)$$

where x is the transverse distance across the diffracted probe beam, c is the speed of light in air, θ_{in} is the angle between the incident beam and the grating normal, and θ_{out} is the angle between the diffracted beam and the grating normal. At grazing incidence $\theta_{\text{in}} = 90^\circ$ and $\theta_{\text{out}} = 0^\circ$, so that Eq. (2) simplifies to $\tau(x) = x/c$. The maximum delay τ is limited by the size of the diffraction grating, and was ~ 190 ps with our 5.8-cm-wide grating.

Equation (1) requires a measurement of the incident probe beam profile $I_{\text{in}}(x)$ at the entrance of the crystal. In practice it is simpler to measure the transmitted probe beam after the crystal but in the absence of any two-beam coupling, $I_{\text{no coupling}}(x)$, by blocking the reference beam. Equation (1) becomes

$$\frac{I_{\text{out}}(x) - I_{\text{no coupling}}(x)}{I_{\text{no coupling}}(x)} = |G(\tau)|^2 [e^{\Gamma L} - e^{\alpha L}] + e^{\alpha L} - 1. \quad (3)$$

This equation includes the effects of Fresnel reflections at the crystal faces, which happen to cancel out nicely. Note that in the absence of linear absorption α , Eq. (3) becomes identical to Eq. (1). For the case of coherent cw illumination, $|G| = 1$, and Eq. (3) reverts to the usual expression describing photorefractive gain.

We tested our device by measuring the average coherence length of the frequency-doubled ($\lambda = 532$ nm) pulses from a mode-locked cw Nd:YAG laser (Coherent Antares 76-s). This laser is actively mode locked and emits pulses at a rate of 76 MHz. Figure 3 shows the relative gain [defined as the left-hand side of Eq. (3)] across the probe beam for a series of $\sim 10^8$ laser pulses (i.e., we averaged for ~ 1 s). The solid line is a least-squares fit of Eq. (3) obtained by varying three parameters: the maximum two-beam coupling gain Γ of the crystal, a vertical offset related to absorption, and the coherence time τ_c of the incident laser pulse. Here we assume that the laser pulses are Gaussian in time, and we take the coherence time τ_c to be the half width at half maximum of the electric field autocorrelation function.¹⁰ From this fit we obtain a value of $\tau_c = 48$ ps. However, we found that τ_c could drift slowly with time by ~ 8 ps over 30 min, which we attribute to a mode-locking instability of our laser.

In order to test Eq. (3), we tried using two different single-domain crystals of BaTiO₃, having dissimilar two-beam coupling gain coefficients Γ . We obtained the same value for the average coherence length of our laser pulses, within experimental error, using either crystal. We also inspected our laser pulses with a 1/4-in.-thick solid glass

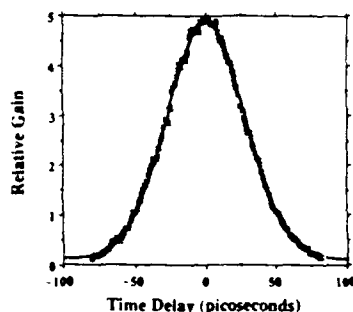


FIG. 3. Plot of the relative intensity gain across the probe beam. Each portion of the beam experiences a different gain because it has been delayed by a different amount of time relative to the reference beam. The horizontal axis shows the relative delay of each portion of the probe beam. The solid line is a best fit to Eq. (3), and yields a coherence time of $\tau_c = 48$ ps.

Fabry-Perot étalon; the appearance of the ring pattern was consistent with the coherence length measured by our two-beam coupling technique. However, the Fabry-Perot also revealed that the center frequency of the laser jittered on the time scale of a few seconds, possibly due to thermally induced fluctuations in the laser's effective cavity length.

What is the resolution limit of this device? Dispersion of the grating will cause spatial broadening of the measured output beam profile $I_{out}(x)$.¹² For the geometry and coherence times used here, this broadening is negligible, but it places a lower limit of 0.1 ps on the shortest pulse we can measure. Also, the finite crossing angle of the two beams will cause a broadening of the output beam profile. The worst case would be for a crossing angle of 90°, which would cause a smearing in time equal to the time it takes light to traverse the wider of the two beams in the crystal. In our experiments, we estimate this smearing to be ~ 1 ps. Our calculations indicate that the effect of a finite recombination time of the photorefractive crystal is to alter the overall two-beam coupling gain coefficient, but without altering the shape of the output profile of the amplified beam.

In summary, we have demonstrated a simple method for measuring the coherence length of a pulsed laser, and especially for a laser that produces a train of very weak optical pulses. This technique does not require phase matching, is simple to align, and can be used over the entire visible and near-infrared regions of the spectrum. The spectral response of our BaTiO₃ crystals extends only to the near infrared, and so is too small to be useful at 1.06 μm Nd:YAG laser wavelength. We are pursuing the use of other photorefractive crystals to extend this pulse-measuring technique further into the infrared.

This work was supported by contract No. F49620-88-C-0095 of the Air Force Office of Scientific Research. V. Dominic gratefully acknowledges fellowship support from the National Science Foundation and the Joint Services Electronics Program.

¹J.-C. M. Diels, E. W. Van Stryland, and D. Gold, In *Picosecond Phenomena*, edited by C. V. Shank, E. P. Ippen, and S. L. Shapiro, Springer Series Chem. Phys. No. 4 (Springer, New York, 1978), pp. 117-120.

²R. Trebino, E. K. Gustafson, and A. E. Siegman, *J. Opt. Soc. Am. B* **3**, 1295 (1986).

³H. J. Eichler, U. Klein, and D. Langhans, *Appl. Phys.* **21**, 215 (1980).

⁴W. L. Nighan, T. Gong, L. Liou, and P. M. Fauchet, *Opt. Commun.* **69**, 339 (1989).

⁵R. Baltrameynas, Yu. Vaitkus, R. Danelyus, M. Pyatrauskas, and A. Piskarskas, *Sov. J. Quantum Electron.* **12**, 1252 (1982).

⁶V. S. Idiatulin and Yu. N. Teryaev, *Opt. Quantum Electron.* **14**, 51 (1982).

⁷X. Zhu, K. G. Spears, and J. Serafin, *J. Opt. Soc. Am. B* **6**, 1356 (1989).

⁸J. Janszky, G. Corradi, and D. S. Hamilton, *Appl. Opt.* **23**, 8 (1984).

⁹J. Buchert, R. Dorsinville, P. Delfyett, S. Krimchansky, and R. R. Alfano, *Opt. Commun.* **52**, 433 (1985).

¹⁰We use the terms "coherence length" and "coherence time" loosely. Our experimental technique measures the field autocorrelation (or fringe visibility) function versus time delay. The width of this function depends on both the pulse duration and the usual coherence time. For more details, see Ref. 7.

¹¹A. M. Johnson, A. M. Glass, W. M. Simpson, R. B. Bylisma, and D. H. Olson, in *Annual Meeting OSA Technical Digest* No. 11 (Optical Society of America, Washington, DC, 1988), paper ThC4.

¹²R. Wyatt and E. E. Marinero, *Appl. Phys.* **25**, 297 (1981).

¹³X. S. Yao, V. Dominic, and J. Feinberg (unpublished).

Theory of beam coupling and pulse shaping of mode-locked laser pulses in a photorefractive crystal

X. Steve Yao, Vince Dominic, and Jack Feinberg

Departments of Physics and Electrical Engineering, University of Southern California, Los Angeles, California 90089-0484

Received October 18, 1989; accepted June 28, 1990

We describe how optical beams from a mode-locked laser will couple in a photorefractive crystal. We show that the two-beam-coupling gain coefficient is proportional to the square of the electric field correlation of the incoming light pulses. Consequently we show that two-beam-coupling experiments can measure the average coherence length of mode-locked laser pulses. We also describe how the temporal envelopes of the mode-locked optical pulses distort as they couple and propagate through the photorefractive crystal, and we give examples of how pulses can be shaped by using photorefractive coupling.

1. INTRODUCTION

The strong coupling between optical beams in a photorefractive crystal has been extensively studied for continuous-wave optical beams¹ and for single, short, high-irradiance optical pulses.²⁻⁴ Here we consider the coupling between trains of mode-locked pulses in a photorefractive crystal. We are especially interested in photorefractive crystals that have a long dark-storage time, which permits the light-induced changes caused by successive optical pulses to accumulate in the crystal. We consider the case in which each optical pulse is quite weak, so that it takes a large number of pulses ($>10^6$) to build up a quasi-steady-state refractive-index grating in the crystal. We derive the time-averaged response of the crystal to these pulses. We show that, once formed, the photorefractive grating can alter the temporal shape of the laser pulses as they traverse the crystal. We also show that a photorefractive crystal can be used to measure the average coherence length of a train of mode-locked laser pulses, as was recently demonstrated in experiments by Johnson *et al.*⁵⁻⁷ and Dominic *et al.*⁸

2. SPACE-CHARGE ELECTRIC FIELD

Consider an infinite and periodic train of laser pulses, such as from a cw-pumped mode-locked laser. Let two such pulse trains intersect in a photorefractive crystal. If in some region of the crystal the two beams are coherent (and so produce an intensity-interference pattern there), then charge carriers in the crystal will be rearranged by the pattern of bright and dark fringes. The migration of these charge carriers causes a space-charge field $E_{sc}(\mathbf{r}, t)$ to grow and eventually reach a quasi-equilibrium. Suppose that the energy of each pulse is small, so that many pulses are required in order to reach the steady state. Then, once E_{sc} reaches its quasi-equilibrium value, each subsequent laser pulse causes E_{sc} to make only small excursions that always return it to its initial value, as we show below.

The time dependence of this space-charge field is governed by a first-order differential equation, as derived by Strohkendl *et al.*⁹ for the case of constant incident intensity. However, the same equation holds even if the intensity is changing in time, as long as the peak intensity is weak enough to satisfy the restriction of Eq. (8) of Ref. 9. For the case in which the recombination rate of free carriers is much shorter than the pulse duration, the space-charge field evolves according to

$$\frac{\partial E_{sc}(\mathbf{r}, t)}{\partial t} + aI_0(t)E_{sc}(\mathbf{r}, t) = ibE_1(\mathbf{r}, t)E_2^*(\mathbf{r}, t), \quad (1)$$

where E_{sc} is the magnitude of the (quasi-dc) space-charge field, $E_1(\mathbf{r}, t)$ and $E_2^*(\mathbf{r}, t)$ are the slowly varying complex optical-field envelopes, and $I_0(t) = |E_1(\mathbf{r}, t)|^2 + |E_2(\mathbf{r}, t)|^2$ is proportional to the total intensity. [Note that, in the absence of absorption, energy conservation requires the intensity to be a constant in space, which is why $I_0(t)$ has no spatial dependence.] The quantities a and b are complicated functions of material parameters and beam geometry but not of the optical intensities.⁹

Equation (1) indicates that the space-charge field is driven by the interference term $E_1(\mathbf{r}, t)E_2^*(\mathbf{r}, t)$ and is erased by the uniform intensity I_0 . If many pulses are required in order to reach steady state, then no one pulse can change E_{sc} by a large amount, and E_{sc} will reach a quasi-steady-state value that is determined by the balance of the driving and erasing terms. Equation (1) holds when the free-carrier recombination time is much less than the duration of a single mode-locked laser pulse, so that the free-carrier density created by light in the photorefractive material closely follows any variation of the light intensity with time. If this is not the case, the situation becomes more complicated, for we must then couple Eq. (1) to another differential equation that describes the time evolution of the free-carrier density. We discuss this case at the end of this section.

Because in general the incoming laser pulses are not identical, we must average over the ensemble of possible

pulses. The laser pulses may fluctuate both in amplitude and in phase. We choose to model the pulses as having identical amplitudes but randomly varying phases. To our knowledge there is no satisfactory statistical description of phase fluctuations of mode-locked laser pulses, so we will not specify the statistics of the phase fluctuations; instead, we simply characterize the optical electric field of the pulses by a parameter τ_c , which specifies the characteristic length of time (averaged over many pulses) during which the optical electric fields evolve sinusoidally in time without interruption. (An analogy may be an electron drifting freely through a solid, with some average time between collisions.)

Using our amplitude-stabilized pulses, we take the ensemble average of Eq. (1):

$$\frac{\partial \overline{E_{sc}(\mathbf{r}, t)}}{\partial t} - a I_0(t) \overline{E_{sc}(\mathbf{r}, t)} = ib \overline{E_1(\mathbf{r}, t) E_2^*(\mathbf{r}, t)}, \quad (2)$$

where the overbar denotes an ensemble average.¹⁰ For the case of cw illumination, Eq. (2) can be solved by a steady-state space-charge field E_{sc} that is proportional to the modulation of the intensity interference pattern.¹¹ For the case of pulsed illumination, we expect the equilibrium value of the space-charge field to depend in a similar manner also on the modulation of the optical intensity and therefore on the relative coherence of the two optical pulses at the crystal. We postulate that the steady-state solution of Eq. (2) is

$$\overline{E_{sc}} = \frac{ib}{a} \frac{\langle \overline{E_1(\mathbf{r}, t) E_2^*(\mathbf{r}, t)} \rangle}{\langle |E_1(\mathbf{r}, t)|^2 + |E_2(\mathbf{r}, t)|^2 \rangle}, \quad (3)$$

where the notation $\langle \rangle$ denotes an average over time T :

$$\langle F(t) \rangle = \frac{1}{T} \int_{-T/2}^{T/2} F(\tau) d\tau. \quad (4a)$$

Note that, if the interfering beams are cw, then the time averages in Eq. (3) may be dropped, and we obtain the usual dependence of the steady-state space-charge field on the modulation of the intensity-interference pattern.¹¹ For periodic optical pulses, the postulated dependence of Eq. (3) may be viewed as the dc term in a temporal Fourier expansion of E_{sc} . We show below that this dc term is by far the largest term (by a factor of 10^6) in the expansion, again because many pulses are required in order to reach the quasi-equilibrium, so that no one pulse can push E_{sc} far from its equilibrium value.

Using the notation of Trebino *et al.*¹² we can express the electric-field envelope of the optical pulses as

$$E_1(\mathbf{r}, t) = A_1(\mathbf{r}, t) u_1(\mathbf{r}, t), \quad (4b)$$

$$E_2(\mathbf{r}, t) = A_2(\mathbf{r}, t - \tau_d) u_2(\mathbf{r}, t - \tau_d), \quad (4c)$$

where in Eqs. (4) the functions $A_1(\mathbf{r}, t)$ and $A_2(\mathbf{r}, t)$ are the deterministic amplitude of the pulses of beams 1 and 2, respectively. The functions $u_1(\mathbf{r}, t)$ and $u_2(\mathbf{r}, t)$ are statistical factors that contain information about the phase fluctuations of the two beams; both of these functions are normalized to unity: $|u_1| = |u_2| = 1$. For convenience we have defined beam 2 with a built-in delay time τ_d , because in practice the two interfering optical beams are usually derived by splitting one single beam into two and

then delaying one beam with respect to the other by a time τ_d . Using this notation, we may rewrite the numerator of Eq. (3) as

$$\begin{aligned} G(\tau_d) &\equiv \overline{E_1(\mathbf{r}, t) E_2^*(\mathbf{r}, t)} \\ &= \overline{A_1(\mathbf{r}, t) A_2^*(\mathbf{r}, t - \tau_d) u_1(\mathbf{r}, t) u_2^*(\mathbf{r}, t - \tau_d)}. \end{aligned} \quad (5)$$

When the phase fluctuations are governed by jointly wide-sense stationary statistics,¹³ so that the quantity $u_1(\mathbf{r}, t) u_2^*(\mathbf{r}, t - \tau_d)$ is independent of time,¹⁴ we express Eq. (5) as

$$G(\tau_d) = \langle A_1(\mathbf{r}, t) A_2^*(\mathbf{r}, t - \tau_d) \rangle \gamma^2(\tau_d), \quad (6)$$

where $\gamma^2(\tau_d)$ is the second-order coherence function, which depends on the relative delay τ_d between the two pulses (and implicitly on the parameter τ_c , the average phase-coherence time of a pulse):

$$\gamma^2(\tau_d) \equiv \overline{u_1(\mathbf{r}, t) u_2^*(\mathbf{r}, t - \tau_d)}. \quad (7)$$

Substituting Eq. (7) into Eq. (3) yields

$$\overline{E_{sc}} = \frac{ib}{a} \frac{\langle A_1(\mathbf{r}, t) A_2^*(\mathbf{r}, t - \tau_d) \rangle \gamma^2(\tau_d)}{I_0}. \quad (8)$$

In order to verify our guess that Eq. (8) is indeed the quasi-steady-state solution for the space-charge field, we numerically integrated Eq. (1) for the case of a periodic train of pulses, with the amplitude of each pulse taken to be Gaussian in time. At first we assumed that each pulse was transform limited. Using a fourth-order Runge-Kutta method, we computed how E_{sc} changed during each light pulse. Figures 1 and 2 show the deviation of E_{sc} from the steady-state value predicted by Eq. (8). In Fig. 1(a) we set the relative delay between the two writing beams (one strong and the other weak) to be $\tau_d = -30$ psec (so that the strong beam arrives before the weak beam). In Fig. 1(b) the space-charge field is seen first to decay and then to grow during each laser pulse but always to return to its initial value. Figure 2 shows the result for $\tau_d = +70$ psec (where now the strong beam arrives after the weak beam). Here each laser pulse causes the space-charge field first to decay (slightly) when the weak beam arrives, then to grow, and then to decay back to its steady-state value. Note that the vertical scale in Figs. 1(b) and 2(b) is in parts in 10^6 ; the maximum excursion of the space-charge field from its steady-state value (which it maintains between laser pulses) is quite small. When we picked a value for E_{sc} that was too small, we found that after the next light pulse E_{sc} would be left at a slightly larger value than when it started, until after many light pulses it attained the steady-state value specified by Eq. (8). Similarly, when we initially picked E_{sc} too large, then the next light pulse would leave it slightly smaller. Only with the value of E_{sc} given by Eq. (8) would each light pulse cause the space-charge field to return to exactly the same value that it had before the light pulse.

To generate Figs. 1 and 2, we used material parameters that are typical for photorefractive BaTiO₃ and optical beams with average beam intensities of tens of milliwatts per square millimeter and pulse durations of 70 psec (intensity FWHM). For this calculation we assumed that (a) the dark decay rate is much less than the pulse repeti-

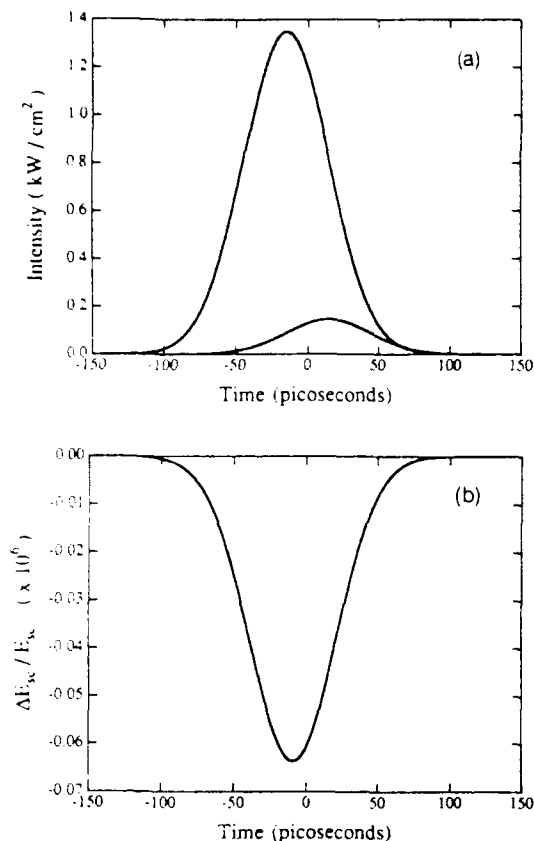


Fig. 1. (a) A strong optical beam leads a weak beam by 30 psec. (b) While these optical pulses are present in the crystal, the space-charge field momentarily deviates from its steady-state value: It initially decays and then recovers.

tion rate, (b) the average modulation of the photorefractive grating is much less than unity, (c) there are no shallow traps, (d) there is no spatially uniform dc electric field in the crystal, (e) the spatially periodic free-carrier number density is much less than the spatially periodic deep-trap number density,⁹ (f) and the recombination time of charges in the band is much less than the duration of each laser pulse.

We also considered the case in which the optical pulses have phases that vary randomly in time, and we found that the quasi-steady-state space-charge field is still given by the correlation of the two optical fields, as predicted by Eq. (8). Encouraged by these results, we then tried relaxing condition (f) above by making the recombination time longer than the pulse duration by factors ranging from 1 to 140 (while keeping constant the product of mobility and recombination time). We found that the space-charge field still attained the value given by Eq. (8) to within 1 part in 10^7 .

3. COUPLED-WAVE EQUATIONS

As discussed in Section 2, the interference of two weak, infinite trains of optical pulses eventually produces a quasi-steady-state space-charge field in a photorefractive crystal. This electric field alters the refractive index of the crystal; it creates a refractive-index grating. Here we

discuss how the optical beams are coupled by this grating. In particular, as the beams traverse the crystal their temporal shapes are modified by their coupling with the grating, which then alters the grating, which then alters the beams, which makes the equations difficult to solve. Coupled-wave treatments¹ of this problem usually ignore any variation in the temporal envelopes of the pulses as they propagate through the crystal. Here we include these variations.

To derive the coupled-wave equations, we consider a material with no free currents. Maxwell's equations then yield

$$\nabla^2 \mathcal{E}(\mathbf{r}, t) - \mu_0 \frac{\partial^2 \mathcal{D}(\mathbf{r}, t)}{\partial t^2} = 0, \quad (9)$$

where $\mathcal{E}(\mathbf{r}, t)$ is the total real optical electric field in the material and $\mathcal{D}(\mathbf{r}, t)$ is the corresponding real displacement vector. In Eq. (9) we ignore the term $\nabla(\nabla \cdot \mathcal{E})$.¹³

Now let the total optical field comprise two light beams with the same nominal frequency ω_0 , respective complex electric fields E_1 and E_2 , wave vectors \mathbf{k}_1 and \mathbf{k}_2 , and eigenpolarizations \hat{e}_1 and \hat{e}_2 in the crystal. The total optical electric field and displacement vectors are

$$\begin{aligned} \mathcal{E}(\mathbf{r}, t) = \text{Re}\{ & [\hat{e}_1 E_1(\mathbf{r}, t) \exp(i\mathbf{k}_1 \cdot \mathbf{r}) \\ & + \hat{e}_2 E_2(\mathbf{r}, t) \exp(i\mathbf{k}_2 \cdot \mathbf{r})] \exp(-i\omega_0 t) \}, \end{aligned} \quad (10)$$

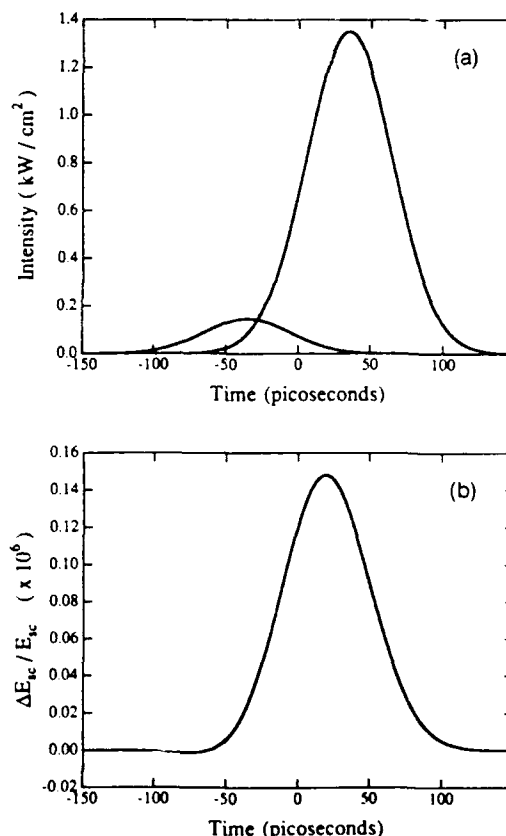


Fig. 2. (a) A strong optical beam follows a weak beam by 70 psec. (b) While these pulses are present, the space-charge field grows and then decays, but it never deviates by even 1 part in 10^6 from its steady-state value.

$$\mathcal{D}(\mathbf{r}, t) = \text{Re}\{[\mathbf{D}_1(\mathbf{r}, t)\exp(i\mathbf{k}_1 \cdot \mathbf{r}) + \mathbf{D}_2(\mathbf{r}, t)\exp(i\mathbf{k}_2 \cdot \mathbf{r})]\exp(-i\omega_0 t)\}, \quad (11)$$

$$\mathbf{D}_i(\mathbf{r}, t) \equiv \epsilon_0 \bar{\epsilon}(\mathbf{r}) \cdot \hat{e}_i E_i(\mathbf{r}, t), \quad i = 1, 2. \quad (12)$$

In Eqs. (10)–(12), ϵ_0 is the permittivity of free space, $\bar{\epsilon}(\mathbf{r})$ is the relative dielectric tensor of the medium, and $\mathbf{D}_i(\mathbf{r}, t)$ and $\hat{e}_i E_i(\mathbf{r}, t)$ are the slowly varying envelopes of the displacement and the electric-field vectors at the optical frequency ω_0 . Note that Eq. (12) ignores any material dispersion. For laser pulses that are picoseconds or longer, this approximation is justified by the short length of typical photorefractive crystals. For example, a 2-mm sample of barium titanate would require a pulse duration of less than 100 fsec before group-velocity dispersion would become noticeable.

The interference pattern of the two light beams will have a periodicity $\cos(\mathbf{k}_g \cdot \mathbf{r})$, where $\mathbf{k}_g \equiv \mathbf{k}_1 - \mathbf{k}_2$. The dielectric tensor of the crystal will be altered by the light pattern at the same spatial frequency \mathbf{k}_g :

$$\bar{\epsilon}(\mathbf{r}) = \bar{\epsilon} + \text{Re}[\Delta \bar{\epsilon} \cdot \exp(i\mathbf{k}_g \cdot \mathbf{r})], \quad (13)$$

where $\bar{\epsilon}$ is the crystal's average dielectric tensor. The spatially periodic part of the dielectric tensor $\text{Re}[\Delta \bar{\epsilon} \cdot \exp(i\mathbf{k}_g \cdot \mathbf{r})]$ will couple the two optical waves. Substituting Eqs. (10)–(13) into Eq. (9) yields equations that couple the slowly varying electric-field envelopes E_1 and E_2 of the two optical beams:

$$\left(\frac{\partial}{\partial z} + \frac{1}{v} \frac{\partial}{\partial t}\right) E_1(z, t) = \frac{i\omega}{4n_1 c \cos \theta} (\hat{e}_1^* \cdot \Delta \bar{\epsilon} \cdot \hat{e}_2) E_2(z, t), \quad (14a)$$

$$\left(\frac{\partial}{\partial z} + \frac{1}{v} \frac{\partial}{\partial t}\right) E_2(z, t) = \frac{i\omega}{4n_2 c \cos \theta} (\hat{e}_2^* \cdot \Delta \bar{\epsilon} \cdot \hat{e}_1) E_1(z, t). \quad (14b)$$

In Eqs. (14), z is the distance along the bisector of \mathbf{k}_1 and \mathbf{k}_2 in the crystal, θ is the half-angle between \mathbf{k}_1 and \mathbf{k}_2 , and v is defined as

$$v \equiv (c/n) \cos \theta. \quad (15)$$

For cw beams the time derivatives in the coupled-wave equations (14) are zero, but for pulsed laser beams these time derivatives must be included. Smirl *et al.*² included these time derivatives in their analysis of beam coupling in photorefractive crystals with single-shot, high-irradiance laser pulses. However, they did not discuss the evolution of the laser pulses' temporal shapes, and with good reason: in the case that they considered, the energy coupling between the two beams was so small that its effect on the temporal shape of the laser pulses could safely be neglected. Here the energy coupling between the beams can be quite strong, and it can drastically alter the temporal shapes of the light pulses. We discuss such pulse shaping in Section 6.

In deriving the coupled-wave equations (14), we made the following assumptions: The optical electric-field envelope changes slowly with distance:

$$\left|\frac{\partial^2 E_i}{\partial z^2}\right| \ll k_i \left|\frac{\partial E_i}{\partial z}\right|, \quad (16)$$

and with time:

$$\left|\frac{\partial^2 (\bar{\epsilon} \cdot \hat{e}_i E_i)}{\partial t^2}\right| \ll \omega \left|\frac{\partial (\bar{\epsilon} \cdot \hat{e}_i E_i)}{\partial t}\right|, \quad (17a)$$

$$\left|\frac{\partial (\Delta \bar{\epsilon} \cdot \hat{e}_i E_i)}{\partial t}\right| \ll \omega \Delta \bar{\epsilon} \cdot \hat{e}_i E_i. \quad (17b)$$

We assume that the perturbation of the dielectric tensor is small:

$$\Delta \bar{\epsilon} \ll \bar{\epsilon}, \quad (18)$$

and that all the frequency components of the laser pulses are perfectly Bragg matched to the grating. We also assume that these frequency components all write the same grating. (For a millimeter-sized grating, this implies a minimum laser pulse width of a few tens of picoseconds.)

4. PHOTOREFRACTIVE GRATING

The space-charge field E_{sc} of Eq. (8) will induce a change in the dielectric tensor by the electro-optic (Pockels) effect¹¹:

$$\Delta \bar{\epsilon} = -\bar{\epsilon} \cdot (\bar{\mathbf{R}} \cdot \hat{k}_g) \cdot \bar{\epsilon} \bar{E}_{sc}, \quad (19)$$

where $\bar{\mathbf{R}}$ is the electro-optic tensor of the crystal. Equation (19) ignores any contribution of $\Delta \bar{\epsilon}$ from electrons in the conduction band, i.e., the free-electron grating.²⁻⁴ Because this transient grating disappears in the time between each laser pulse, at the intensities used in our calculations the free-carrier grating will be negligible compared with the steady-state photorefractive grating, which accumulates over many laser pulses. For example, even with a pulse energy as large as 6 mJ/cm², the peak diffraction efficiency of just the transient free-carrier grating in BaTiO₃ is only 10⁻⁴,³ which is 200 times smaller than the steady-state diffraction efficiency with cw beams in the same geometry. Because the diffraction efficiency from a free-carrier grating depends quadratically on the fluence of the writing pulses,³ with a cw mode-locked laser having a fluence of microjoules per square centimeter, the diffraction efficiency from the free-carrier grating will be on the order of 10⁻⁹, which can certainly be ignored. Note that any contribution to $\bar{\epsilon}$ from an absorption grating¹⁶⁻¹⁹ can be included in our coupled-wave equations by changing the overall two-beam-coupling gain coefficient.

Substituting Eqs. (8) and (19) into the coupled-wave equations (14) yields

$$\left(\frac{\partial}{\partial z} + \frac{1}{v} \frac{\partial}{\partial t}\right) E_1(z, t) = \eta_{12} \frac{G(z, \tau_d)}{I_0} E_2(z, t), \quad (20a)$$

$$\left(\frac{\partial}{\partial z} + \frac{1}{v} \frac{\partial}{\partial t}\right) E_2(z, t) = -\eta_{21} \frac{G^*(z, \tau_d)}{I_0} E_1(z, t), \quad (20b)$$

where, with plane waves incident upon the crystal, the field correlation function G defined in Eq. (5) is now permitted to vary only along the z direction. In Eqs. (20a) and (20b) the coupling constants η_{ij} are

$$\eta_{12} = \frac{\omega}{4n_1 c \cos \theta} \frac{b}{a} [\hat{e}_1^* \cdot \bar{\epsilon} \cdot (\bar{\mathbf{R}} \cdot \hat{k}_g) \cdot \bar{\epsilon} \cdot \hat{e}_2], \quad (21a)$$

$$\eta_{21}^* = \frac{\omega}{4n_2 c \cos \theta} \frac{b^*}{a^*} [\hat{e}_2^* \cdot (\hat{E}_1 \cdot (\hat{R} \cdot \hat{k}_2) \cdot \hat{E}_1)^* \cdot \hat{e}_1]. \quad (21b)$$

We combine Eqs. (20), perform an ensemble average over many pulses, and average over the time T between optical pulses:

$$\frac{\partial \langle |\bar{E}_1(z, t)|^2 \rangle}{\partial z} = +2 \operatorname{Re}(\eta_{12}) \frac{|G(z, \tau_d)|^2}{I_0}, \quad (22a)$$

$$\frac{\partial \langle |\bar{E}_2(z, t)|^2 \rangle}{\partial z} = -2 \operatorname{Re}(\eta_{21}) \frac{|G(z, \tau_d)|^2}{I_0}, \quad (22b)$$

$$\frac{\partial G(z, \tau_d)}{\partial z} = \frac{G(z, \tau_d)}{I_0} (\eta_{12} \langle |\bar{E}_2|^2 \rangle - \eta_{21} \langle |\bar{E}_1|^2 \rangle). \quad (22c)$$

In deriving Eqs. (22) we eliminate the time derivatives by using the fact that

$$\left\langle \frac{\partial}{\partial t} F(z, t) \right\rangle = 0 \quad (23)$$

for any function F that has a period T .

If the time-averaged intensity of beam 1 is much less than that of beam 2, ($\langle |\bar{E}_1|^2 \rangle \ll \langle |\bar{E}_2|^2 \rangle$), then the intensity of the strong beam remains constant over the interaction length ($\langle |\bar{E}_2|^2 \rangle \cong I_0$), and the above equations have the simple solutions:

$$G(z, \tau_d) = G(0, \tau_d) \exp(\eta_{12} z), \quad (24)$$

$$\langle |\bar{E}_1(z, t)|^2 \rangle - \langle |\bar{E}_1(0, t)|^2 \rangle = \frac{|G(0, \tau_d)|^2 \exp[(g_{12} z) - 1]}{I_0}, \quad (25)$$

where the gain coefficient g_{12} is defined as

$$g_{12} \equiv 2 \operatorname{Re}(\eta_{12}). \quad (26)$$

Equation (25) states that the average intensity gain of the weak beam is proportional to the magnitude squared of the correlation function of the two incident beams. One factor of the correlation function appears because the two beams must first interfere to create the refractive-index grating; the second factor appears because each beam, after diffraction off the grating, interferes with the transmitted fraction of the other beam. Our result is an interesting contrast to that of Trebino *et al.*,¹² who analyzed the interaction of two beams in a rapidly responding absorptive medium.²⁰⁻²⁴ In that case the grating was newly formed by each laser pulse and decayed to zero between pulses. Consequently the average intensity of their diffracted beam was proportional to the fourth-order correlation function of the two interacting beams. In contrast, in our case the grating in the photorefractive crystal is formed by a large number of pulses and reaches a steady state. The early pulses create the grating; the later pulses diffract off the grating. Consequently, the intensity of the transmitted beam is proportional to the product of two second-order coherence functions and not to the fourth-order coherence function.

Equation (25) also shows that the average intensity of the weak beam grows at a rate determined by the electric-field correlation function $G(0, \tau_d)$ evaluated at the entrance face of the crystal, even though the temporal profiles of the two beams can change dramatically during

propagation, as we show below. It is convenient to separate the incident, deterministic optical-field envelopes $A_i(0, t)$ into a real amplitude E_{i0} and a normalized complex temporal profile $\bar{J}_i(t)$ [so that the peak value of $\bar{J}_i(t)$ is unity]:

$$A_i(0, t) = E_{i0} \bar{J}_i(t), \quad i = 1, 2. \quad (27)$$

This permits us to define the normalized field correlation function $\Gamma(\tau_d)$:

$$\Gamma(\tau_d) \equiv \frac{\langle \bar{J}_1(t) \bar{J}_2^*(t - \tau_d) \rangle}{[\langle \bar{J}_1(t)^2 \rangle \langle \bar{J}_2(t)^2 \rangle]^{1/2}} \gamma^2(\tau_d). \quad (28)$$

Then substitution into Eq. (25) yields

$$\frac{\langle |\bar{E}_1(z, t)|^2 \rangle - \langle |\bar{E}_1(0, t)|^2 \rangle}{\langle |\bar{E}_1(0, t)|^2 \rangle} = [\exp(g_{12} z) - 1] |\Gamma(\tau_d)|^2. \quad (29)$$

Equation (29) is the central result of our theory; it shows that after the weak beam has traversed a distance z in the crystal, its intensity gain depends on the magnitude squared of the normalized electric-field correlation function $\Gamma(\tau_d)$. For a given time delay τ_d , the function $\Gamma(\tau_d)$ is a measure of the fringe visibility of the interfering optical beams. Note that, for the case of cw light beams having infinite coherence time, $|\Gamma(\tau_d)|$ becomes unity, and the intensity of the weak wave grows exponentially with distance, as expected¹:

$$\langle |\bar{E}_1(z, t)|^2 \rangle = \langle |\bar{E}_1(0, t)|^2 \rangle \exp(g_{12} z). \quad (30)$$

5. MEASURING COHERENCE OF LIGHT PULSE

Now we show how a slow photorefractive crystal can be used to measure the autocorrelation of a fast laser pulse, as experimentally demonstrated by Johnson *et al.*⁵⁻⁷ and by Dominic *et al.*⁸

Let the incident laser beam be split into two beams and recombined in a photorefractive crystal, with a relative time delay τ_d between the two beams. Measure the coupling gain [defined by Eq. (29)] as a function of τ_d . According to Eq. (29), the resulting plot will be proportional to the square of the electric-field autocorrelation of the incoming laser pulses.

As an example, consider transform-limited laser pulses whose intensity profiles are Gaussian in time with a FWHM of τ_p . A plot of the measured intensity-coupling gain versus τ_d for these pulses will be a Gaussian curve with a FWHM of $2\tau_p$.

One can also consider the case of a cw beam with a limited coherence length, for example, a beam with a Gaussian power spectrum (and therefore a Gaussian coherence function, from the Wiener-Khinchin theorem):

$$\gamma^{(2)}(\tau_d) = \exp[-(\tau_d^2/\tau_c^2) \ln 2], \quad (31)$$

where τ_c is the average phase coherence time. In that case the plot of beam-coupling gain versus τ_d will trace out a Gaussian with a FWHM of $2\tau_c$.

Finally, we consider the more general case in which the light is pulsed and not transform limited. The electric-field envelope of the optical wave is

$$E(0, t) = E_0 \exp[i\varphi(t)] \exp[-2(t^2/\tau_p^2) \ln 2], \quad (32)$$

where the phase $\varphi(t)$ of the wave may be varying randomly with time. For this pulse Eq. (28) gives a coherence function $\Gamma(\tau_d)$:

$$\Gamma(\tau_d) = \exp\left[-\tau_d^2 \left(\frac{1}{\tau_p^2} + \frac{1}{\tau_s^2}\right) \ln 2\right], \quad (33)$$

where, in analogy with the cw case, we assume that the phase correlation is also Gaussian, so that the ensemble average of the correlation of the phase functions [as described in Eq. (7)] is

$$\gamma^2(\tau_d) = \exp[-(\tau_d^2/\tau_s^2) \ln 2], \quad (34)$$

where τ_s is the average phase coherence time. For this case of non-transform-limited pulses the measured gain will be a Gaussian function of the relative time delay τ_d with a FWHM²⁵ of

$$\text{FWHM} = \frac{2\tau_p\tau_s}{(\tau_p^2 + \tau_s^2)^{1/2}}. \quad (35)$$

6. PULSE SHAPING

The photorefractive grating not only alters the intensity of each beam but also alters the temporal shape of the pulses as they traverse the crystal. These pulse-shape changes are not limited by the response time of the crystal.

Consider the case in which two optical beams have already built up a steady-state grating in the crystal. Each beam diffracts off this grating and interferes with the other beam, which drastically alters the temporal pulse shapes of both beams, as shown in Fig. 3.

To describe pulse shaping by photorefractive two-beam coupling quantitatively, we use a Fourier representation of the optical-pulse envelopes E_1 and E_2 :

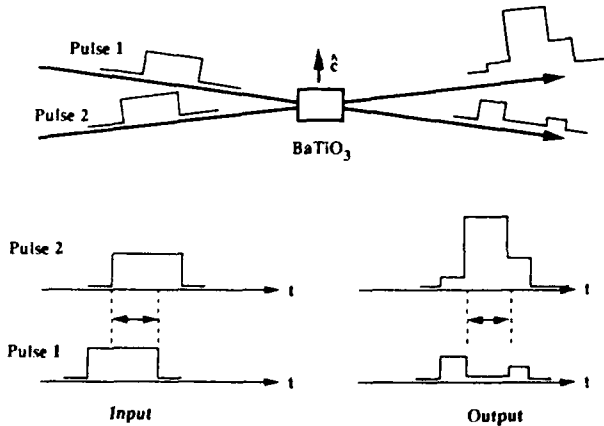


Fig. 3. Schematic illustrating pulse shaping by two-beam coupling in a photorefractive crystal. The square temporal profiles of the two incident pulses are altered after coupling in the crystal. [A steady-state grating has already been built up in the crystal, and each new light pulse barely perturbs this grating (see Figs. 1 and 2)]. Note that when the two pulses overlap in time the transmitted field of pulse 2 constructively interferes with the diffracted field of pulse 1, while the transmitted field of pulse 1 destructively interferes with the diffracted field of pulse 2. When the two pulses do not overlap, there is no interference.

$$E_{1,2}(z, t) = \frac{1}{2\pi} \int_{-\infty}^{\infty} E_{1,2}(z, \omega) e^{-i\omega t} d\omega. \quad (36)$$

In the frequency domain the coupled-wave equations (20) become

$$\frac{\partial F_1(z, \omega)}{\partial z} = +\eta_{12} \frac{G(z, \tau_d)}{I_0} F_2(z, \omega), \quad (37a)$$

$$\frac{\partial F_2(z, \omega)}{\partial z} = -\eta_{21}^* \frac{G^*(z, \tau_d)}{I_0} F_1(z, \omega), \quad (37b)$$

where for convenience we have defined

$$F_1(z, \omega) \equiv \exp\left(-\frac{i\omega z}{v}\right) E_1(z, \omega), \quad (38a)$$

$$F_2(z, \omega) \equiv \exp\left(-\frac{i\omega z}{v}\right) E_2(z, \omega). \quad (38b)$$

Equations (37a) and (37b) are solved using Eq. (24) and the boundary conditions

$$F_1(0, \omega) = E_1^0, \quad (39a)$$

$$F_2(0, \omega) = E_2^0, \quad (39b)$$

$$\left. \frac{\partial F_1(z, \omega)}{\partial z} \right|_{z=0} = +\eta_{12} \frac{G(0, \tau_d)}{I_0} E_2^0, \quad (39c)$$

$$\left. \frac{\partial F_2(z, \omega)}{\partial z} \right|_{z=0} = -\eta_{21}^* \frac{G^*(0, \tau_d)}{I_0} E_1^0 \quad (39d)$$

and then transforming the solutions $F_1(z, \omega)$ and $F_2(z, \omega)$ back into the time domain. The resulting solution for the electric-field envelope of each pulse as it propagates a distance z through the crystal is then

$$E_1(z, t) = E_1\left(0, t - \frac{z}{v}\right) \cos[\beta(z, \tau_d)] + \frac{\Gamma(\tau_d)}{|\Gamma(\tau_d)|} E_2\left(0, t - \frac{z}{v}\right) \sin[\beta(z, \tau_d)], \quad (40a)$$

$$E_2(z, t) = E_2\left(0, t - \frac{z}{v}\right) \cos[\beta(z, \tau_d)] - \frac{\Gamma^*(\tau_d)}{|\Gamma(\tau_d)|} E_1\left(0, t - \frac{z}{v}\right) \sin[\beta(z, \tau_d)], \quad (40b)$$

where the function $\beta(z, \tau_d)$ is defined as

$$\begin{aligned} \beta(z, \tau_d) &\equiv \frac{G(0, \tau_d)}{I_0} (e^{\eta z} - 1) \\ &= \left[\frac{\langle |E_1(0, t)|^2 \rangle}{\langle |E_2(0, t)|^2 \rangle} \right]^{1/2} \Gamma(\tau_d) (e^{\eta z} - 1). \end{aligned} \quad (41)$$

In Eqs. (40) we have assumed that the time-averaged intensity of beam 1 is much less than that of beam 2: i.e., $\langle |E_1|^2 \rangle \ll \langle |E_2|^2 \rangle$. For simplicity we have also assumed that both of the coupling constants η_{12} and η_{21} are real and equal, so that $\eta = \eta_{12} = \eta_{21}^*$. $\Gamma(\tau_d)$ is the normalized field correlation of beams 1 and 2, as defined in Eq. (28). Beam 1 will either gain or lose energy during its propagation through the crystal according to whether the sign of η is positive or negative.

Equations (40) show that $E_1(z, t)$ is a weighted sum of the input fields $E_1[0, t - (z/v)]$ and $E_2[0, t - (z/v)]$ at the entrance face of the crystal, with a similar expression for beam 2. The relative weights in the sum depend on the correlation between the two input fields, their relative time delay, and the ratio of their average intensity. To confirm Eqs. (40) we used Eq. (40a) to calculate the time-averaged intensity of the weak beam at an arbitrary position z , and we obtained the same result as with Eq. (25).

As an example of how two-beam coupling can dramatically alter the shape of an optical pulse, consider a train of short pulses (E_2) and a train of somewhat longer pulses (E_1) incident upon the crystal. The short and the long pulses are assumed to have the same spectral width. Assume that the short pulse is transform limited and Gaussian in time and that the long pulse is also Gaussian in time but is chirped. Let these two pulse trains interfere in a photorefractive crystal. Orient the c axis of the crystal so that the longer pulse loses energy as it propagates through the crystal (i.e., make the coupling constant

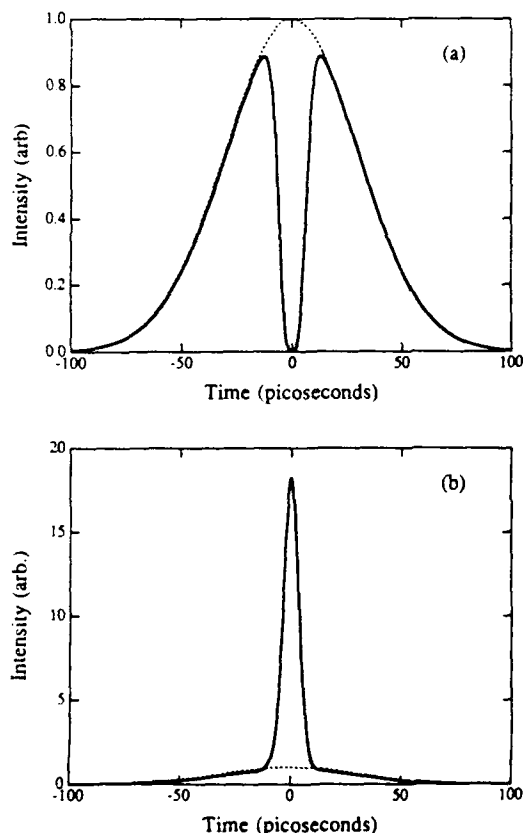


Fig. 4. Pulse shaping by using Gaussian pulses with the same spectral width. The peaks of both beams reach the entrance face of the crystal at the same time ($\tau_d = 0$), but the duration of beam 1 is 10 times greater than that of beam 2. (a) The temporal profile of beam 1 before (dotted curve) and after (solid curve) the photorefractive crystal. Note that beam 2 couples energy out of beam 1. We assume an incident average intensity ratio of $I_2/I_1 = 100$ and a coupling strength $\eta L = -1.23$. (b) The temporal profile of beam 1 before (dotted curve) and after (solid curve) coupling in the crystal. Here we reverse the direction of energy coupling in the crystal, so that beam 2 couples energy into beam 1. We use an incident average intensity ratio of $I_2/I_1 = 100$ and a coupling strength $\eta L = +1.23$.

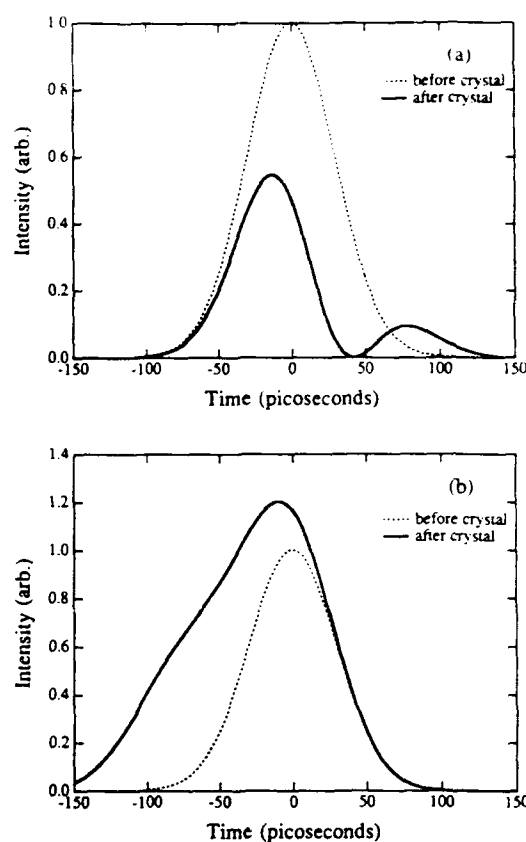


Fig. 5. Pulse shaping in a photorefractive crystal by using equal-width, transform-limited Gaussian pulses (FWHM intensity = 70 psec). The curves show the temporal envelope of incident beam 1 before the crystal (dotted curves) and after the crystal (solid curves). (a) Beam 1 arrives 50 psec before beam 2. The coupling strength is set at $\eta L = -2$ (so that beam 1 loses energy), and the average intensity ratio is set at $I_2/I_1 = 10$. (b) Beam 1 arrives 85 psec before beam 2. The coupling strength is set at $\eta L = +1.5$ (so that beam 1 gains energy), and the average intensity ratio is set at $I_2/I_1 = 100$.

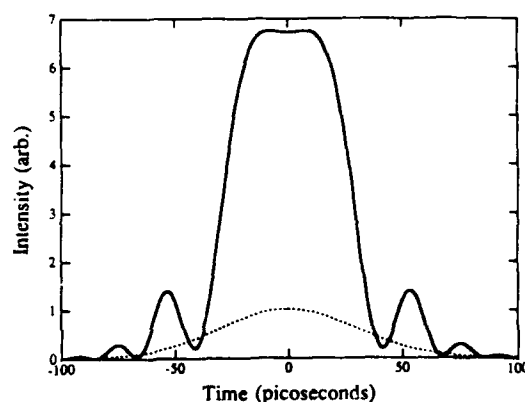


Fig. 6. Pulse shaping in a photorefractive crystal by using Gaussian pulses with the same temporal width (FWHM intensity 70 psec). The temporal envelope of the incident beam (1) is shown before the crystal (dotted curve) and after the crystal (solid curve). Here beam 1 is transform limited, but beam 2 is chirped and has a spectral width 8 times that of beam 1. The time delay between the two beams is zero, and the coupling strength is $\eta L = 1.5$ (beam 1 gains energy).

$\eta < 0$). For these conditions Fig. 4(a) shows that the long pulse will have a deep hole carved out of its center: a dark pulse. Such a pulse may prove useful for the experiments with dark pulses.^{26,27} (See Appendix A for further discussion of this calculation.)

If we reorient the crystal so that the longer pulse gains energy during propagation ($\eta > 0$), then it will emerge with a sharp spike, as shown in Fig. 4(b). Beam shaping will also occur if the two pulses have similar temporal envelopes, as shown in Figs. 5 and 6. In Fig. 5 we chose the two beams to be identical, transform-limited Gaussians. In Fig. 6 we chose a transform-limited weak beam and a strong beam that is linearly chirped and with a somewhat wider spectral width. Note the strong ringing caused by the temporal overlap of the two pulses.

7. CONCLUSION

In summary, we have derived an analytical expression for the two-beam-coupling gain of a photorefractive crystal when it is illuminated by two light beams that contain infinite trains of amplitude-stabilized pulses. We demonstrated that the photorefractive space-charge field reaches a quasi-steady-state value proportional to the local fringe visibility in the crystal. We find that the time-average intensity gain of each beam is proportional to the magnitude squared of the electric-field correlation of the interfering beams at the entrance face of the crystal. Consequently, the correlation between two optical pulse trains can be measured by performing two-beam coupling experiments in a photorefractive crystal. We have also shown that optical pulses will be shaped by their coupling in a photorefractive crystal, and we have derived analytic expressions describing how each pulse transforms during propagation through the crystal.

APPENDIX A: PULSE-SHAPE CALCULATIONS

We can use Eqs. (40a) and (40b) to calculate how the intensities of two interacting pulses will change with time because of beam coupling. In general, we must first choose the shapes of the incident pulses before the crystal and then calculate the normalized electric-field correlation function. In the example shown in Fig. 4, we chose one pulse to be transform limited and Gaussian in time and the other pulse also to be Gaussian in time, with the same spectral width, but chirped. We might generate such pulses by splitting a transform-limited Gaussian pulse into two pulses and sending one of the pulses through a Treacy grating pair.²⁸ This pulse will be chirped and temporally stretched. If the duration τ_{p1} of the stretched pulse (1) is q times the duration τ_{p2} of the unstretched pulse $\tau_{p1} = q\tau_{p2}$, then the normalized complex temporal amplitudes of these pulses can be expressed as

$$\mathcal{T}_1(t) = \exp\left[\frac{-2 \ln 2(1 + i\sqrt{q^2 - 1})t^2}{\tau_{p1}^2}\right], \quad (42a)$$

$$\mathcal{T}_2(t - \tau_d) = \exp\left[-2\frac{(t - \tau_d)^2}{\tau_{p2}^2} \ln 2 + i\omega_0\tau_d\right], \quad (42b)$$

where τ_{p1} is the FWHM intensity width of the long pulse and ϕ_0 is a constant phase. Both pulses are Gaussian with the same spectral width $\Delta\omega = (4/\tau_{p2}) \ln 2$, as can be shown by taking their Fourier transforms. Because the original pulse is assumed to be transform limited, the coherence function $\gamma^{(2)}$ is unity. The corresponding correlation function, calculated using Eq. (25), becomes

$$\Gamma(\tau_d) = \frac{\sqrt{2} \exp\left[-\frac{i}{2} \tan^{-1}\left(\frac{\sqrt{q^2 - 1}}{q^2 + 1}\right) - i\omega_0\tau_d\right]}{(q^2 + 3)^{1/4}} \times \exp\left[-\frac{2 \ln 2}{q^2 + 3} \left(2 + i\sqrt{q^2 - 1}\right) \frac{\tau_d^2}{\tau_{p2}^2}\right]. \quad (43)$$

If the average intensity of beam 1 is much smaller than that of beam 2, e.g., $\langle \mathcal{E}_1^2 \rangle \ll \langle \mathcal{E}_2^2 \rangle$, then substitution into Eq. (40a) yields

$$E_1(z, t) = E_{10} \{ \mathcal{T}_1[t - (z/v)] + \sqrt{q} \Gamma(\tau_d) (e^{i\eta} - 1) \mathcal{T}_2[t - (z/v) - \tau_d] \}. \quad (44)$$

Substituting Eqs. (42) and (43) into Eq. (44), we can calculate the intensity of pulse 1 as a function of time and distance in the crystal. The results are shown in Figs. 4 and 5. [In Fig. 5 both beams are transform limited, so that $q = 1$ in Eqs. (41)–(44).]

In Fig. 6 we consider pulses with the same temporal width but different spectral widths and with a linear chirp on the spectrally wider beam. If the spectral width of pulse 2 is m times that of pulse 1, then the two pulses can be expressed as

$$\mathcal{T}_1(t) = \exp\left(-2 \ln 2 \frac{t^2}{\tau_p^2}\right), \quad (45)$$

$$\mathcal{T}_2(t - \tau_d) = \exp\left[-2 \ln 2 \times (1 + i\sqrt{m^2 - 1}) \frac{(t - \tau_d)^2}{\tau_p^2} + i\omega_0\tau_d\right]. \quad (46)$$

Pulse 1 is transform limited, and the coherence function $\gamma^{(2)}$ is unity. The corresponding correlation function, calculated using Eq. (28), is

$$\Gamma(\tau_d) = \frac{\sqrt{2} \exp\left[\frac{i}{2} \tan^{-1}\left(\frac{\sqrt{m^2 - 1}}{2}\right) - i\omega_0\tau_d\right]}{(m^2 + 3)^{1/4}} \times \exp\left[-\frac{2 \ln 2}{m^2 + 3} (1 + m^2 + i\sqrt{m^2 - 1}) \frac{\tau_d^2}{\tau_p^2}\right]. \quad (47)$$

Substituting Eqs. (45)–(47) into Eq. (44) and setting $q = 1$ (the two pulses are given the same temporal width), we obtain Fig. 6.

ACKNOWLEDGMENTS

We thank R. Pierce, J.-M. C. Jonathan, D. Mahgerefteh, and C. M. Caves for fruitful discussions. This research is supported by the Joint Services Electronics Program and contract F49620-88-C-9905 of the U.S. Air Force Office of Scientific Research. V. Dominic gratefully acknowledges fellowship support from the National Science Foundation and the Joint Services Electronics Program.

REFERENCES AND NOTES

1. L. Solymar, "Theory of volume holographic formation in photorefractive crystals," in *Electro-Optic and Photorefractive Materials*, P. Günter, ed. (Springer-Verlag, Berlin, 1987), pp. 223-245.
2. A. L. Smirl, G. C. Valley, K. M. Bohnert, and T. F. Boggess, Jr., "Picosecond photorefractive and free-carrier transient energy transfer in GaAs at 1 μm ," *IEEE J. Quantum Electron.* **24**, 289-302 (1988).
3. A. L. Smirl, K. Bohnert, G. C. Valley, R. A. Mullen, and T. F. Boggess, "Formation, decay, and erasure of photorefractive gratings written in barium titanate by picosecond pulses," *J. Opt. Soc. Am. B* **6**, 606-615 (1989).
4. A. L. Smirl, G. C. Valley, R. A. Mullen, K. Bohnert, C. D. Mire, and T. F. Boggess, "Picosecond photorefractive effect in BaTiO₃," *Opt. Lett.* **12**, 501-503 (1987).
5. A. M. Johnson, A. M. Glass, W. M. Simpson, R. B. Bylisma, and D. H. Olson, "Microwatt picosecond pulse autocorrelator using photorefractive GaAs:Cr," in *OSA Annual Meeting*, Vol. 11 of 1988 Optical Society of America Technical Digest Series (Optical Society of America, Washington, D.C., 1988), p. 128.
6. A. M. Johnson, A. M. Glass, W. M. Simpson, and D. H. Olson, "Infrared picosecond pulse diagnostics using photorefractive beam coupling," in *Conference on Lasers and Electro-Optics*, Vol. II of 1989 Optical Society of America Technical Digest Series (Optical Society of America, Washington, D.C., 1989), p. 226.
7. A. M. Johnson, W. M. Simpson, A. M. Glass, M. B. Klein, D. Rytz, and R. Trebino, "Infrared picosecond pulse correlation measurements using photorefractive beam coupling and harmonic generation in KNbO₃ and BaTiO₃," in *OSA Annual Meeting*, Vol. 18 of 1989 Optical Society of America Technical Digest Series (Optical Society of America, Washington, D.C., 1989), p. 53.
8. V. Dominic, X. S. Yao, R. M. Pierce, and J. Feinberg, "Measuring the coherence length of mode-locked laser pulses in real time," *Appl. Phys. Lett.* **53**, 521-523 (1990).
9. F. P. Strohkendl, M. C. Jonathan, and R. W. Hellwarth, "Hole-electron competition in photorefractive gratings," *Opt. Lett.* **11**, 312-314 (1986).
10. Here we use the fact that the ensemble average of the derivative of a function equals the derivative of the ensemble average of the function. See, for example, A. Papoulis, *Probability, Random Variables, and Stochastic Process* (McGraw-Hill, New York, 1965), Chap. 9, pp. 314-318.
11. J. Feinberg, "Optical phase conjugation in photorefractive materials," in *Optical Phase Conjugation*, R. Fisher, ed. (Academic, New York, 1983), pp. 417-443.
12. R. Trebino, E. K. Gustafson, and A. E. Siegman, "Fourth-order partial-coherence effects in the formation of integrated-intensity gratings with pulsed light sources," *J. Opt. Soc. Am. B* **3**, 1295-1304 (1986).
13. J. W. Goodman, *Statistical Optics* (Wiley, New York, 1985), Chap. 3, pp. 63-68.
14. For example, if both of the optical fields are derived from the same mode-locked laser, then Eq. (6) will hold as long as the laser exhibits no long-term changes in the statistics of its phase fluctuations during an experiment. However, if the alignment of the mirrors of the laser should drift with time, for example, then the laser's pulse statistics might change, and Eq. (6) would no longer follow from Eq. (5).
15. The coupling coefficients η_{12} and η_{21} in the coupled-wave equations (21a) and (21b) will be slightly different if the term $\nabla(\nabla \cdot \hat{\epsilon})$ is retained. Namely, $\cos \theta$ will be replaced by $\cos \theta - \text{Re}[(\hat{\epsilon}_1 \cdot \hat{\epsilon}_2)(\hat{s}_1 \cdot \hat{s}_2)]$ with $i = 1$ in Eq. (21a) and $i = 2$ in Eq. (21b), where \hat{s}_1 and \hat{s}_2 are the unit vectors along \mathbf{k}_1 and \mathbf{k}_2 , respectively, $\hat{\epsilon}$ is a unit vector in the z direction, and we assume that the optical field amplitudes vary only along the z direction.
16. A. V. Alekseev-Popov, A. V. Knyaz'kov, and A. S. Saikin, "Recording volume amplitude-phase holograms in a lead-lanthanum zirconate-titanate ceramic," *Sov. Tech. Phys. Lett.* **9**, 475-477 (1983).
17. K. Walsh, T. J. Hall, and R. E. Burge, "Influence of polarization state and absorption gratings on photorefractive two-wave mixing in GaAs," *Opt. Lett.* **12**, 1026-1028 (1987).
18. Y. Lee, "Studies of the photorefractive effect in barium titanate: higher-order spatial harmonics and two-beam energy coupling," (University of Southern California, Los Angeles, Calif., 1989).
19. R. M. Pierce, R. S. Cudney, G. D. Bacher, and J. Feinberg, "Measuring photorefractive trap density without the electro-optic effect," *Opt. Lett.* **17**, 411-416 (1990).
20. H. J. Eichler, U. Klein, and D. Langhans, "Coherence time measurement of picosecond pulses by light-induced grating method," *Appl. Phys.* **21**, 215-219 (1980).
21. Z. Vardeny and J. Tauc, "Picosecond coherence coupling in the pump and probe technique," *Opt. Commun.* **39**, 396-400 (1981).
22. R. Baltrameynas, Yu. Vaitkus, R. Danelyus, M. Pytrauskas, and A. Piskarskas, "Applications of dynamic holography in determination of coherence times of single picosecond light pulses," *Sov. J. Quantum Electron.* **12**, 1252-1254 (1982).
23. S. L. Palfrey and T. F. Heinz, "Coherent interactions in pump-probe absorption measurements: the effect of phase gratings," *J. Opt. Soc. Am. B* **2**, 674-678 (1985).
24. W. L. Nighan, Jr., T. Gong, L. Liou, and P. M. Fauchet, "Self-diffraction: a new method for characterization of ultrashort laser pulses," *Opt. Commun.* **69**, 339-344 (1989).
25. In Ref. 8 we defined the coherence time of the pulse as one-half of the FWHM of the field correlation function. This definition leads to a coherence time $\tau_c = (2 \ln 2)/(\pi \Delta\nu)$ for an optical field having a Gaussian power spectral density with a FWHM of $\Delta\nu$ (Hz). With this definition the coherence time τ_c equals the pulse duration τ_p for a transform-limited pulse. A more common definition¹² of τ_c for cw beams is $\tau_c = \int_{-\infty}^{\infty} |\Gamma(\tau_d)|^2 d\tau_d$. In this case $\tau_c = [(2 \ln 2)/\pi]^2 1/(\Delta\nu)$ for an optical field having a Gaussian spectrum with a FWHM of $\Delta\nu$ (Hz).
26. D. Krokul, N. J. Halas, G. Giuliani, and D. Grischowsky, "Dark-pulse propagation in optical fibers," *Phys. Rev. Lett.* **60**, 29-32 (1988).
27. A. M. Weiner, J. P. Heritage, R. J. Hawkins, R. N. Thurston, E. M. Kirschner, D. E. Leaird, and W. J. Tomlinson, "Experimental observation of the fundamental dark soliton in optical fibers," *Phys. Rev. Lett.* **61**, 2445-2448 (1988).
28. E. D. Treacy, "Optical pulse compression with diffraction gratings," *IEEE J. Quantum Electron.* **QE-5**, 454-458 (1969).

Explanation of the Apparent Sublinear Photoconductivity of Photorefractive Barium Titanate

Daniel Mahgerefteh and Jack Feinberg

Department of Physics, University of Southern California, Los Angeles, California 90089-0484

(Received 28 December 1989)

We explain the apparent sublinear intensity dependence of photoconductivity in barium titanate. In our model shallow acceptors act as a reservoir for charges optically excited from the donors. As this reservoir fills, the fraction of occupied donors changes appreciably, changing the lifetime of the free carriers. We identify two types of barium-titanate crystals having quite different photorefractive characteristics depending on their relative density of donors and acceptors, and we find that the depth of the shallow acceptor level is $\sim 0.4 \pm 0.1$ eV in both types of crystals.

PACS numbers: 72.20.Jv, 42.70.Gi, 72.40.+w

The photoconductivity of BaTiO₃ does not scale linearly with light intensity. In 1977, Fridkin and Popov measured an $I^{0.5}$ dependence using electrodes attached to the crystal.¹ In 1984, Ducharme and Feinberg² found an $I^{0.68}$ dependence of the speed-of-light-induced charge migration (which is proportional to the photoconductivity). In most photorefractive materials doubling the incident optical intensity doubles the charge migration rate, but not so in BaTiO₃. Here we show that the apparent sublinear photoconductivity of BaTiO₃ is caused by shallow acceptors, and that the empirical I^x functional dependence, while producing a reasonable fit to the data, is not the fundamentally correct functional dependence.

We identify two types of barium-titanate crystals which we call type *A* and type *B*. A type-*A* crystal has an erasure speed that increases almost linearly with light intensity (and can be approximated as speed $\propto I^{x \sim 0.9}$), a steady-state photorefractive grating strength that varies very little with intensity, and a small dark conductivity. A type-*B* crystal has an erasure speed that increases decidedly less than linearly with light intensity (and can be approximated as speed $\propto I^{x \sim 0.6}$), a steady-state photorefractive grating strength with a marked intensity dependence, and a large dark conductivity. We show below that a simple two-level model of deep donors and shallow acceptors explains the very different behaviors of these two types of BaTiO₃ crystals.

We postulate that in type-*A* crystals the density of donors greatly exceeds that of acceptors ($N_D \gg N_A$), while in type-*B* crystals the density of donors is comparable or slightly less than the density of acceptors ($N_D \leq N_A$). Previous models of the photorefractive effect assumed that either the donors or the acceptors (but not both) took part in charge transport,^{3,4} or neglected thermal excitations,⁵ or invoked additional levels.^{6,7} In our model charges (assumed to be holes) in both the donors and the acceptors can be excited by light, and we also permit thermal excitation of holes from the acceptors into the valence band. We position the donors near the middle of the band gap of the crystal (which is ~ 3.1 eV for BaTiO₃) and the acceptors close to the top of the

valence band, so that at room temperature the only likely thermal excitation is from the acceptors. The Fermi level is located on the donor levels for $N_D > N_A$ and on the acceptor level for $N_D < N_A$. A key feature of this model is that holes optically excited from the donors can accumulate in the shallow acceptors, where they can be thermally reexcited. The equations describing the change in the populations of these levels are a two-level adaptation of those found in Ref. 7:

$$\frac{\partial N_D^+}{\partial t} = -s_D I N_D^+ + \gamma_D n (N_D - N_D^+), \quad (1)$$

$$\frac{\partial N_A^-}{\partial t} = (s_A I + \beta) (N_A - N_A^-) - \gamma_A n N_A^-, \quad (2)$$

$$\frac{\partial n}{\partial t} + \frac{\partial N_D^+}{\partial t} - \frac{\partial N_A^-}{\partial t} + \frac{1}{e} \nabla \cdot \mathbf{J} = 0, \quad (3)$$

$$\mathbf{J} = e \mu n \mathbf{E} - \mu k_B T \nabla n, \quad (4)$$

$$\nabla \cdot \mathbf{E} = (e/\epsilon) (n + N_D^+ - N_A^-), \quad (5)$$

where I is the total optical intensity, N_D^+ is the density of ionized donors, N_A^- is the density of full acceptors, n is the density of free holes, s_D and s_A are the light excitation cross sections from the donors and acceptors, γ_D and γ_A are the free-carrier recombination constants for donors and acceptors, β is the thermal excitation rate from the shallow acceptors, \mathbf{J} is the current density, \mathbf{E} is the total static electric field, μ and ϵ are the carrier mobility and dielectric constant of the crystal, respectively, along the direction of charge migration, e is the electric charge, and $k_B T$ is the thermal energy.

We solve these equations for light intensities $I < 10^7$ W/cm², where the generation rate of free carriers is small compared with the fast (10^{10} Hz) recombination rate to the traps.⁸ For this case, the density of free holes is small compared to the light-induced change in either the density of ionized donors or full acceptors,

$$n \ll |N_D^+ - (N_D^+)_{I=0}|, \quad n \ll |N_A^- - (N_A^-)_{I=0}|. \quad (6)$$

Note that because holes optically excited from the donors can accumulate in the acceptors, both N_D^+ and N_A^- can be appreciably changed by light, even though n

remains small.

Consider a photorefractive grating with wave vector $k = 4\pi(\sin\theta)/\lambda$ along the z direction. This grating is formed by two coherent writing beams with intensities I_1 and I_2 and wavelength λ in the crystal crossing at a full angle 2θ inside the crystal. Let an intense erasing beam (not coherent with the writing beams) simultaneously flood the crystal with a uniform intensity I_0 . This makes the total light intensity $I = (I_1 + I_2 + I_0)\text{Re}(1 + me^{-ikz})$, and the modulation of the grating $m \equiv 2(I_1 I_2)^{1/2}/(I_1$

$+ I_2 + I_0)$ much less than 1. If the writing beams are suddenly removed, the grating will begin to decay. We find that the energy density Φ needed to erase the grating to $1/e$ of its initial value is

$$\Phi = \frac{\epsilon}{e\mu f(k)} \frac{\gamma_D(N_D - N_{D0}^+)}{s_D N_{D0}^+}, \quad (7)$$

where N_{D0}^+ is the spatially uniform density of ionized donors. Solving Eqs. (1)–(3) to eliminate the intensity-dependent quantity N_{D0}^+ yields

$$\Phi = \frac{\Phi_0}{1 + \beta/s_A I_0} \left[\text{sgn}(N_A - N_D) + \left(1 + \frac{4s_D \gamma_A N_A N_D}{s_A \gamma_D (N_A - N_D)^2 (1 + \beta/s_A I_0)} \right)^{1/2} \right]^{-1}, \quad (8)$$

where

$$\Phi_0 \equiv \frac{2\epsilon}{e\mu f(k)} \frac{\gamma_A N_D}{s_A |N_A - N_D|}, \quad (9)$$

and $\text{sgn}(N_A - N_D) \equiv -1$ for type-A crystals, and $\text{sgn}(N_A - N_D) \equiv +1$ for type-B crystals.

For all type-B crystals that we studied the approximation

$$\frac{4s_D \gamma_A N_A N_D}{s_A \gamma_D (N_A - N_D)^2} \gg 1 + \frac{\beta}{s_A I_0} \quad (10)$$

holds, as long as the light-induced conductivity of the crystal exceeds its dark conductivity. In this case, Eq. (8) for a type-B crystal simplifies to

$$\Phi_B = \frac{\Phi_{0B}}{(1 + \beta/s_A I_0)^{1/2}}, \quad (11)$$

where

$$\Phi_{0B} \equiv \frac{\epsilon}{e\mu f(k)} \left(\frac{\gamma_A \gamma_D N_D}{s_A s_D N_A} \right)^{1/2}. \quad (12)$$

Figure 1 shows the calculated intensity dependence of

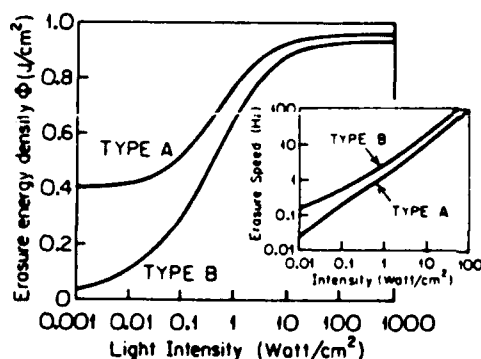


FIG. 1. Predicted dependence of Φ (the energy density required to erase a photorefractive grating to $1/e$ of its initial value) on light intensity for the two types of BaTiO_3 crystals. Inset: A log-log plot of the calculated erasure speed vs intensity showing the apparent I^{-1} behavior.

Φ , the energy density needed to erase a previously written grating to $1/e$ of its initial value. Note that at high intensity Φ becomes constant in both type-A and type-B crystals, which implies that the photoconductivity becomes linear at these high intensities. Also, at low intensities in type-A crystals the photoconductivity is linear with intensity I , while in type-B crystals it is proportional to \sqrt{I} . These features of the photoconductivity can be easily missed if the same information is displayed in the traditional log-log plot of speed versus intensity (as shown in the inset), where the curves appear to be straight lines of constant slope x ($0.5 < x < 1$), implying an oversimplistic I^x functional dependence for the photoconductivity.

To verify our two-level model we measured the light-induced erasure rate of photorefractive gratings as a function of the incident light intensity. Three as-grown BaTiO_3 samples (named Cat, Free, and Rob) were selected for their different characteristics. The Rob crystal is type A with a long dark storage time ($T_{\text{dark}} > 10^4$ sec at room temperature). Both the Cat and Free crystals are type B and have short dark storage times ($T_{\text{dark}} \sim 1$ sec at room temperature). The same Cat crystal was previously studied in Ref. 2; we repeated the measurements over a wider range of crystal temperature and light intensity. Two optical writing beams, of comparable intensity, intersected in the crystal at a full internal angle of $2\theta = 25^\circ$. After the writing beams had written a photorefractive grating to steady state, both writing beams were blocked and the grating was allowed to decay. An intense erasing beam flooded the crystal at all times, and thereby avoided large changes in the shallow trap population when the writing beams were turned off. The erasing intensity was 10 times the total writing intensity. All these optical beams were at 514.5 nm and polarized perpendicular to the c axis of the crystal. The crystal temperature was stabilized to $\pm 1^\circ$. The relative grating strength was measured by a weak, extraordinary polarized 632.8-nm laser beam incident at the Bragg angle.

Figure 2 is the plot of Φ vs I_0 in the Rob crystal (a

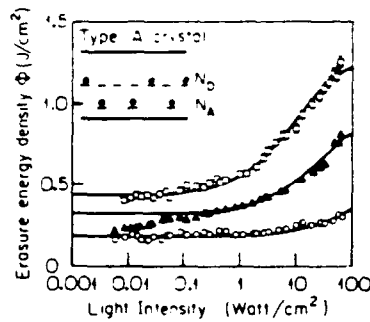


FIG. 2. Φ vs I_0 at various temperatures of the Rob crystal of BaTiO_3 , a type-A crystal: $T=25^\circ\text{C}$ (\square), $T=47^\circ\text{C}$ (\blacktriangle), $T=90^\circ\text{C}$ (\circ). Solid curves are simultaneous best fits by Eq. (8).

type-A crystal) for three temperatures. The solid curves are simultaneous least-squares fits of the data by Eq. (8) which contains three parameters: Φ_0 (which sets the amplitude), β/s_A (which determines the point of inflection), and $p_2 \equiv 4s_D\gamma_A N_A N_D / \gamma_D s_A (N_D - N_A)^2$. (From a simultaneous least-squares fit of all of the data we obtain $p_2 = 23$.) According to theory, β (the thermal excitation rate out of the shallow traps) increases with temperature T according to

$$\beta = \beta_0 e^{-E_T/k_B T}, \quad (13)$$

where E_T is the energy separation of the shallow trap level from the valence band, and β_0 is a constant. Fitting the values of β/s_A at the various temperatures by Eq. (13) we estimate the depth of the shallow trap levels in the Rob crystal to be $E_T \sim 0.36$ eV.

Figure 3 shows a semilogarithmic plot of Φ vs I_0 for the Cat crystal. Note that the function Φ increases with light intensity even at low intensities; this is caused by the light-induced change in the density of un-ionized donors. Comparison with Fig. 1 shows that the Cat crystal is a type-B sample with $N_D \leq N_A$. At high intensity Φ flattens, because the density of holes in the shallow acceptors (and the corresponding density of un-ionized donors) is beginning to saturate. Note that the data at higher crystal temperatures flatten at higher intensities, because it requires more light to saturate an acceptor that has a larger thermal excitation rate. The solid curves are least-squares fits by Eq. (11) using Φ_{0B} and β/s_A as the two fitting parameters.

Figure 4 shows a semilogarithmic plot of the parameter β/s_A as a function of the inverse thermal energy $1/k_B T$ for both the Cat and Free crystals (both type B). From the slope of these graphs and using Eq. (13), we obtain the depth of the shallow traps in the Cat crystal to be $E_{T\text{Cat}} = 0.5 \pm 0.15$ eV, and $E_{T\text{Free}} = 0.3 \pm 0.1$ eV in the Free crystal.

The depth of the shallow traps in type-B crystals can also be determined by measuring the rate of decay of photorefractive gratings in the dark as a function of the

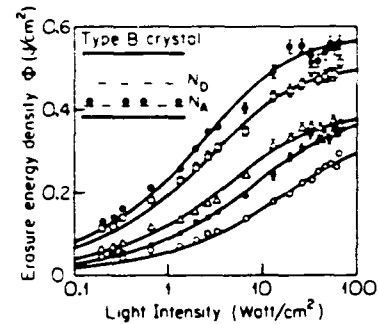


FIG. 3. Φ vs I_0 at various temperatures of the Cat crystal of BaTiO_3 , a type-B crystal: $T=17^\circ\text{C}$ (\bullet), $T=25^\circ\text{C}$ (\square), $T=35^\circ\text{C}$ (\triangle), $T=43^\circ\text{C}$ (\blacksquare), $T=52^\circ\text{C}$ (\circ). Solid curves are best fits by Eq. (11).

crystal temperature. If the total intensity is sufficiently low ($I \ll \beta/s_A$), the grating forms only on the shallow acceptors in type-B crystals, and will decay in the dark exponentially at a rate

$$\Gamma_{\text{dark}} = \frac{e\mu f(k)}{\epsilon} \frac{\beta_0}{\gamma_A N_D} e^{-E_T/k_B T}.$$

In order to obtain E_T , we first correct for the strong temperature dependence of the mobility μ by multiplying the dark-decay rate by Φ_{0B} at each temperature. A semilogarithmic plot of $\Gamma_{\text{dark}}\Phi_{0B}$ vs $1/k_B T$ yielded a straight line for the Cat and Free crystals with $E_T \sim 0.4$ eV in both cases, in good agreement with the values of E_T determined above.

We now understand why the dark conductivity is much smaller for a type-A crystal than for a type-B crystal. In a type-A crystal in the dark and in thermal equilibrium, the acceptors will be empty of holes and there will be negligible conduction in the dark. In contrast, in a type-B crystal there are always some holes in the acceptors available for thermal excitation, so the dark conductivity is relatively large.

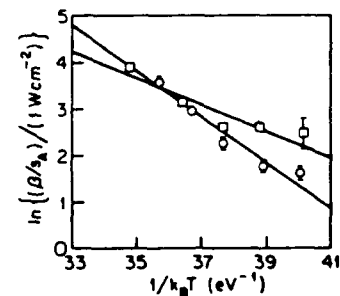


FIG. 4. Plot of the measured intensity needed to saturate the shallow traps (normalized to 1 W/cm^2) vs the inverse thermal energy for two type-B crystals. (a) Circles, Cat crystal. The slope of the line yields $E_T \sim 0.5 \pm 0.15$ eV. (b) Squares, Free crystal. The slope of the line yields $E_T \sim 0.3 \pm 0.1$ eV.

We also predict the intensity dependence of the space-charge field. In general, photorefractive gratings will form on both the donors and the acceptors. Equations (1)–(5) predict that the amplitude E_{sc} of the steady-state space-charge field $E_{sc}e^{-ikz}$ will vary strongly with intensity in type-*B* crystals but only weakly in type-*A* crystals. We obtain

$$E_{sc} = +im \frac{k_B T}{e} \eta(I) \frac{k}{1 + k^2 / (k_{D,donor}^2 + k_{D,acceptor}^2)}, \quad (14)$$

where

$$\eta(I) \equiv \frac{k_{D,donor}^2 + k_{D,acceptor}^2 / (1 + \beta/s_A I)}{k_{D,donor}^2 + k_{D,acceptor}^2}. \quad (15)$$

The function $\eta(I) \leq 1$ approaches unity at high intensity. The Debye screening wave vectors for the donors and acceptors are defined by

$$k_{D,donor}^2 \equiv \frac{e^2}{\epsilon k_B T} \frac{N_{D0}^+ (N_D - N_{D0}^+)}{N_D}, \quad (16)$$

and

$$k_{D,acceptor}^2 \equiv \frac{e^2}{\epsilon k_B T} \frac{N_{A0}^- (N_A - N_{A0}^-)}{N_A}. \quad (17)$$

Here N_{D0}^+ and N_{A0}^- are the spatially uniform densities of ionized donors and filled acceptors, respectively, both of which vary with light intensity.

For a type-*B* crystal operated in a regime where the light-induced photoconductivity exceeds the dark conductivity, Eq. (10) holds, and the function η in Eq. (15) becomes $\eta(I) = \frac{1}{2} [1 + 1/(1 + \beta/s_A I)]$. This causes E_{sc} to increase by a factor of 2 as the light intensity is increased from low intensities $I \ll \beta/s_A$ to high intensities $I \gg \beta/s_A$. For a type-*A* crystal, $\eta \sim 1$ for all intensities, so that E_{sc} should vary only weakly with intensity.

We confirmed the above by measuring the magnitude of the photorefractive space-charge field and found that, as predicted by theory, E_{sc} varied appreciably with optical intensity in type-*B* crystals but not in type-*A* crystals. For the Cat and Free crystals the space-charge field increased with increasing light intensity by a factor of

more than 2.3 over the intensity range $I = 0.1$ – 70 W/cm², consistent with their assignment as type-*B* crystals. In contrast, for the Rob crystal (a type-*A* crystal) the grating strength changed by only $\sim 20\%$ over the same intensity range for all temperatures studied.

Equation (8) also explains our cw and pulsed erasure data of Ref. 9. In those experiments we erased gratings with pulsed light beams of high peak intensity but low average intensity in two additional type-*A* crystals of BaTiO₃ (Swiss and Hop). Our theory predicts that in this case it takes the same amount of energy to erase a photorefractive grating by continuous illumination as by a train of light pulses having the same average intensity.

The critical parameter controlling whether a crystal is type *A* or type *B* is $\chi \equiv N_A N_D / (N_A - N_D)^2$, which varies rapidly near the compensation point $N_A = N_D$. This suggests that our as-grown BaTiO₃ crystals are nearly compensated, which explains why their photorefractive characteristics vary so much from one sample to the next.

This work was supported by Contracts No. F49620-88-C-0095 of the Air Force Office of Scientific Research and No. F49620-88-C-0067 of the Joint Services Electronics Program.

¹V. M. Fridkin and B. N. Popov, *Ferroelectrics* **21**, 611 (1978).

²S. Ducharme and J. Feinberg, *J. Appl. Phys.* **56**, 839 (1984).

³N. V. Kukhtarev, V. B. Markov, S. G. Odulov, M. S. Soskin, and V. L. Vinetskii, *Ferroelectrics* **22**, 949 (1979).

⁴J. Feinberg, D. Heiman, A. R. Tanguay, Jr., and R. W. Hellwarth, *J. Appl. Phys.* **51**, 1297 (1980); **52**, 537(E) (1981).

⁵G. C. Valley, *Appl. Opt.* **22**, 3160 (1983).

⁶L. Holtmann, *Phys. Status Solidi (a)* **113**, K89 (1989).

⁷A. L. Smirl, G. C. Valley, R. A. Mullen, K. Bohnert, C. D. Mire, and T. F. Boggess, *Opt. Lett.* **12**, 501 (1987).

⁸P. Tayebati, Ph.D. dissertation, University of Southern California, Los Angeles, 1989 (unpublished).

⁹D. Mahgerefteh and J. Feinberg, *Opt. Lett.* **13**, 1111 (1988).

Theory of the photorefractive effect for $\text{Bi}_{12}\text{SiO}_{20}$ and BaTiO_3 with shallow traps

Parviz Tayebati* and Daniel Mahgerefteh

Department of Physics, University of Southern California, University Park, Los Angeles, California 90089-0484

Received July 17, 1990; accepted December 17, 1990

We analytically solve charge-transport equations for a photorefractive crystal with shallow and deep traps. We predict that, if shallow traps can accumulate a high density of charge, the photorefractive trap density and space-charge field will be strong functions of light intensity and the photoconductivity will scale sublinearly with intensity. We show that, depending on light intensity and grating spacing, shallow-trap charge gratings form either in phase or out of phase with the light pattern. As shallow traps thermally depopulate in the dark, the space-charge field either partially decays or partially develops for a few seconds. The amount of decay increases as grating spacing increases in $\text{Bi}_{12}\text{SiO}_{20}$ and as grating spacing decreases in BaTiO_3 .

1. INTRODUCTION

The early models of the photorefractive effect,¹⁻³ which we refer to as deep-trap models, predict that the photorefractive grating strength is independent of the light intensity that is used to write the grating as long as the photoconductivity exceeds the dark conductivity. However, the magnitude of the photorefractive space-charge field in some BaTiO_3 samples is a strong function of intensity^{4,5} even for intensities for which the thermal-equilibrium dark conductivity is negligible compared with the photoconductivity. Also, deep-trap models predict that the photorefractive grating will decay exponentially in the dark. Yet in $\text{Bi}_{12}\text{SiO}_{20}$ (BSO) and in some BaTiO_3 crystals a certain fraction of the grating decays in the dark on a time scale of a few seconds, whereas the rest of the grating remains for several minutes to hours.⁶⁻⁸ Other such deviations from the predictions of deep-trap models are the wavelength dependence of the photorefractive trap density^{2,9,10} and the oscillatory behavior of the diffraction efficiency in the dark in BSO.¹¹ There is also the recently resolved problem of the sublinear dependence of the light-induced grating-erasure rate on optical intensity in BaTiO_3 .¹²⁻¹⁵ Recently Brost *et al.* explained the intensity dependence of optical absorption and the photorefractive space-charge field in their BaTiO_3 sample by using a model of the photorefractive effect with shallow traps.⁶ However, they arrived at their results numerically and considered only the steady state. Strohkendl used a similar shallow-trap model to explain the dark decay of photorefractive gratings in BSO.⁶ Yet his treatment neglects the formation and dynamics of shallow-trap charge gratings, which we show to be important, and does not consider the steady state.

In this paper we present a complete analytical solution of a charge-transport model of the photorefractive effect with shallow traps. We derive a general expression for the charge gratings in the shallow and the deep traps and for the resulting space-charge field in the steady state. We also solve for the time development of photorefractive gratings in the dark in an approximate regime.

Our model includes shallow traps in addition to the usual deep donors and inactive compensative acceptors of the single-carrier Kukhtarev model.¹ For simplicity we consider shallow electron traps for n-type BSO (Fig. 1) and shallow hole traps for p-type BaTiO_3 . (It is not yet established whether the shallow traps in BSO and BaTiO_3 are electron traps or hole traps.) Light populates the shallow traps with charges, which are thermally reexcited to the nearest band on a time scale of microseconds to seconds. In our model light can excite charges to the nearest band from both the deep donors and the shallow traps. We neglect thermal excitation of charges from the deep donors, which causes photorefractive gratings to decay in the dark on time scales of the order of minutes to hours.

When a photorefractive crystal is illuminated by a sinusoidal light pattern, charge gratings form in both the shallow and the deep traps. We show that, depending on crystal temperature, light intensity, and grating spacing, the steady-state charge grating in the shallow traps forms in phase or 180° out of phase with the light pattern. When the shallow-trap charge grating is in phase with the light pattern, it can be larger than the grating in the deep traps.

We predict that if the shallow traps can accumulate a charge density that is comparable with or higher than the density of donors ionized in the dark, the photoconductivity will increase less than linearly with the light intensity. In the same regime the photorefractive trap density and space-charge field will be strong functions of the light intensity. On the other hand, if the density of charges in the shallow traps remains low compared with the density of ionized donors in the dark, the space-charge field changes little with intensity and the photoconductivity is nearly linear with the light intensity.

It was shown that the thermal depopulation of the charges that are stored in the shallow traps during illumination causes the photorefractive grating to decay in the dark.^{6,8} Here we show that the grating in the shallow traps plays a significant role in the dynamics of photorefractive dark decay and cannot be neglected. As the shallow traps depopulate, they erase the grating in the shallow

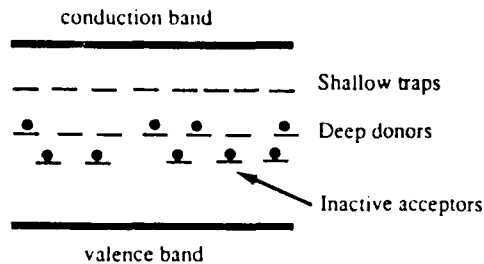


Fig. 1. Band diagram of the shallow-trap model for n-type crystals.

traps as well as some or all of the grating in the deep traps in a time of the order of microseconds to seconds. In most cases this causes the space-charge field partially to decay (coast) in the dark; however, the coupling between the shallow- and the deep-trap gratings can result in more complicated behavior. For example, when the charge grating in the shallow traps is 180° out of phase with the charge grating in the deep traps, thermal depopulation of shallow traps in the dark can, under certain conditions, cause the space-charge field to increase.

We solve for the time development of photorefractive gratings in the dark for the case in which the density of charges in the shallow traps is small compared with both the density of donors ionized in the dark and the total density of shallow traps. The time dependence of the dark decay of a photorefractive grating as well as the amount of decay is a function of the intensity of light that is used to write the grating, the grating spacing, the Debye screening length, and the diffusion length of the free carriers. In BSO the diffusion length of the free carriers is much larger than the Debye screening length, whereas the opposite is true in BaTiO_3 . This causes the dark decay behavior of photorefractive gratings to be quite different in the two crystals. For example, our model predicts that the dark decay of a grating in BaTiO_3 is a sum of two exponentials that decay to a constant background, whereas the dark decay of a grating in BSO is highly nonexponential in time. Also, the amount of dark decay increases as the grating spacing is increased in BSO and as the grating spacing is decreased in BaTiO_3 . These predictions are in agreement with recent experimental results in BSO and BaTiO_3 .^{11,14}

In Section 2 we describe the basic equations of our model and derive expressions for the density of filled shallow traps, steady-state charge gratings in the deep and the shallow traps, the space-charge field, photoconductivity, and absorption during cw illumination. In Section 3 we derive an expression for the time development of the space-charge field in the dark and discuss the solutions for BSO and BaTiO_3 .

2. THEORY

In the presence of shallow traps, the photorefractive effect is described by a simple extension of the Kukhtarev equations¹:

$$\frac{\partial N_D'}{\partial t} = s_D I (N_D - N_D') - \gamma_D n N_D', \quad (1)$$

$$\frac{\partial M}{\partial t} = -(s_T I + \beta) M + \gamma_T n (M_T - M), \quad (2)$$

$$\frac{\partial}{\partial t} (N_D' - M - n) + \frac{1}{e} \nabla \cdot \mathbf{J} = 0, \quad (3)$$

$$\mathbf{J} = e \mu n \mathbf{E} + \mu k_B T \nabla n, \quad (4)$$

$$\nabla \cdot \mathbf{E} = -\frac{e}{\epsilon} (n - N_D' + N_A + M). \quad (5)$$

Here N_D is the density of donors, N_A is the density of (inactive) acceptors, M_T is the total shallow-trap density, N_D' is the density of ionized donors, M is the density of filled shallow traps, n is the free-carrier density, \mathbf{J} is current density, \mathbf{E} is the electrostatic field, s_D and s_T are the light-excitation cross sections for donors and for shallow traps, γ_D and γ_T are the recombination constants for donors and for shallow traps, β is the thermal-excitation rate from the shallow traps, μ and ϵ are the mobility and the dielectric constant along the direction of charge migration, $e = 1.6 \times 10^{-19}$ C, and $k_B T$ is thermal energy. Here we assume that electrons are the charge carriers, so that these equations apply directly to n-type BSO. In the case of p-type BaTiO_3 crystals, our results can be converted to hole-dominated transport by simple substitutions and a change of terminology (see Appendix A). We also neglect the photogalvanic effect.

Assume that a sinusoidal light pattern, $I = I_0 \text{Re}[1 + m \exp(ikz)]$, illuminates the crystal. Here k is the grating wave vector, z is position, and m is the modulation index of the grating. Since the intensity varies only in the z direction, the problem reduces to one dimension. Also, if the modulation is small, $m \ll 1$, then all physical quantities that light can alter will have a spatially uniform part and a component that varies as $\exp(ikz)$. So, for example,

$$N_D' = N_A + N_0 + \text{Re}[N_1 \exp(ikz)],$$

$$M = M_0 + \text{Re}[M_1 \exp(ikz)], \quad (6)$$

with similar expressions for n , \mathbf{J} , and \mathbf{E} . We assume that the density of free carriers is low compared with both the density of the donors ionized by light and the density of filled shallow traps:

$$n_0 \ll N_0, \quad n_0 \ll M_0. \quad (7)$$

This replaces the low-intensity approximation used by Kukhtarev.¹ In this regime the charge-conservation equation, $N_0 = M_0 + n_0$, becomes

$$N_0 \approx M_0, \quad (8)$$

so the mean density of donors ionized by light is equal to the mean density of filled shallow traps. Note that relations (7) and (8) constitute two key differences between our model and deep-trap models. In the Kukhtarev model¹ the density of donors ionized by light is equal to the density of free carriers and is negligible compared with the density of donors ionized in the dark, $N_0 = n_0 \ll N_A$. Also, in Valley's two-species model, the spatially uniform components of the density of ionized donors and filled acceptors are unchanged by illumination.³ In our model light can significantly alter the mean density of ionized donors, because the electrons excited out of the donors can accumulate in the shallow traps. In fact dark decay experiments in BSO (Refs. 6 and 11) and BaTiO_3 (Ref. 8) showed that there are enough charges

stored in the shallow traps during illumination to cause a large fraction of a photorefractive grating to decay in a few seconds in the dark. This gives an order-of-magnitude estimate for the density of filled shallow traps of $M_0 \approx 10^{14}$ – 10^{15} cm $^{-3}$ for $I \sim 10$ mW/cm 2 , whereas the density of free carriers is $n_0 \sim 10^7$ – 10^8 cm $^{-3}$ for the same light intensity.

We also assume that the free-carrier grating is small compared with the total space-charge grating in the traps:

$$|n_1| \ll |N_1 - M_1|. \quad (9)$$

Inequalities (7) and (9) are satisfied in BSO and BaTiO $_3$ for $I < 10^7$ W/cm 2 .

A. Mean Density of Filled Shallow Traps at Steady State

Using the low-intensity approximation, inequality (7), we obtain the mean density of filled shallow traps at steady state from Eqs. (1)–(3) and Eq. (5) as

$$N_0 = M_0 = \frac{1}{2[\rho(I_0) - 1]} \{ [\rho(I_0)(N_{DA} + M_T) + N_A] - \{ [\rho(I_0)(N_{DA} + M_T) + N_A]^2 - 4\rho(I_0) \times [\rho(I_0) - 1]N_{DA}M_T \}^{1/2} \}, \quad (10)$$

where

$$\rho(I_0) = \frac{s_D \gamma_T}{s_T \gamma_D (1 + \beta/s_T I_0)}, \quad N_{DA} \equiv N_D - N_A. \quad (11)$$

The density of filled shallow traps, M_0 , which is a saturating function of intensity, determines the magnitude of the charge gratings in the shallow and the deep traps as well as the amount of dark decay after illumination.

The time development of the space-charge field in the dark can be obtained analytically in the special case in which the density of filled shallow traps is small compared with both the density of ionized donors in the dark and the total shallow-trap density, $M_0/M_T \ll 1$ and $M_0/N_A \ll 1$. These conditions are satisfied when

$$\frac{s_D \gamma_T}{s_T \gamma_D} \ll \frac{N_A^2}{4M_T N_{DA}}, \quad 1 \quad (\Rightarrow M_0/N_A \ll 1), \quad (12)$$

$$\frac{s_D \gamma_T}{s_T \gamma_D} \ll \frac{N_A}{N_{DA} + M_T} \quad (\Rightarrow M_0/M_T \ll 1). \quad (13)$$

In this case the density of filled shallow traps is given by

$$M_0 = \frac{M_*}{(1 + \beta/s_T I_0)} \quad (\text{if } M_0/N_A \ll 1, M_0/M_T \ll 1), \quad (14)$$

where

$$M_* = \frac{s_D \gamma_T M_T N_{DA}}{s_T \gamma_D N_A} \quad (15)$$

is the density of filled shallow traps above the saturation intensity $I_0 \gg \beta/s_T$.

B. Light-Induced Change in Absorption

The redistribution of charges between the deep and the shallow energy levels causes the optical absorption to vary

with light intensity. In our model the optical absorption of the traps is given by

$$\alpha_{\text{traps}} = (s_D N_{DA} + (s_T - s_D) M_0) h\nu. \quad (16)$$

The first term on the right-hand side of Eq. (16) is the trap absorption in the dark and in thermal equilibrium, and the second term is the light-induced change in absorption. Since the magnitude of the change in absorption is proportional to the density of filled shallow traps, it increases with as light intensity is increased and saturates at high intensities according to Eq. (10). Note that Eq. (16) for trap absorption predicts induced absorption for $s_T > s_D$ and induced transparency for $s_T < s_D$. Brost *et al.*⁴ observed that optical absorption of their BaTiO $_3$ sample at $\lambda = 514.5$ nm increased as intensity increased (by as much as 0.3 cm $^{-1}$ at $I = 20$ W/cm 2), indicating that $s_T > s_D$ in BaTiO $_3$ for that wavelength.

C. Sublinear Photoconductivity and Grating-Erasure Rate

The light-induced redistribution of electrons between deep and shallow levels also causes the photoconductivity to become a sublinear function of intensity.^{13,15} The intensity dependence of photoconductivity, $\sigma_{\text{light}} = e\mu n_0$, is determined by the density of free carriers, n_0 . From the spatially uniform part of Eq. (1) in steady state, the density of free carriers can be written as

$$n_0 = s_D I_0 (N_{DA} - N_0) \tau_D(I_0), \quad (17)$$

where

$$\tau_D(I_0) = \frac{1}{\gamma_D(N_A + N_0)} \quad (18)$$

is the recombination time of the electrons to the deep donors. As the light intensity increases, the density of donors ionized by light, N_0 , increases. Since the electrons ionized from the donors can accumulate in the shallow traps, N_0 can become comparable with or larger than N_A . Hence the recombination time of the free electrons to the deep donors, $\tau_D(I_0)$, decreases appreciably, and the photoconductivity increases less than linearly as intensity increases. At extremely low intensities for which the density of donors ionized by light is negligible compared with the density of ionized donors in the dark, $N_0 \ll N_A$, the recombination time $\tau_D(I_0)$ is a constant, and the photoconductivity increases linearly with intensity. Also, at extremely high cw intensities, for which the density of filled shallow traps (and the corresponding density of donors ionized by light) saturates, $M_0 = N_0 = \text{constant}$, the photoconductivity is a linear function of intensity. Another factor that tends to make photoconductivity a sublinear function of intensity is the decrease in the absorption from the deep donors, $s_D(N_{DA} - N_0) h\nu$. This occurs when the density of donors ionized by light becomes comparable with the density of un-ionized donors in the dark.

The explicit intensity dependence of the density of free carriers is given by

$$n_0 = \frac{s_D I_0}{2\gamma_D(N_A + M_T)} \left\{ (N_{DA} - M_T) - \frac{N_A}{\rho(I_0)} \right. \\ \left. + \left[\left((N_{DA} - M_T) - \frac{N_A}{\rho(I_0)} \right)^2 + \frac{4N_{DA}(M_T + M_T)}{\rho(I_0)} \right]^{1/2} \right\}. \quad (19)$$

In the intermediate range of light intensities, where the density of free carriers is a sublinear function of light intensity, Eq. (19) for n_0 can be approximated by the function I_0^x with $0.5 < x < 1$.¹⁵ The $x \sim 0.5$ limit is reached for $I_0 \ll \beta/s_T$ and when all donors are un-ionized in the dark and in thermal equilibrium, $N_A = 0$.

In grating-erasure experiments for which the average light intensity illuminating the crystal does not change during the write-erase cycle the population of the filled shallow traps and the density of the free carriers will be independent of time. In this case the grating-erasure rate will be proportional to the steady-state photoconductivity and is therefore expected to be a sublinear function of the erasing intensity. This prediction has been experimentally verified in a few BaTiO₃ samples.¹³

D. Steady-State Charge Gratings

In this subsection we present expressions for the steady-state charge gratings in the deep and the shallow levels for sinusoidal illumination. When the crystal is illuminated, the charges that are transferred from the partially filled donor level to the empty shallow traps allow gratings to form in both levels.

In the low-intensity approximation, $n_0 \ll N_0, M_0$ and $|n_1| \ll |N_1 - M_1|$, and in the absence of an externally applied field the amplitude of the charge grating in the deep donors is given by

$$(+e)N_1 = meN_F \frac{k^2}{(k^2 + k_0^2)} + meM_E \frac{1}{(1 + s_T I_0/\beta)} \frac{k_0^2}{(k^2 + k_0^2)}, \quad (20)$$

and the amplitude of the shallow-trap charge grating is

$$(-e)M_1 = meM_E \frac{1}{(1 + \beta/s_T I_0)} \frac{k^2}{(k^2 + k_0^2)} - meM_E \frac{1}{(1 + s_T I_0/\beta)} \frac{k_0^2}{(k^2 + k_0^2)}. \quad (21)$$

Here

$$N_E = \frac{(N_{DA} - N_0)(N_A + N_0)}{N_D}, \quad M_E = \frac{M_0(M_T - M_0)}{M_T}, \quad (22)$$

$$k_0^2 = \frac{e^2 N_E}{\epsilon k_B T}, \quad k_0^2 = \frac{e^2 M_E}{\epsilon k_B T}, \quad (23)$$

and

$$k_0^2 = k_{0D}^2 + k_{0T}^2 \quad (24)$$

is the square of the Debye screening wave vector. [In the presence of an applied electric field, Eqs. (20) and (21) for N_1 and M_1 are modified by replacing k^2 by $k(k - ieE_0/k_B T)$. Note that the Debye screening wave vector is a function of light intensity through its dependence on N_0 .

In the absence of an applied field, the charge gratings in the shallow and the deep traps, $(-e)M_1$ and $(+e)N_1$, are each a sum of an in-phase and a screening grating. The in-phase gratings, given by the first terms on the right-hand sides of Eqs. (20) and (21), are positive for both levels and are proportional to k^2 , corresponding to the transport

of charge by diffusion. The space-charge field is generated by the sum of the in-phase charge gratings of the two levels. The screening gratings, given by the second terms on the right-hand sides of Eqs. (20) and (21), have equal magnitudes and opposite signs and correspond to the lateral transfer of charge from the deep donors to the shallow traps. The screening gratings of the two levels exactly cancel each other and hence do not contribute to the space-charge field.

It is interesting to note that the phase of the shallow-trap charge grating, $(-e)M_1$, with respect to the light pattern changes with intensity (Fig. 2). In the absence of an applied field, $(-e)M_1$ is 180° out of phase with the light pattern for intensities $I_0 < \beta k_{0D}^2/s_T k^2$ and becomes in phase with it at higher intensities. For $I_0 < \beta k_{0D}^2/s_T k^2$ the screening grating in the shallow traps is larger than the in-phase grating, so that $(-e)M_1$ is 180° out of phase with the light pattern. In this case thermal excitations from shallow traps dominate light excitations, and charges accumulate in the bright regions, where there are more electrons in the conduction band that can recombine into the shallow traps. For $I_0 > \beta k_{0D}^2/s_T k^2$ optical excitations dominate thermal excitations, forcing charges to accumulate in the dark regions. In this case the screening grating is smaller than the in-phase grating, making the total shallow-trap charge grating, $(-e)M_1$, in phase with the light pattern. At the critical intensity $I_0 = \beta k_{0D}^2/s_T k^2$ the grating in the shallow traps vanishes. The charge grating in the deep traps, $(+e)N_1$, is in phase with the light pattern independent of intensity.

Although the shallow-trap charge grating can be either in phase or 180° out of phase with the light pattern (Fig. 2), the total space-charge field (hence the electro-optic, two-wave mixing gain) will not switch signs.⁴ Since only the in-phase components of the charge gratings contribute to the space-charge field, the light pattern will always be in phase with the total charge grating and 90° out of phase with the (electro-optic) refractive-index grating.

Note also that the screening gratings remain finite as $k \rightarrow 0$, while the in-phase gratings vanish. The screening gratings do not contribute to the electro-optic index grating. However, the charge transfer between the deep and

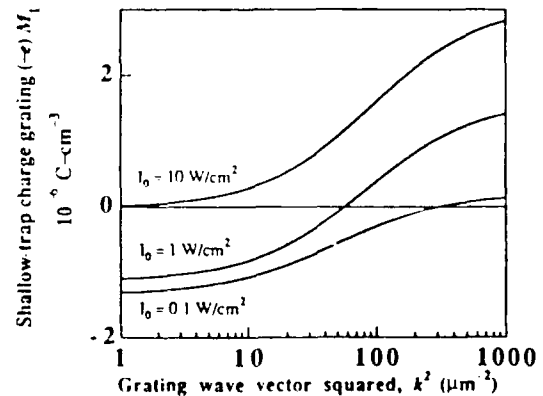


Fig. 2. Steady-state shallow-trap grating M_1 as a function of the grating wave vector squared for three writing intensities. The parameters used are $\beta = 10$ Hz, $\beta/s_T = 100$ mW/cm², $N_A = 1.9 \times 10^{18}$ cm⁻³, $M_T = 1.9 \times 10^{18}$ cm⁻³, $N_D = 10^{19}$ cm⁻³, $\kappa_D^2/\kappa_T^2 = 0.5$. (Only the ratio of the recombination rates affects the value of the steady-state charge gratings.)

the shallow levels creates an absorption (and corresponding refractive-index) grating that diffracts light and can therefore be observed. Using a geometry in which the effective electro-optic coefficient vanishes, Bacher *et al.* recently reported that a component of the absorption gratings in their BaTiO₃ sample remains finite as $k \rightarrow 0$ and is relatively large for $\lambda = 457.9$ nm.¹⁶ Their results are in excellent quantitative agreement with the predictions of our model. The change in sign of the shallow-trap charge grating with intensity can be observed also by measuring both the amplitude and the phase of absorption gratings. In Section 3 we suggest another experiment for observing the grating in the shallow traps.

E. Steady-State Space-Charge Field

The steady-state space-charge field is determined from the spatially oscillating part of the Poisson equation

$$ikE_1 = -\frac{e}{\epsilon}(N_1 - M_1). \quad (25)$$

We substitute Eqs. (20) and (21) for N_1 and M_1 in Poisson's equation, Eq. (25), and solve for the space-charge field to obtain

$$E_1 = -im \frac{k_B T}{e} \eta(I_0) \frac{k}{1 + k^2/k_0^2}, \quad (26)$$

where

$$\eta(I_0) = \frac{1}{k_0^2} \left(k_0 D^2 + \frac{k_0 r^2}{1 + \beta/s_T I_0} \right). \quad (27)$$

Note that Eq. (26) for the space-charge field has the same form as the familiar result of the Kukhtarev or Hopping model^{1,2} except for the intensity-dependent factor $0 < \eta \leq 1$. In addition the Debye screening wave vector, given by Eqs. (22)–(24), is a function of light intensity in our model.

In the hypothetical case that $s_T \sim 0$ and the density of shallow traps far exceeds the density of un-ionized donors, $M_T \gg N_D - N_A$, the Debye screening wave vector and the factor η will decrease as intensity is increased, and $\eta \rightarrow 0$ at high intensities. Such a material would become transparent, and its photoconductivity would saturate at high illumination intensities.

Inspection of Eqs. (26) and (27) shows that $1/2 \leq \eta \leq 1$ as long as the space-charge field is an increasing function of light intensity, which is the case for most crystals studied so far. When the density of shallow traps is comparable with the density of donors, $M_T \sim N_D$, and all the donors are un-ionized in the dark and in thermal equilibrium, $N_A = 0$, then the factor η varies between $1/2$ (for $I_0 \ll \beta/s_T$) and 1 (for $I_0 \gg \beta/s_T$). Under the same conditions the Debye screening wave vector k_0 and the space-charge field vanish for low intensities, because the donor level is full, and a spatial redistribution of charge is not possible. As the intensity increases, shallow traps are populated and deep traps are unpopulated, making k_0 and the space-charge field increasing functions of light intensity. These conditions seem to hold, for example, for the BaTiO₃ sample of Ref. 4 and for the Free and Cat crystals of BaTiO₃ used in Ref. 13. If, on the other hand, the density of filled shallow traps remains low compared with the density

of donors ionized in the dark and in thermal equilibrium, $M_0 \ll N_A$, the factor η is nearly unity and the Debye screening wave vector k_0 varies little with light intensity. We believe that most BSO crystals,^{8,11,17} and some BaTiO₃ samples (e.g., the Swiss and Hop crystals of Refs. 8 and 18 and the Rob crystal of Ref. 13), fall into this category.

The value of the space-charge field measured in two-wave mixing experiments is often less than that predicted by the single-carrier Kukhtarev or Hopping model. This discrepancy is usually attributed to electron-hole competition,^{17,19,20} which reduces the space-charge field by a k -dependent factor $0 \leq |\xi(k)| \leq 1$. However, in some BaTiO₃ crystals shallow traps alone reduce the space-charge field by a factor $1/2 \leq \eta \leq 1$, which could be mistaken for a k -independent electron-hole competition factor. Since the thermal-equilibrium dark conductivity of the crystal also decreases the photorefractive space-charge field at low intensities, it is common to choose the writing intensity such that the photoconductivity exceeds the dark conductivity. However, this does not guarantee that $\eta = 1$, because the intensity that is necessary to saturate the shallow traps (and therefore make $\eta \sim 1$) is often much higher. The saturation intensity can be determined in experiments in which the light-induced erasure rate of a photorefractive grating is measured as a function of intensity.¹³

Figure 3 shows a theoretical plot of the steady-state space-charge field E_1 as a function of the square of the grating wave vector k^2 for various writing intensities. Note that, as the light intensity increases, the amplitude of E_1 increases and the peak of the curve ($k = k_0$) moves to higher k values. Chang¹⁸ reported that the Debye screening wave vector k_0 increased by $\sim 15\%$ as the intensity increased from $I = 10 \times 10^{-3}$ W/cm² to $I = 0.4$ W/cm² in their sample of BaTiO₃ (Hop crystal). Brost *et al.*⁴ showed that k_0 increased by $\sim 50\%$ between $I = 2 \times 10^{-3}$ W/cm² and $I = 2$ W/cm² in their BaTiO₃ sample. Apparently $M_0 \ll N_A$ in the Hop crystal, while $M_0 \geq N_A$ in the BaTiO₃ sample used by Brost *et al.*

Our model also predicts that the Debye screening wave vector k_0 is a function of the wavelength of light. Since the density of donors ionized by light, n_0 , depends on the

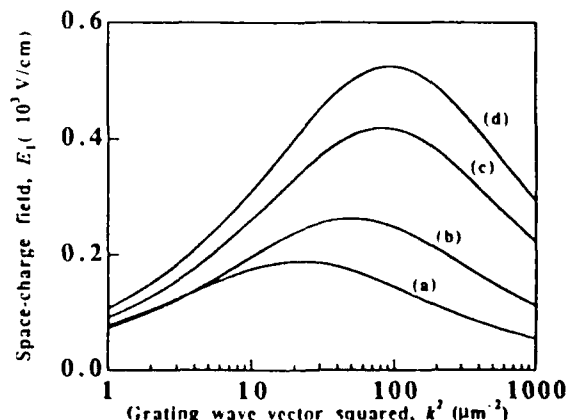


Fig. 3. Steady-state space-charge field E_1 as a function of the grating wave vector squared for various writing intensities. (a) $I = 0.001$ W/cm², (b) $I = 0.01$ W/cm², (c) $I = 0.1$ W/cm², (d) $I = 10$ W/cm². The parameters used are the same as those for Fig. 2.

ratio of the light-excitation cross sections from the deep and the shallow traps, $s_T(\lambda)/s_D(\lambda)$, the effective density of photorefractive traps (and k_0) is expected to vary with the wavelength of light. Many researchers^{2,10} have reported that the effective density of photorefractive traps varies with the wavelength of light, but to our knowledge no explanation has been given before this study.

3. DARK DECAY

A. Persistent Photoconductivity

In the absence of shallow traps the conductivity decays to its thermal-equilibrium value within a recombination time (approximately nanoseconds) after the lights are switched off. In the presence of shallow traps the conductivity drops to an intermediate value within a recombination time and decays to the thermal-equilibrium conductivity in microseconds to seconds after the illumination is switched off.¹¹ This so-called persistent photoconductivity is determined by the density of free carriers in the dark, $n_0(t)$.

In this subsection we derive an equation for $n_0(t)$ in the dark after cw illumination. We assume that the recombination time of free carriers to either the shallow or the deep level is much shorter than the relaxation time of the density of filled shallow traps. In this case the time derivative of n_0 in Eq. (3) can be neglected for times longer than a recombination time. Using the rate equations, Eqs. (1)–(3), with $I_0 = 0$ and the low-intensity approximation, relations (7) and (9), we find a transcendental equation for the density of filled shallow traps:

$$\left[\frac{M_0(t)}{M_T} \right] \left[\frac{M_0(t) + N_A}{M_T} \right]^{-(1 + N_A M_T / (1 + \gamma_D N_A \gamma_T M_T))} = \text{const.} \exp \left(- \frac{\beta t}{1 + \gamma_T M_T / \gamma_D N_A} \right), \quad (28)$$

where the constant is determined by the initial conditions. The density of filled shallow traps decays nonexponentially in the dark unless $M_0/N_A \ll 1$. The density of free carriers in the dark is given from the rate equations, Eqs. (1) and (2), in terms of M_0 by

$$n_0(t) = \frac{\beta M_0(t)}{\gamma_D N_A + \gamma_T M_T + (\gamma_D - \gamma_T) M_0(t)}. \quad (29)$$

Even if $M_0/N_A \ll 1$, the density of free carriers decays nonexponentially in the dark unless $|\gamma_D - \gamma_T| M_0 \ll \gamma_D N_A + \gamma_T M_T$. In this case the lifetime of free carriers in the conduction band remains constant during the decay, and the density of free carriers decays exponentially in the dark.

B. Equations for Dark Decay of Charge Gratings

When the lights are switched off, the shallow traps begin to depopulate thermally. A charge is thermally excited out of a shallow trap and retrapped several times before it recombines with a deep donor. The thermal depopulation of shallow traps in the dark causes the space-charge field to decay or, in certain cases, develop in the dark. It is also possible for the space-charge field to undergo damped oscillations in the dark even in the absence of an applied field.¹¹

In this subsection we derive equations for the time dependence of the charge gratings in the dark. We assume

that the grating amplitudes vary slowly compared with the recombination rate of the free carriers, $\gamma_D(N_A + N_0) + \gamma_T(M_T - M_0)$, so that we can neglect the time derivative of n_1 in Eq. (3). The spatially oscillating parts of Eqs. (1)–(5) with $I_0 = 0$ give a set of two coupled differential equations for the grating amplitudes $N_1(t)$ and $M_1(t)$:

$$\begin{aligned} \frac{\partial N_1}{\partial t} &= - \frac{(k^2 + K_T^2) \gamma_D n_0 + e \mu n_0 K_D^2 / \epsilon}{(k^2 + K^2)} N_1 \\ &\quad - \frac{(\beta + \gamma_T n_0 - e \mu n_0 / \epsilon) K_D^2}{(k^2 + K^2)} M_1, \\ \frac{\partial M_1}{\partial t} &= - \frac{(\gamma_D n_0 - e \mu n_0 / \epsilon) K_T^2}{k^2 + K^2} N_1 \\ &\quad - \frac{(k^2 + K_D^2)(\beta + \gamma_T n_0) + e \mu n_0 K_T^2 / \epsilon}{k^2 + K^2} M_1, \end{aligned} \quad (30)$$

where

$$\begin{aligned} K_D^2 &= \frac{e \gamma_D (N_A + N_0)}{\mu k_B T}, \\ K_T^2 &= \frac{e \gamma_T (M_T - M_0)}{\mu k_B T}, \\ K^2 &= K_D^2 + K_T^2. \end{aligned} \quad (31)$$

Here K_D^{-1} is the average distance an electron moves before recombining to a deep trap, and K_T^{-1} is the average distance an electron moves before recombining to a shallow trap. Note that n_0 , $M_0 = N_0$, K_T^2 , and K_D^2 are functions of time in Eqs. (30) and (31). These equations can be solved analytically only in the special case that the density of filled shallow traps is low compared with both the total density of shallow traps and the density of donors ionized in the dark.

C. Special Case ($M_0 \ll N_A, M_T$)

In this subsection we derive an analytical expression for the time dependence of the charge gratings, N_1 and M_1 , and the space-charge field, E_1 , in the dark. We consider the case for which the density of shallow traps that are filled during illumination is low compared with both the density of donors that are ionized in the dark and the total density of shallow traps:

$$M_0/N_A \ll 1, \quad (32)$$

$$M_0/M_T \ll 1. \quad (33)$$

We believe that these conditions are met in most BSO crystals and in BaTiO₃ crystals with a large dark-storage time. If $M_0/N_A \ll 1$ during illumination, the steady-state space-charge field and effective trap density vary little with intensity, and the photoconductivity scales nearly linearly with light intensity. In BSO photoconductivity scales approximately as I^x , with $x \sim 0.8$ – 1.0 ,²¹ and the steady-state space-charge field varies little with intensity, so that $M_0/N_A \ll 1$ in this crystal. The photorefractive properties of BaTiO₃ vary greatly from sample to sample. For example, photoconductivity scales approximately as I^x with $x \sim 0.8$ – 0.9 in the Hop crystal used in Refs. 8 and 18, the Swiss crystal of Ref. 18, and the Rob crystal of Ref. 13, so that $M_0/N_A \ll 1$ in these BaTiO₃ samples. However, the condition $M_0/N_A \ll 1$ is not valid for the BaTiO₃ sample used in Ref. 4, in which the effective trap density is a

strong function of intensity, or for the Free and Cat crystals of Ref. 13, in which photoconductivity scales approximately as I^x with $x \sim 0.6-0.7$. The condition that the density of shallow traps filled during illumination be low compared with the total, $M_0/M_T \ll 1$, can be indirectly verified in dark decay experiments.

Applying the condition $M_0/N_A \ll 1$ to the transcendental equation for the density of filled shallow traps, Eq. (28), we obtain

$$M_0(t) = M_0(t=0)\exp(-at), \quad (34)$$

where

$$a = \frac{\beta}{(1 + \gamma_T M_T / \gamma_D N_A)} \quad (35)$$

and $M_0(t=0)$ is the density of filled shallow traps at $t=0$ when the lights are switched off. Note that the decay rate a of the filled shallow trap population is slower than the thermal excitation rate β because of multiple trapping of charges by the shallow traps. When $M_0/N_A \ll 1$ and $M_0/M_T \ll 1$, the density of free carriers will decay exponentially in the dark and is given by

$$n_0(t) = \frac{\beta M_0(t=0)}{\gamma_D N_A + \gamma_T M_T} \exp(-at), \quad (36)$$

where we have used Eq. (34) for the density of filled shallow traps. Substituting Eq. (34) for the density of filled shallow traps and Eq. (36) for the density of free carriers into Eq. (30) for the charge gratings and after some mathematical manipulation, (see Appendix B), we obtain

$$M_1(t) = \exp[(f + g - q)\zeta_0 \exp(-at)] \times \left[A_0 \zeta_0 \exp(-at) F\left(1 - \frac{b}{2} - \frac{r}{2q}, 2 - b; 2q\zeta_0 \exp(-at)\right) + B_0 \exp(-abt) F\left(\frac{b}{2} - \frac{r}{2q}, b; 2q\zeta_0 \exp(-at)\right) \right], \quad (37)$$

$$N_1(t) = \frac{1}{c} \exp[(f + g - q)\zeta_0 \exp(-at)] \times \left\{ A_0 [(f - g - q)\zeta_0 \exp(-at) + 1 - b] \times F\left(1 - \frac{b}{2} - \frac{r}{2q}, 2 - b; 2q\zeta_0 \exp(-at)\right) + A_0 \zeta_0 \exp(-at) \left(q - \frac{r}{2 - b}\right) \times F\left(2 - \frac{b}{2} - \frac{r}{2q}, 3 - b; 2q\zeta_0 \exp(-at)\right) + B_0 \exp(-abt) (f - g - q) \times F\left(\frac{b}{2} - \frac{r}{2q}, b; 2q\zeta_0 \exp(-at)\right) + B_0 \exp(-abt) \left(q - \frac{r}{b}\right) \times F\left(1 + \frac{b}{2} - \frac{r}{2q}, 1 + b; 2q\zeta_0 \exp(-at)\right) \right\}. \quad (38)$$

Here F is the confluent hypergeometric function,

$$\zeta_0 = \frac{M_0(t=0)}{M_T} \quad (39)$$

is the fraction of the shallow traps that are filled at $t=0$ and is a function of the intensity of light used to write the grating,

$$b = \frac{1 + k^2/\kappa_D^2}{1 + k^2/\kappa^2}, \quad c = \frac{M_T \kappa_T^2 (1 - k_{0A}^2/\kappa_D^2)}{N_A \kappa^2 (1 + k^2/\kappa^2)}, \quad f = \frac{1}{2} \frac{M_T \kappa_T^2}{N_A \kappa^2} \frac{1 + (k^2 + k_{0A}^2)/\kappa_T^2}{1 + k^2/\kappa^2}, \quad g = \frac{1}{2} \frac{\kappa_T^2}{\kappa^2} \frac{1 + (k^2 + k_{0S}^2)/\kappa_D^2}{1 + k^2/\kappa^2}. \quad (40)$$

Also,

$$q^2 \equiv [(f - g)^2 - ch], \quad r \equiv [b(f - g) - cd], \quad h = -\frac{\kappa_T^2 (1 - k_{0S}^2/\kappa_T^2)}{\kappa^2 (1 + k^2/\kappa^2)}, \quad d = \frac{1}{1 + k^2/\kappa^2}. \quad (41)$$

In the presence of an applied electric field E_0 the definitions, Eqs. (40) and (41), are modified by replacing k^2 with $k(k - ieE_0/k_B T)$. The constants of the material, which are independent of the intensity of light used to write the grating, are

$$k_{0A}^2 = \frac{e^2 N_A}{\epsilon k_B T}, \quad k_{0S}^2 = \frac{e^2 M_T}{\epsilon k_B T},$$

$$\kappa_D^2 = \frac{e \gamma_D N_A}{\mu k_B T}, \quad \kappa_T^2 = \frac{e \gamma_T M_T}{\mu k_B T}, \quad \kappa^2 = \kappa_T^2 + \kappa_D^2. \quad (42)$$

Note that the lengths k_{0A}^{-1} and k_{0S}^{-1} that characterize dark decay are different from their corresponding values for cw illumination. The constants A_0 and B_0 are determined by the amplitudes of the gratings in the deep and the shallow traps at $t=0$ when the lights are switched off, $N_1(t=0)$ and $M_1(t=0)$. The time dependence of the space-charge field in the dark is determined from the Poisson equation and inequality (12) with Eqs. (37) and (38) for the charge gratings in the shallow and the deep traps:

$$E_1(t) = \frac{ie}{k\epsilon} [N_1(t) - M_1(t)]. \quad (43)$$

Dark decay of photorefractive gratings can be observed by introducing a weak probing beam that is incident upon the grating at the Bragg angle and by measuring the intensity of the diffracted signal as a function of time. In the limit of weak diffraction efficiency, the diffracted signal intensity is proportional to the absolute square of the space-charge field: $I_{\text{sig}}(t) \propto |E_1(t)|^2$. As expected, Eqs. (37) and (38) predict that for times longer than the decay time of the filled shallow-trap population, $t \gg 1/a$, the grating in the shallow traps will be completely erased, $M_1(t \gg 1/a) \rightarrow 0$, while a portion of the deep-trap grating will remain, $N_1(t \gg 1/a) \rightarrow A_0(1 - b)/c$; hence $I_{\text{sig}}(t \gg 1/a) = \text{constant}$. This partial erasure of a photorefractive grating in the dark that is caused by shallow traps is called coasting.⁸

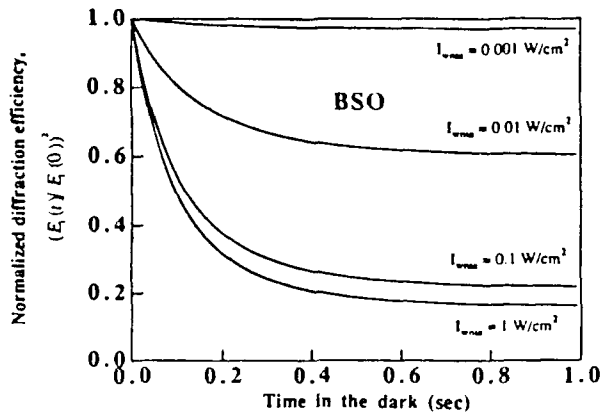


Fig. 4. Grating diffraction efficiency as a function of time in the dark, normalized to its value at $t = 0$ for various writing intensities in BSO. The parameters used are $\beta = 5$ Hz, $\beta/s_T = 10$ mW/cm², $k_{0A}^2 = 150 \mu\text{m}^{-2}$, $k_{0T}^2 = 100 \mu\text{m}^{-2}$, $\kappa_D^2 = 0.2 \mu\text{m}^{-2}$, $\kappa_T^2 = 0.02 \mu\text{m}^{-2}$.

The temporal behavior of the charge gratings in the dark, $M_1(t)$ and $N_1(t)$, depends on the intensity of light, I_0 , that is used to write the grating, the grating wave vector, and the Debye screening and diffusion wave vectors of the material. The only intensity-dependent quantities in Eqs. (37) and (38) are $A_0(I_0)$ and $B_0(I_0)$, which are determined by the amplitudes of the charge gratings in the two levels during illumination, and $\zeta_0(I_0)$, the fraction of shallow traps filled during illumination. $\zeta_0(I_0)$ increases as light intensity increases, saturates at high intensities according to Eq. (14), and is much less than 1 in the approximate regime that we are considering.

For a fixed writing intensity the temporal behavior of the charge gratings in the dark is most dramatically affected by the factor q in the argument of the hypergeometric functions and by the sum $f + g$, which appears in the exponent of the exponential prefactor. All the other parameters of the hypergeometric functions remain of order unity for all values of the grating wave vector. For large grating wave vectors, $k^2 \gg k_{0S}^2, k_{0A}^2, \kappa^2$, the sum of $f + g$ and q are less than or equal to 1, so that $q\zeta_0 \ll 1$ and $(f + g)\zeta_0 \ll 1$. In this case the hypergeometric functions and the exponential prefactor in the expressions for the charge gratings, Eqs. (37) and (38), can be approximated by the first two terms of their respective series, and the decay of the space-charge field can be described by a sum of two exponentials. This prediction can be used to test the validity of our assumption that the shallow traps are only partially populated, $\zeta_0 = M_0/M_T \ll 1$.

For smaller grating wave vectors, the time dependence of the gratings in the dark is more complicated and depends on the ratio of the Debye screening wave vectors k_{0A} and k_{0S} to the diffusion wave vectors κ_D and κ_T . The Debye screening wave vector is typically $k_0 \sim 10 \mu\text{m}^{-1}$ in both BaTiO₃ and BSO, whereas the diffusion wave vector in BaTiO₃, $\kappa_{\text{BaTiO}_3} \sim 24 \mu\text{m}^{-1}$, is much larger than that in BSO, $\kappa_{\text{BSO}} \sim 0.5 \mu\text{m}^{-1}$. (Here we suppose, for the sake of argument, that the Debye screening and diffusion wave vectors for the deep donors are of the same order of magnitude as the corresponding wave vectors for the shallow traps, $k_{0A} \sim k_{0S}$ and $\kappa_D \sim \kappa_T$.) Hence the dark decay of gratings with small grating wave vectors will have sub-

stantially different behavior in BaTiO₃ and in BSO. In Subsections 3.D and 3.E we discuss the solutions obtained above for the dark decay of photorefractive gratings in BSO and BaTiO₃ crystals.

D. Dark Decay in BSO

For small grating wave vectors, $k < k_0$, and for typical parameters of BSO, $\kappa_{\text{BSO}} \sim 0.5 \mu\text{m}^{-1}$ and $k_0 \sim 10 \mu\text{m}^{-1}$, the argument of the hypergeometric functions, $2q\zeta_0$, is much larger than unity because $q \sim 10^{-4}$, so that many terms of each series have to be retained for an accuracy of the order of ζ_0^2 . In addition the exponential prefactor in Eqs. (37) and (38) deviates from a simple exponential because the sum $f + g$ and q become large. Hence the functions $M_1(t)$ and $N_1(t)$ will be highly nonexponential in time for small- k gratings in BSO. Note that although the filled shallow-trap population and the free-carrier density decay exponentially in the dark, the dark decay of the charge gratings and the space-charge field are highly nonexponential in time.

Figure 4 shows theoretical plots of grating diffraction efficiency in BSO as a function of time in the dark, normalized to its value at $t = 0$ when the lights are switched off, $|E_1(t)|^2/|E_1(0)|^2$, for $k = 3.3 \mu\text{m}^{-1}$ and various writing-beam intensities. Note that the rate and the total amount of decay increase as writing intensity increases. As the writing intensity increases, the fraction of shallow traps filled during illumination, ζ_0 , increases, and the dark decay of the photorefractive grating becomes faster and more nonexponential. Also, since there are more charges stored in the shallow traps at higher intensities, more of the grating will decay in the dark.

Figure 5 shows theoretical plots of normalized grating diffraction efficiency, $|E_1(t)|^2/|E_1(0)|^2$, in BSO as a function of time in the dark for gratings of various wave vectors, k 's, written at an intensity $I_0 = 1 \text{ W/cm}^2$, where the shallow traps are saturated. Note that the decay rate and the total amount of decay are larger for gratings with smaller k 's. The decay of gratings with large wave vectors can be described by a sum of two exponentials, and the total amount of decay is small. For gratings with large k 's in BSO the grating erasure is inefficient, and the

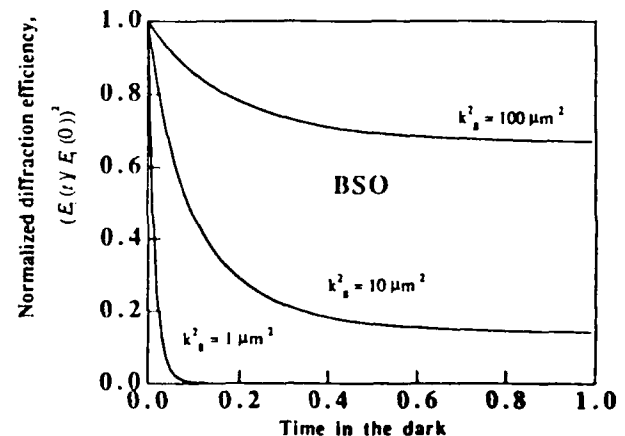


Fig. 5. Grating diffraction efficiency as a function of time in the dark normalized to its value at $t = 0$ for various grating wave vectors in BSO. The parameters used are the same as those for Fig. 4.

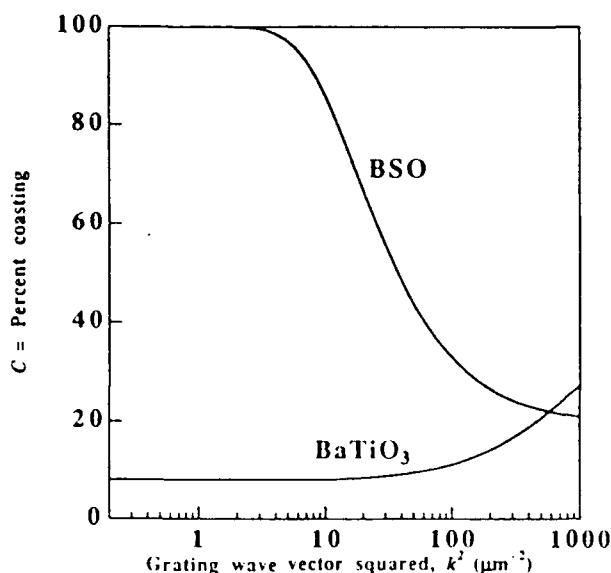


Fig. 6. Percent coasting C as a function of the grating wave vector squared. The parameters used for BSO are the same as those for Fig. 4, and the parameters for BaTiO₃ are $\beta = 2$ Hz, $\beta/s_T = 15$ mW/cm², $k_{0A}^2 = 260$ μm^{-2} , $k_{0T}^2 = 340$ μm^{-2} , $\kappa_D^2 = 1200$ μm^{-2} , $\kappa_T^2 = 200$ μm^{-2} .

photorefractive grating decays in the dark at nearly the same rate as the density of free carriers. Also, it takes a large charge to write or to erase a grating with a large k (small spacing), so that the charge stored in the shallow traps during illumination is not enough to erase a substantial part of the grating in the dark. On the other hand, the decay of gratings with small wave vectors in the dark is nonexponential in time, and the amount of decay is substantial. In BSO, grating erasure is quite efficient for small- k gratings, so that the decay of the grating in the dark is much faster than the decay of the density of free carriers. Also, it takes little charge to write or to erase a grating with a small k (large spacing), so that the charge stored in the shallow traps during illumination is sufficient to erase nearly completely the grating in the dark.

In order to characterize dark decay of photorefractive gratings without having to confront the full complexity of the solutions, we define two new quantities:

$$C \equiv 100 \frac{I_{\text{sig}}(t=0) - I_{\text{sig}}(t \gg 1/a)}{I_{\text{sig}}(t=0)} \quad (44)$$

is the percentage of the signal diffracted from the photorefractive grating that decays in the dark because of shallow traps (coasting) and

$$R \equiv \frac{1}{I_{\text{sig}}} \left(\frac{dI_{\text{sig}}}{dt} \right)_{t=0} \quad (45)$$

is the decay rate of the diffracted signal at $t = 0$ when the lights are switched off. Figures 6 and 7 show the percent coasting, defined by Eq. (44), and the decay rate at $t = 0$ as functions of the grating wave vector in BSO for a writing intensity $I_0 = 1$ W/cm². Coasting reaches 100% for small k 's but decreases as the grating wave vector increases, eventually reaching a plateau for $k \geq k_{0A}$. Increasing the density of shallow traps increases coasting,

but the location of the plateau at large grating wave vectors remains fixed at $k \sim k_{0A}$. The initial dark decay rate R is a constant for small k 's, begins to decrease as the grating wave vector increases when $k \sim \kappa_D$, and reaches a second plateau at $k \sim \kappa_{0A}$. The dependence of the initial dark decay rate on the grating wave vector is the same as that for light-induced grating decay,⁷ except that the characteristic wave vector k_{0A} for dark decay is different from the corresponding wave vector for cw illumination. Also, both the percent coasting C and the initial dark decay rate R increase with increased writing intensity and saturate (Figs. 8 and 9), showing a behavior similar to the intensity dependence of the fraction of shallow traps filled during illumination.

E. Dark Decay in BaTiO₃

For typical material parameters of BaTiO₃ the decay of the space-charged field in the dark can be approximated to order ζ_0^2 by a sum of two exponentials, because $q\zeta_0 \ll 1$ and $(f + g)\zeta_0 \ll 1$ for all values of the grating wave vector. Figure 10 shows the theoretical plots of $|E_1(t)|^2/|E_1(0)|^2$ for BaTiO₃ as a function of time in the dark for gratings of various wave vectors written at a fixed intensity $I_0 = 1$ W/cm². The total decay in the dark increases with increased wave vectors in BaTiO₃ (opposite the trend for BSO), and the functional form of the decay remains double exponential for all k 's. As the grating wave vector increases, grating erasure becomes more efficient in BaTiO₃, and the total decay in the dark increases. However, the amount of decay in the dark remains small for all k 's. It takes a large charge to write or to erase a grating with a large k (small spacing), and there is not enough charge stored in the shallow traps during illumination to erase a substantial fraction of the grating. For small- k gratings, which take little charge to erase, the shallow traps do have enough charge to erase the entire grating. However, in BaTiO₃ erasure is inefficient for gratings with small k 's, so that the shallow traps can erase only a small fraction of

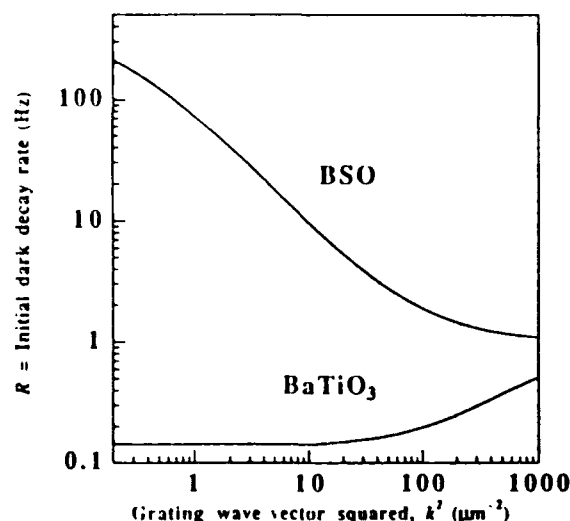


Fig. 7. Initial dark decay rate R as a function of the grating wave vector. The parameters used for BSO are the same as those for Fig. 4, and the parameters for BaTiO₃ are the same as those for Fig. 6.

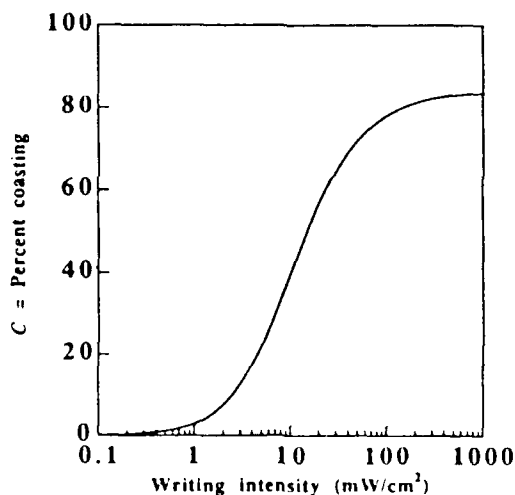


Fig. 8. Percent coasting in the dark C as a function of the writing intensity for BSO. The parameters used are the same as those for Fig. 4. The curve for BaTiO_3 has the same shape.

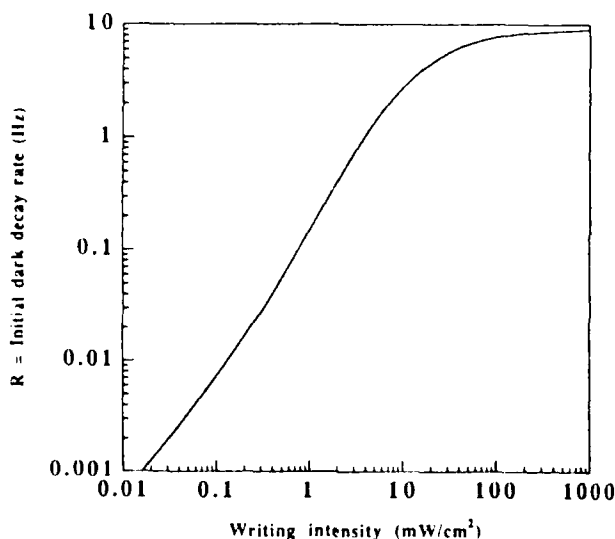


Fig. 9. Initial dark decay rate R as a function of the writing intensity for BSO. The parameters used are the same as those for Fig. 4. The curve for BaTiO_3 has the same shape.

the grating in the dark during the short (few seconds) time that they have before they are depopulated.

Figure 6 shows a plot of percent coasting, defined by Eq. (44), as a function of the grating wave vector in BaTiO_3 . Note that coasting increases as the wave vector increases in BaTiO_3 , opposite the trend in BSO, with plateaus at $k \sim k_{0A}$ and $k \sim \kappa_D$ (which is off scale on the horizontal axis). As in the case of BSO, the percent coasting increases with increased light intensity and saturates at high intensities, because more charge is stored in the shallow traps at higher writing intensities. The initial dark decay rate R of the signal diffracted from a grating in BaTiO_3 also increases as the grating wave vector k increases (Fig. 7). R has the same k dependence as the light-induced erasure rate,¹⁸ except that the plateau in Fig. 7 occurs at the Debye screening wave vector that corresponds to dark decay, k_{0A} .

F. Enhancement of the Space-Charge Field in the Dark
Inspection of Eq. (30) for the time dependence of the grating amplitudes reveals that $\partial(N_1 - M_1)/\partial t$ can be positive. Hence the space-charge field can grow (or have damped oscillations) in the dark, even in the absence of an applied field.¹¹ Here we give an example.

Suppose that the charge gratings formed during illumination in the deep and the shallow traps have equal magnitudes and opposite signs and that the space-charge field is quite small, $E_1 \propto (N_1 - M_1) \sim 0$. This can occur, for example, when a grating with $k \sim 0$ is written to steady state or when low-energy pulsed light is used to write a grating of arbitrary k that has not reached steady state. When the writing beams are switched off, the total charge grating and the resulting space-charge field will initially increase, because the gratings in the shallow and the deep traps decay at different rates. Figure 11 shows a theoretical plot of the normalized grating diffraction efficiency in

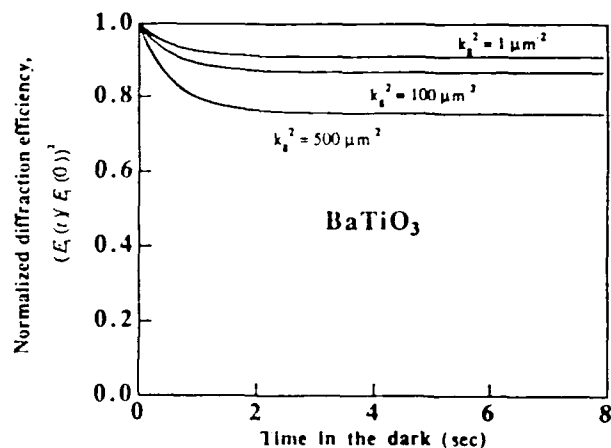


Fig. 10. Grating diffraction efficiency as a function of time in the dark normalized to its value at $t = 0$ for various grating wave vectors in BaTiO_3 . The parameters used are the same as those for Fig. 6.

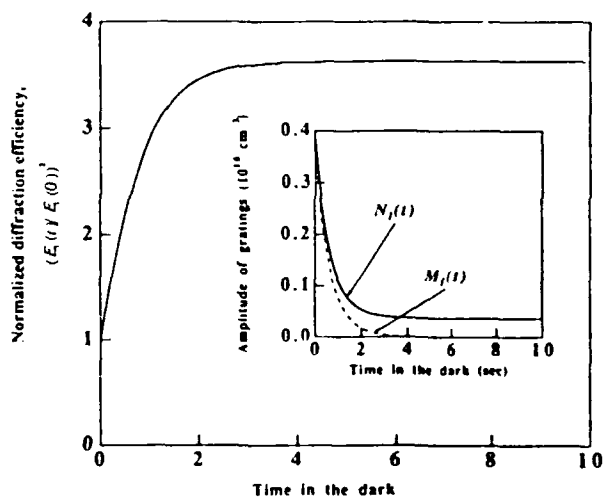


Fig. 11. Grating diffraction efficiency as a function of time in the dark normalized to its value at $t = 0$ for BaTiO_3 , assuming that the charge gratings in the deep and the shallow traps have equal magnitudes and opposite signs at $t = 0$. Note that the space-charge field develops in the dark. The inset shows the decay of N_1 , the grating in the deep traps, and M_1 , the grating in the shallow traps.

the dark, $|E_1(t)|^2/|E_1(t=0)|^2$, for BaTiO₃ for $k = 10 \mu\text{m}^{-1}$ and initial conditions that demonstrate the above situation. The inset shows the time dependence of the grating amplitudes $M_1(t)$ and $N_1(t)$. Note that the shallow-trap grating decays faster than the deep-trap grating. Recently Smirl *et al.* observed that the grating diffraction efficiency increased in the dark for a few seconds after illumination of a BaTiO₃ sample by two 30-ps writing pulses.²² Oscillatory behavior of the space-charge field in the dark (with no applied field) was also recently observed in BSO and can be understood in terms of our model.¹¹

SUMMARY

In summary, we have solved the charge-transport equations for a photorefractive insulator with shallow and deep traps and have derived analytical expressions for the photorefractive charge grating and space-charge field, Debye screening wave vector, photoconductivity, and absorption at steady-state for cw illumination. We have shown that, if shallow traps can accumulate a large density of charge, then the photoconductivity is a nonlinear function of light intensity and that the photorefractive space-charge field and the Debye screening wave vector are strong functions of the intensity and the wavelength of light.

We have also solved for the time development of the space-charge field in the dark in an approximate regime, which, we believe, applies both to BSO and to BaTiO₃ crystals with large dark-storage times. We have shown that the grating in the shallow traps also plays a significant role in the dark decay of the photorefractive space-charge field. According to our model, even if conductivity decays exponentially in the dark, the decay of the space-charge field is highly nonexponential for gratings with small wave vectors in BSO. In BaTiO₃ crystals (with long dark-storage times) and for gratings with large wave vectors in BSO, the grating decay consists of two exponentials that decay to a constant background that lasts for hours. The amount of decay in the dark increases with increasing grating wave vectors in BaTiO₃ and with decreasing grating wave vectors in BSO. We have also shown that thermal depopulation of shallow traps in the dark can, in certain cases, cause the photorefractive space-charge field to increase in the dark.

APPENDIX A: CHANGES FOR HOLE-DOMINATED CRYSTALS

The following recipe converts our electron-dominated shallow-trap model and its results to a hole-dominated model:

1. Replace the shallow electron traps near the bottom of the conduction band by shallow hole traps near the top of the valence band.
2. Replace light excitation of electrons to the conduction band by the light excitation of holes to the valence band. Hence S_D and S_T become the cross sections for hole excitation from the donors and shallow traps, and γ_D and γ_T are coefficients of hole recombination to the donors and shallow traps.
3. Make the following substitutions in the theoretical expressions: $e \rightarrow -e$, $\mu \rightarrow -\mu$, $N_{DA} \rightarrow N_A$, $N_A \rightarrow N_{DA}$, $M_T - M \rightarrow M$, and $M \rightarrow M_T - M$; N_D is unchanged.

APPENDIX B: DERIVATION OF $N_1(t)$ AND $M_1(t)$ (DARK DECAY)

Using Eq. (34) for the density of filled shallow traps and Eq. (36) for the density of free carriers in Eq. (30) for the charge gratings, we obtain

$$\frac{1}{a} \frac{\partial N_1}{\partial t} = -[d - h\zeta_0 \exp(-at)]M_1 - 2f\zeta_0 \exp(-at)N_1, \quad (\text{B1})$$

$$\frac{1}{a} \frac{\partial M_1}{\partial t} = -(b + 2g\zeta_0 \exp(-at))M_1 - c\zeta_0 \exp(-at)N_1. \quad (\text{B2})$$

The coefficients appearing in Eqs. (B1) and (B2) are defined by Eqs. (40)–(42). We change variables to $x = \exp(-at)$ and obtain a second-order differential equation for M_1 :

$$\frac{\partial^2 M_1}{\partial x^2} - \left[2(f + g)\zeta_0 + \frac{b}{x} \right] \frac{\partial M_1}{\partial x} + \left[(ch + 4fg)\zeta_0^2 + \frac{(2fb - cd)}{x} \zeta_0 + \frac{b}{x^2} \right] M_1 = 0. \quad (\text{B3})$$

The solutions of Eq. (B3) are given by

$$M_1(\zeta_0 x) = \exp(f + g - q)\zeta_0 x \left[A_0 x \zeta_0 F \left(1 - \frac{b}{2} - \frac{r}{2q}, 2 - b; 2q\zeta_0 x \right) + B_0 x^b F \left(\frac{b}{2} - \frac{r}{2q}, b; 2q\zeta_0 x \right) \right], \quad (\text{B4})$$

where F is the confluent hypergeometric function and A_0 and B_0 are determined by the initial conditions.²³ Equation (37) for the time development of the shallow-trap grating in the dark, $M_1(t)$, is then obtained by changing back to the time variable by the substitution $x = \exp(-at)$. The amplitude of the deep-trap grating in the dark, $N_1(t)$, given by Eq. (38), is obtained by substituting the solution for $M_1(t)$ into Eq. (B2).

ACKNOWLEDGMENTS

This research was supported by contracts F49620-88-C-0095 and F49620-88C-0027 with the U.S. Air Force Office of Scientific Research and grant ECS-8821507 from the National Science Foundation.

*Present address, Foster-Miller Inc., 350 Second Avenue, Waltham, Massachusetts 02154.

REFERENCES

1. N. V. Kukhtarev, V. B. Markov, S. G. Odulov, M. S. Soskin, and V. L. Vinetskii, "Holographic storage in electrooptic crystal. I. Steady state," *Ferroelectrics* **22**, 949 (1979).
2. J. Feinberg, D. Heiman, A. R. Tanguay, Jr., and R. W. Hellwarth, "Photorefractive effect and light-induced charge migration in BaTiO₃," *J. Appl. Phys.* **51**, 1297 (1980); erratum **52**, 537 (1981).
3. G. C. Valley, "Erasable rates in photorefractive materials with two photoactive species," *Appl. Opt.* **22**, 3160 (1983).
4. G. A. Brost, R. A. Motes, and J. R. Rotge, "Intensity-dependent absorption and photorefractive effects in barium titanate," *J. Opt. Soc. Am. B* **5**, 1879 (1988).
5. D. A. Temple and C. Warde, "Photoinduced absorption effects in BaTiO₃," in *OSA Annual Meeting*, Vol. 11 of 1988 OSA

- Technical Digest Series (Optical Society of America, Washington, D.C., 1988), p. 137.
6. F. P. Strohkendl, "Light-induced dark decays of photorefractive gratings and their observation in $\text{Bi}_{12}\text{SiO}_{20}$," *J. Appl. Phys.* **65**, 3773 (1989).
 7. R. A. Mullen, "Measurement of bulk space-charge grating in photorefractive $\text{Bi}_{12}\text{SiO}_{20}$," Ph.D. dissertation (University of Southern California, Los Angeles, Calif., 1984).
 8. D. Mahgerefteh and J. Feinberg, "Erasure rate and coasting in photorefractive barium titanate at high optical power," *Opt. Lett.* **13**, 1111 (1988).
 9. S. Ducharme, "Photorefraction in BaTiO_3 ," Ph.D. dissertation (University of Southern California, Los Angeles, Calif., 1986).
 10. M. E. Lasher and D. M. Gookin, "Wavelength dependence of the photorefractive effect in photorefractive barium titanate," in *Conference on Lasers and Electro-Optics*, Vol. 7 of 1990 OSA Technical Digest Series (Optical Society of America, Washington, D.C., 1990), p. 92.
 11. P. Tayebati, "Characterization of the effect of shallow traps on photorefractive properties of $\text{Bi}_{12}\text{SiO}_{20}$," submitted to *J. Appl. Phys.*
 12. S. Ducharme and J. Feinberg, "Speed of the photorefractive effect in a BaTiO_3 single crystal," *J. Appl. Phys.* **66**, 839 (1984).
 13. D. Mahgerefteh and J. Feinberg, "Explanation of the apparent sublinear photoconductivity of photorefractive barium titanate," *Phys. Rev. Lett.* **64**, 2195 (1990).
 14. D. Mahgerefteh, "The speed of the photorefractive effect, shallow traps, photogalvanic currents, and light-induced surface damage in barium titanate," Ph.D. dissertation (University of Southern California, Los Angeles, Calif., 1990).
 15. L. Holtmann, "A model for the nonlinear photoconductivity of BaTiO_3 ," *Phys. Status Solidi A* **113**, K89 (1989).
 16. R. S. Cudney, R. M. Pierce, G. D. Bacher, and J. Feinberg, "Absorption grating having multiple levels," submitted to *J. Opt. Soc. Am. B*.
 17. F. P. Strohkendl, P. Tayebati, and R. W. Hellwarth, "Comparative study of photorefractive BSO crystals," *J. Appl. Phys.* **66**, 6024 (1989).
 18. T. Y. Chang, "Nonlinear optical studies of BaTiO_3 ," Ph.D. dissertation (University of Southern California, Los Angeles, Calif., 1986).
 19. F. P. Strohkendl, J. M. C. Jonathan, and R. W. Hellwarth, "Hole-electron competition in photorefractive gratings," *Opt. Lett.* **11**, 312 (1986).
 20. G. C. Valley, "Simultaneous electron/hole transport in photorefractive materials," *J. Appl. Phys.* **59**, 2363 (1986).
 21. P. Tayebati, "Characterization and modeling of the photorefractive effect in bismuth silicon oxide," Ph.D. dissertation (University of Southern California, Los Angeles, Calif., 1989).
 22. A. L. Smirl, K. Bohnert, G. C. Valley, R. A. Mullen, and T. F. Boggesa, "Formation, decay, and erasure of photorefractive gratings written in barium titanate by picosecond pulses," *J. Opt. Soc. Am. B* **6**, 606 (1989).
 23. P. M. Morse and H. Feshbach, *Methods of Theoretical Physics* (McGraw-Hill, New York, 1953).

Measuring photorefractive trap density without the electro-optic effect

R. M. Pierce, R. S. Cudney, G. D. Bacher, and Jack Feinberg

Department of Physics, University of Southern California, University Park, Los Angeles, California 90089-0484

Received October 30, 1989; accepted February 5, 1990

Two optical beams can couple in a photorefractive crystal without using the electro-optic effect. Beam coupling is due to a spatially modulated absorption caused by the rearrangement of trapped charges. We use these gratings to determine the effective photorefractive trap density for several barium titanate crystals.

In a photorefractive effect, light rearranges charges among trapping sites in a crystal, and the resulting electric field alters the crystal's refractive index by the electro-optic effect. However, if the polarizability of a full trap differs from that of an empty trap, the trapping sites themselves will alter the susceptibility of the crystal. A periodic light intensity pattern will induce a periodic population of empty and full trap sites, in turn making the crystal's susceptibility periodic. This trap grating can couple light beams even in the absence of an electro-optic effect.

In most photorefractive crystals any beam coupling from a trap grating will be masked by the much larger coupling from the electro-optic grating. In this Letter we present measurements of optical beam coupling caused by trap gratings alone, using a geometry that prohibits electro-optic beam coupling. Trap gratings in photorefractive materials have been observed in lead-lanthanum zirconate-titanate ceramic.^{1,2} More recently, the effects of trap gratings have been noted in GaAs^{3,4} and BaTiO₃.⁵ We present, for the first time to our knowledge, the use of trap gratings alone to measure the effective trap density in photorefractive materials.

Two-beam coupling by a trap grating has a unique signature: it causes the transmitted energy to increase or decrease in *both* beams. (In the BaTiO₃ samples studied here the transmitted energy increases.) This is in contrast to coupling by an electro-optic grating, in which one transmitted beam gains energy while the other loses energy. Energy is conserved in trap-grating coupling since the grating simply reduces the effective absorption for both beams.

The coupling of optical beams by a trap grating can be explained heuristically as follows. Let two beams interfere in a crystal, creating a spatially periodic intensity pattern. Charge carriers from trap sites will diffuse out of the bright regions and accumulate in the dark regions. If the (complex) polarizability of an empty trap differs from that of a full trap, the spatially periodic distribution of full traps will cause a periodic change in the crystal's optical dielectric constant. For the case of no external or intrinsic uniform electric field, the distribution of charge will be 180° out of phase with the light pattern. The imaginary part of this grating alters the energy of each of the optical beams, while the real part alters their phases.

After charge migration the brightly lit regions of the crystal will have fewer charge carriers in the traps than the darker regions. If these full trap sites absorb more than the empty sites, then the effect of charge migration is to bunch the absorbers away from the light and so decrease the absorbed energy. Where the light is the brightest the absorption is now the least. This reduction in absorption can be large only if the absorption from the traps is large. This heuristic picture only shows why an absorption grating can increase the transmission of both beams. In order to investigate this effect quantitatively, a coupled-wave solution must be performed.

Consider two coherent optical beams, having electric fields $E_1 \hat{e}_1 \exp(i\mathbf{k}_1 \cdot \mathbf{x} - i\omega t)$ and $E_2 \hat{e}_2 \exp(i\mathbf{k}_2 \cdot \mathbf{x} - i\omega t)$, interfering in a photorefractive crystal. The resulting optical intensity pattern $I(\mathbf{x}) = I_0 \text{Re}[1 + m \exp(i\mathbf{k}_g \cdot \mathbf{x})]$, with its modulation $m \equiv 2(\hat{e}_1 \cdot \hat{e}_2^*) E_1 E_2^* / (|E_1|^2 + |E_2|^2)$, will impose a periodicity on the distribution of full and empty traps, giving rise to a trap grating with wave vector $\mathbf{k}_g = \mathbf{k}_1 - \mathbf{k}_2$. Here \hat{e}_1 and \hat{e}_2 are optical polarization unit vectors.

The crystal's relative dielectric tensor $\tilde{\epsilon}(\mathbf{x})$ is

$$\tilde{\epsilon}(\mathbf{x}) = \tilde{\epsilon}_{\text{host}} + \tilde{\epsilon}_{\text{traps}}(\mathbf{x}) + \tilde{\epsilon}_{\text{eo}}(\mathbf{x}), \quad (1)$$

where $\tilde{\epsilon}_{\text{host}}$ is the crystalline host contribution, $\tilde{\epsilon}_{\text{eo}}$ is due to the electro-optic (Pockels) effect, and $\tilde{\epsilon}_{\text{traps}}$ depends on the polarizability tensors of full and empty traps, \tilde{p}_{full} and \tilde{p}_{empty} ,

$$\tilde{\epsilon}_{\text{traps}}(\mathbf{x}) = \tilde{p}_{\text{full}} N_{\text{full}}(\mathbf{x}) + \tilde{p}_{\text{empty}} N_{\text{empty}}(\mathbf{x}), \quad (2)$$

where we have assumed a single species of active trap sites. The spatially periodic component of the total dielectric tensor $\tilde{\epsilon}(\mathbf{x})$ couples the amplitudes of the two optical waves E_1 and E_2 . Using coupled-wave equations and assuming that $|E_2| \ll |E_1|$, we find that the intensity $I_2(l)$ of the weak beam after propagating a distance l is

$$I_2(l) = I_2(0) \exp[-\alpha + \gamma_{\text{abs}}(k_g) + \gamma_{\text{eo}}(k_g)]l, \quad (3)$$

where α is the total background absorption coefficient and $\gamma_{\text{abs}}(k_g)$ and $\gamma_{\text{eo}}(k_g)$ are the coupling gains per unit length due to absorption gratings and electro-optic gratings, respectively.

For simplicity, we consider a single charge-carrier model.^{6,7} Let N_{full} and N_{empty} be the spatial average of

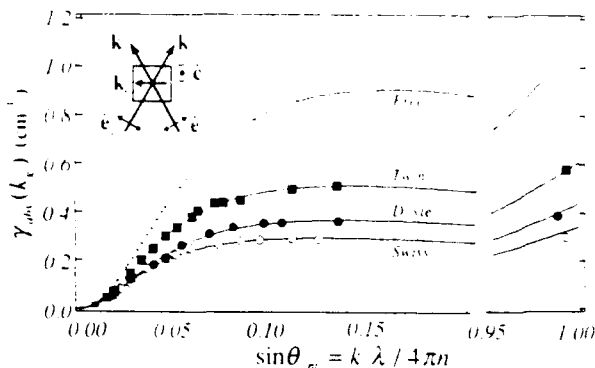


Fig. 1. Absorptive coupling versus the sine of the internal beam-crossing half-angle in four strangely named BaTiO₃ crystals. The experimental geometry is shown in the inset. The single large-angle data point for each crystal was obtained by directing the two beams into opposite faces of the crystal. The solid curves are two-parameter fits to Eq. (6).

the full and empty trap site densities, respectively. The coupling gain becomes

$$\gamma_{\text{abs}}(k_g) = \frac{\omega}{nc} \text{Im}(p_{\text{full}} - p_{\text{empty}}) \times |\hat{e}_1 \cdot \hat{e}_2|^2 \frac{(k_g/k_o)^2}{1 + (k_g/k_o)^2} N_{\text{eff}}, \quad (4)$$

where the effective trap density $N_{\text{eff}} \equiv \bar{N}_{\text{full}} \bar{N}_{\text{empty}} / (\bar{N}_{\text{full}} + \bar{N}_{\text{empty}})$ and n is the index of refraction. In Eq. (4) we have made the polarizabilities isotropic. The inverse Debye screening length k_o in Eq. (4) is given by

$$k_o^2 = \frac{e^2}{\epsilon_o \epsilon_{\text{dc}} k_B T} N_{\text{eff}}, \quad (5)$$

where $k_B T/e$ is the thermal energy per charge, ϵ_o is the vacuum permittivity, and ϵ_{dc} is the relative static dielectric constant of the crystal along the grating wave vector \mathbf{k}_g . Equations (4) and (5) allow us to determine the effective density of traps by measuring the absorption grating gain $\gamma_{\text{abs}}(k_g)$ as a function of k_g .

In order to measure $\gamma_{\text{abs}}(k_g)$ exclusively, we first had to eliminate any coupling from the electro-optic effect. This is accomplished in BaTiO₃ by choosing both of the beam polarizations, \hat{e}_1 and \hat{e}_2 , and \mathbf{k}_g all to be perpendicular to the crystal's c axis (see the inset of Fig. 1).

Because $\gamma_{\text{abs}}(k_g)$ can be small, extra care was taken in the measurement of this coupling strength. Any light scattered from the reference beam by crystal imperfections will interfere with the transmitted probe beam at the detector and introduce a systematic error. This noise is especially strong at small beam-crossing angles. This scattered light was largely blocked by a 250- μm -diameter pinhole placed 10 cm after the crystal (the probe beam was focused through this pinhole by a lens). Still, the remaining scattered light could cause large errors in the measurement. These were eliminated by varying the relative phase between the scattered light and the probe light by stepwise changes in the reference beam's path length and then averaging the coupling measurements. We

avoided errors from bulk light-induced absorption⁷ by never turning the light beams on or off; instead, we destroyed the absorption grating (and thus its coupling) by rapidly vibrating the reference beam's mirror. When we stopped the vibration, the two-beam coupling would increase from zero to a steady-state value in a time typical for photorefractive charge transport.

To check that no part of our measured coupling was due to a remnant electro-optic effect, we performed experiments using probe and reference beams of equal intensity ($|m| = 1$). As expected for a pure absorption grating, we observed gain of equal sign and magnitude for both beams, to within 5%. (Any contribution from an electro-optic grating would have decreased the gain for one beam and increased it for the other.) As a further check, we made one beam much weaker than the other, measured its coupling gain, and then rotated the crystal by 180° around the c axis. We obtained the same gain to within 2%; any electro-optic coupling would have ruined this symmetry.

To determine the effective charge density, we measured $\gamma_{\text{abs}}(k_g)$ versus k_g in several BaTiO₃ crystals. The intensity of the strong beam was $\sim 1 \text{ W/cm}^2$, and the intensity of the weak beam was 700 times less than that of the strong beam, giving a modulation of $m < 0.1$. The coupling gain is shown in Fig. 1, where θ_{int} is the half-angle between the two optical beams inside the crystal. The data are fitted to

$$\gamma_{\text{abs}}(k_g) = \Gamma_{\text{abs}} \cos^2 2\theta_{\text{int}} \frac{k_g^2/k_o^2}{1 + k_g^2/k_o^2}, \quad (6)$$

where Γ_{abs} and k_o are fitting parameters. This equation follows from Eq. (4) for the geometry and polarizations of the inset in Fig. 1. We find that $k_g = k_o$ for an internal full crossing angle of $2\theta_{\text{int}} = 4\text{--}7^\circ$, depending on the sample of BaTiO₃. The large-angle data points in Fig. 1 were obtained by directing the two beams through opposite faces of the crystal. At these large angles $\gamma_{\text{abs}}(k_g)$ is dominated by the $\cos^2 2\theta_{\text{int}}$ factor in Eq. (6). The fitting parameters k_o and Γ_{abs} , and the inferred N_{eff} , are listed in Table 1.

We also measured two-beam coupling with the conventional geometry shown in the inset of Fig. 2, in

Table 1. BaTiO₃ Crystal Parameters^a

	BaTiO ₃ Crystal			
	Swiss	Doyle	Twin	Free
$N_{\text{eff}} (\text{cm}^{-3})$	3.1×10^{16}	3.5×10^{16}	4.5×10^{16}	7.4×10^{16}
$k_o^{\text{abs } b}$	0.038	0.045	0.046	0.060
$k_o^{\text{eo } b}$	0.24	0.25	0.32	0.37
$\Gamma_{\text{abs}} (\text{cm}^{-1})$	0.34	0.44	0.61	1.13
$\Gamma_{\text{eo}} (\text{cm}^{-1})$	4.13	4.3	3.2	4.6
$\alpha (\text{cm}^{-1})$	0.74	1.28	1.67	2.73
ϵ_a	4200	3450	4200	4050
ϵ_c	130	125	130	120
$(k_o^{\text{eo}}/k_o^{\text{abs}})^2$	40	31	48	38
ϵ_a/ϵ_c	32	28	32	34
$\Gamma_{\text{abs}}/\alpha$	0.46	0.34	0.37	0.41

^a The fitting parameters are k_o^{abs} , k_o^{eo} , Γ_{abs} , and Γ_{eo} ; the measured parameters are ϵ_a , ϵ_c , and α . All measurements are at $T = 24^\circ\text{C}$, $\lambda = 514.5 \text{ nm}$, o polarization, and a total intensity of 1 W/cm^2 .

^b Units of $4\pi n/\lambda$ at $\lambda = 514.5 \text{ nm}$.

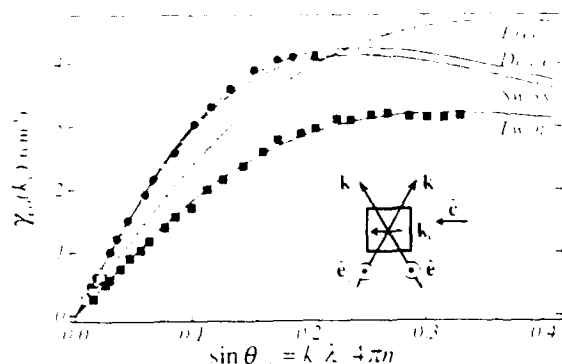


Fig. 2. Electro-optic coupling versus the sine of the internal beam-crossing half-angle in four BaTiO₃ crystals. The experimental geometry is shown in the inset. The solid curves are two-parameter fits to Eq. (7).

which the electro-optic coupling $\gamma_{eo}(k_g)$ is large. We oriented the crystal's c axis so that the electro-optic grating depleted the weak beam. Figure 2 shows the measured $\gamma_{eo}(k_g)$ versus k_g . Since absorption coupling is also present (and can be as large as $\sim 10\%$ of the electro-optic grating depletion at $k_g = k_o$) we used the previously determined value of the parameter Γ_{abs} to perform a two-parameter fit to

$$\gamma_{eo}(k_g) = \Gamma_{eo} \frac{2k_g/k_o}{1 + k_g^2/k_o^2} - \Gamma_{abs} \frac{k_g^2/k_o^2}{1 + k_g^2/k_o^2}. \quad (7)$$

The fitted values of Γ_{eo} and k_o for these electro-optic measurements are also listed in Table 1. In the geometry of the inset of Fig. 2 a much larger beam-crossing angle, in the range $2\theta_{int} = 26\text{--}45^\circ$, was required to reach $k_g = k_o$. The required crossing angle is large because the static dielectric constant is relatively small ($\epsilon_c \approx 120$) when k_g is parallel to \hat{c} . In contrast, with the absorption grating geometry of the inset of Fig. 1, k_g is perpendicular to the c axis of the crystal, and the dielectric constant is large ($\epsilon_a \approx 4100$), making the corresponding crossing angle small. From Eq. (5),

$$(k_o^{eo}/k_o^{abs})^2 = \epsilon_o/\epsilon_c \approx 34, \quad (8)$$

so that the absorption grating k_o should be approximately six times smaller than its electro-optic counterpart. This implies that N_{eff} can be determined in BaTiO₃ by measuring two-beam coupling from absorption gratings at small crossing angles. This is a definite advantage over the usual electro-optic beam-coupling technique, in which the required large crossing angles, with their varying beam overlap, often lead to errors.

We note that the data of Table 1 do not satisfy Eq. (8) precisely; the ratio $(k_o^{eo}/k_o^{abs})^2$ always exceeds the ratio of dielectric constants. This may be caused by inaccuracies in our capacitance-bridge measurement of the dielectric constants, although the data are within 10% of previously published values (except for one sample). Another possible error is the fitted value of k_o obtained from our electro-optic coupling experiments, since these measurements are prone to errors caused by the required large crossing angles.

We can show that two-beam coupling from an absorptive grating can never completely overcome the

crystal absorption: at best it can only nearly balance it. The total absorption α is due to the host crystal and to both full and empty traps: $\alpha = \alpha_{host} + \alpha_{traps}$. In our simple model the trap absorption is

$$\alpha_{traps} = \frac{\omega}{nc} \text{Im}(p_{empty} \bar{N}_{empty} + p_{full} \bar{N}_{full}) \approx \alpha_{empty} + \alpha_{full}. \quad (9)$$

The ratio of the maximum absorption grating gain to the total absorption loss is then

$$\frac{\Gamma_{abs}}{\alpha} \leq \frac{\Gamma_{abs}}{\alpha_{full} + \alpha_{empty}} \leq \frac{\Gamma_{abs}}{\alpha_{full}} = \frac{\bar{N}_{empty}}{\bar{N}_{full} + \bar{N}_{empty}}, \quad (10)$$

which is always less than one. In Table 1 we list Γ_{abs}/α values for four BaTiO₃ crystals. If BaTiO₃ obeyed the simple charge-transport model considered here, then Eq. (5) and relation (10) could also provide values for the separate donor and acceptor densities. However, charge transport in BaTiO₃ is known to be considerably more complex than the simple model presented here (there is more than one active trap level, and both electrons and holes are mobile).^{9,10} In fact, we have observed a noticeable dependence on intensity in our values for Γ_{abs} and k_o .

In conclusion, we have used absorption gratings in BaTiO₃ to determine the effective trap density. These gratings are invariably present during electro-optic beam-coupling experiments and can lead to errors if not accounted for.³⁻⁵ We also note that trap gratings can occur even in centrosymmetric materials and so can be used to study charge transport and excitation in any material.

We thank Robert Hellwarth, Yeon Lee, Daniel Mahgerefteh, and Jouni Partanen for their useful suggestions. We gratefully acknowledge support from U.S. Air Force Office of Scientific Research contract F49620-88-C-0095.

The authors are also with the Department of Electrical Engineering, University of Southern California, Los Angeles, California.

References

1. A. V. Alekseev-Popov, A. V. Kynaz'kov, and A. S. Saikin, *Sov. Tech. Phys. Lett.* **9**, 475 (1983).
2. A. V. Kynaz'kov and M. N. Lobanov, *Sov. Tech. Phys. Lett.* **11**, 365 (1985).
3. K. Walsh, T. J. Hall, and R. E. Burge, *Opt. Lett.* **12**, 1026 (1987).
4. R. B. Bylsma, D. H. Olson, and A. M. Glass, *Opt. Lett.* **13**, 853 (1988).
5. Y. Lee, Ph.D. dissertation (University of Southern California, Los Angeles, Calif., 1989).
6. N. V. Kukhtarev, V. B. Markov, S. G. Odoulov, M. S. Soskin, and V. L. Vinetskii, *Ferroelectrics* **22**, 949 (1979).
7. J. Feinberg, D. Heiman, A. R. Tanguay, Jr., and R. W. Hellwarth, *J. Appl. Phys.* **51**, 1297 (1980); erratum **52**, 537 (1981).
8. A. Motes and J. J. Kim, *J. Opt. Soc. Am. B* **4**, 1379 (1987).
9. D. Mahgerefteh and J. Feinberg, *Opt. Lett.* **13**, 1111 (1988).
10. F. P. Strohkendl, J. M. C. Jonathan, and R. W. Hellwarth, *Opt. Lett.* **11**, 312 (1986).

Absorption gratings in photorefractive crystals with multiple levels

R. S. Cudney, R. M. Pierce, G. D. Bacher, and Jack Feinberg

Department of Physics and Department of Electrical Engineering, University of Southern California, Los Angeles, California 90089-0484

Received July 31, 1990; accepted January 23, 1991

Two coherent light beams can couple in any absorbing material owing to a light-induced modulation of the material's dielectric constant. In photorefractive crystals the coupling caused by these absorption gratings appears in addition to any electro-optic coupling, complicating the interpretation of data. However, in contrast with the electro-optic gratings formed by charge diffusion, absorption gratings do not necessarily vanish as the beam-crossing angle approaches zero if there is more than one absorbing level. We show that a plot of the coupling strength of the absorption gratings versus the beam-crossing angle is characterized by only three parameters, independent of the number of absorbing levels. We use absorption gratings with a two-level model to determine experimentally some important crystal parameters, including the relative density of donors and acceptors in a barium titanate crystal. Our values agree with those obtained from measurements of the bulk light-induced absorption of the crystal.

1. INTRODUCTION

The photorefractive effect has outgrown its early models. These models assume that charges are trapped by both donor and acceptor levels in a crystal, but they also assume that the charges can be excited from only one of these levels.^{1,2} These models predict, for example, that the photoconductivity increases linearly with intensity and, if the dark conductivity is small compared with the photoconductivity, that the photorefractive coupling strength and the effective Debye screening length are independent of optical intensity. Also, these models predict that the magnitude of the two-beam coupling coefficient is the same whether a beam is depleted or amplified. However, none of these predictions is true in the photorefractive crystal BaTiO₃.

Much of the anomalous behavior of photorefractive BaTiO₃ can be explained if charges are permitted to be optically excited from more than one level. For example, Holtmann³ and also Mahgerefteh and Feinberg⁴ recently explained the sublinear dependence of the photoconductivity of BaTiO₃ by using a model that included an additional trap site level or, equivalently, by permitting charges in both the donor and acceptor levels to be excited by light. A multilevel model also accounts for the observed intensity dependence of the photorefractive coupling strength and the effective Debye screening length in BaTiO₃.^{4,5} Motes and Kim⁶ showed that part of the asymmetry between gain and depletion in two-beam coupling is caused by the bulk light-induced absorption of the crystal, and Brost *et al.*⁷ showed that light-induced absorption requires more than one active level in the crystal. Alekseev-Popov *et al.*⁸ showed that for a single photoactive level the coupling asymmetry in photorefractive materials can also be caused by a spatial modulation of the absorption because this absorption grating produces either gain or loss for both of the optical beams.⁸⁻¹¹

The above papers established the presence of absorption gratings and the existence of at least two photoactive lev-

els in BaTiO₃. In this paper we combine these two concepts by investigating the effects of absorption gratings when there is more than one active level. We solve the band-conduction model and obtain expressions for the steady-state two-beam coupling gain due to absorption gratings as well as to electro-optic gratings. Our two-beam coupling experiments clearly reveal an intensity dependence of the absorption-grating coupling strength γ_{abs} , the electro-optic-grating coupling strength γ_{eo} , and the inverse effective Debye screening length k_0 . Our multilevel model predicts all these effects. The model also predicts that more than one trapping level can cause an offset in the coupling constant γ_{abs} , so that the absorption-grating gain does not vanish as the magnitude of the grating wave vector k_g approaches zero. This absorption-grating offset also appears in all electro-optic beam-coupling measurements, as we will demonstrate in Subsection 3.C. We measured this offset in several crystals of BaTiO₃, and we present data for the variation of this offset with intensity. By fitting our data to the special case of one active donor level and one active acceptor level, we determine the ratio of the densities of donor and acceptor sites, as well as other material parameters of one of our crystals.

2. THEORY

A. Band-Conduction Model for Multiple Levels

We derive expressions for the two-beam coupling gains per unit length of absorption gratings and electro-optic gratings for the case of l levels, some of which are electron donors and others of which are electron acceptors. We will show that the absorption-grating gain as a function of the magnitude of the grating wave vector k_g contains an offset term, which does not exist in a single-level model. Additionally, we will show that the functional dependence of the gain on k_g is independent of the number of photoactive levels.

We consider only one type of charge carrier, either electrons or holes but not both. The band-conduction model for an arbitrary number of trap levels is described by the following set of equations:

$$\frac{\partial N_j^E}{\partial t} = (\beta_j + s_j I) N_j^F - \gamma_j n N_j^E, \quad (1)$$

$$\mathbf{j} = e\mu n \mathbf{E} \mp k_B T \mu \nabla n, \quad (2)$$

$$\sum_{j=1}^l \left(\xi_j^F \frac{\partial N_j^F}{\partial t} + \xi_j^E \frac{\partial N_j^E}{\partial t} \right) \pm \frac{\partial n}{\partial t} + \frac{\nabla \cdot \mathbf{j}}{e} = 0, \quad (3)$$

$$\nabla \cdot \mathbf{E} = \frac{e}{\epsilon_0 \epsilon} \left[\sum_{j=1}^l (\xi_j^F N_j^F + \xi_j^E N_j^E) \pm n \right], \quad (4)$$

where N_j^E and N_j^F are the number densities of the j th sites that are empty and full, respectively, of the mobile charge. (By definition, the total trap density of the j th level is $N_j = N_j^F + N_j^E$.) In Eq. (1) n is the number density of charges in the appropriate band, and the optical, thermal, and recombination constants for the j th level are denoted by s_j , β_j , and γ_j , respectively. In Eq. (2) \mathbf{j} is the total current density, $k_B T$ is the thermal energy, e is the magnitude of the electric charge, μ is the mobility of the charge carrier, and \mathbf{E} is the electric field. In Eqs. (2)–(4) the upper or lower sign applies according to whether the charge carriers are holes or electrons, respectively. In Eq. (4) ϵ is the relative dc dielectric constant of the crystalline host, and ϵ_0 is the permittivity of the vacuum.

The factors ξ_j^F and ξ_j^E in Eqs. (3) and (4) denote the sign of the charge at full and empty sites, respectively, of the j th level. The values of ξ_j^F and ξ_j^E depend on whether the site is an electron donor or acceptor and on the type of charge carrier. For example, if the mobile charges are holes, then $\xi_j^F = 0$ and $\xi_j^E = -1$ for acceptor levels, while $\xi_j^F = +1$ and $\xi_j^E = 0$ for donor levels. These ξ_j terms are a bookkeeping device used to ensure charge neutrality, but they play no role in our subsequent results since they appear only as a difference in the formulas. In general, $\xi_j^F - \xi_j^E = +1$ for holes and $\xi_j^F - \xi_j^E = -1$ for electrons.

For clarity, we have neglected the photogalvanic effect, as well as any externally applied electric field. Although Eqs. (1)–(4) can also be solved if these effects are included, the results are cumbersome. In any case, for the absorption-grating geometry used in Subsection 3.A, the photogalvanic effect is forbidden by the crystal's symmetry, and no external field was applied during the experiments. Equations (1)–(4) and the results derived from them can also be generalized to the case of a continuous distribution of levels. However, we find that such a generalization adds no new insights to the interpretation of our experiments.

In order to recover the one-active-level model,¹¹ we set $l = 2$ in Eqs. (3) and (4) and make one of the levels the active donor level and the other an inactive acceptor level by setting its recombination constant and its optical and thermal excitation rates all equal to zero.

Consider two coherent optical beams with electric fields $\text{Re}[E_1 \hat{e}_1 \exp(i\mathbf{k}_1 \cdot \mathbf{x} - i\omega t)]$ and $\text{Re}[E_2 \hat{e}_2 \exp(i\mathbf{k}_2 \cdot \mathbf{x} - i\omega t)]$ intersecting at a full crossing angle $2\theta_{\text{int}}$ measured inside a photorefractive crystal. The resulting optical intensity is $I(\mathbf{x}) = I \text{Re}[1 + m \exp(i\mathbf{k}_g \cdot \mathbf{x})]$, where the modulation is given by $m \equiv 2(\hat{e}_1 \cdot \hat{e}_2^*) E_1 E_2^* / (|E_1|^2 + |E_2|^2)$, the

grating wave vector is $\mathbf{k}_g = \mathbf{k}_1 - \mathbf{k}_2$, and I is the total average intensity. Here \hat{e}_1 and \hat{e}_2 are the unit polarization vectors of the incident optical beams. For $m \ll 1$ we can approximate the number density of full sites of the j th level by $N_j^F = N_j^I + [N_j^I \exp(i\mathbf{k}_g \cdot \mathbf{x}) + \text{c.c.}]/2$. The linearized solution for the first-order term $N_j^{F(1)}$ is

$$N_j^{F(1)}(I, \mathbf{k}_g) = m N_j^{\text{eff}}(I) \left(\frac{s_j I}{\beta_j + s_j I} \right) \frac{k_g^2 k_0^2(I) + \phi_j(I)}{1 + k_g^2/k_0^2(I)}, \quad (5)$$

where N_j^{eff} is the intensity-dependent effective number density of the j th level [$N_j^{\text{eff}}(I) = N_j^F(N_j - N_j^F)/N_j$]. The term N_j^{eff} is equivalently written as $N_j^{\text{eff}} = N_j f_j(1 - f_j)$, where f_j is the fraction of full sites of the j th level. The steady-state filling fraction $f_j(I) = \gamma_j n_0(I) / [\beta_j + s_j I + \gamma_j n_0(I)]$ is a complicated function of intensity because it depends on the average density of free charge carriers, $n_0(I)$, which varies nonlinearly with intensity. The particular functional form of $n_0(I)$ depends on the number of active levels. The magnitude of the grating wave vector is $k_g = (2n\omega/c) \sin \theta_{\text{int}}$, where n is the crystal's index of refraction at optical frequency ω , and θ_{int} is the crossing half-angle between the two beams inside the crystal. The effective inverse screening length k_0 for the j th level is defined by $k_0^2(I) = e^2 N_j^{\text{eff}}(I) / \epsilon \epsilon_0 k_B T$, and the total effective inverse screening length k_0 is defined by $k_0^2(I) = e^2 n_0(I) / \epsilon \epsilon_0 k_B T + \sum_{j=1}^l k_0^2(I)$. The parameter ϕ_j in Eq. (5) is a function of the thermal and optical excitation rates from the different levels:

$$\phi_j = 1 - \left(\frac{\beta_j + s_j I}{s_j I} \right) \sum_{i=1}^l \frac{k_{0i}^2}{k_0^2} \left(\frac{s_i I}{\beta_i + s_i I} \right). \quad (6)$$

The two terms in the last factor in the numerator of Eq. (5) may be understood physically as follows. The term proportional to k_g^2 arises from charges that are excited in one location, migrate, and are trapped elsewhere, as depicted in Fig. 1(a). In the absence of any uniform dc electric field these charges are propelled only by diffusion, and so their contribution to the spatially varying number density $N_j^{F(1)}$ is expected to scale as k_g^2 for small spatial frequencies, just as in the one-active-level model. However, a new term ϕ_j appears in the numerator of Eq. (5); it is caused by charges that are excited from one level and recombine into another level without diffusing, as shown

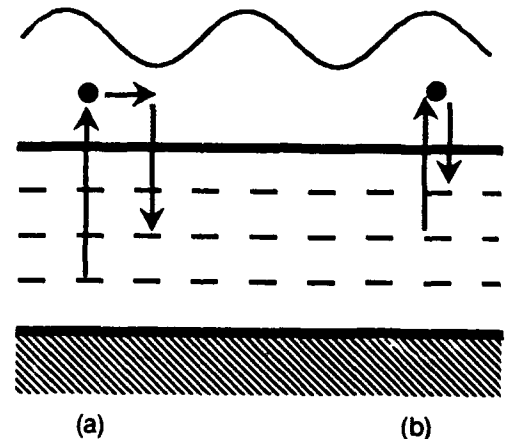


Fig. 1. (a) Diffusive charge transport; (b) no diffusion.

in Fig. 1(b). These two processes of (i) charge diffusion and (ii) local charge excitation between levels without diffusion are linked by Eqs. (5) and (6). To our knowledge, the presence of this ϕ term was first derived analytically by Tayebati and Mahghefteh¹² and independently by Knyazkov and Lobanov¹³ for the special case of two active levels.

B. Absorption-Grating Gain

We now use these results to derive an expression for the absorption-grating gain per unit length coefficient. The spatially varying relative dielectric constant $\epsilon_{\text{trap}}(\mathbf{x})$ produced by the trap sites of the crystal is given by

$$\epsilon_{\text{trap}}(\mathbf{x}) = \sum_j p_j^F N_j^F(\mathbf{x}) + p_j^E N_j^E(\mathbf{x}), \quad (7)$$

where p_j^F and p_j^E are the polarizabilities of the full and empty trap sites, respectively, of the j th level. Note that this effect is local: the change in the polarizability at location \mathbf{x} is due only to the occupation of the various trapping sites at that location. [This is in contrast with the usual electro-optic (Pockels) grating, where a charge at one place produces an electric field that alters the crystal's refractive index elsewhere.] Using Eqs. (5) and (7) and the usual coupled-wave approach, we find that the imaginary part of the polarizabilities, i.e., the absorption, causes a change in the transmitted energy of the two beams. In the undepleted-pump approximation the intensity of the weak beam grows (or decreases, according to the particular crystal) exponentially with a gain per unit length, γ_{abs} , given by

$$\gamma_{\text{abs}}(I, k_g) = \frac{\Gamma_{\text{abs}}(I) [k_g/k_0(I)]^2 + \Phi(I)}{1 + [k_g/k_0(I)]^2} \hat{e}_1 \cdot \hat{e}_2^{*2}, \quad (8)$$

where $\Gamma_{\text{abs}}(I)$ is given by

$$\Gamma_{\text{abs}}(I) \equiv \frac{\omega}{nc} \sum_{j=1}^l N_j^{\text{eff}}(I) \left(\frac{s_j I}{\beta_j + s_j I} \right) \text{Im}(\Delta p_j) \quad (9)$$

and $\Delta p_j = p_j^F - p_j^E$. Note that the inverse screening length $k_0(I)$ becomes intensity dependent, as mentioned in Subsection 2.A.

For comparison, the coupling gain per unit length in the simple one-active-level model is given by¹¹

$$\gamma_{\text{abs}}(k_g) = \Gamma_{\text{abs}} \frac{(k_g/k_0)^2}{1 + (k_g/k_0)^2} \hat{e}_1 \cdot \hat{e}_2^{*2}. \quad (10)$$

In the low-intensity limit, i.e., when $n_0(I)$ is negligible, k_0 is independent of intensity in Eq. (10).

The most significant difference between the single-level and multilevel models is the appearance of an offset term $\Phi(I)$ in Eq. (8), where

$$\Phi(I) \equiv -\frac{\omega}{nc} \sum_{j=1}^l N_j^{\text{eff}}(I) \phi_j(I) \left(\frac{s_j I}{\beta_j + s_j I} \right) \text{Im}(\Delta p_j). \quad (11)$$

If the number density $n_0(I)$ of free carriers contributes negligibly to the inverse screening length (low-intensity limit), one can show from Eqs. (5), (6), and (11) that

$$\begin{aligned} \Phi(I) = & -\frac{\omega}{nc} \frac{\epsilon_F \epsilon_B T}{e^2} \sum_{i=1}^l \sum_{j=1}^l \frac{k_{0i}^2(I) k_{0j}^2(I)}{k_0^2(I)} \left(\frac{s_j I}{\beta_j + s_j I} \right) \\ & \times \text{Im}(\Delta p_j - \Delta p_i). \end{aligned} \quad (12)$$

Note that the offset $\Phi(I)$ depends on the difference between the imaginary parts of Δp_j for different levels. If this difference is zero, the offset disappears. Both $\Gamma_{\text{abs}}(I)$ and $\Phi(I)$ depend on the optical frequency, primarily through the spectral response of the different polarizabilities. In the case of one active level, $\Phi(I)$ is zero, since ϕ vanishes.

The offset term $\Phi(I)$ is the grating analog to the bulk light-induced absorption discussed in Ref. 7, in which a spatially uniform light beam alters the populations of the various trapping levels. Since the polarizabilities of full and empty traps are different in general, the bulk absorption of the crystal can change with the light intensity. The change in the bulk absorption of the crystal, $\Delta\alpha(I)$, is given by

$$\Delta\alpha(I) = \frac{\omega}{nc} \sum_{j=1}^l [N_{j0}^F(I) - N_{j0}^F(0)] \text{Im}(\Delta p_j). \quad (13)$$

In Eq. (13) we have neglected the absorption of any free charges in the band.

Both the offset term $\Phi(I)$ and the light-induced absorption coefficient $\Delta\alpha(I)$ result from the redistribution of charge among different levels at the same spatial location. Nevertheless, these coefficients are not the same. The offset term $\Phi(I)$ originates from diffraction off a grating. This is a coherent process, unlike bulk light-induced absorption, which does not require interference. Also, it can be shown that $\Phi(I)$ tends to zero at low and high optical intensities, while in general the light-induced absorption saturates at a nonzero value at high optical intensities.

Because of the offset term $\Phi(I)$ in Eq. (8), the gain per unit length, $\gamma_{\text{abs}}(I, k_g)$, does not vanish as k_g approaches zero. Note that a grating cannot be defined when $k_g = 0$. In fact, our beam-coupling approach breaks down when the grating spacing becomes comparable with the spot size of the smaller optical beam.

C. Electro-optic Gain

The electro-optic gain per unit length in the multilevel model has the surprisingly simple form⁵

$$\gamma_{\text{eo}}(I, k_g) = \Gamma_{\text{eo}}(I) \frac{2k_g/k_0(I)}{1 + k_g^2/k_0^2(I)} \hat{e}_1 \cdot \hat{e}_2^{*2}, \quad (14)$$

where the dependence on k_g is the same as in the single-level model. The intensity dependence of the maximum gain per unit length, $\Gamma_{\text{eo}}(I)$, is now given by a weighted sum similar in form to Eq. (9):

$$\Gamma_{\text{eo}}(I) = \frac{\omega}{2nc} \frac{k_B T}{e} r_{\text{eff}} \sum_{j=1}^l \frac{k_{0j}^2(I)}{k_0(I)} \left(\frac{s_j I}{\beta_j + s_j I} \right), \quad (15)$$

where r_{eff} is the effective Pockels coefficient. An offset does not appear in the electro-optic gain; the ϕ_j terms cancel out exactly. Physically, these terms cancel because the electro-optic effect requires a space-charge field, and exciting a charge from one level to another at the same location does not produce an electric field.

3. EXPERIMENT

We measured the two-beam coupling gain due only to absorption gratings by using a geometry in which electro-optic coupling was effectively eliminated. In BaTiO₃ the

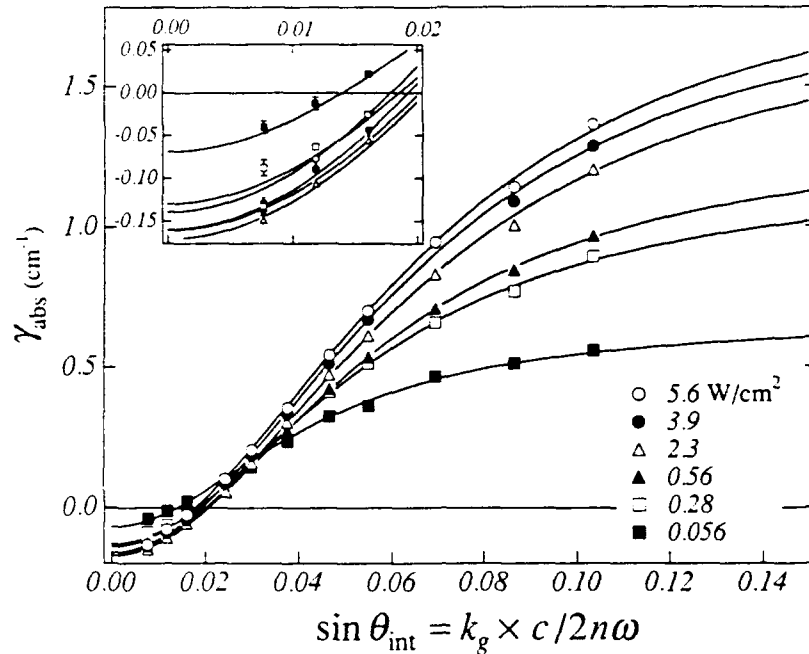


Fig. 2. Two-beam coupling absorption grating gain per unit length, γ_{abs} , versus internal half-angle θ_{int} in BaTiO₃ (the Free crystal) at six intensities for $\lambda = 488$ nm. The solid curves are fits to Eq. (8). The gain does not vanish as the crossing angle goes to zero, but it reaches an offset value Φ . In the inset the offset can clearly be seen to be negative. The magnitude of the offset and the absorption-grating gain both vary with intensity.

electro-optic coupling vanishes if the c axis of the crystal is aligned perpendicularly to the plane of incidence and if two beams (which we call the reference and the probe beam) are polarized in the plane of incidence, making them ordinary rays in the crystal. The reference beam (beam 2) was always at least ten times more intense than the probe beam (1), so that we were always in the low-modulation, undepleted-pump regime. We define an experimental coupling gain per unit length, γ , by

$$\gamma = \frac{1}{L} \ln \left[\frac{I_{probe}(\text{with a grating present})}{I_{probe}(\text{without a grating present})} \right], \quad (16)$$

where I_{probe} is the intensity of the transmitted probe beam and L is the interaction length. As Eq. (16) implies, we want to measure that gain caused by diffraction from a grating and not from any light-induced change in the bulk absorption. We accomplish this by never turning off the optical beams; when we need to eliminate the grating, we wash it out by rapidly vibrating one of the mirrors in the reference beam's optical path. In this way we eliminate any contribution from light-induced absorption because the total intensity incident on the crystal is never altered. More details on this experimental procedure are given in Ref. 11.

A. Absorption-Grating Measurements

Figure 2 shows the measured two-beam coupling gain per unit length, γ_{abs} , due to absorption gratings in one BaTiO₃ crystal (called the Free crystal). Here we have fixed the wavelength at $\lambda = 488$ nm and varied the crossing angle between the two optical beams. We varied the total intensity of the two beams over a range of 100 while keeping the ratio of their intensities fixed. The solid curves in Fig. 2 are fits to Eq. (8). The inset of this figure is a blowup of

the data near the origin. A single-level model would require the absorption-grating coupling to pass through the origin¹¹; this clearly does not occur here. Figure 3(a) shows the absorption-grating gain per unit length in the same crystal at $\lambda = 458$ nm and $\lambda = 488$ nm. (We also performed experiments at $\lambda = 515$ nm and $\lambda = 476$ nm.) At all these wavelengths the gain changed similarly with intensity, but the size of the offset decreased with increasing wavelength. At $\lambda = 515$ nm the offset was so small that we missed it in our previous study.¹¹ This absorption-grating offset must still be present in a geometry that permits an electro-optic grating. This accounts for the offset seen in Fig. 3(b), which was obtained with the crystal orientation shown in the inset and which permits electro-optic beam coupling by means of the Pockels coefficient r_{13} .

In order to compare the intensity dependence of the offset $\Phi(I)$ with the theoretical model, we must choose the number of active levels. The simplest multilevel case is to assume that there are only two levels: one active donor level and one active acceptor level. We also assume that only hole conduction occurs, and we ignore thermal excitation from the deep donor level but not from the shallow acceptor level. With these approximations we find that

$$\Phi(I) = \frac{\omega}{nc} \frac{\beta_A}{\beta_A + s_A I} \frac{N_{D0}^F \text{Im}(\Delta p_D - \Delta p_A)}{\frac{N_A}{N_A - N_{D0}^F} + \frac{N_D}{N_D - N_{D0}^F}}. \quad (17)$$

The intensity dependence of $N_{D0}^F(I)$ is given by

$$N_{D0}^F(I) = \frac{N_D + N_A \pm [(N_D + N_A)^2 - 4N_D N_A G]^{1/2}}{2G}, \quad (18)$$

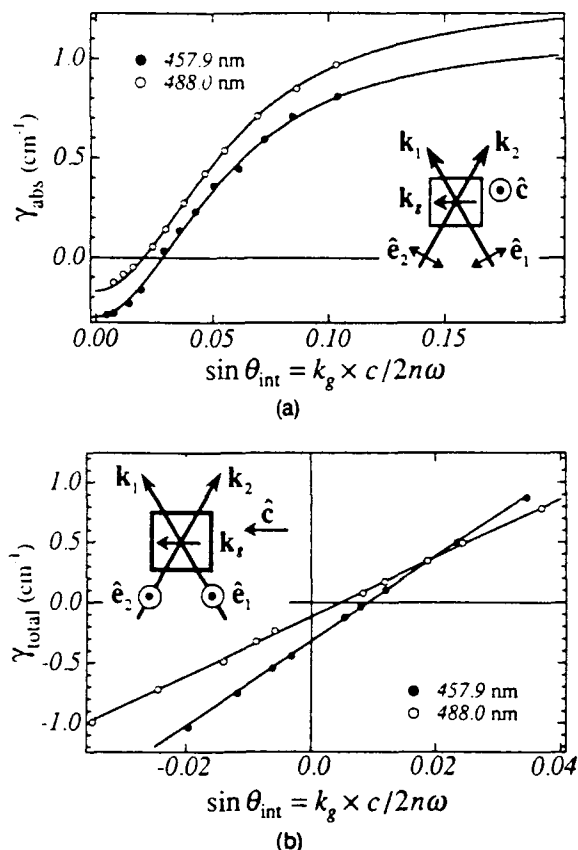


Fig. 3. Two-beam coupling gain per unit length at $\lambda = 458$ nm and $\lambda = 488$ nm in BaTiO_3 (the Free crystal) at $I = 0.6$ W/cm^2 with (a) the pure absorption-grating configuration and (b) the absorption-plus-electro-optic grating configuration. In (b) the sign of the crossing angle is the same as the sign of $\mathbf{k}_x \cdot \hat{\mathbf{c}}$, where the positive direction of $\hat{\mathbf{c}}$ is chosen as in Ref. 2. The solid curves in (a) and (b) are fits to Eqs. (8) and (21), respectively. The insets show the beam-coupling geometry used for these two experiments. For a given wavelength the gain for both electro-optic and absorption measurements at $k_x = 0$ is the same, corresponding to the absorption-grating offset discussed in the text.

where

$$G \equiv 1 - \frac{\gamma_A s_D}{\gamma_D s_A} \frac{s_A I}{\beta_A + s_A I}. \quad (19)$$

The subscripts A and D in Eqs. (17)–(19) refer to the acceptor and donor levels, respectively. Even with only two levels there are four free parameters in these equations, enough to require a large number of data points over a wide range of intensities in order to make a meaningful theoretical fit. We measured the absorption-grating two-beam coupling gain per unit length coefficient at $\lambda = 488$ nm in the Free crystal of BaTiO_3 at a small crossing angle (external half-angle 0.4°) with an intensity variation spanning more than four orders of magnitude. At this small angle the offset $\Phi(I)$ dominates the coupling. Since β_A is temperature dependent, the crystal was mounted on a copper block and immersed in a water bath maintained at a temperature $T = (17.7 \pm 0.2)^\circ\text{C}$. Figure 4 shows these data and the curve fit to Eq. (17). The fitting parameters are

$$N_A/N_D = 0.97 \pm 0.02,$$

$$\beta_A/s_A = 0.95 \pm 0.06 \text{ W/cm}^2,$$

$$(\gamma_A/\gamma_D)(s_D/s_A) = 0.031 \pm 0.006, \text{ and}$$

$$(\omega/\text{nc})N_D \text{Im}(\Delta p_D - \Delta p_A) = -6.2 \pm 0.5 \text{ cm}^{-1}.$$

A striking aspect of our fit to the data in Fig. 4 is that N_A/N_D is nearly unity; the crystal is nearly compensated. When we use this value for N_A/N_D and the other curve-fit parameters, this two-level model predicts that the inverse screening length k_0 should be small at low intensities and increase monotonically with intensity.⁴ Figure 5 shows the values of k_0 obtained from the curve fits of the data in Fig. 2 above. As predicted, the magnitude of k_0 is small at low intensities and appears to saturate at intensities close to 3 W/cm^2 ; over the range of intensities used, the variation of k_0 shown in Fig. 5 is 60%.

B. Bulk Light-Induced Absorption Measurements

As mentioned in Subsection 2.B, the offset grating gain is related to the light-induced absorption. Again, when we

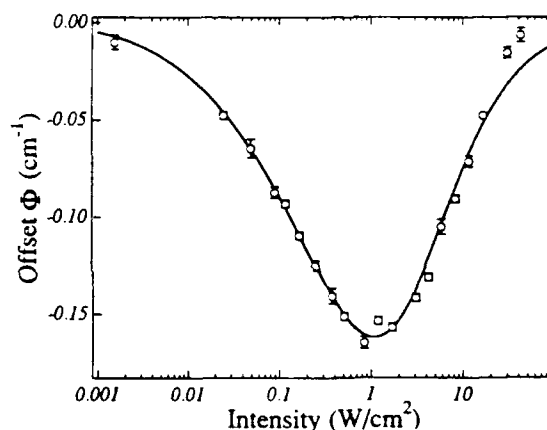


Fig. 4. Absorption-grating gain per unit length as a function of incident intensity at $\lambda = 488$ nm at an external crossing half-angle of 0.4° in the Free crystal of BaTiO_3 . [Note that at this angle the gain is due only to the offset $\Phi(I)$, to within a maximum error $< 0.004 \text{ cm}^{-1}$.] The solid curve is a four-parameter fit to a two-level model using Eq. (17). The temperature was $(17.7 \pm 0.2)^\circ\text{C}$.

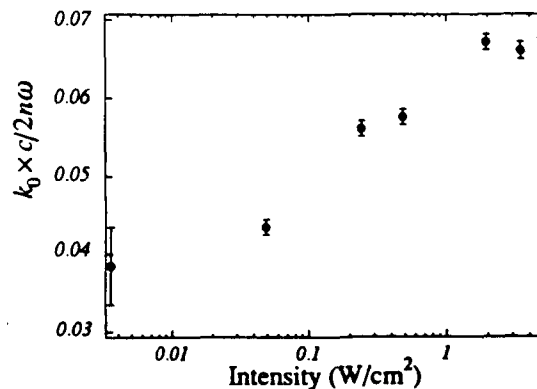


Fig. 5. Inverse screening length k_0 in units of $2n_0/c$ versus incident intensity at $\lambda = 488$ nm in the Free crystals of BaTiO_3 . The data points were obtained from curve fits to the data in Fig. 2. In the two-level model the magnitude of k_0 is expected to saturate at high intensities and to reach a constant value at low intensities.

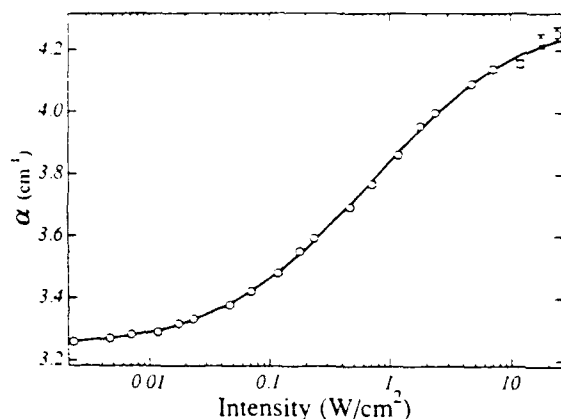


Fig. 6. Measured bulk absorption versus incident intensity in the Free crystal at $\lambda = 488$ nm, ordinary polarization, and $T = (17.8 \pm 0.2)^\circ\text{C}$. The solid curve is a fit to Eq. (20).

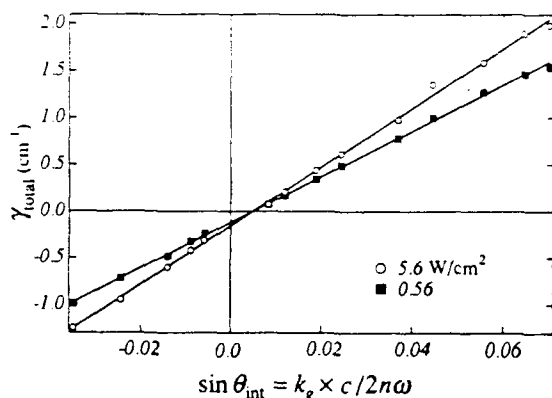


Fig. 7. Total (absorption-plus-electro-optic) two-beam coupling gain per unit length versus k_g in the Free crystal of BaTiO_3 , obtained with the geometry of Fig. 3(b). The data are curve fits to Eq. (21).

use the two-level model described above, the bulk absorption is given by

$$\alpha(I) = \alpha_0 + (\omega/nc)(N_{D0}^F - N_A)(\Delta p_D - \Delta p_A) \quad (20)$$

for $N_A < N_D$. Here α_0 is the absorption as the light intensity approaches zero. For an ordinary ray incident at Brewster's angle (to eliminate reflections) we measured $\alpha_0 = 3.25 \text{ cm}^{-1}$ at 488 nm in the Free crystal. Figure 6 shows the measured absorption $\alpha(I)$ versus intensity in the Free crystal at 17.7°C for an ordinary ray at 488 nm and a fit to Eq. (20) made using our measured values for α_0 . The parameters used in this fit correspond to those used in the curve fit of the offset data in Fig. 4 above, and the values obtained for these parameters are in good agreement with those determined from Fig. 4: $N_A/N_D = 0.96 \pm 0.02$, $\beta_A/s_A = 0.73 \pm 0.06 \text{ W/cm}^2$, $\gamma_{ASD}/\gamma_{DSA} = 0.033 \pm 0.007$, and $(\omega/nc)N_D \text{Im}(\Delta p_D - \Delta p_A) = -7.6 \pm 0.7 \text{ cm}^{-1}$.

In our curve fits for both the bulk light-induced absorption and the offset grating gain we have taken into account the intensity variation of the optical beams in the crystal caused by both background and light-induced absorption. All the intensities in this paper are the incident

intensities, corrected for calculated Fresnel losses, as would be measured just inside the crystal face.

C. Electro-Optic Grating Measurements

Absorption gratings and electro-optic gratings can exist simultaneously. In particular, the absorption-grating offset $\Phi(I)$ appears as an offset in any measurement of electro-optic coupling, becoming evermore apparent as k_g approaches zero. Since the size of the offset does not depend on the relative dc dielectric constants of the crystal, its magnitude does not depend on the crystal's orientation. We verified this by measuring the two-beam coupling gain in a geometry where the effective Pockels coefficient was not zero, so that both absorption gratings and electro-optic gratings were present, as shown in Fig. 3(b) above. We aligned the c axis of the crystal in the plane of incidence and parallel to the grating wave vector k_g and made the optical polarizations perpendicular to the plane of incidence, so that both beams were ordinary rays as before. The total observed coupling is given by the sum of Eqs. (8) and (14), which for small values of k_g can be approximated by

$$\gamma_{\text{total}}(I) = \gamma_{\text{eo}}(I) + \gamma_{\text{abs}}(I) \approx 2\Gamma_{\text{eo}}(I)[k_g/k_0(I)] + \Phi(I). \quad (21)$$

Figure 3(b) shows two sets of data taken in the Free crystal at $\lambda = 488$ nm and $\lambda = 458$ nm. The solid lines are linear fits according to Eq. (21). The values of the offset $\Phi(I)$ obtained from these fits agree with those obtained from the absorption-grating data. At $\lambda = 458$ nm and $I = 0.6 \text{ W/cm}^2$ the offset determined from the pure absorption-grating experiment is $\Phi(I) = -0.30 \text{ cm}^{-1}$, while that determined from the combined absorption-plus-electro-optic coupling configuration is almost identical, namely, $\Phi(I) = -0.33 \text{ cm}^{-1}$. Similarly, at $\lambda = 488$ nm and $I = 0.55 \text{ W/cm}^2$ the offsets in the pure absorption and the absorption-plus-electro-optic coupling experiments were $\Phi(I) = -0.12 \text{ cm}^{-1}$ and $\Phi(I) = -0.17 \text{ cm}^{-1}$, respectively. We also varied the total intensity and noted that the slopes of these graphs increased, as shown in Fig. 7, owing to the expected increase of $\Gamma_{\text{eo}}(I)$ with I . The same set of experiments was performed on another crystal (called the Swiss crystal). Compared with the Free crystal, the Swiss crystal has less absorption and shows little light-induced absorption. Consequently, the magnitudes of the absorption-grating coupling and the offset $\Phi(I)$ are smaller. For example at $\lambda = 456$ nm and $I = 0.7 \text{ W/cm}^2$, $\Phi(I) = -0.050 \text{ cm}^{-1}$ and $\Phi(I) = -0.067 \text{ cm}^{-1}$ for the Swiss crystal, as determined by pure absorption gratings and absorption-plus-electro-optic gratings, respectively. As in the other crystals, the magnitude of this negative offset was largest for $\lambda = 456$ nm, somewhat smaller at $\lambda = 488$ nm, and too small to be measured by our techniques at $\lambda = 515$ nm.

The offset term of absorption gratings can confuse the interpretation of two-beam coupling experiments. For example, in the usual beam-coupling geometry [shown in Fig. 3(b) above], where both absorption gratings and electro-optic gratings are present, the offset causes the coupling strength to flip sign at a finite crossing angle. In BaTiO_3 this may not be noticed at $\lambda = 515$ nm, where the offset is small, but it becomes increasingly prominent as the wavelength is decreased. In fact, Klein and Valley¹⁴

observed that at $\lambda = 442$ nm the sign of the two-beam coupling strength flipped sign in one of their BaTiO₃ crystals (GB-5) as the beam-crossing angle was increased. Strohkendl *et al.*¹⁵ later explained this anomaly by invoking electron-hole competition from a single active level. We had considered an alternative explanation for their experimental data, namely, the presence of a large offset from absorption gratings. However, we performed beam-coupling experiments on this same crystal GB-5 at $\lambda = 442$ nm, and we found that the offset (and the magnitude of the absorption grating) was small, which rules out absorption gratings as an explanation for this crystal's anomalous behavior.

4. CONCLUSION

We have shown that there are two ways that charge can redistribute in a multilevel crystal: among various spatially separated trapping centers or between different trapping levels at roughly the same location. This latter contribution does not produce any electro-optic coupling, since no electric field is produced; however, it causes an additional absorption grating that remains finite even as the crossing angle of the beams approaches zero. By measuring this offset gain, we are able to determine certain physical parameters of a barium titanate crystal that agree well with the values obtained through bulk light-induced absorption measurements. We find that the magnitude of this offset gain per unit length, $\Phi(I)$, varies strongly with wavelength in our BaTiO₃ crystals, ranging from almost zero at $\lambda = 515$ nm to more than 0.3 cm^{-1} at $\lambda = 458$ nm. We have also shown that once there are at least two active levels, the functional dependence of the absorption-grating gain and the electro-optic gain on k_x is independent of the number of active levels.

ACKNOWLEDGMENTS

We would like to thank Marvin Klein for the loan of the crystal GB-5 and Armand Tanguay, Jr., for the loan of a He-Cd laser. We gratefully acknowledge support from U.S. Air Force Office of Scientific Research contract F49620-88-C-0095.

REFERENCES

1. N. V. Kukhtarev, V. B. Markov, S. G. Odoulov, M. S. Soskin, and V. L. Vinetskii, "Holographic storage in electrooptic crystals. I. Steady state," *Ferroelectrics* **22**, 949 (1979).
2. J. Feinberg, D. Heiman, A. R. Tanguay, Jr., and R. W. Hellwarth, "Photorefractive effects and light-induced charge migration in barium titanate," *J. Appl. Phys.* **51**, 1297 (1980); **52**, 537(E) (1981).
3. L. Holtmann, "A model for the nonlinear photoconductivity of BaTiO₃," *Phys. Status Solidi (A)* **K89**, 113 (1989).
4. D. Mahgerefteh and J. Feinberg, "Explanation of the apparent sublinear photoconductivity of photorefractive barium titanate," *Phys. Rev. Lett.* **64**, 2195 (1990).
5. D. D. Nolte, D. H. Olson, and A. M. Glass, "Nonequilibrium screening of the photorefractive effect," *Phys. Rev. Lett.* **63**, 891 (1989).
6. A. Motes and J. J. Kim, "Intensity-dependent absorption coefficient in photorefractive BaTiO₃ crystals," *J. Opt. Soc. Am. B* **4**, 1379 (1987).
7. G. A. Brost, R. A. Motes, and J. R. Rotge, "Intensity-dependent absorption and photorefractive effects in barium titanate," *J. Opt. Soc. Am. B* **5**, 1879 (1988).
8. A. V. Alekseev-Popov, A. V. Knyaz'kov, and A. S. Saikin, "Recording volume amplitude-phase holograms in a lead-lanthanum zirconate-titanate ceramic," *Sov. Tech. Phys. Lett.* **9**, 475 (1983).
9. K. Walsh, T. J. Hall, and R. E. Burge, "Influence of polarization state and absorption gratings on photorefractive two-wave mixing in GaAs," *Opt. Lett.* **12**, 1026 (1987).
10. R. B. Bylisma, D. H. Olson, and A. M. Glass, "Photochromic gratings in photorefractive materials," *Opt. Lett.* **13**, 853 (1988).
11. R. M. Pierce, R. S. Cudney, G. D. Bacher, and J. Feinberg, "Measuring photorefractive trap density without the electro-optic effect," *Opt. Lett.* **15**, 414 (1990).
12. P. Tayebati, "Characterization and modeling of the photorefractive effect in bismuth silicon oxide," Ph.D. dissertation (University of Southern California, Los Angeles, Calif., 1989); P. Tayebati and D. Mahgerefteh, "Theory of the photorefractive effect for Bi₁₂SiO₂₀ and BaTiO₃ with shallow traps," *J. Opt. Soc. Am. B* **8**, 1053 (1991).
13. A. V. Knyaz'kov and M. N. Lobanov, "Absorption modulation under hologram formation in photorefractive materials," in *Topical Meeting on Photorefractive Materials, Effects and Devices II* (Optical Society of America, Washington, D.C., 1990), pp. 112-113.
14. M. B. Klein and G. C. Valley, "Beam coupling in BaTiO₃ at 442 nm," *J. Appl. Phys.* **57**, 4901 (1985).
15. F. P. Strohkendl, J. M. C. Jonathan, and R. W. Hellwarth, "Hole-electron competition in photorefractive gratings," *Opt. Lett.* **11**, 312 (1986).

JF
AS SENT
4/26/91
JOSA

SELF-BENDING OF LIGHT BEAMS IN PHOTOREFRACTIVE PHASE CONJUGATORS

V.V. Eliseev

*General Physics Institute, Academy of Sciences of the USSR,
38 Vavilov St., Moscow, 117924, USSR.*

A. A. Zozulya

*P. N. Lebedev Physical Institute, Academy of Sciences of the USSR,
Leninsky pr. 53, Moscow, 117924, USSR.*

G. D. Bacher and Jack Feinberg

*Departments of Physics and Electrical Engineering
University of Southern California, Los Angeles, CA 90089-0484
Tel. (213) 740-1134*

ABSTRACT

Stimulated photorefractive phase-conjugators often exhibit well-defined, curved beam paths, which cannot be accounted for by simple beam fanning. We propose a model that suggests that these apparently curved paths are composed of a series of straight-line segments, with beams propagating in both directions along these paths. These line segments initially form by the amplification of scattered light between regions of the crystal already

possessing counterpropagating pump beams. As these line segments form they create new interaction regions that generate new segments, thereby making the final beam path appear to be curved. Application of our model to a single-interaction-region mutually-pumped phase-conjugator shows that the threshold coupling strength required for the appearance of these new segments is only slightly larger than the threshold for the phase-conjugate mirror itself.

INTRODUCTION

Light beams propagating through a photorefractive crystal are like politicians: if given the opportunity they choose the path that maximizes their own gain. Here we propose a detailed though necessarily simplistic description of how light beams spring up inside a photorefractive crystal, and why under some conditions these stimulated light beams follow curved paths. We show that these curves are formed by a sequence of straight-line segments connecting many four-wave mixing regions inside the crystal.

In recent years a variety of photorefractive devices have been demonstrated that rely on stimulated light beams to perform optical phase conjugation. These self-pumped and mutually-pumped phase conjugators, which include the cat mirror¹, the double phase-conjugate mirror², the bird-wing³, the frog-legs⁴, the bridge conjugator⁵ and the unnamed-geometry of Smout and Eason⁶ are all closely related⁷ and differ only in the number and angle of their input beams.

Figure 1 is a photomicrograph of stimulated beams inside a cat conjugator.¹ The stimulated beams have collapsed into narrow filaments (for reasons that will not be discussed here). These filaments appear to follow curved paths but upon close inspection the curves are seen to consist of a series of straight-line segments connected by distinct bends. Our model requires that the filaments themselves consist of counterpropagating waves. We show that two separated regions inside the crystal, each having its own pair of counterpropagating waves, can "find" each other with new

light beams, provided that the total round-trip reflectivity of a small seed wave between these regions is greater than unity. Our model predicts a sequence of such couplings, so that the path of the filaments eventually resembles a curved trajectory.

Consider the case of two counterpropagating beams already present inside a photorefractive crystal, as shown in Fig. 2. If a reflecting surface, such as a mirror or a wedding ring, is placed nearby, then a beam of light will spring up between the crystal and the reflecting surface, provided that the photorefractive coupling strength exceeds a certain threshold.⁸ These stimulated beams grow and reach steady state when the reflectivity of the photorefractive phase conjugator declines to $1/M$, where M is the reflectivity of the mirror. The crystal acts as a phase conjugator with gain: it returns light from the mirror back to the mirror. If the mirror surface is replaced by a second photorefractive crystal, also pumped by two counterpropagating beams, then a beam of light can spring up between the two crystals; they will "find" each other and direct counterpropagating light beams from one to the other,⁹ as shown in Fig. 2b. Instead of two crystals one could consider two separate regions inside the same crystal, as shown in Fig. 2c. In that case a pair of counterpropagating beams can spring up between these two regions. These new counterpropagating beams now make new interaction regions available, allowing new beams to spring up, as shown in Fig. 3. This "bifurcation" can occur repeatedly, with each new pair of counterpropagating beams serving as a springboard for the generation of more such beam pairs.

STIMULATED SCATTERING AND PHASE CONJUGATION

When a single laser beam traverses a photorefractive crystal, imperfections and defects in the crystal scatter the incident light. The scattered light can coherently interfere with the incident beam to create a multitude of photorefractive gratings in the crystal. A subset of the light scattered from these gratings will reinforce the originally scattered beams, and these beams grow exponentially with distance in the crystal and emerge in a broad fan of light.

Now let two (preferably mutually incoherent) laser beams be incident on the right and left crystal boundaries with optical intensities I_R and I_L , respectively. Let the two beams intersect inside the crystal, as shown in Fig. 3a. Because the two beams are mutually incoherent, they will not interfere with each other. However, each incident beam will interfere with its own randomly scattered beams to create its own armada of photorefractive gratings inside the crystal. The particular grating that diffracts beam R into the phase-conjugate of beam L will also diffract beam L into the phase conjugate of beam R, by time-reversal symmetry.² Because this grating is common to both beams, it is preferentially reinforced. In the simplest such mutually-pumped phase conjugator (the geometry of Fig. 3a) the intensity transmission T_0 of the device, defined as the fraction of the light input into one face that emerges phase-conjugate to the beam at the other face, is found by solving the following equations:²

$$T_0 = \frac{c^2(q^{1/2} + q^{-1/2}) - (q^{1/2} - q^{-1/2})}{4} \quad (1)$$

$$c = \tanh\left(\frac{\Gamma_0 c}{2}\right) \quad (2)$$

where $q = I_R/I_L$ is the ratio of intensities of the two incident beams, and Γ_0 is the coupling strength. These equations yield non-trivial solutions only if the coupling strength exceeds a threshold value $\Gamma_0 \geq [(q+1)/(q-1)] \ln q$.

NEW BEAMS

Just above threshold the configuration of a single interaction region turns out to be unstable: arbitrarily weak beams will grow between two new regions of the nonlinear medium, with each region pumped by two counterpropagating waves as shown in Fig. 3b. The threshold for this instability occurs when the round-trip reflectivity of a weak "seeding" beam between the right and left regions in Fig. 3b exceeds unity:

$$R_{Right} R_{Left} \geq 1. \quad (3)$$

In Eq. (3) R_{Right} is the phase-conjugate intensity reflectivity for the beam incident on the right region from the left region, and similarly R_{Left} for the left region. These reflectivities can be computed from the traditional four-wave mixing equations of Ref. 10, where the usual counterpropagating pumping beams are here taken to be the conjugate pairs I_L and I_L^C in the right region, and I_R and I_R^C in the left region. We obtain:

$$R_{Left} = \frac{I_L}{I_L^C} \frac{[1 - \exp(-\Gamma_{left})]^2}{[1 + (I_L/I_L^C) \exp(-\Gamma_{left})]^2}$$

$$R_{Right} = \frac{I_R}{I_R^C} \frac{[1 - \exp(-\Gamma_{right})]^2}{[1 + (I_R/I_R^C) \exp(-\Gamma_{right})]^2}.$$

In general, the values of coupling coefficients in the various regions are all different. However, for simplicity we will here take them all to be the same $\Gamma_0 = \Gamma_{left} = \Gamma_{right} \equiv \Gamma$ for the remainder of our analysis. Even in this case we show that the system prefers to generate new beams, and that (except near threshold) these new beams increase the overall phase-conjugate reflectivity of the device.

Figure 4 shows the calculated threshold for phase conjugation vs. the incident beam ratio q when there is only one interaction region, and also for the case in which the system has already "bifurcated" once to create three interconnected regions. Note that a single interaction region will become unstable for a coupling strength even slightly larger than the single-region threshold. For example, for the case $q = 1$ the single region threshold (no bifurcations) is $\Gamma_{th}^{(0)} = 2$, while the three-region threshold (one bifurcation) is only slightly larger: $\Gamma_{th}^{(1)} = 2.026$. For even larger values of Γ the system may undergo further bifurcation, as shown in Fig.3c. This process will continue, with new beams springing up to connect new interaction regions, and so carve out a path made of many straight-line segments that approximates a curved trajectory. Because there is no unique

path for the bifurcation, it is possible for different paths to be favored sequentially. This would cause the phase-conjugate signal to oscillate in time, as has been observed in the bird-wing and cat conjugators.¹¹⁻¹³

COUPLED-WAVE EQUATION

We analyze the 3-region geometry of Fig. 3b by inspecting the slowly-varying amplitudes A_j ($j=1-4$) of the electromagnetic waves in each of the three interaction regions. For the geometry of Fig. 5 these amplitudes vary according to:¹⁰

$$\begin{aligned}
 \frac{\partial A_1}{\partial x} &= v A_4 \\
 \frac{\partial A_2^*}{\partial x} &= v A_3^* \\
 \frac{\partial A_3}{\partial x} &= -v A_2 \\
 \frac{\partial A_4^*}{\partial x} &= -v A_1^* \\
 v &= \frac{\gamma}{I_0} (A_1 A_4^* + A_2^* A_3)
 \end{aligned} \tag{4}$$

In Eqs. (4) $I_0 \equiv \sum_{j=1}^4 A_j^2$, $0 \leq x \leq l$, and $\gamma = \Gamma / l$ is the coupling coefficient

per unit length. Here we will consider only the case of a purely real coupling coefficient γ (which corresponds to a 90° phase shift between the light pattern and the resulting refractive-index pattern in the

photorefractive crystal).¹⁴ For this case the wave amplitudes A_j can all be taken as real without loss of generality.

The boundary conditions on the four wave amplitudes A_j ($j=1-4$) differ here from those usually used. Consider the right region shown in Fig. 3b with the beams labeled as in Fig.5. The usual boundary condition is to set the conjugate-wave amplitude to be zero at the right-hand boundary: $A_3(l) = 0$. Instead, here we let the conjugate wave be seeded by scattered light, so that $A_3(l) = \sqrt{\epsilon} A_2(l)$. Physically, this seed is caused by the scattering from crystal defects of wave 2 into wave 3. We let the total amount of scattering remain constant but let the "seeding" parameter $\sqrt{\epsilon} \ll 1$ determine the fraction of the scattered light from amplitude $A_2(l)$ that is scattered into precisely the amplitude $A_3(l)$. In the left region we use a similar seeded boundary condition, and for simplicity we have set the scattering strength to be the same in both of these regions. We set the phase of these scattered beams so that the light scattered from the left region exactly reinforces the grating forming in the right region, and vice versa.

In the top region we could also replace the usual boundary conditions for a double phase-conjugate mirror with the seeded boundary conditions, but we found that for $\epsilon \ll 1$ the presence of finite seeding beams in this top region have a negligibly small influence on the behavior of the various waves except when the coupling coefficient is very near the threshold $\Gamma \equiv \Gamma_{th}^{(0)}$. Therefore we set $\epsilon = 0$ in the top region but keep ϵ finite in the other two regions. The presence of these seed beams in the left

and right regions becomes especially important at large coupling strengths; they determine the asymptotic behavior of the system as $\Gamma \rightarrow \infty$.

In Figure 3b light entering from the bottom left has the choice of two different paths before it exits at the bottom right, either by a single diffraction from the grating at the top or by two successive diffractions at the left and right regions. These two paths will interfere provided the difference in their lengths is within the coherence length of the incident laser beam. (A similar interference will also occur for light beams propagating from the right to the left.) For the case of a purely real coupling coefficient γ this interference will always be exactly constructive irrespective of the lengths of the two optical paths. For example, consider the beam that propagates from the left region directly to the right region. This beam will always add constructively to the beam coming from the top region (as in two-beam energy coupling).

RESULTS

When bifurcations occur new beams spring up and the overall transmission T of the system changes. For the case of equal intensity input beams ($q=1$) the dependence of the transmission on the coupling strength Γ is shown in Fig. 6. Here the effect of the additional beam path is seen in the sharp jump in the transmission when Γ increases above the first bifurcation threshold $\Gamma_{th}^{(1)}$ as shown in the inset of Fig. 6. The bifurcation increases the overall transmission of the device because the portion of the input not diffracted by the grating in the left region will still be partially redirected by the grating at the top and will recombine coherently with the diffracted beam in the right region. The original grating serves to 'catch'

some of the light that slips through the new gratings and redirects it into the phase-conjugate beam.

Consider the symmetric case of equal intensity input beams ($q=1$). Define T^* to be the fraction of beam I_L input into the left side of the crystal that is deflected by the left interaction region into the right interaction region (i.e., the intensity diffraction efficiency of beam 2 into beam 4 described in the Appendix). Then we obtain $T^* = (\sqrt{T} - \sqrt{T_0}) / (1 - \sqrt{T_0})$, where T_0 is defined before Eq. (1) and T is the overall intensity transmission of the entire three-region device. Figure 7 illustrates the dependence of the diffraction efficiency T^* of either the left or right region (these two diffraction efficiencies are equal when $q=1$) on the coupling strength, for several different values of the seeding parameter ϵ . For any finite value of ϵ , T^* asymptotically approaches unity for large coupling strength Γ , but the form of the approach depends on the value of the seed. For $q=1$ and for large values of coupling strength we find that

$$T^* = 2\Gamma \exp(-\Gamma) + \sqrt{\frac{\epsilon(1-T^*)}{T^*}} \exp(\Gamma). \quad (5)$$

As T^* approaches 1, an increasing amount of light is channeled between regions the left and right interaction regions, so that the A shaped pattern in Fig. 8a begins to resemble the sawed-off pattern of Fig. 8b. Note that Fig. 8b can be viewed as two mutually-pumped phase conjugators sharing a common set of beams, and both the dynamic behavior and the

stationary states of such a system have been shown to be critically dependent on the values of the seeds.^{15,16}

In order to explore the behavior of the system with unequal input beam intensities ($q \neq 1$), we repeated our analysis for the case of $q=2$. The equations are less symmetric now, and each interaction region has a different diffraction efficiency. Nevertheless the overall transmission of the device is quite similar to the $q=1$ case, as shown in Fig. 9. However with $q=2$ there is now a small region of Γ just past threshold where the overall transmission decreases when the additional beams appear, as shown in the inset of Fig. 9. In Fig. 10 we plot the diffraction efficiencies of each of the left and right regions vs. the coupling strength. The stronger beam is input on the left, and the weaker beam on the right. Note that the diffraction efficiency is larger in the region with the weaker input beam. The asymmetry in the strength of the two bifurcation gratings is evident in Fig. 10, especially near threshold. Just above threshold we found a region of Γ for which the system oscillates between two states, first bifurcating and then relaxing back to the initial un-bifurcated state.

For $q \neq 1$ there is no longer a simple relation among the various grating efficiencies as in Eq. (5). We find numerically that the asymptotic behavior as $\Gamma \rightarrow \infty$ of each region's diffraction efficiency is similar to the $q=1$ case, so that for any finite seed the bifurcation path dominates as Γ becomes large.

In summary, we have presented a simple model to explain the bending of light beams in various self-pumped and mutually-pumped phase conjugators. This model attributes the growth of curved beam paths inside

the crystal to a series of straight-line segments caused by a couplings between adjacent regions inside the crystal, each pumped by counterpropagating waves. We have shown that including a small but finite amount of scattered light is crucial for describing this self-bending. The bifurcation occurs even when the gratings in all three regions are taken to have the same coupling strength. In practice, one should include the dependence of coupling strength on both the crossing angle and the orientation of the light beams inside the crystal, which can make the bifurcation path even more favorable. Also, we note that there are usually a multitude of possible bifurcation paths which compete for the available light energy, and that the light path could oscillate repeatedly between them.

MATHEMATICAL APPENDIX

Consider a four-wave mixing region, described by the set of equations:¹⁷

$$\begin{aligned}\frac{\partial A_1}{\partial x} &= \nu A_4 \\ \frac{\partial A_2^*}{\partial x} &= \nu A_3^* \\ \frac{\partial A_3}{\partial x} &= -\nu A_2 \\ \frac{\partial A_4^*}{\partial x} &= -\nu A_1^* \\ \nu &= \frac{\gamma}{I_0} (A_1 A_4^* + A_2^* A_3)\end{aligned}\tag{A1}.$$

The values of waves 1, 2, and 4 are fixed at the beginning of the interaction region:

$$A_1(0), A_4(0), A_2(l),$$

and wave 3 is seeded:

$$A_3(l) = \sqrt{\epsilon} A_2(l)\tag{A2}$$

We assume that γ is real. In this case, the fields can be taken to be real.

We introduce the variable

$$z = \int_0^x dx' \frac{\Gamma}{I_0} (A_1 A_4 + A_2 A_3) = \int_0^x \nu dx'$$

The output amplitudes become a function of z :

$$\begin{aligned} A_1(l) &= A_1(0)\cos(z_l) + A_4(0)\sin(z_l) \\ A_4(l) &= -A_1(0)\sin(z_l) + A_4(0)\cos(z_l) \\ A_2(0) &= A_2(l)\cos(z_l) - \sqrt{\epsilon}\sin(z_l) \\ A_3(0) &= A_2(l)\sin(z_l) + \sqrt{\epsilon}\cos(z_l) \end{aligned} \quad (A3).$$

where $z_l \equiv z(x=l)$

From (A1)–(A3), we obtain:

$$\tanh(\Gamma a) = b \quad (A4)$$

where $\Gamma \equiv \gamma l$,

$$a \equiv \frac{\Delta}{2(I_1 + I_2 + I_3)},$$

$$b \equiv \frac{\Delta}{I_4 - I_1 + I_2 + 2\cot(z_l)(A_1(0)A_4(0) + \sqrt{\epsilon}I_2)},$$

$$\begin{aligned} \Delta^2 &\equiv (I_1 + I_4)^2 + I_2^2 + 2I_2(I_1 - I_4)\cos(2z_l) \\ &\quad + 4I_2A_1(0)A_4(0)\sin(2z_l) \\ &\quad + 4I_2\sqrt{\epsilon}[(I_4 - I_1)\sin(2z_l) + 2A_1(0)A_4(0)\cos(2z_l)] \end{aligned}$$

Here $I_1 \equiv A_1^2(0)$, $I_4 \equiv A_4^2(0)$, $I_2 \equiv A_2^2(l)$. If the three input fields are known, then Eq. (4) can be solved for z_l . The expressions for a and b are given here only to the lowest order in ϵ . One may write down exact expressions, but since $\epsilon \ll 1$ there is no advantage.

For the three-region geometry of Fig. 3b, one has three Eqs. (A4) (one for each region) which are coupled via the boundary conditions. Since the presence of the seeding light has no effect on the top region except very near threshold, we will neglect the seeds in this region and use Eq.(2) from the text to calculate its transmission. The boundary conditions are:

Left region:

$$\begin{aligned} A_2(l) &= \sqrt{I_L} \\ A_1(0) &= \sqrt{T_0} A'_2(0) \\ A_4(0) &= A'_3 \end{aligned}$$

Right region:

$$\begin{aligned} A'_2(l) &= \sqrt{I_R} \\ A'_1(0) &= \sqrt{T_0} A_2(0) \\ A'_4(0) &= A_3(0) \end{aligned}$$

Here all of the primed amplitudes refer to the right region and the unprimed amplitudes refer to the left region as indicated in Fig. A1. Note that the left and right regions are laid out as mirror images, so that the external beams are input at $x=l$ in both of these regions. T_0 is the intensity transmission of the double phase conjugator in the top region where $A_2(0)$ and $A'_2(0)$ are its two input beams. Using Eq. (3), these boundary conditions are rewritten as:

Left region:

$$\begin{aligned} A_2(l) &= \sqrt{I_L}, \\ A_1(0) &= \sqrt{I_R T_0} (\sin(z_2) - \sqrt{\epsilon} \cos(z_2)), \\ A_4(l) &= \sqrt{I_R} (\sin(z_2) + \sqrt{\epsilon} \cos(z_2)), \end{aligned}$$

Right region:

$$\begin{aligned} A'_2(l) &= \sqrt{I_R}, \\ A'_1(0) &= \sqrt{I_L T_0} (\sin(z_1) - \sqrt{\epsilon} \cos(z_1)), \\ A'_4(l) &= \sqrt{I_L} (\sin(z_1) + \sqrt{\epsilon} \cos(z_1)), \end{aligned}$$

One determines z_1 and z_2 , and all other quantities are expressed through them. We could solve these equations analytically only for a few special cases. For example if $q = 1$ ($I_L = I_R = I$) and $\Gamma_1 = \Gamma_2 = \Gamma$, then further analytic results can be obtained. In this case $z_1 = z_2 = z$. Since the system is left-right symmetric for input beams having equal intensities, q is always equal to 1 for the top region, regardless of the values of ϵ and Γ , and the transmission of the top region depends only on Γ .

For $q=1$ one can solve for z in Eq. (4) using the boundary conditions:

$$\begin{aligned} A_2(l) &= \sqrt{I}, \\ A_1(0) &= \sqrt{T_0 I} (\cos(z) - \sqrt{\epsilon} \sin(z)), \\ A_4(0) &= \sqrt{I} (\sin(z) + \sqrt{\epsilon} \cos(z)) . \end{aligned}$$

The overall transmission of the device is then given by

$$T = \frac{(A_1(0)\cos(z) + A_4(0)\sin(z))^2}{I}$$

$$= [\sin^2(z) + \sqrt{T_0} \cos^2(z) + \sqrt{\varepsilon}(1 - \sqrt{T_0})\sin(z)\cos(z)]^2.$$

REFERENCES

1. J. Feinberg, "Self-pumped, continuous-wave phase conjugator using internal reflection," *Opt. Lett.* **7**, 486-488 (1982).
2. S. Weiss, S. Sternklar, B. Fischer, "Double phase-conjugate mirror: analysis, demonstration, and applications," *Opt. Lett.* **12**, 114-116 (1986).
3. M.D. Ewbank, "Mechanism for photorefractive phase conjugation using incoherent beams," *Opt. Lett.* **13**, 47-49 (1988).
4. M.D. Ewbank, R.A. Vasquez, R.R. Neurgaonkar, and J. Feinberg, "Mutually pumped phase conjugator in photorefractive SBN: theory and experiment," *J. Opt. Soc. Amer.* **B-7**, 2306-2316 (1990).
5. D. Wang, Z. Zhang, Y. Zhu, S. Zhang, and P. Ye, "Observations on the coupling channel of two mutually incoherent beams without internal reflection in BaTiO₃," *Opt. Commun.* **73**, 495-500 (1989).
6. R.W. Eason and A.M.C. Smout, "Bistability and noncommutative behavior of multiple-beam self-pulsing and self-pumping in BaTiO₃," *Opt. Lett.* **12**, 51-53 (1987).
7. M. Cronin-Golomb, "Almost all transmission grating self-pumped phase conjugating mirrors are equivalent," *Opt. Lett.* **15**, 897-899 (1990).
8. J. Feinberg and R.W. Hellwarth, "Phase-conjugating mirror with continuous-wave gain," *Opt. Lett.* **5**, 519-521 (1980); Erratum **6**, 257 (1981).
9. M.D. Ewbank, P. Yeh, M. Khoshnevisan, and J. Feinberg, "Time-reversal by an interferometer with coupled phase-conjugate reflectors," *Optics Letters* **10**, 282-284 (1985).
10. M. Cronin-Golomb, B. Fischer, J.O. White and A. Yariv, "Theory and applications of four-wave mixing in photorefractive media," *IEEE J. Quant. Electr.* **20**, 12-29 (1984).

11. G. Hussain, S. W. James and R.W. Eason, "Observation and modeling of dynamic instabilities in the mutually pumped bird-wing phase conjugator in BaTiO₃," J. Opt. Soc. Amer. **B-7**, 2294-2298 (1990).
12. D.J. Gauthier, P. Narum, R.W. Boyd, "Observation of deterministic chaos in a phase conjugate mirror," Phys. Rev. Lett **58**, 1640-1643, (1987).
- 13) A.V. Nowak, T.R. Moore, and R.A. Fisher, "Observation of internal beam production in a barium titanate phase conjugator, " J. Opt. Soc. Amer. **B-9**, 1864-1878 (1988).
14. J. Feinberg, D. Heiman, A.R. Tanguay, Jr., and R.W. Hellwarth, "Photorefractive effects and light-induced charge migration in barium titanate," J. Appl. Phys. **51**, 1297-1305 (1980); Erratum **52**, 537 (1981).
15. A.V. Mamaev, A.A. Zozulya, "Dynamics and stationary states of a photorefractive phase-conjugate semilinear mirror," Opt. Comm. **79**, 373-376 (1990).
16. V.T. Tikhonchuk, M.G. Zhanuzakov, A.A. Zozulya, "Stationary states of two coupled double phase-conjugate mirrors," Opt. Lett. **16**, 288-290 (1991).
17. Note: these equations are the same as those used in Ref. 10 but with the substitution $\gamma \rightarrow -\gamma$.

Figure captions

Fig. 1. Photomicrograph of stimulated beams inside a BaTiO_3 "cat" conjugator, showing the segmented bent trajectories of the light beams.

Fig. 2. a) Light beams (in gray) springing up between a pumped crystal and the normal to a mirror. b) Light beams springing up between two pumped crystals. c) Light beam springing up between separate pumped regions of a single crystal, with the pumping beams connected by a photorefractive grating inside the crystal.

Fig. 3. Schematic of beam paths in a mutually-pumped phase conjugator a) before bifurcation, b) after one bifurcation, c) after a second bifurcation. The circles indicate interaction regions.

Fig. 4. Coupling strength at threshold vs. incident beam ratio q for a mutually-pumped phase conjugator with no bifurcations (solid line, see Fig. 3a) and one bifurcation (dotted line, see Fig. 3b).

Fig. 5. Assignment of the interacting waves in a four-wave mixing region.

Fig. 6. Calculated transmission (throughput) of a mutually-pumped phase conjugator with no bifurcation (i.e. the one-region geometry of Fig.3a) and with one bifurcation (i.e. the three-region geometry of Fig.3b) vs. the coupling coefficient Γ , for equal intensity incident beams into the device ($q=1$). The bifurcated data correspond to seeding values of $\varepsilon = 0, 10^{-4}$, and 10^{-3} . The inset shows the region near threshold.

Fig. 7. Diffraction efficiency of the grating in the left (or right) interaction region (Fig.3b) vs. coupling strength Γ for $q = 1$. The different curves correspond to seeding values of $\varepsilon = 0, 10^{-4}$, and 10^{-3} .

Fig. 8. Appearance of the beams of Fig.3b for a) small coupling strength Γ , b) large Γ .

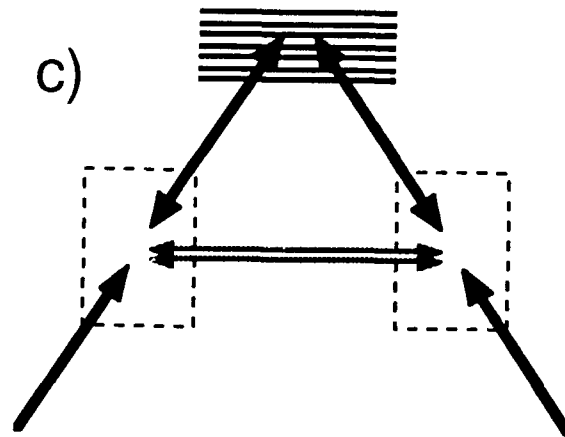
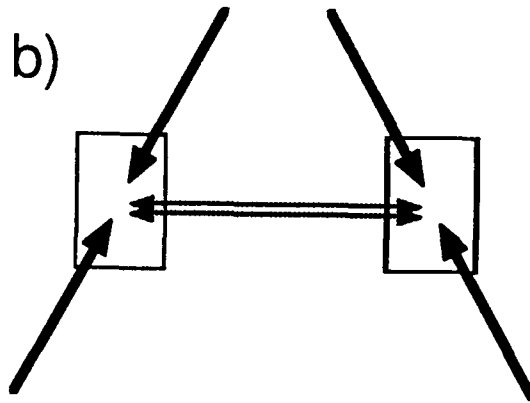
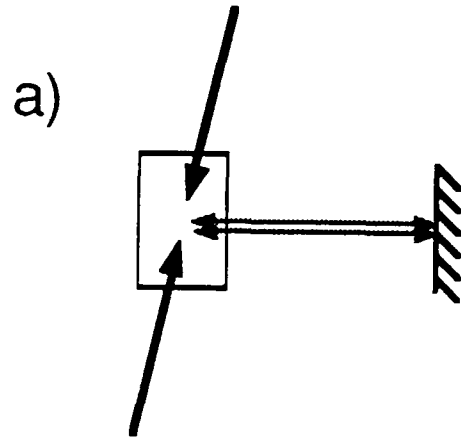
Fig. 9. Transmission in the one-region geometry of Fig. 3a, and in the three-region geometry of Fig. 3b vs. coupling coefficient Γ for *unequal* incident beam intensities ($q = 2$). The curves for the geometry of Fig 3b correspond to seed values of $\varepsilon = 0, 10^{-4}$, and 10^{-3} . The inset shows the region near threshold.

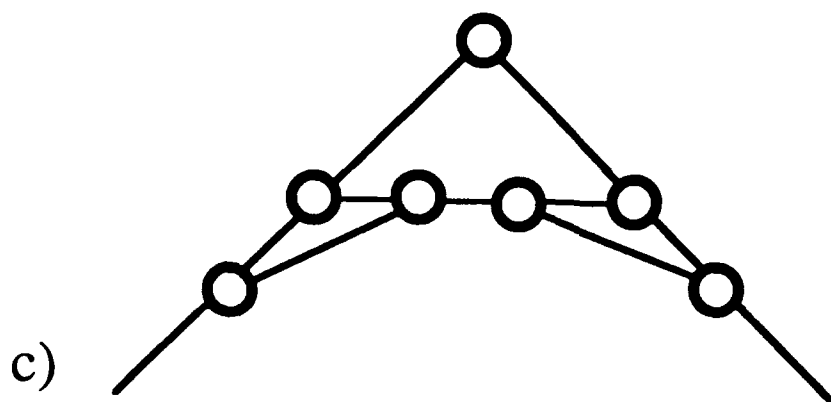
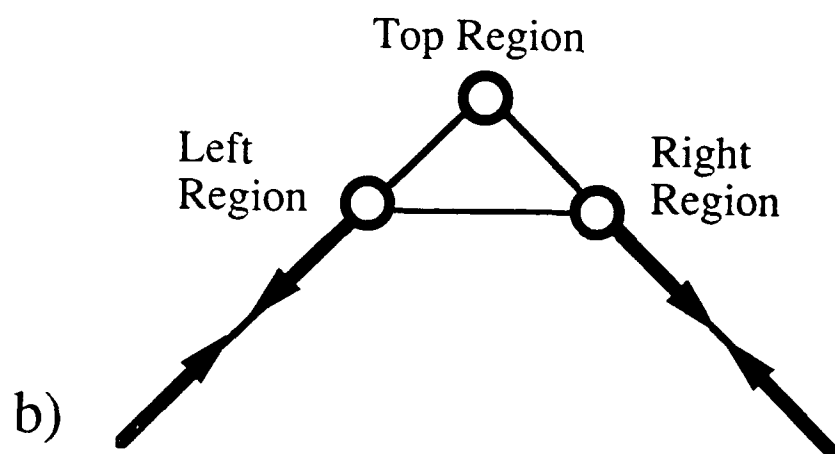
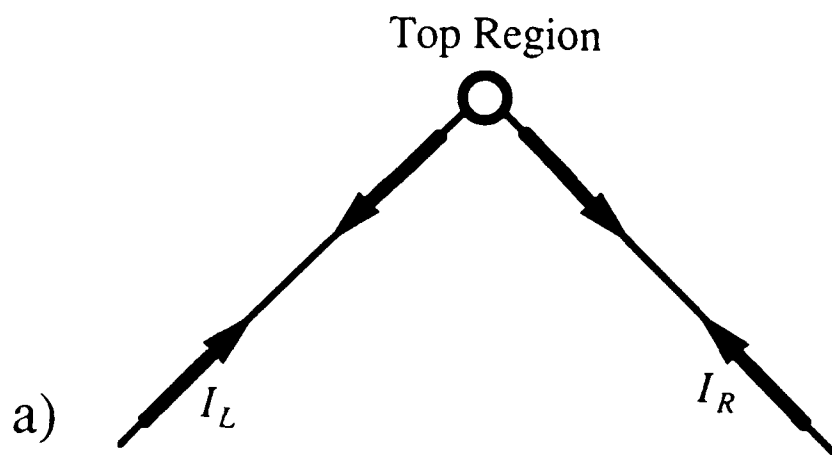
Fig. 10. Diffraction efficiency of the gratings in the left and right interaction regions versus Γ for $q = 2$. Here the stronger beam is incident

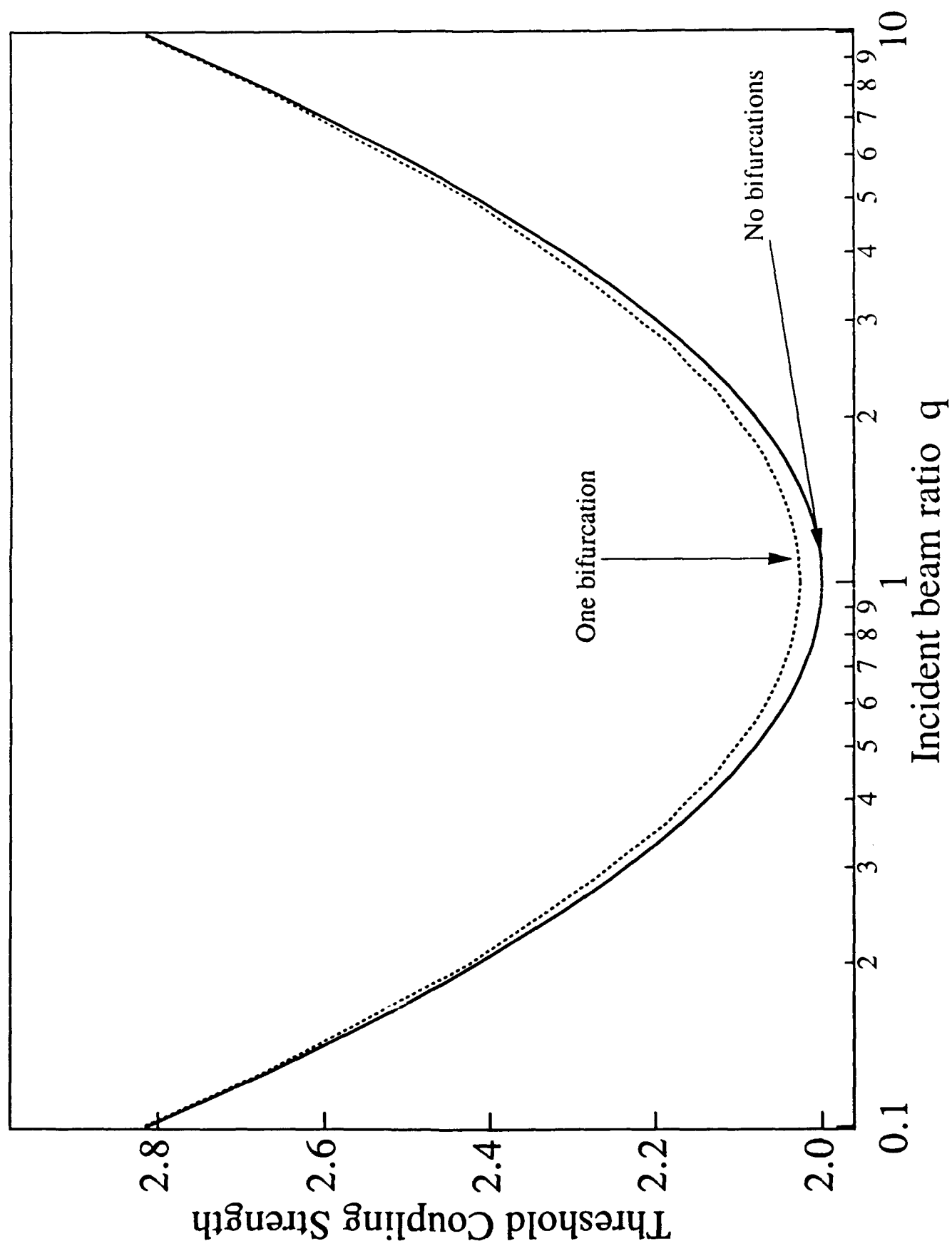
on the crystal from the right and the weaker beam is incident from the left. The curves correspond to seeding values of $\varepsilon = 0$ and 10^{-3} .

Fig. A1. Diagram of the three-interaction region geometry labeling the beams used in the analysis. All beams in the right region are primed. Note that the left and right regions are laid out as mirror images.









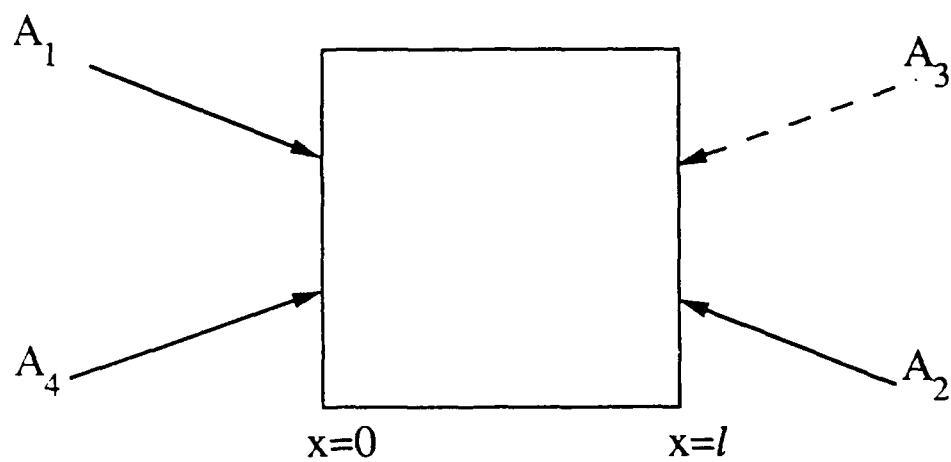


Figure 5

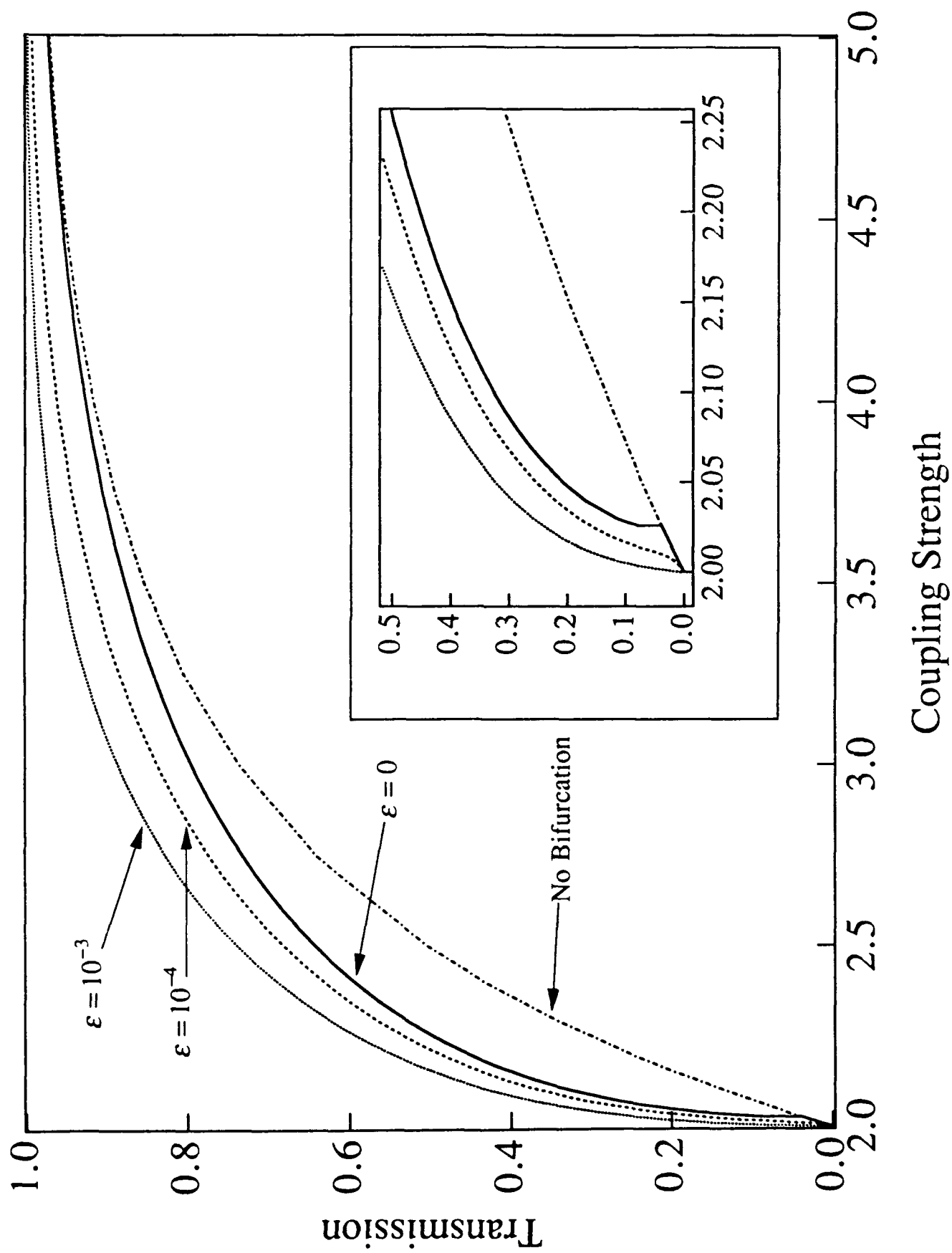


Figure 6

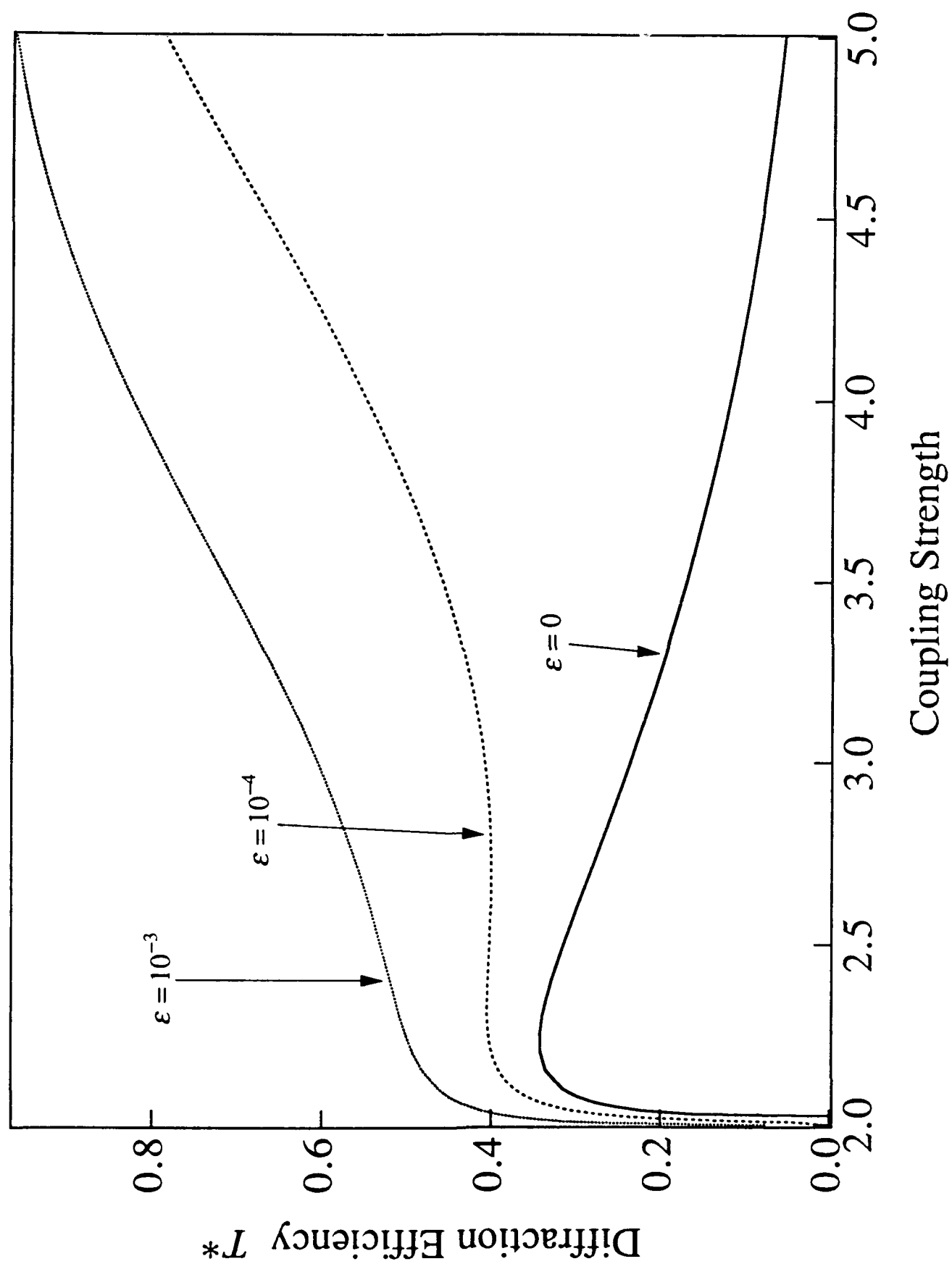


Figure 7

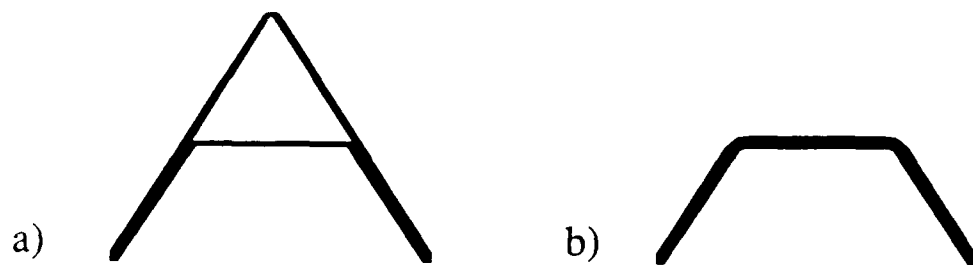


Figure 8

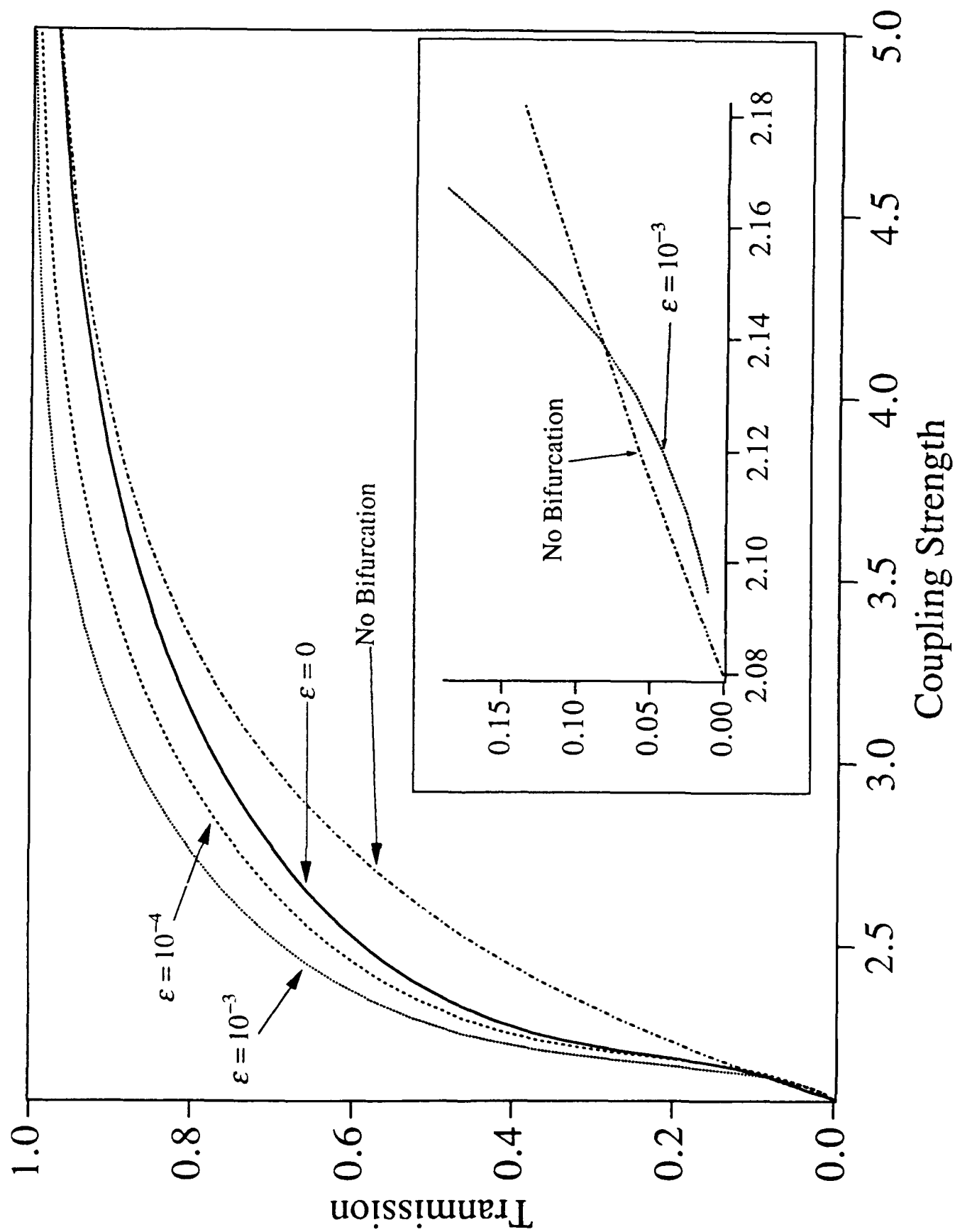


Figure 9

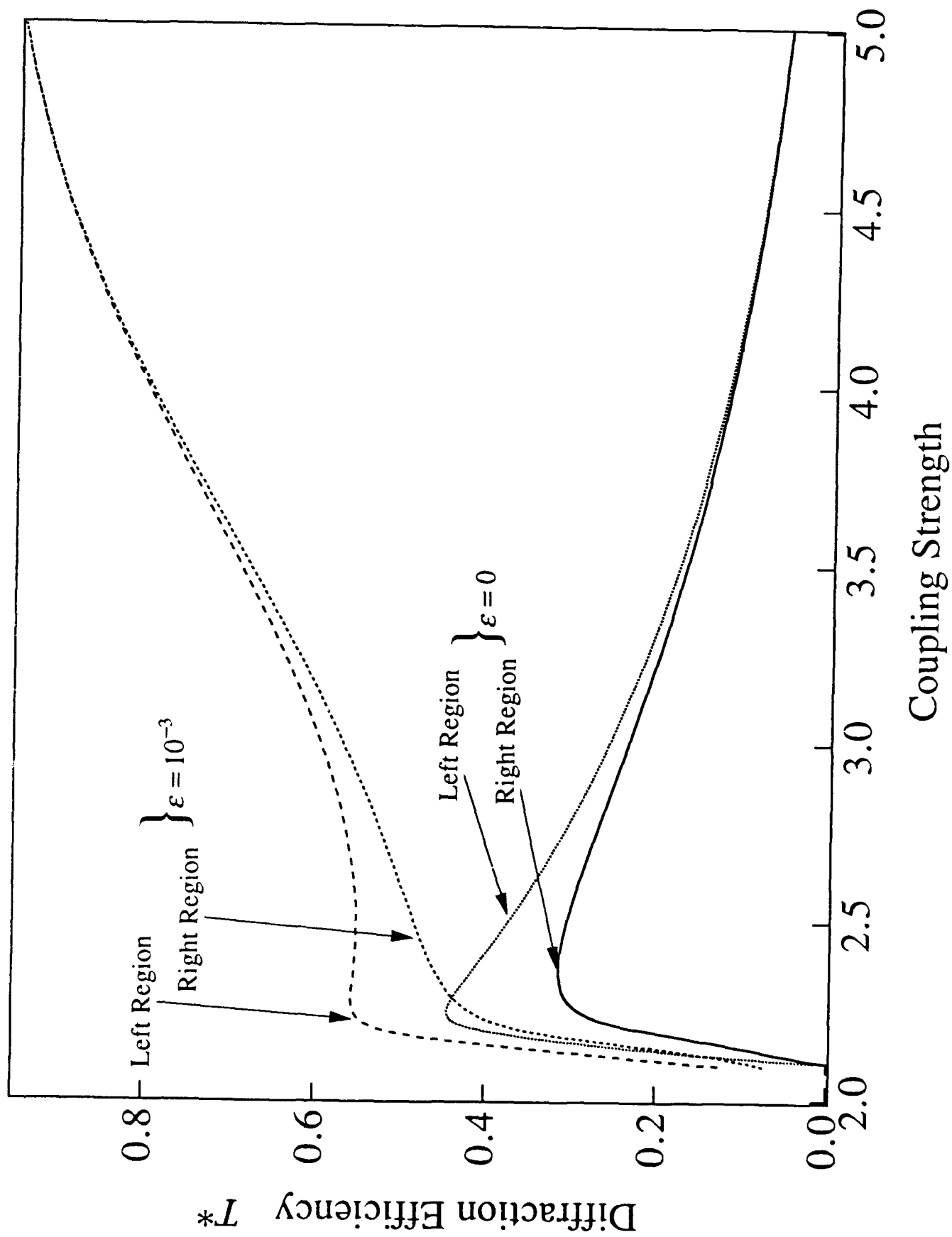
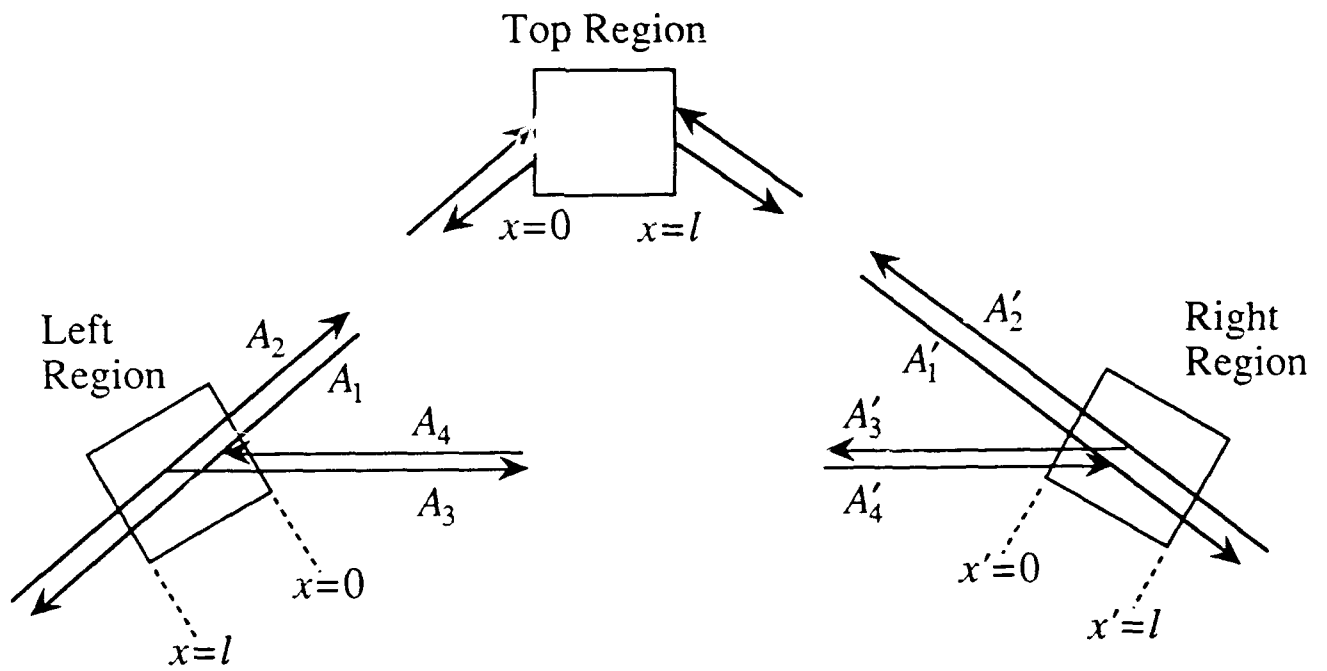


FIGURE 10

Figure **A1**

Time-resolved holography

A. Rebane* & Jack Feinberg

Department of Physics, University of Southern California, Los Angeles, California 90089-0484, USA

In a conventional hologram, a photographic film records the interference pattern of monochromatic light, scattered from the object to be imaged, with a reference beam of unscattered light. Illumination of the developed film with a replica of the reference beam then creates a virtual image of the original object. Here we show how a molecular resonance can be used to record an interference pattern between light signals that arrive at different times, and with this technique create a hologram with time resolution. Using a timed reference pulse as a 'light shutter', we can record holographic images selectively, according to the time taken by light travelling from the object to the hologram. We use this method to image an object behind a semi-opaque screen, and indicate how a similar method could be used to inspect objects embedded in a dense scattering medium. Ultimately, this technique might be applied to the medical imaging of tumours.

Consider two optical pulses incident on a holographic recording medium as shown in the inset of Fig. 1. Let pulse F arrive T_0 seconds before pulse G . If we use photographic film as the recording medium, then an interference pattern will be recorded only if the pulses overlap with each other at least partially in time. But suppose we replace the photographic film by a bank of resonators such as atoms, with each atom tuned to a slightly different optical frequency ω_j . In this case, the interference pattern of the two optical pulses F and G can be recorded even if the pulses are never present in the material at the same time¹.

If the optical pulse F is sufficiently brief, then its frequency spread will be wide enough to excite all of the atoms, much as a brief kick to a piano will excite all of the piano's strings. Each atom will continue to ring at its own natural frequency ω_j . After a delay time T_0 , the second light pulse G arrives, and it will transfer energy either into or out of the j th atom depending on the relative phase between the optical electric field of G and the phase $\phi_j = \omega_j T_0$ of the still-ringing atom. Because each atom's phase depends on its particular resonant frequency ω_j , a given time delay T_0 between the two incident light pulses will produce a unique pattern of excited and unexcited atoms in frequency space.

After interacting with both of the light pulses F and G , let the absorption of the j th atom be permanently altered by an amount proportional to the atom's final energy (by a mechanism described below). If the now altered atoms are illuminated by a replica of pulse F , they will absorb and re-radiate light, again at the frequencies ω_j appropriate to each atom. At first, the phases of the re-radiated light will be incoherent, but after a time of exactly T_0 , the phases of the different frequencies come together to reproduce coherently a duplicate of the pulse G (ref. 1). It can be shown², however, that application of a replica of pulse G to the altered atoms causes a re-radiation of light that loses rather than gains phase coherence with the passage of time. Unlike conventional off-axis holography, where either light beam can be used to reconstruct the other, the bank of atoms here records the direction of time's arrow.

In fact, as we describe below, it is possible to reproduce an image of the scattered light that strikes the hologram before the reference pulse arrives. To produce such an image, the hologram is read out by a replica of pulse F applied in the opposite direction to the original pulse: reversing the spatial orientation of the readout pulse reverses the relative phase relation of the re-radiated light, and thereby leads to the recreation of the 'before' rather than 'after' scattered light.

Now consider illuminating an entire scene with a pulsed laser. Record the reflected light G using a bank of tuned resonators, and let a reference pulse F also illuminate the resonators, as described above. If the reference pulse arrives at the resonators before any of the reflected light, then the entire scene can be recalled by simply reading with another reference pulse. But if the initial reference pulse is delayed so that it arrives after some of the reflected light, then reading (with another reference pulse) will only recreate the parts of the image that arrived after that first reference pulse, which are the parts of the scene that were located farthest from the resonators. For example, if the scene consisted of the street view of a bookshop, then, with a suitably timed reference pulse, the reconstructed image would show the books on display deep inside the store, and would not show the reflections off the shop's front window.

We constructed a bank of narrow-band resonators by doping a solid block of polystyrene with the organic dye protoporphyrin³⁻⁶. Each dye molecule acts as a lightly damped resonator, but because of inhomogeneities in the plastic matrix, each dye molecule has a slightly different resonant frequency. When illuminated by narrow-band light of frequency ω , the molecules that happen to be in resonance with the light become excited. A fraction of these excited molecules subsequently relaxes into a metastable state (thought to be a tautomerization of the original molecule). Once in this transformed state the molecule's absorption is shifted to a completely different spectral region, so a narrow 'hole' is burned into the sample's absorption spectrum at the frequency ω . This spectral hole remains as long as the sample is kept cold. If cooled to a temperature of 2 K, the phase-relaxation time, T_2 , of the molecule's upper level becomes quite long ($T_2 \approx 1$ ns), so that the absorption hole has a narrow homogeneous spectral width of $\Delta\omega = 1/(\pi T_2) \approx 0.01$ cm⁻¹. The polystyrene matrix causes the net absorption spectrum of all of the molecules to form an inhomogeneously broadened band extending over a range of 200 cm⁻¹. Consequently, this material resembles a bank of 200/0.01 = 20,000 narrow-bands of resonators and we use this 'spectral-hole-burning' material to record and store the spectral (and, as we show below, spatial) contents of an incident light beam.

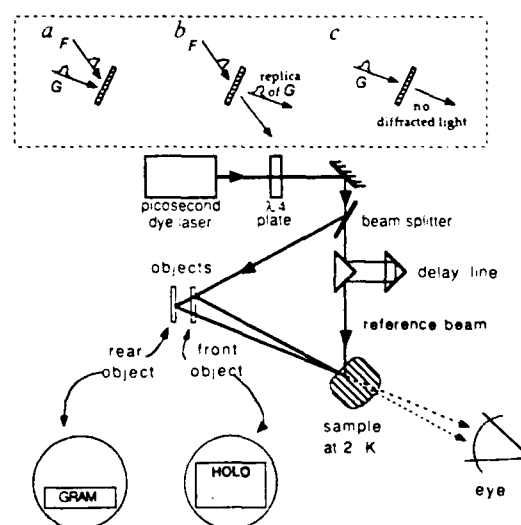


FIG. 1 Main figure: experimental set up. The front object is a frosted slide with the letters 'HOLO' pasted on the front. The rear object is the letters 'GRAM' pasted on the back of the same slide. Inset: a. Writing the hologram with two light pulses separated in time. b. Reading with the earlier pulse F recreates the later pulse G . c. Reading with the later pulse G does not produce any diffracted pulse.

* Permanent address: Institute of Physics, Estonian Academy of Science, 142 Rii Street, Tartu, Estonia, USSR.

In our experiments, we used a 3 mm-thick block of polystyrene doped with protoporphyrin at a concentration of 10^{-3} mol l $^{-1}$. The useful sample area was 4 cm 2 . The sample was immersed in liquid helium, and the helium vapours were pumped to reduce the temperature to 2 K. The peak of the broad absorption feature was at $\lambda = 621$ nm, at which the optical density was 1.6. The light source was a continuous-wave modelocked Nd:YAG laser (Coherent Antares 76s) which synchronously pumped a tunable dye laser (Coherent 701) to produce pulses having an intensity width of 8 ps full width at half maximum (FWHM). (These pulses are not transform-limited; they have a coherence width of only 0.5 ps.) The repetition rate of the laser pulses was 76 MHz. A beamsplitter divided the beam from the picosecond dye laser into a reference beam and a separate beam to illuminate the various objects in the scene, as shown in Fig. 1. The reference beam was expanded by a telescope to illuminate the entire polystyrene block. Scattered light from the illuminated objects simply propagated to the polystyrene block with no intervening lens. The angle between the reference beam and the image-bearing beam was $\sim 14^\circ$.

The recorded scene consisted of two objects. The nearby object was a 1.0-mm-thick glass slide with the letters 'HOLO' attached to its front surface. The distant object was a white paper screen carrying the letters 'GRAM', which was pressed against the back of the transparent slide so the separation between the two objects was ~ 1 mm. To increase the amount of light scattered by the slide, its front surface was coated with a frosting aerosol spray (New York Bronze Powder Co.) The slide was illuminated from the front. Of the scattered light from the slide reaching the polystyrene block, $\sim 80\%$ came from the front sprayed surface of the slide, and only $\sim 20\%$ came from the rear surface. Viewing the laser-illuminated slide by eye from

the position of the polystyrene block, one could clearly read the words HOLO, but the intense glare from the front surface almost completely obscured the letters GRAM located near the back of the slide.

Light from the laser reached the front of the slide 5 ps before it reached the back of the slide. Consequently, light from the front of the slide reached the storage medium 10 ps (twice the glass travel-through time) before light from the back of the slide. In the first experiment a hologram was recorded with the reference beam timed to arrive before both of these object waves. In the second experiment a hologram was recorded with the reference beam carefully timed to arrive within the 10-ps interval between the two object waves.

The reference beam and the object beam each had an average intensity of 0.2 mW cm^{-2} at the location of the storage medium. An exposure time of 2–3 minutes was needed to record a hologram with a fluence of $70\text{--}100 \text{ mJ cm}^{-2}$, corresponding to 10^{10} identical pairs of laser pulses. To write the first hologram we tuned the laser wavelength to the absorption maximum of the medium at 621 nm ($19,950 \text{ cm}^{-1}$). Because the absorption spectrum is 200 cm^{-1} wide and the dye-laser pulses have a spectral bandwidth of only $\sim 30 \text{ cm}^{-1}$, we could change the wavelength of the dye laser by $\sim 30 \text{ cm}^{-1}$ and then record a new hologram in a 'fresh' spectral region of the storage medium without affecting any previously stored holograms. The different holograms written at different centre wavelengths were later selectively read out by simply adjusting the centre wavelength of the reading dye-laser pulse. In the absence of all illumination these holograms lasted for as long as the sample was kept cold.

We read the holograms by blocking the light coming from the objects and illuminating the hologram with only the reference beam. Figure 2a shows the reconstructed image when the

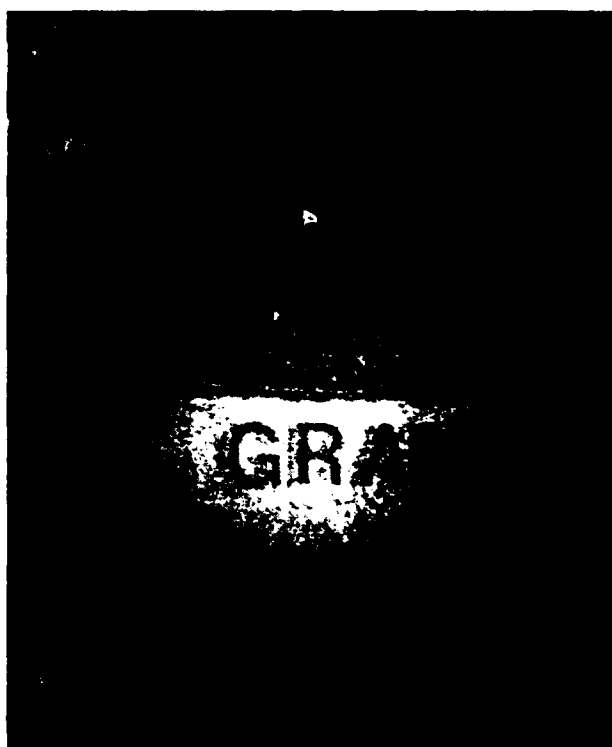
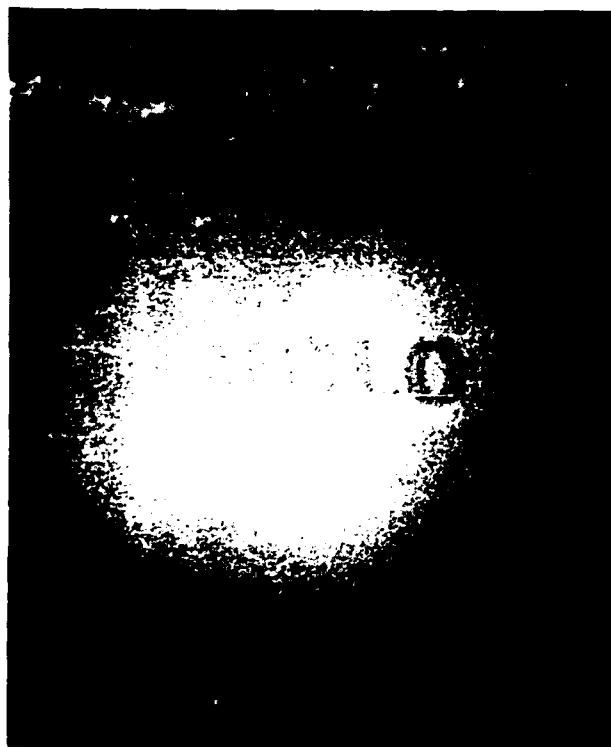


FIG. 2 *a*, Holographic reconstruction of both objects. The reference pulse was set to arrive before light from either of the objects. The glare from the frosted glass in front with the word HOLO obscures the object GRAM behind it. *b*, In this hologram the reference pulse was delayed to arrive after

light from the front object (frosted glass) but before light from the rear object. The front object is no longer reconstructed, whereas the rear object (GRAM) is now plainly visible.

hologram was recorded using a reference beam that arrived a few picoseconds before any of the light from the glass slide. The letters HOLO on the front of the slide are plainly visible, but the glare from the front of the slide almost obscures the letters GRAM near the back of the slide. Figure 2b shows the reconstructed image when the reference beam pulse was carefully set to arrive after light from the distant object but before light from the nearby object. Now only the distant object was reconstructed, and the nearby object was eliminated. We emphasize that the light from these objects need not arrive at the polystyrene block at the same time as light in the reference pulse for the hologram to be recorded. In fact, because the coherence time of the light pulses was only 0.5 ps, and because we set the reference beam to arrive at the storage medium ~ 5 ps before the light from the back of the slide, the reference and object beams could not have produced a conventional intensity interference pattern in the storage medium. We note that the maximum time delay permitted between the object and reference beams was 10^3 ps and is set by the phase-decay time T_2 of the sample.

In the experiment reported here we could selectively reconstruct those objects that sent light to the hologram after the reference pulse had arrived. For some applications, however, it is desirable to do the opposite and recreate the light that arrived before the reference pulse. For example, consider the problem of imaging an object that is embedded in a scattering medium, such as a tumour embedded in breast tissue. Illuminate the

tissue from behind with a short laser pulse. Light transmitted through the tissue without any scattering will emerge before light that has been multiply scattered by the tissue⁷. Because the eye records all of this light, and because the scattered light overwhelms the unscattered light, the tumour remains unseen. But if light that arrived earlier at the eye could be selectively enhanced, than a shadowgram of the tumour would become visible.

This selection of early light over late light can be accomplished by simply altering the direction of the readout beam used in the experiments above. Instead of using a readout beam in the same direction as the reference beam, one should use a readout beam that is directed exactly opposite to the direction of the original reference beam. This is the 'four-wave mixing' geometry of traditional phase-conjugation experiments⁸, but with a spectral-hole-burning material now only the light that arrived before the reference beam is holographically reconstructed in the final image. In this way light scattered from back-lighted tissue could be eliminated, while light travelling directly through the tissue could be preserved, and would form a shadowgram of features embedded in the tissue. We caution that this scheme requires a very large dynamic range for the hologram, because in thick tissue the scattered light can be much more intense than the unscattered light. We estimate that our present spectral-hole-burning medium has a dynamic range limited to $\sim 10^3$. Experiments to demonstrate such selective imaging are in progress. \square

Received 11 February; accepted 29 April 1991

1. Longuet-Higgins, H. C. *Nature* **217**, 104 (1968).
2. Saar, P., Kaari, R. & Rebane, A. *J. opt. Soc. Am.* **B3**, 527-533 (1986).
3. Mossberg, T. W. *Opt. Lett.* **7**, 77-79 (1982).
4. Rebane, A., Kaari, R., Saar, P., Anjalg, A. & Timpmann, K. *Opt. Comm.* **47**, 173-176 (1983).
5. Rebane, A. *Opt. Comm.* **65**, 175-178 (1988).

6. Moerner, W. E. *Persistent Spectral Hole Burning: Science and Applications* (Springer, Berlin, Heidelberg, 1988).

7. Yoo, K. M. & Alfano, R. R. *Opt. Lett.* **15**, 320-322 (1990).

8. Hellwarth, R. W. *J. opt. Soc. Am.* **67**, 1-3 (1977).

ACKNOWLEDGEMENTS J. F. is grateful for support from the US Air Force Office and their University Research Initiative.

The Photorefractive Effect

A laser beam passing through a crystal can suddenly burst into a spray of light. This photorefractive effect may be the key to developing computers that exploit light instead of electricity

by David M. Pepper, Jack Feinberg and Nicolai V. Kukhtarev

When Arthur Ashkin and his colleagues at Bell Laboratories first noticed the photorefractive effect some 25 years ago, they considered the phenomenon a curiosity at best and a complete nuisance at worst. Today photorefractive materials are being shaped into components for a new generation of computers that exploit light instead of electricity.

Ashkin was experimenting with a crystal of lithium niobate (LiNbO_3) that he hoped would convert one color of intense laser light to another (a process technically called second-harmonic generation). As part of his tests, he directed a laser beam through the crystal. At first, the crystal performed quite admirably, allowing light to pass through undisturbed. But after a few minutes, the crystal began to distort the beam, scattering light around the laboratory. Somehow the laser light had altered the optical properties of the crystal itself. This photorefractive effect would persist in the crystal for days. If the workers bathed the crystal in a uniform beam of light, however,

the crystal would once again transmit an undistorted beam.

During the past 25 years investigators have discovered a wide variety of photorefractive materials, including insulators, semiconductors and organic compounds. Photorefractive materials, like film emulsions, change rapidly when exposed to bright light, respond slowly when subjected to dim light and capture sharp detail when struck by some intricate pattern of light. Unlike film, photorefractive materials are erasable: images can be stored or obliterated at whim or by design.

By virtue of their sensitivity, robustness, and unique optical properties, photorefractive materials have the potential to be fashioned into data-processing elements for optical computers. In theory, these devices would allow optical computers to process information at much faster rates than their electronic counterparts. Employing photorefractive materials, workers have already developed the optical analogue to the transistor: if two laser beams interact within a photorefractive material, one beam can control, switch or amplify the second beam. Photorefractive materials also lie at the heart of devices that trace the edges of images, that connect networks of lasers and that store three-dimensional images.

Because the optical properties of photorefractive materials can be modified by the very light that passes through them, they are categorized as nonlinear optical media. In linear optical media—such as lenses, prisms and polarizing filters—light beams merely pass through one another, without changing the properties of the material.

The photorefractive effect is closely related to another nonlinear phenomenon known as the photochromic effect. The light that strikes a photochromic material can change the amount of light that the medium absorbs. Photochromic materials, which are incorpo-

rated in certain brands of sunglasses, darken in bright sunlight and lighten in dark rooms.

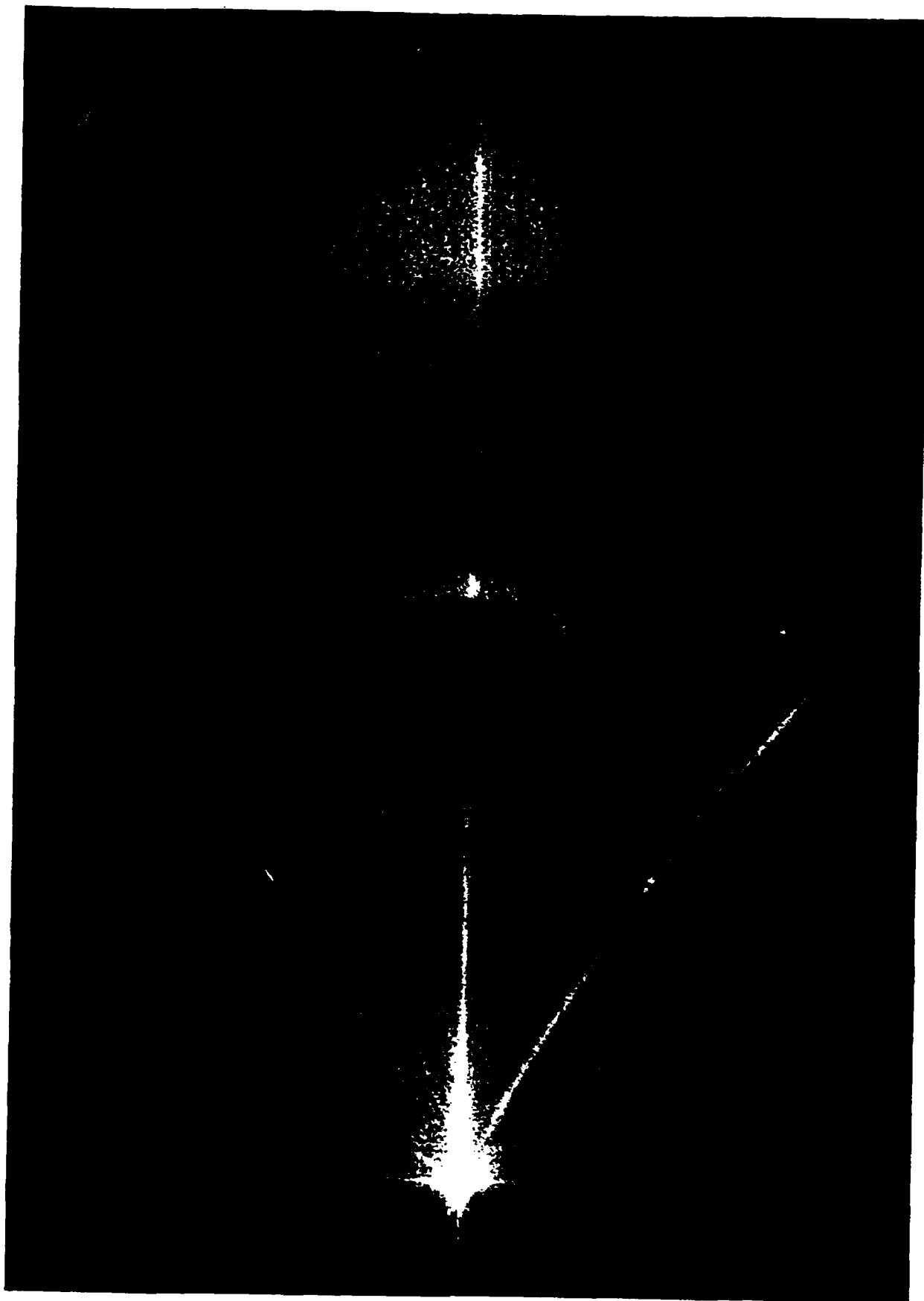
In photorefractive materials, the light that bombards the material affects how fast light travels through it. More specifically, the photorefractive effect is a process in which light alters the refractive index of a material. (The refractive index is the ratio of the speed of light in a vacuum to that in the material.)

Most transparent materials will change their refractive index if bombarded by light of sufficient intensity. Light is a traveling electromagnetic wave whose electric field strength is proportional to the square root of the intensity of light. For instance, an optical beam whose intensity is 100 million watts per square centimeter is equivalent to an electric field strength of about 100,000 volts per centimeter. When such intense light is directed at a transparent material, it disrupts the positions of the atoms, changing the refractive index by a few parts in one million. As a result of the change, the material can act like a prism or a lens to deflect light.

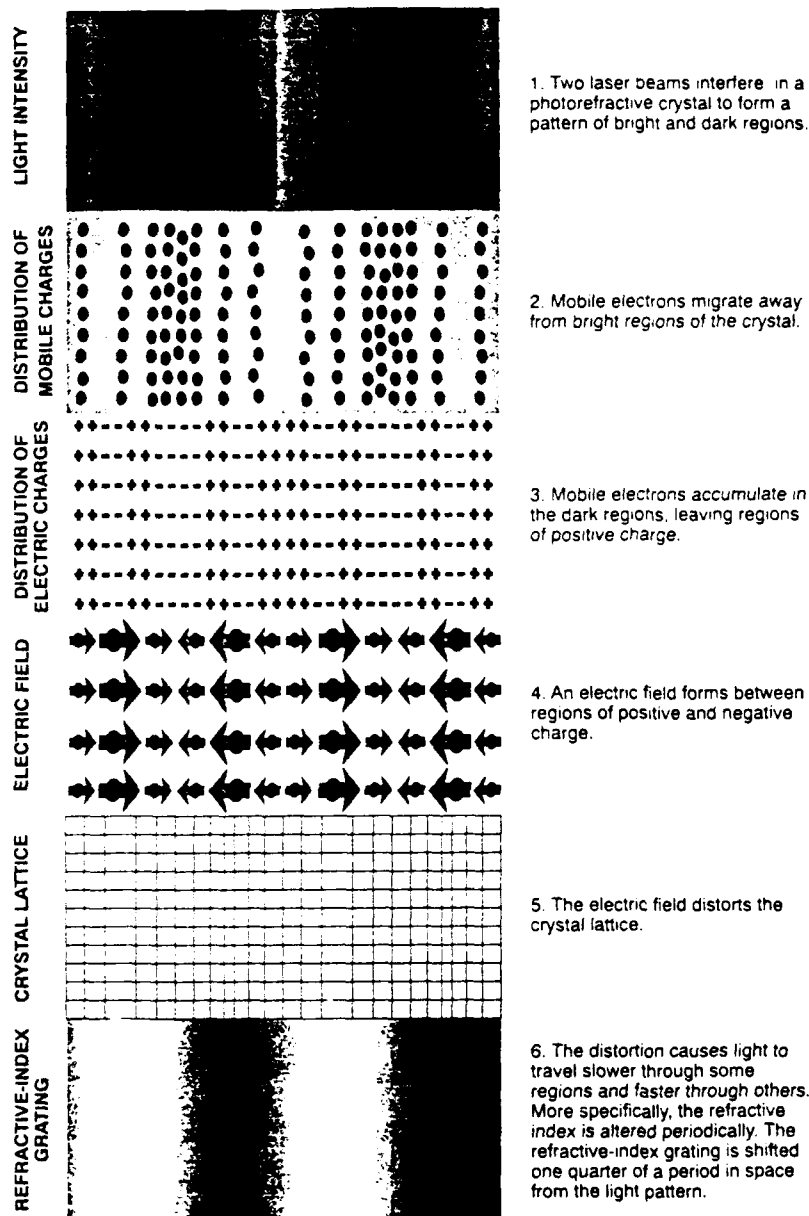
The term "photorefractive" is usually reserved, however, for materials whose refractive index changes in response to light of low intensity. In photorefractive materials, light beams as weak as one thousandth of a watt per square centimeter can alter the arrangement of atoms in a crystal, changing the refractive index as much as a few parts in 10,000. And unlike most transparent materials, the change in photorefractive crystals is semipermanent: if an altered crystal is isolated from all sources of light, the change in the refractive index can last from milliseconds to years, depending on the material. In this manner, one can store information in the form of images in a crystal.

LASER BEAM striking a 5-mm crystal of barium titanate scatters into a fan of light owing to the photorefractive effect.

DAVID M. PEPPER, JACK FEINBERG and NICOLAI V. KUKHTAREV wrote part of this article on the beaches of Hawaii and simultaneously participated in an experiment on the photochromic effect: they developed sunglasses. Pepper is a senior staff physicist in the optical physics department at Hughes Research Laboratories and adjunct professor at Pepperdine University. In 1980 he received his Ph.D. in applied physics from the California Institute of Technology. This is his second article for SCIENTIFIC AMERICAN. Feinberg is associate professor of physics and electrical engineering at the University of Southern California. In 1977 he earned his Ph.D. in physics from the University of California, Berkeley. Kukhtarev is a senior scientist at the Institute of Physics in Kiev, Ukraine, U.S.S.R. In 1983 he received a doctorate degree for his studies of the theory of dynamic holography.



HOW LIGHT ALTERS THE OPTICAL PROPERTIES OF A PHOTOREFRACTIVE CRYSTAL



How can a weak beam of light cause such a strong change in the refractive index of a crystal? In the late 1960s F. S. Chen of Bell Laboratories advanced the basic model of the photorefractive effect. Just as a single ant can move a large mound of sand one grain at a time, a weak beam of light can gradually build up a strong electric field by moving electric charges one by one. In photorefractive crystals, charges diffuse away from bright regions and pile up in dark regions. As more and more charges are displaced, the electric field inside the crystal in-

creases, attaining a strength as high as 10,000 volts per centimeter. The electric field will distort the crystal lattice slightly (about .01 percent), thereby modifying the refractive index.

The source of these electric charges apparently lies in defects in the crystal lattice of the material. The defects can be mechanical flaws in the lattice structure (missing atoms at certain lattice sites), substitutional dopants (a foreign atom at some lattice site) or interstitial dopants (a foreign atom wedged between native atoms). Very small amounts of these defects, on the

order of parts per million, can cause the photorefractive effect.

Each crystal defect can be the source of an extra charge, which can be either electrons (particles of negative charge) or holes (regions of positive charge), depending on the particular crystal. In the dark, these charges are trapped; in the presence of light, they are free to roam within the crystal until they eventually become caught again. If light illuminates charges in one region of the crystal, they will diffuse away from that region and accumulate in the dark, in the way cockroaches scurry underneath furniture to avoid light.

Each charge that moves inside the crystal leaves behind an immobile charge of the opposite sign. In the region between these positive and negative charges, the electric field is strongest, and the crystal lattice will distort the most. A beam of light that passes through this region of the crystal will experience a different refractive index from that of the unaffected regions.

The time it takes for light to rearrange charges in a crystal depends on the intensity of the light and also on how fast charges migrate in the crystal. Weak light takes longer than strong light to build up the same electric field. For low-intensity light (about .01 watt per square centimeter), it can take minutes for the charges to reach their equilibrium pattern. For high-intensity light (about a billion watts per square centimeter), the response time can be less than a nanosecond. A photorefractive crystal, like photographic film, requires a certain amount of light to complete its "exposure."

The change in refractive index is linearly proportional to the strength of the electric field if the crystal lattice lacks a certain property called an inversion symmetry. The electric field will remain in the crystal long after the light is removed, just as the mound of sand remains in its new location long after the ants have left.

One of the most useful consequences of the photorefractive effect is the exchange of energy between two laser beams, which is also known as two-beam coupling. If two laser beams of the same frequency intersect, they will interfere and produce a stationary pattern of bright and dark regions—or more specifically a pattern whose intensity varies sinusoidally with position in the crystal. If this sinusoidal pattern of light forms within a photorefractive crystal, electric charges will move to generate an electric field whose strength also varies sinusoidally. The resultant field will distort the

crystal lattice in a similar periodic manner, producing changes in the refractive index. Ultimately a "refractive-index grating" (also called a refractive-index volume hologram) will be formed within the crystal.

The electric field and the refractive-index grating will have the same periodicity as the light pattern, but they will be shifted by one quarter of a period in space from the incident light. This displacement—called a 90-degree phase shift—is the optimal configuration for the exchange of energy between the original two laser beams.

Once the refractive-index grating has been established in the crystal, some of the light of one beam will be deflected, or diffracted, by the grating in the direction of the other beam (and vice versa). Hence, the two deflected beams will interfere with the two original beams—constructively in one case and destructively in the other. In the case of constructive interference, the peaks of the light waves in one of the deflected beams combine with the peaks of one of the original beams, and the beams therefore reinforce each other. In the case of destructive interference, the peaks of the waves from the other deflected beam combine with the valleys from the other original beam, and the light waves diminish each other. The beam formed from constructive interference will emerge from the crystal stronger than when it entered, whereas

the beam formed from destructive interference will emerge weaker. Hence, one of the beams will have gained energy from the other. Which beam gains and which beam loses is determined by the orientation of the crystal and whether the charge carriers are holes or electrons.

Photorefractive materials exhibit two-beam coupling because the optical pattern and the refractive-index grating are shifted in space. Two-beam coupling is not found in most nonlinear materials, however, because they respond "locally" to optical beams (for example, atomic orbitals are deformed by the intense electric fields of the laser beams). In most nonlinear materials, therefore, the optical pattern and grating precisely overlap. The light deflected by the grating interferes with each of the undeflected beams in exactly the same way. Thus, the two beams exchange an equal amount of energy; so neither grows in intensity.

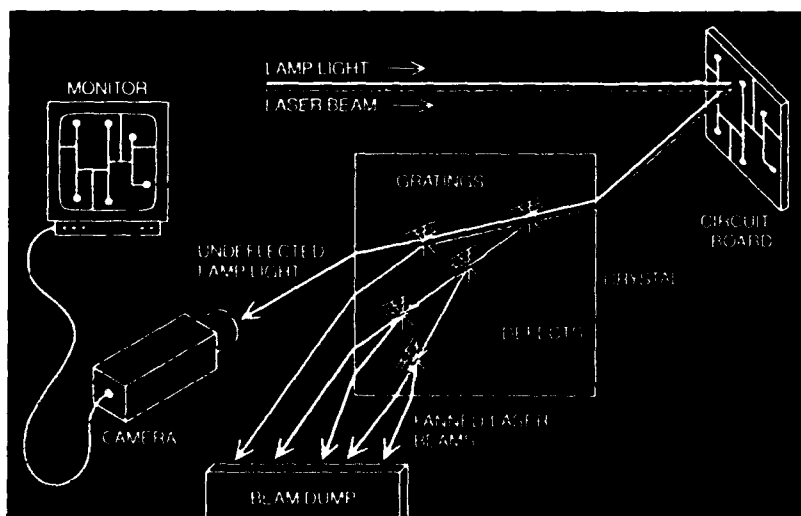
To enhance the photorefractive effect, investigators have learned to control the flow of charge within a material. The two mechanisms that control the flow of charge in a crystal are diffusion and drift. They are analogous to the diffusion and drift of smoke from a burning ember. Left on its own, smoke will diffuse to regions of low smoke density. If a slight breeze is blowing, however, the smoke will

drift in a particular direction. The particles in the smoke behave like mobile charges in a photorefractive material: the charges tend to move toward regions of low charge density, and they drift in response to any electric field.

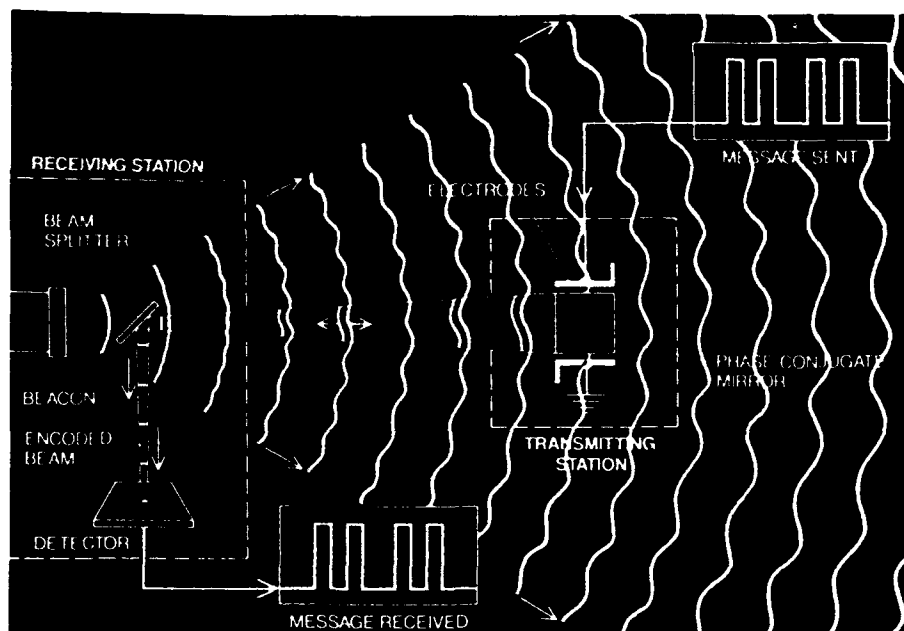
The simple diffusion of charges from bright regions to dark regions of a crystal does not produce the strongest electric field possible. In 1981 Jean-Pierre Huignard and Abdellatif Marakchi of Thomson-CSF Laboratories in Orsay, France, applied an electric field externally to a photorefractive crystal to build up a spatially varying field stronger than that produced by diffusion alone. The applied electric field, however, shifted the refractive-index grating away from the optimal quarter-cycle phase shift.

To prevent this nonoptimal spatial shifting of the grating, Sergei I. Stepanov and Mikhail P. Petrov of the A. F. Ioffe Physico-Technical Institute of the Soviet Academy of Sciences in Leningrad developed a clever technique. When they applied an external electric field that rapidly alternated its direction, the charges would preferentially drift in one direction for the first half cycle of the applied field and in the opposite direction for the next half cycle. The process is similar to having two people alternately blow on a burning ember from opposite sides. The resulting smoke pattern is both intensified and spread out farther in space but has the same average location as if no net wind were present. In photorefractive crystals the process yields an internal electric field larger than that produced by diffusion alone, and the refractive-index grating has the same average quarter-cycle phase shift as if no drift field were present.

Workers have used this technique to enhance the efficiency of two-beam coupling as well as an effect called beam fanning (technically known as stimulated, forward photorefractive scattering). Discovered in the 1970s, beam fanning is perhaps one of the most intriguing nonlinear optical phenomena. It can be observed, for example, when a pencil-thin, weak beam from a helium-neon laser illuminates a crystal such as barium titanate (BaTiO_3). Initially the beam passes through the crystal unaltered. After a second or so (the time depends on the intensity of the light), the beam begins to spread out in the crystal, curving to one side. In the process the curved beam divides into many rays that appear to spray out into a broad fan of light—hence the term "beam fanning." Depending on the choice of photorefractive crystal, the emerging light in cross section can



COHERENT OPTICAL EXCISOR scatters intense light from a laser but transmits weak light from a lamp. Here the excisor protects a camera from the damaging laser rays. The laser beam, which consists of a single frequency of light, scatters off defects in the photorefractive crystal and then interferes with itself. The interference pattern creates a refractive-index grating. As a result, most of the laser light is scattered to one side of the crystal, a process called beam fanning. Because the lamp light consists of many frequencies, neither an interference pattern nor a grating is created, and so most of the lamp light is transmitted through the crystal.



PHASE-CONJUGATE MIRROR made from a photorefractive crystal allows communication through the atmosphere. The receiving station emits a beam of light. As the beam travels through the atmosphere, it spreads out and distorts. At the transmitting station a photorefractive crystal either reflects or transmits the light that hits it, depending on the voltage applied through the electrodes. Because the crystal acts as a phase-conjugate mirror, the reflected light is time-reversed. A message can be encoded by alternately reflecting and transmitting the light. As the time-reversed message beam interacts with the atmosphere, all distortions are removed from the beam, and the message can be decoded at the receiving station.

assume the shape of a beautiful array of elliptical patterns and can have differing polarization components.

Beam fanning results from an energy exchange between the incident beam of light and light randomly scattered by crystal defects. Light scattered by a defect interferes with the unscattered beam, forming a refractive-index grating because of the photorefractive effect. Once this occurs, the unscattered light can transfer additional energy to the scattered beam. It turns out that the energy-exchange mechanism is not isotropic, and so the scattered beams of light become preferentially intensified only over a finite range of angles. This intensified, scattered beam is then randomly scattered by other crystal defects, and the process is repeated. As a result, a large number of scattered beams fan out from the original beam. Depending on the orientation of the crystal and the point at which the incident laser beam enters the crystal, the fanned beam can be made to curve through shallow angles (barely curving through the crystal) or over rather large angles (striking an extreme corner of the crystal).

Beam fanning and other photorefractive effects have been exploited in such applications as coherent beam excisors, optical interconnection elements, phase-conjugate mirrors,

novelty filters and edge enhancement of images.

The coherent optical excisor—first described in 1985 by Mark Cronin-Golomb and Amnon Yariv of the California Institute of Technology—can potentially filter out light that scatters from high-intensity laser beams. The excisor has the potential to protect sensitive optical detectors, which may be necessary to monitor high-power lasers during industrial processes such as annealing and welding. The excisor can also prevent damage to video cameras [see illustration on page 66].

The key component of the coherent optical excisor is a photorefractive crystal, which is placed in front of the detector or the camera's lens. The intense beam can be diverted away from the detector because the beam-fanning effect essentially guides the coherent laser light to the side as it travels through the crystal. The detector or camera can view the object in the presence of intense light, however, because the background room light scattered from the rest of the object passes through the crystal essentially unaltered.

Beam fanning also plays an important role in phase-conjugate mirrors made from photorefractive materials. These mirrors possess the peculiar property that an optical beam "reflected" from them will travel exactly backward in space as if time were reversed.

Because of this property, phase-conjugate mirrors have myriad applications in the fields of optical communications, high-power lasers and optical computing. As an example, they can be incorporated into a system to correct undesirable aberrations that laser beams sometimes acquire during propagation through distorting media or powerful laser amplifiers [see "Applications of Optical Phase Conjugation" by David M. Pepper; *SCIENTIFIC AMERICAN*, January, 1986].

In 1977 Robert W. Hellwarth of the University of Southern California suggested a basic configuration for phase-conjugate mirrors, and two years later Sergei G. Odulov and one of us (Kukhtarev) and independently Huignard and his co-workers produced such a mirror that incorporated photorefractive materials. In 1982 one of us (Feinberg) serendipitously discovered a class of phase-conjugate mirrors that many investigators use today. Feinberg had focused three laser beams on a crystal of barium titanate. One beam contained the light waves whose time-reversed replica was sought; the two additional "pump" beams were needed to form the phase-conjugate mirror (or so Feinberg and his colleagues thought at the time). To check the experiment, Feinberg blocked the pump beams to ensure that the presumed time-reversed beam did not arise merely from a simple reflection from a crystal face. At first, the time-reversed beam obediently vanished. But after a short time, the time-reversed beam surprisingly reappeared. Feinberg had found a phase-conjugate mirror that required only a single beam. Feinberg's elegant device is an example of a more general class of self-pumped, phase-conjugate mirror, which was pioneered by Jeffrey O. White, Mark Cronin-Golomb, Baruch Fischer and Amnon Yariv of Cal Tech.

Although phase-conjugate mirrors can be made from many classes of nonlinear optical materials, photorefractive elements have several distinct advantages: first, the mirrors require only one input beam—the very beam whose phase-conjugate replica is sought—thus forming the so-called self-pumped phase conjugator; and second, very low laser powers and intensities can initiate the process leading to the time-reversed beam.

Why does nature love the phase-conjugate beam? A partial answer to this question posed by Hellwarth can be advanced at least in the case of barium titanate, as postulated by Kenneth MacDonald, then at the University of Southern California, and one of us (Feinberg). After a short time, beam fanning caus-

es the incident laser light to be swept preferentially to one side of the crystal. If the incident beam and crystal are positioned so that the fanned beam is swept into a far corner of the crystal, the fanned beam undergoes two internal reflections, essentially folding back onto itself. This reflected beam fans again back along the direction of the incident beam. Out of all the scattered beams inside the crystal, the time-reversed beam—by virtue of its backward trajectory—gains more energy than the other scattered beams. This beam-reversal process can be very efficient: 60 percent of the power in the incident beam can emerge as the phase-conjugate beam.

One of us (Pepper) has added an additional twist to this novel phase-conjugate mirror. Pepper attached electrodes to a photorefractive crystal to apply a time-varying electric field across the crystal. When a laser beam strikes this crystal, it not only is time-reversed but also can be pulsed in time like a shuttered mirror. In this manner, pulsed information can be relayed from the conjugate mirror back to the laser source; the time-reversed nature of the beam guarantees that the two communication points remain locked onto each other. This scheme can be used to establish a communications channel between two satellites or to relay information from a remote sensor placed at one end of an optical fiber link [see illustration on page 70].

Another application that takes advantage of the energy-exchange mechanism is a device called a novelty filter, which highlights whatever is changing in a highly complex scene. Such devices can pick out moving airplanes against a background of buildings, a sportswoman diving into a still pond or bacteria swimming against

a background of motionless algae.

One type of novelty filter demonstrated by Cronin-Golomb (now at Tufts University) involves two beams that illuminate a photorefractive crystal. An image is encoded spatially onto the first laser beam. The crystal is oriented so that this image-bearing beam transfers most of its energy to the second beam. After the image-bearing beam passes through the crystal, it becomes almost completely dark. Whenever something in the image-bearing beam changes, however, the energy-exchange mechanism is disturbed momentarily, and the part of the image beam that has changed will pass through the crystal. This part of the beam can then be viewed on a video monitor. Once the motion has ceased, the image-bearing beam will become dark once again after passing through the crystal.

Photorefractive crystals can also be employed in other applications to enhance the edges of an image. An image is encoded onto an "object" beam, which is directed into a photorefractive crystal along with a "reference" beam. The two beams interfere inside the crystal and produce a hologram of the original image. The image can be recovered by a third "readout" beam, which is aimed in a direction opposite to the reference beam. If the object beam is relatively weak, then the reconstructed image will be a faithful replica of the original picture. If the object beam is more intense than the other two beams, however, then the edges of the reconstructed image will be enhanced.

The intensity of the object beam varies locally in the crystal because the beam contains an image. Hence, its intensity will match that of the reference beam at every edge in the image, because an edge contains a full range of intensities, from dark to bright. Where-

ver the intensities of the two beams match, the optical interference pattern at that particular region in the crystal will have the largest modulation from bright to dark to bright and so on. The strong interference pattern will then generate a strong refractive-index grating. When the readout beam interacts with the strong grating, it will be most efficiently deflected, or diffracted, at that location, and so the reconstructed image will emerge with all of its edges highlighted.

Because photorefractive crystals can act as both energy couplers and phase-conjugate mirrors, they are particularly useful for reconfigurable optical interconnects and frequency-locking of lasers. Photorefractive crystals can relay information from one optical element (say, an optical fiber) to another (a data-processing element), free of complicated optical elements or electronic interconnects. This optical relaying scheme can also force two (or more) separate lasers to "lock" onto each other so that the two lasers oscillate at precisely the same optical wavelength; in this way, the two separate lasers essentially behave as one larger laser.

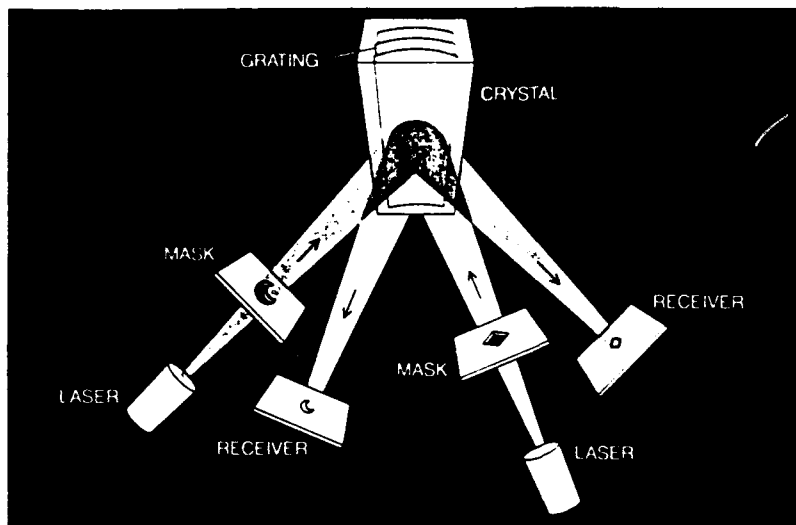
How do two or more mutually incoherent beams of light become connected in a photorefractive crystal? When the different beams illuminate a photorefractive crystal, each will produce its own armada of scattered beams and random refractive-index gratings (or holograms) within the crystal. If one hologram from one beam exactly matches one of the holograms from the other beam, then that hologram will grow faster in strength than the others. The result is that the two beams will be connected to each other. This device is called a mutually pumped, or doubly pumped, phase-conjugate mirror.

The device—first demonstrated in 1987 by Fischer, now at the Technion-Israel Institute of Technology in Haifa, and his co-workers, by Robert W. Eason and A.M.C. Smout of the University of Essex in Great Britain and subsequently by Mark D. Ewbank of the Rockwell International Science Center in Thousand Oaks, Calif.—can connect any two beams originating from any direction. If the two beams contain images, then each image will be converted into the other as the beams traverse the crystal [see illustration on page 74]. If one beam is pulsed rapidly, the temporal information is relayed back toward the other beam.

If two beams come from different lasers that oscillate at slightly different frequencies, then the beam from one laser will be diverted into the approximate conjugate, or time-reversed, di-



PARAMECIUM is hidden among algae and debris (left), but when the scene is viewed through a novelty filter, only the swimming microorganism appears (right). Novelty filters can highlight any object that moves against a stationary background. This filter was designed by R. M. Pierce, R. Cudney, G. D. Bacher and J. Feinberg.



PHOTOREFRACTIVE CRYSTAL couples two laser beams, a process that may be exploited in communications systems, optical computers or other laser networks.

rection of the beam from the other laser, and vice versa. If two such lasers are optically connected by a crystal, they can, under the proper conditions, be made to oscillate coherently, thereby locking the frequency of the two lasers. With this scheme, workers hope that thousands of semiconductor lasers can be efficiently combined into a high-power source of coherent light.

To construct better optical components and devices, investigators are searching among the many different kinds of photorefractive materials to find the most efficient and reliable crystals. Photorefractive materials vary greatly in their optical, electrical and structural properties—for example, the insulator barium titanate, the semiconductor gallium arsenide and the organic compound 2-cyclooctylamino-5-nitropyridine doped with 7,7,8,8-tetracyanoquinodimethane.

These seemingly different materials nonetheless exhibit similar photorefractive effects. They all have a crystal lattice that is relatively easy to distort, and they all contain defects, which act as a source of charge carriers and charge traps. Under the influence of an electric field, however, charges move about 10,000 times faster in gallium arsenide than they do in barium titanate. For the same incident light intensity, therefore, the photorefractive effect evolves much more rapidly in gallium arsenide than it does in barium titanate. The resulting refractive-index grating is not as strong in gallium arsenide, however, as it is in barium titanate. The optical properties of the

crystals in the different materials vary greatly as well: gallium arsenide and other semiconductors are typically photosensitive in the near infrared part of the optical spectrum, whereas most insulators and organic compounds are sensitive in the visible spectrum.

A flurry of experiments currently in progress aim to identify and possibly control the defects responsible for the photorefractive effect in various crystals. As an example, the source of the photorefractive effect in barium titanate is an open question: many researchers attribute the effect to the presence of various ionization states of transition metal impurities such as iron, cobalt and manganese; oxygen vacancies in the lattice may also contribute to the charge carriers. In gallium arsenide, on the other hand, the photorefractive effect is attributed to an intrinsic lattice defect thought to be formed by a combination of an arsenic atom replacing a gallium atom in the lattice and an additional arsenic atom placed in the same lattice cell, forming the so-called EL2 center.

Regardless of the character of the crystalline defects, the properties of most photorefractive crystals can be altered by doping them with impurities or by drawing atoms out of the lattice. For example, one of us (Feinberg) and Stephen Ducharme of U.S.C. found that when a crystal of barium titanate is heated in an oxygen-free environment to remove some oxygen from the crystal lattice, its photorefractive properties are altered markedly because the dominant charge carriers are changed from holes to electrons.

As workers increase the concentration of the defects in a photorefractive material, they have found that the number of available charges increases, thereby enhancing the strength of the internal electric field and the refractive-index gratings. On the other hand, defects scatter and absorb light from the incident beams. Defect concentrations of from one to 100 parts per million appear to be optimal in terms of providing a reasonable number of charges without appreciably attenuating the input light.

Perhaps the best photorefractive materials will be those painstakingly fashioned out of semiconductor materials. Stephen E. Ralph, David D. Nolte and Alastair M. Glass of AT&T Bell Laboratories have recently shown that layers of gallium aluminum arsenide alloys only a few atoms thick can be assembled into structures—called superlattices and quantum wells—that exhibit a measurable photorefractive effect. Such materials are currently being studied for their novel electrical properties and high speed of response. These crystals may also lead to a new class of integrated processors based on optics and electronics.

What makes photorefractive materials so promising for optical computing is their high sensitivity to light, coupled with their ability to connect light beams from different lasers and to change one information pattern into another. The future of photorefractive materials will depend on whether their optical properties can be as meticulously tailored as semiconductors are today. Ideally, photorefractive devices would be integrated with semiconductor lasers and detectors to form a single, compact device capable of processing millions of bits of data simultaneously in each microsecond, yielding a total data-processing rate of trillions of bits per second.

FURTHER READING

- OPTICAL PHASE CONJUGATION IN PHOTOREFRACTIVE MATERIALS. Jack Feinberg in *Optical Phase Conjugation*. Edited by R. A. Fisher. Academic Press, 1983.
- PHOTOREFRACTIVE NONLINEAR OPTICS. Jack Feinberg in *Physics Today*, Vol. 41, No. 10, pages 46-52; October, 1988.
- PHOTOREFRACTIVE MATERIALS AND THEIR APPLICATIONS I & II: TOPICS IN APPLIED PHYSICS. Volumes 61 and 62. Edited by P. Gunter and J.-P. Huignard. Springer-Verlag, 1988.
- NONLINEAR OPTICAL PHASE CONJUGATION. Special Issue. Guest edited by David M. Pepper. *IEEE Journal of Quantum Electronics*, Vol. 25, No. 3, pages 312-647; March, 1989.

Science Times

117

The New York Times

TUESDAY, JUNE 4, 1991

SCIENCE WATCH

Beyond X-Rays

It may eventually be possible to use ordinary light rather than harmful X-rays to obtain images of bones and organs within living beings, several groups of scientists have reported. In reports published by the British journal *Nature* last week and presented at a recent conference on lasers and optics, physicists showed that the faint light that penetrates animal tissue can reveal underlying details, if it is carefully controlled.

Dr. Jack Feinberg of the University of Southern California at Los Angeles said in an interview that light passing through skin and muscle is normally scattered so strongly that it conveys no image of internal structure. But experiments have shown, he said, that the first fraction of a light pulse to pass through tissue actually contains enough information to yield images of internal details. Scattered light, which must travel over longer paths than the light that goes straight through, takes a few trillionths of a second longer to reach the other side. By cutting off the transmitted light pulse before the scattered fraction has time to arrive, fairly clear images of internal details have been preserved in experiments using lasers.

In a method developed by Dr. Feinberg and his colleague, a beam of laser light passing through an object is brought together with a second "reference" beam that follows a path of different length. By careful adjustment of path lengths, the scientists can make them interfere, canceling out the unwanted scattered light that arrives at a photodetector target after the light that directly penetrated the object.

The Economist

VOLUME 320
NUMBER
2715



Leaders

- 13 Lots to do at the summit
- 14 Behind BCCI's closed doors
- 15 A prospect of economic growth
- 16 Yugoslavia: In from the wings
- 17 The financial rot in Japan
- 18 Defending Britain's realm

Special

- 21 Remaking the Soviet Union

Books and Arts

- 91 Woody Allen meets Julia Phillips
- 92 Another war with Japan?
- 92 This month's new novel
- 92 Israel's clumsy spies
- 93 A.J.P. Taylor's love letters
- 93 Not the Royal Academy
- 94 France: Graffiti as art
- 94 Books for the small screen

Letters

- 6 On ICI and Hanson, the Philippines, the Falklands and Argentina, Federconsorzi, Ethiopia, Saddam's promises

The Economist

FIRST PUBLISHED IN SEPTEMBER 1843

to take part in "a severe contest between intelligence, which presses forward, and an unworthy, timid ignorance obstructing our progress."

JULY 13TH 1991

World Politics and Current Affairs

American Survey

- 25 Foreign quagmires for George Bush
- 26 Chinese games in Congress
- 26 California's rebellious conservatives
- 27 Insanity pleas change sides
- 27 The Mormons' money
- 28 Clamping kerb-crawlers
- 29 Farmers reap a bumper crop of gloom
- 32 Lexington: Jay Rockefeller

Asia

- 33 Kaifu begins his campaign
- 34 Taiwan thinks of China
- 34 Mongolia's brave experiment
- 35 Maoist memorabilia
- 35 Pakistan and Kashmir
- 36 India's economic radicalism
- 41 Tittle-tattle in Thailand
- 41 Philippine politics

International

- 43 Iraq's bomb
- 44 The fate of the Kurds
- 45 Algeria's experiment ends
- 45 Litter in paradise
- 45 The Palestinians in Lebanon
- 48 South Africa after sanctions
- 50 Durban's July fever
- 50 The new African National Congress

Europe

- 51 Yugoslavia's civil war
- 52 Sub-atomic Soviet Union
- 53 Will Slovakia secede?
- 54 Separatism in Spain
- 54 Defining minority rights
- 55 Europe's regional clubs
- 55 Switzerland and the EC
- 58 Eurobuzz: EC enlargement

Britain

- 59 THIS WEEK
- 61 Worries about the trade deficit
- 62 Exporting to the Soviet Union
- 62 A white paper on defence
- 63 A change of tack on inner cities
- 64 Asian victims of the BCCI collapse
- 65 Bagehot: Politics and the unions

Business, Finance and Science

66 THIS WEEK

Business

- 67 The future for oil
- 68 Profitable Mr Schwarzenegger
- 69 Management focus: Skill-based pay
- 70 Whirlpool's European adventure
- 70 Japan's booming domestic airlines
- 71 Cosmetics companies' new look
- 72 Ted Turner's TV ad blitz
- 77 Economics brief: Out of poverty
- 78 How Hanson manages

Finance

- 81 The crumbling of BCCI
- 82 Tokyo's shamed stockmarket
- 83 Economics focus: The ecu
- 84 Unhappy Nomura
- 84 The SEC helps shareholders
- 85 Soft commissions in London
- 86 Insider trading in Germany

Science and Technology

- 87 The future of Bell Labs
- 88 Knowing the nose
- 88 Seeing through people
- 89 Stacking the genetic deck

Economic and financial indicators

- 107 Output, demand, jobs, prices, wages and commodities, plus a closer look at global diets and groundnuts
- 108 Stockmarkets, money supplies, interest rates, trade, exchange rates and reserves, plus a closer look at current-account imbalances

Editorial offices in London and also Bangkok, Bonn, Brussels, Hong Kong, Los Angeles, Moscow, New York, Paris, Tokyo and Washington.

INQUIRIES TO:

25 St James's Street, London SW1A 1HG
Tel: 071 839 7000 Fax: 071 839 2968

111 West 57th Street, New York, NY 10019
Tel: 212 541 5730 Fax: 212 541 9378

1329 The Prince's Building, 10 Queen's Road, Victoria, Hong Kong
Tel: 955 555 0078 Fax: 955 868 1425

another sells credit cards, and so on. It is from these units that Bell Labs now gets most of its budget: as a result it has been pressed to concentrate on areas with immediate potential, and to cut costs. "It makes my life more difficult but more interesting," says Arno Penzias, who won the Nobel prize for that crucial bit of Big-Bang cosmology and has risen through working on basic research to be head of Bell Labs' research division. Not all his colleagues are so enthusiastic. "Bell Labs people see themselves as the elite, the aristocracy of the system," says one researcher. "Right now there is a big morale issue, because they don't have the predominance they used to."

Mr Mayo, Bell Labs' new director, is likely to make the laboratory even more commercial. He is seen as more business-minded than his predecessor, Ian Ross, who spent nearly all his 40-year career with AT&T at Murray Hill. Although Mr Mayo insists that basic science will not be cut back, employees expect a continued swing away from research and towards development, and away from the physical sciences towards software and systems. "The fact is that software is now the mainstream of technology and you have to recognise that," admits Mr Mayo.

Should Bell Labs be shrunk and turned into just another R&D department? Not necessarily. Its glorious history provides tangible advantages, which could be lost if the nature of the institution changed. Because Bell Labs does exciting work, it attracts the best scientists; over time they can be edged into commercial areas. The laboratory also gives a gloss to AT&T's corporate image, both inside and outside the firm. Even employees who have nothing to do with the place speak of it with pride; regulators may be prepared to go easier on a dominant ex-monopoly if it is doing lots of unremunerative public work. The image does AT&T good, but at a high price; the trick will be to keep it, while spending less.

The nose

Smelly genes

WHEN you sniff a glass of wine, about 10m trillion odorous molecules get up your nose. Your brain senses a smooth, stimulating bouquet. But what happens in between? Neuroscientists have devised detailed maps of the ways in which sights and sounds get picked up and processed. Just how the brain recognises more than 10,000 different smells remains a mystery. Recent work by Linda Buck and Richard Axel of the Howard Hughes Medical Institute at Columbia University offers a useful clue.

Scientists have known for some time that smelly molecules, called odorants,

bind to receptor proteins on the surface of nerve cells in the nose. The nerves then send signals to the brain. The question is, how are the signals made sense of?

If each nerve carried a receptor tailored to a specific odorant, then the brain would know what it was smelling simply by knowing which cells were active. There would be as many types of receptor as there were smells. On the other hand, there could be just a few types of receptor. In that case, each receptor would respond to many smells, each in a slightly different manner. The brain would have to compare lots of messages from different types of receptors in order to work out what it was smelling. Such systems are common in the other senses. The eyes have only three types of colour receptors—it is by comparing the responses of all three that the brain turns a few nerve signals into all the hues of the spectrum.

There is, of course, a middle way. Gordon Shepherd of Yale University has long argued that signals from a range of receptors are gathered into "labelled lines" in the olfactory bulb of the brain. The relative strength of the messages passing down each of the lines—there might be dozens, but not hundreds—would be further processed to produce an "odour image".

While Dr Shepherd has some evidence to support this view, a few other researchers continue to prefer the idea that there are as many receptors as there are smells. To choose between the ideas, you need to get your hands on the receptors. That has proved a daunting task. In the early 1980s Solomon Snyder and his colleagues at Johns Hopkins University in Maryland tried to do it by mixing radioactive odorants with proteins from the nose, then separating the odorants out again with proteins attached. This approach has led to the discovery of various receptors on cells elsewhere in the body; this time the scientists just ended up with a minor constituent of mucus.

Where Dr Snyder and many others failed, Dr Buck and Dr Axel may have succeeded. Instead of seeking out the receptor proteins themselves, they looked for the genes that produce them. They took short fragments of DNA from genes that describe other receptors, and used them as "probes" to look for similar genes in the nose's nerves.



Receptors in action

They found a large family of genes that look as though they make receptors, and have shown that 18 of them produce receptors which are all similar to each other, but not identical. Dr Buck thinks that the family could include several hundred different genes. Other researchers are talking about 1,000. If the number of receptor types really is that large, the workload on the brain may not be terribly heavy.

Dr Buck and Dr Axel still have to prove that the receptor proteins produced by these genes actually bind odorants. To do so, they plan to put the genes into other cells and see whether that makes them sensitive to odorants. Then there are more questions to answer. For example, how many types of receptor are there on each individual cell? André Holley of Claude Bernard University in Lyons and others have shown that single cells respond to many different molecules. He thinks this may show that a nerve cell can carry

several types of receptor. But it is also possible that one receptor protein could detect more than one odour. Thanks to Dr Buck and Dr Axel these nasal mysteries, while far from solved, are at least becoming tractable.

Medical holograms

Translucent

PRESS a powerful torch against your palm. The back of your hand will glow a faint pink. It is a diffuse light: the bones, tendons and blood vessels do not show up, because almost all the light is scattered around the tissues inside the hand. Some of the light, however, goes straight through. If you saw only that light, the internal structure would show up like a shadow—providing a picture similar to an x-ray, but produced without the use of x-ray radiation. Such a picture might be useful for screening against breast cancer, among other things. After all, there is some uneasiness about screening for cancer with repeated x-rays, as it carries a faint chance of causing that which it seeks to reveal—although the benefits outweigh the risks.

The light that comes straight through also comes through fastest. So, in principle,

all you need to catch the direct light is a camera shutter that can open and shut in a millionth of a millionth of a second. Unfortunately, no mechanical shutter can work that fast. However, Jack Feinberg, of the University of Southern California, and Alex Rebane, of the Institute of Physics in Tartu, Estonia, announced in a recent issue of *Nature* that the same goal can be achieved by a technique called time-resolved holography.

To understand, first think of a normal hologram—a portrait of yourself, perhaps. A laser beam shines on your face (at which point you should keep your eyes closed). The light bounces off and hits a photographic plate. Since no lens is used, the light is not focused; normally the plate would just be fogged. However, in a hologram, a second beam, called the reference beam, is shone on to the plate at the same time. The plate records the interference pattern made by the reference beam and the beam that has bounced off your face. The recorded interference pattern is a hologram. If another laser beam, like the reference beam, is then shone at the hologram, it gets diffracted in such a way that it now looks like the original reflected light—so it provides a seemingly three-dimensional image of your face.

Time-resolved holography works in the same way, but the reference beam is limited to being a very brief pulse. Lasers can be turned on and off far quicker than shutters can be opened and closed. Going back to the example of the torch and the hand, suppose the aim is to make an image using only the light which first leaves the hand. First put the hand over a block of plastic impregnated with a light-absorbing dye. Then shine one laser through the hand, and another on to the plastic as a reference beam. The reference beam is switched on and off again in an instant.

The dye molecules which are excited by both beams record a form of interference pattern in the plastic. Because of the dye's "memory", the beams do not even have to arrive at exactly the same time. The record can later be made to yield an image of the inside of the hand. Although the dye also absorbs the scrambled light that comes more slowly through the tissue, this does not wipe out the original pattern.

Time-resolved holography is not yet ready to be used for scanning breasts; the light-detection system has to be further developed. But now that the principle has been demonstrated, the two or three academic research teams working on it may well be reinforced by the resources of big medical-equipment makers. And the technology is not limited to medical uses; various industrial and military problems could be tackled too. For example, time-resolved holography might be used to see through cloudy water, helping to keep an eye on seabed installations.

Genetic imprinting

Shuffling with marked cards

BIOLGISTS have long believed in at least one underlying equality between the sexes: a gene is a gene, no matter which parent it came from. Now they are not so sure. Genes are turning up which seem to work only if they have come from the father. Others need a mother's touch to switch them on. All this is a bit disturbing: it questions the established wisdom of nearly a century. But it is not inexplicable.

The phenomenon is called genetic imprinting—not to be confused with behavioural imprinting, which fools young geese into following elderly biologists around. It surfaced when some researchers tried to breed mice with genes from only one parent. Normally, an embryo gets one set of genes from the father, and a similar set of genes from the mother. When two sets of genes from the mother were used, the resulting embryos developed virtually no placenta from which to draw sustenance. Paternal genes alone produced a placenta but not much of an embryo.

Without external meddling, embryos get two copies of each gene, one from the mother, one from the father, stored in two sets of chromosomes. But it is not unknown for small muddles to occur in the gene-shuffling which attends the beginning of a new life. In people, this shuffling can cause a disorder in which the fetus grows too fast. This comes about when two copies of one part of a specific chromosome arrive from the father, and none from the mother.

Another human disease—fragile-x syndrome—travels the distaff path. The x chromosome helps determine sex: women normally have two of them, while men have one x and one y. Fragile-x syndrome, a form of mental retardation, can occur in either sex—but only if the eponymous chromosome has come from the mother. Men with a fragile x do not have diseased daughters.

How all this happens is becoming clear. Not all of the genes in a cell are active all of the time. One way to turn genes off is to plaster molecules called methyl groups all over the DNA from which the gene is made. Imprinting seems to boil down to a difference between the sexes, in terms of which genes they choose to methylate. Imprinted genes appear to be methylated by one parent and not by the other—as though one parent wants them to be turned on, and the other is happy to let them lie.

How it happens is one thing; biologists also want to know why. Bio-

logical whys usually require a bit of detective work to unearth an evolutionary motive. What is the benefit to be gained from imprinting? There are three clues. First, most of the effects seem to occur in embryos. Second, the imprinted genes often regulate growth in some way. Third, parents may imprint genes with opposite effects in opposite directions. It is not a case of one sex simply being more disposed to adding methyl groups than the other.

Take, for example, a hormone called IGF-2, which encourages embryos to grow. The gene which tells the body how to make this growth factor is imprinted: the mother's IGF-2 gene will be methylated and silent. But the maternal copy of another gene, one that produces a protein which makes IGF-2 inactive, shouts loudly in the developing embryo—while the paternal copy keeps quiet. The general rule is that the father imprints genes in such a way as to encourage growth. The mother discourages it. This fits with the original observation that male genes were promoting the placenta. It is the placenta which grabs resources from the mother to make the embryo grow.

To make sense of these clues, bear in mind that although all the embryos in a uterus have the same mother, they may not all share a father. Female cats and mice, for instance, often spread their favours widely. David Haig and Chris Graham, of Oxford University, suggest that in these cases imprinting by males has evolved as a sort of metabolic theft—stealing food from the mother which might otherwise be used by embryos unrelated to the father. Each father wants his offspring to do better than the rest of the litter; the mother wants all her offspring to do well. Hence the imprinting by which fathers prime the genes for growth and the grabbing of the placenta, while mothers try to damp such intra-uterine competition down. Even in the womb, the battle of the sexes goes on.



The evidence of infidelity

TECHNOLOGY

Physicists Who Play With Crystals See Serious Applications

* * *
The Photorefractive Effect,
Once a Diverting Puzzle,
Is Being Studied Widely

By DAVID SHIPP

Staff Reporter of THE WALL STREET JOURNAL

Once merely a diverting puzzle for physicists, the photorefractive effect of crystals is being studied for possible applications in communications, computers, and even crime prevention.

The effect is a peculiar reaction of certain crystals to laser light that was discovered in the 1960s. A photorefractive crystal can, among other things, gather light from lasers shone on it and beam the light toward any nearby shiny object. If the object is moved, the beam tracks it like a human-operated spotlight. The crystals also can fuse two laser beams or, like photographic film, record holograms, simulated three-dimensional images.

When shown such odd tricks, "even hardened physicists, weary from decades of proposal writing, instinctively begin to play" with the crystals in the hope of finding new tricks, writes Jack Feinberg in a recent issue of the magazine "Physics Today."

Photorefractive play is getting serious, though. Researchers at Stanford University are experimenting with the crystals to switch light beams into desired channels in optical-fiber communications. At the University of Colorado, scientists are studying the crystals' use in "optical associative memories," computer devices that are structured roughly like the brain's net of neurons but which use light instead of electricity to carry information. Scientists also hope to use the crystals to direct laser beams that etch microscopic circuit patterns in computer chips.

One of the most remarkable photorefractive applications is the "novelty" filter, which is used in conjunction with video systems. Recently developed by a group led by Mr. Feinberg, a researcher at the University of Southern California, and by other scientists, these systems register only moving or changing objects in their visual fields: for instance, one pointed at a parking lot at 2 a.m. might picture only a skulking thief.

The photorefractive effect was discovered by researchers trying to encode information in beams of laser light. To their frustration, the crystals of barium titanate and certain other compounds tended to deform the beams. "It was called 'optical damage,'" says Mr. Feinberg.

Later, scientists found that the damage occurs when light waves rearrange charged particles inside the crystals. That warps the crystal's lattice of atoms, distorting the light.

In the spotlight trick, for example, a shiny object, say a piece of tin foil, reflects laser light into a photorefractive crystal. That alters the crystal's lattice, causing more of the light entering the crystal to be deflected toward the foil. The light, in turn, is reflected right back to the crystal to further alter its structure, causing yet more light to be deflected toward the foil. The process snowballs, quickly building up a beam of light between crystal and foil. When the foil is moved, light from it induces a new crystal pattern that re-establishes the beam within a few seconds.

In the novelty filter, light reflected from a scene is passed through a photorefractive crystal that deflects it, preventing the scene from being registered by the system's video camera. But when something in the scene changes, the light hitting the crystal changes. That momentarily alters the crystal's structure, allowing part of the formerly diverted light to get through to the system's video monitor. The crystal lattice quickly resumes a deflecting pattern when such changes cease.

The novelty filter, aside from its possible crime prevention uses, might help computerized vision systems quickly zero in on the important parts of cluttered images. For instance, "you might be able to see moving bacteria more clearly on a messy background," said Mark Cronin-Golomb, a Tufts University researcher who has developed a prototype novelty filter. The devices might also be employed in automated surveillance systems, such as robots that scan battlefields for advancing enemies, said USC's Mr. Feinberg.

The New York Times

'Magic' Crystals: Key to New Technologies?

Compounds could be used in computers and telephone lines.

By MALCOLM W. BROWNE

It seems more like magic than a laboratory demonstration.

Two transparent crystals are placed at random a few feet apart, and a separate laser beam is pointed at each one. At first the beams pass straight through the crystals as if they were glass, but after a few seconds the emerging beams fan out, and the fans from the two crystals begin to merge. A moment later the fans fade away and a new beam pops into existence between the two crystals.

In reality, the crystals have found each other and created a two-way optical link between themselves, at which each crystal not only propagates its own beam but

acts as a mirror for the other's beam.

The crystals in this demonstration by Dr. Jack Feinberg, a professor of physics at the University of California at Los Angeles, are made of the compound barium titanate. They are not endowed with intelligence or will, but merely exhibit the extraordinary properties of a new class of materials called photorefractive nonlinear optics.

When light shines through these peculiar substances, they respond by rearranging the electric charges in their microscopic structures so as to increase their ability to bend the light, to change its color, or even to act as mirrors. Some photorefractive crystals can "see" weak light coming from any source in their vicinity and modify themselves to reflect the light directly back. This odd behavior is more than a laboratory curiosity. It is, in the view of many physicists, the dawn of a very important new family of technologies.

These materials are expected to make telephone systems more efficient and

cheaper, computers more flexible and intelligent and lasers far more powerful. Photorefractive crystals are already under development as devices for storing holograms. The many organizations backing research in the field include large communication companies and the Defense Department, and discoveries and inventions are coming thick and fast.

Although it has been known for decades that the refractive indexes (light-bending ability) of some materials can be slightly changed by the passage of light, only in recent years have substances been invented or discovered whose light-bending ability changes markedly under the influence of light or electric fields.

Communication engineers say that when these substances are eventually incorporated in new telephone systems based on optical fibers, the transmission

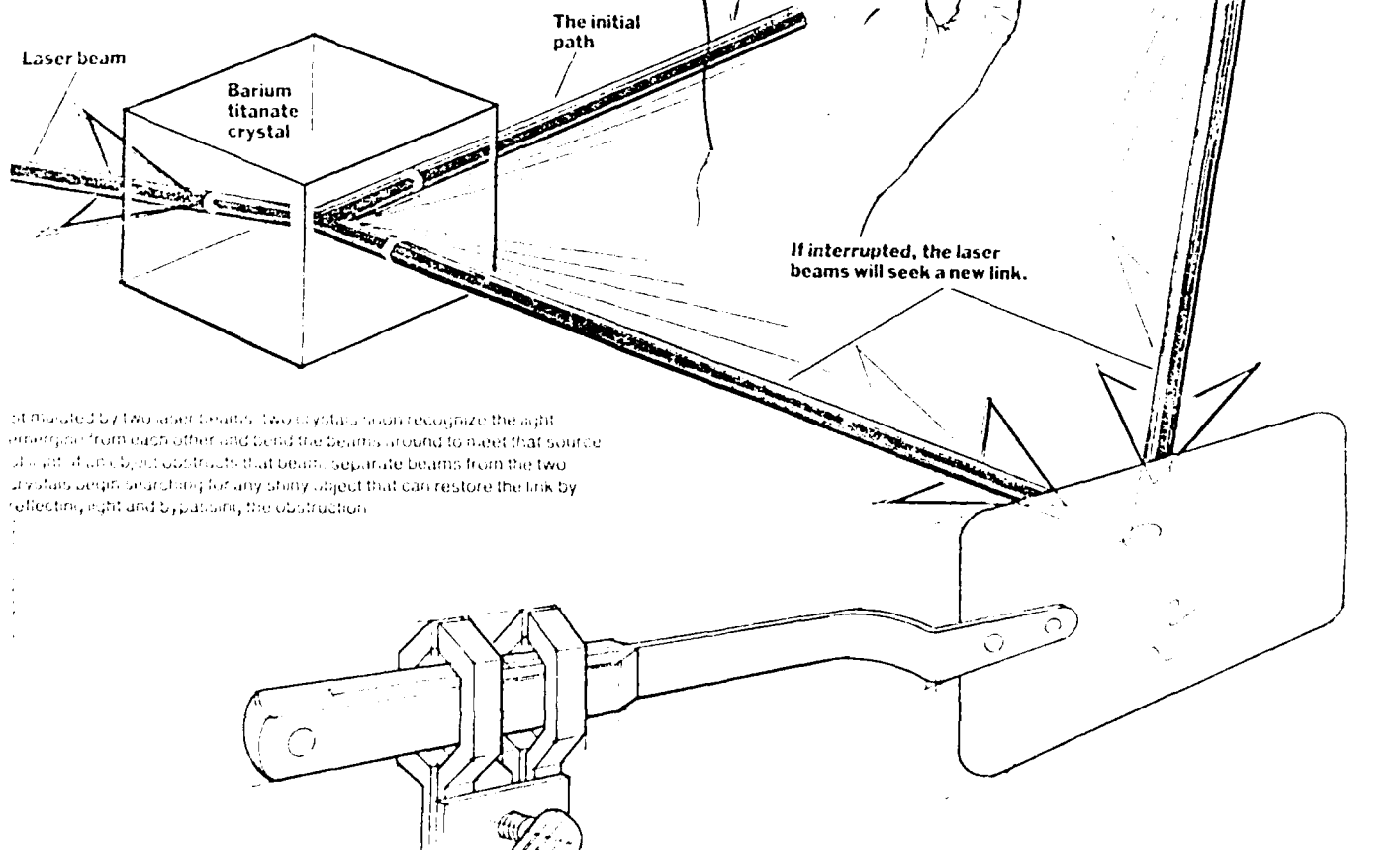
of voices and information will become vastly more efficient.

Because light travels faster than electrons (and has some other advantages), optical fibers have already replaced electric wires in many telephone systems. Optical connections have begun to replace electricity in computer components as well, reducing the time it takes information to travel from one device to another. Scientists believe that optical on-and-off switches and even optical switchboards

Continued on Page 123

Crystals That Make Light Do Tricks

Crystals with special optical properties make light behave in unexpected ways. Photorefractive materials change radically when either an electric field or a strong beam of light is applied. The positive and negative electrical charges within their molecular structure are redistributed, which changes the way they bend light. Scientists believe photorefractive materials may revolutionize telephone communications, computer operation and the storing of information in holographic form.



'Magic' Crystals Can Rearrange Light Rays

Continued from Page B1

will one day replace their electronic counterparts in computers, although there is general agreement that practical optical computers are still many years away. One problem that remains to be solved is size, the crude optical switches devised so far are vastly larger than their electronic counterparts, which can be packed by the million on a thumbnail-size semiconductor chip.

Last month, scientists at A.T.&T. Bell Laboratories unveiled a prototype, a hybrid computer based on chips containing labyrinths of microscopic lasers and tiny optical on-off switches ("gates") that respond to electric fields by becoming either transparent or opaque. The comparatively large devices in the Bell prototype serve the same functions that some electronic transistor switches do in conventional computers. Dr. Alan Huang, who designed the machine, said the chips containing electro-optical switches have as many as 1,500 layers only a few atoms thick, deposited by beams of molecules in a wafer of gallium arsenide.

Recognizing a Familiar Face

Many experts believe that optical materials will eventually take over many tasks now performed by semiconductor electronic devices. Dr. Peter A. L. Smith, a science director of Bellcore, a research institution in Red Bank, N.J., financed by telephone companies, said that if computers can ever function in ways approximately those of the human brain, refractive optics will be important components.

"When we see a familiar face, we are able to recognize it instantly, not at the end of a sequence of digital computation," he said. "The image need not even be very clear for the brain to recognize it." If a computer could store entire images as holographic patterns that could be retrieved whole rather than piece by piece, it might approach some of the brain's remarkable ability to recognize patterns almost instantly, he said.

Bellcore recently devised a holographic system based partly on photorefractive substances that can not only retain a memory of images but also recognize them and learn from its own mistakes. A principal object of the research is to develop "neural networks" of computer interconnections with some of the same associative abilities that a brain has.

Photorefractive materials differ from ordinary glass or plastic, said Dr. Feinberg of U.C.L.A., in that their microscopic structures are changed by the light passing through them, and their altered structures, in turn, change the light.

All transparent materials bend

Special compounds can create two-way optical links between themselves.

beams of light by varying amounts, the amounts are expressed in terms of "refractive index." Diamond has the highest refractive index of all known substances, which accounts for the sparkle of a faceted stone. In most substances the refractive index remains fairly constant, but in photorefractive materials, light-bending ability changes radically when either an electric field or a strong beam of light is applied.

The Rush to Discover More

Electric fields and light beams can rearrange the positive and negative charges in photorefractive materials, and this changes their refractive indexes. In some cases, two or more beams of light entering a photorefractive material interfere with each other to create microscopic bands of positive and negative charges, which form "gratings."

Optical gratings, rows of microscopic lines separated by spaces the widths of the wavelengths of light, can be etched, printed or electronical-

ly implanted on transparent material. They bend and break up light in much the way prisms disperse white light into a rainbow of colors. When such patterns are created by the interference of light beams, they can be used to store complex images encoded as holograms.

Dr. Smith and other leaders in the field say the rush is on to discover photorefractive substances with new and useful properties.

Last month Dr. Samson A. Jenekhe of the University of Rochester announced the invention of a photorefractive polymer that may be the fastest optical switch yet, one whose refractive index changes radically in less than one trillionth of a second after exposure to strong laser light. The material, Dr. Jenekhe said in an interview, is a derivative of polythiophene, a chain of carbon-atom rings linked to sulfur atoms. Dr. Jenekhe, whose research is supported by the Naval Air Development Center and the Honeywell Corporation, said he believes the substance may eventually be used in optical computers, but a more immediate application will be in powerful lasers.

A problem with lasers, including those under investigation by the Strategic Defense Initiative program as antimissile weapons, is that at very high power they generate intense heat that distorts their internal light paths, dissipating and wasting energy.

While a beam is building up inside a laser device, the light is reflected back and forth between two mirrors many times before it gains sufficient energy to penetrate the thin mirror at one end and emerge from the lasing device. As the beam gains energy, heat and other factors tend to distort the lasing medium inside the cavity and rob the beam of energy.

But by replacing one or both of the mirrors in the laser device with photorefractive material, the distortions can be corrected. Instead of acting as simple mirrors that reflect the beam back and forth to build its energy, the photorefractive materials change their structures and create a distorted reflection that exactly cancels the

distortion within the beam itself. Photorefractive material, therefore, "heals" the laser beams they contain, permitting the beams to reach maximum intensity.

An application of vital importance to communication companies is in optical fiber telephone lines. At present, the laser light signals carried by these fibers can travel only relatively short distances before being absorbed and weakened by their glass carriers. The signals must therefore be strengthened at frequent intervals by converting pulses of light into electric pulses, then amplifying the electric pulses electronically and reconvert them into light pulses to be sent on their way to the next

Engineers expect faster transmission of voices and information.

amplifying station.

But if signal strengthening could be achieved optically without electronic amplification, telephone systems would become vastly simpler, more efficient and cheaper to operate. In such a system, Dr. Feinberg has planned, the signal beam would draw fresh energy from a "pumping beam" directed at the medium through which the signal was passing. Thus fortified, the signal would continue on at the speed of light without having to pause for conversion and electronic amplification.

An astonishing new blend of photorefractive plastic and glass was recently patented by Dr. Paras N. Prasad of the State University of New York at Buffalo, working under contract to the Air Force Office of Scientific Research. Such materials are likely to be critical elements in future communication systems and many other applications, according to Dr. Donald R. Ulrich, program manager at the Air Force Office of Scientific Research.

Phase Conjugation with Nonlinear Crystals

Photorefractive optics also point to holographic and interconnect applications.

An Interview with Jack Feinberg



Jack Feinberg is an associate professor of physics and electrical engineering at the University of Southern California, Los Angeles, Calif.

Lasers & Optonics: *What are the basic keys to photorefraction, in terms of the movement of charge carriers in crystals and so forth?*

Jack Feinberg: There is a traditional photorefractive effect and there are some newer photorefractive effects. Let me give you the traditional one first. To start, you need charges in the material, usually due to impurities or perhaps crystal defects. You are not creating the charges by light; they are sitting there already.

The second prerequisite is that these charges can move under the influence of light. Once the charges have moved and made a static electric field in the material, that electric field must create a first-order change in the refractive index of the material. By first-order, I mean that the change in the refractive index is linearly proportional to the space-charge field — the electric field made by the separation of charge.

Other as yet unnamed effects start off the same way. You move charge around but then the change in the refractive index of the material is not linear, but may be through a quadratic term, proportional to E^2 . For example, a paper was published just a few weeks ago in *Optics Letters* by Alastair Glass and his co-workers. They were looking at a photorefractive effect in quantum wells. The space-charge field affects the orbits of the electrons in the quantum wells, which can be sensed by shining a beam of light on them. This is not a first-order effect, but a second-order effect. I'm sure some-

one will coin a name for these other effects soon.

All these effects start out the same way, with light-induced charge migration. They differ in how the electric field acts back on the material. In the traditional photorefractive effect, the electric field causes a first-order change in the refractive index of the material through what is called the Pockels, or electro-optic, coefficient.

In order that the material have a non-zero Pockels coefficient, the material must lack inversion symmetry. It must know the difference between left and right. If it didn't, you couldn't have a first-order effect. It would be forbidden by symmetry.

L&O: *Why must the crystal not exhibit an inversion symmetry if it is to exhibit the traditional photorefractive effect?*

J.F.: You want the electric field in the crystal to change the refractive index to first order. For that to be possible, if I flip the sign of the electric field, then it must flip the change in the refractive index. Suppose, just for discussion, that applying an electric field makes the refractive index increase. Now, if I flip the electric field around, the refractive index must decrease.

You can envision this with a crystal and a battery. Let's say I hook it up so that the electric field points up. Then I leave the room and someone sneaks in and takes the crystal from between the two wires and turns it around. When I

come back, either I can tell the crystal has been turned around or I can't. If the crystal has inversion symmetry, it looks the same in both directions and there is no way I can tell. If the crystal lacks inversion symmetry, then I can tell.

To put it another way, the crystal has to "know" when it sees the electric field whether it should increase its refractive index or decrease it. If the crystal has no sense of direction, it has nothing to measure the field against, then it can't have a first-order effect. It could have a second-order effect, saying in effect "Here comes an electric field, and I don't care if it is up or down, I'm going to increase my refractive index."

You can make ball-and-stick models of these crystals and readily see their lack of symmetry — that up really is different from down — because some atoms are closer to the center and others further away. In barium titanate this is particularly dramatic, because BaTiO_3 is a poled ferroelectric, which is the electrical analog of a poled magnet. It has a lot of little dipoles distributed throughout, with the pluses pointing this way and the minuses pointing that way. Other photorefractive crystals like bismuth silicon oxide, often called BSO, and bismuth germanium oxide, similarly called BGO, are not poled ferroelectrics; nevertheless, their crystal lattices exhibit differences between going one way and going the other way. It is a ranty; most materials have inversion symmetry.

L&O: How far back does the photorefractive effect go? It seems to many observers that the field surfaced more or less spontaneously about a decade ago. Is this a misperception?

J.F.: The first demonstration of the effect was about 25 years ago, when people at Bell Labs were working on frequency doubling in crystals. They were putting intense beams of light into crystals and getting, for the most part, spatially deformed outputs. A nice, clean Gaussian input beam would come out a mess. They realized that the light was causing some kind of semi-permanent change in the material, it was making it into a lens of some sort. F.S. Chen was an early worker in this field and, I believe, was the first person to propose a model of charge migration as being responsible. They called this "optical damage" because it was a pain in the neck. It was

"The ideal crystal has a large Pockels coefficient and is very fast. So far, no one has come up with such a crystal."

annoying and was something they wished would go away. In a sense it did go away, for the subject was pretty much dropped after that.

The photorefractive effect was "rediscovered" about 1979 or 1980 independently in the Soviet Union and in the United States. In the Soviet Union there was a lot of theoretical work going on, and people were able to write down a set of equations to describe the photorefractive effect and actually solve the equations in great detail. In the United States, the approach was more experimental. I was a post-doc for Bob Hellwarth at the time, and we were working on BaTiO_3 . One of the other post-docs in the lab was Don Heiman, who had done his thesis project on BaTiO_3 and had access to the material.

Four-wave mixing had just been invented by Hellwarth, and we were trying it with everything we could think of. When we got around to BaTiO_3 , we found that it worked remarkably well. We got signals much stronger than anything we had ever seen before, even at very low pump intensities. Up until then, four-wave mixing had been a high-power affair; now we were using weak argon and even helium-neon lasers. The behavior of the material was, to us, completely bizarre.

We didn't go to the library and check the literature on the material. We just continued to stumble around, which has its drawbacks and its advantages. The main drawback is that it takes you a long time to make progress. The main advantage is that you are not encumbered by anyone else's thoughts. So we came up with our own theory to explain what was happening in BaTiO_3 . Our theory was completely different from the Russian one. It turns out that, in some limits, the

two theories agree. That was an exciting time to be doing physics.

L&O: It is interesting in your case, not defects, such as impurities, are more important than defects?

J.F.: For quantity, I think it's like money, more is better. Actually, 10% per cm, or roughly one part per million, is beginning to look like a good minimum number. For quality, I don't know which are better, defects or impurities. However, if I were designing a crystal from scratch, impurities would give me more choices. If I were "building" defects into BaTiO_3 , I could leave out a barium, or I could leave out a titanium, or I could leave out an oxygen. I would have only three choices. With impurities, I've got 100 elements to choose from.

Of course, with some materials, the lattices are so densely packed that it is quite difficult to get impurities in except to replace atoms that should be there. That is, they go in substitutionally rather than interstitially. Barium titanate is like that. Other crystals, like strontium barium niobate, or SBN, have a lot of room in the lattice, and you can wedge extra atoms in comfortably without having to displace native atoms.

L&O: Those two crystals, BaTiO_3 and SBN, apparently, had the highest known Pockels coefficients several years ago. Are those two still the preferred materials?

J.F.: Some materials related to SBN have come into play recently, with sodium or potassium substituted for some of the strontium or barium. So now there are lots of things to adjust — two-thirds this, one-sixth that, one-sixth the other, and so on. There is a master crystal grower at Rockwell, Ratnakar Neurgaonkar, who has been working with these crystals. These crystals have high Pockels coefficients, which is one characteristic everyone wants. The ideal photorefractive crystal has a large Pockels coefficient and is very fast; so far, no one has come up with such a crystal.

L&O: Let's move to the speed question, or perhaps it is better described as the rate-of-charge-migration question. If you expect charges to migrate to their final position in a given time, say 1 microsecond, why do they take up to two orders of magnitude longer to reach their destinations in some crystals?

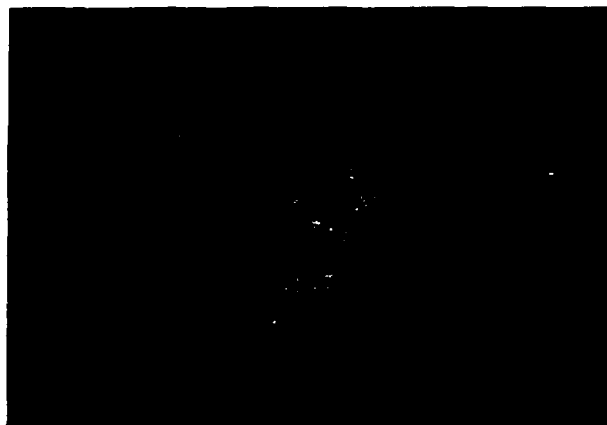


Figure 1. The first image of a cat is badly distorted because it has passed through an aberrator (clear glue smeared on a glass slide). The second image shows what happens if you phase-conjugate the distorted image and pass it back through the same distorter. For these photos, a self-pumping BaTiO₃ crystal served as the phase conjugator.

J.F.: That puzzled us at first, but we understand it now. What you are trying to do in these experiments is put in a light pattern and push the charges from the bright regions into the dark regions. Ideally, you would like to do it in one step — with the light kicking one charge up, which then drifts in the conduction band, and later falls down in a dark region. If that occurred the process would be very efficient; the absorption of one photon would get the job done.

But what happens in BaTiO₃ is that you kick a charge up, it moves about 100 Angstroms and then it comes down again. It absorbs another photon and moves another 100 Angstroms, and so on. It runs out of gas. BaTiO₃ is slow because the typical "hopping" distance is small compared to the typical distances you are trying to move the charge, which are on the order of a micrometer.

L&O: Is this where pump intensity enters the picture?

J.F.: The brighter the pump beam, the more photons you are putting in per second, which means the more hits the charges are getting per second.

L&O: Does that make it a momentum sort of reaction?

J.F.: No, it is just a matter of steps. If you have to walk from here to there and it takes 100 steps, and if you can do the steps quickly, you will get there faster. If you use very weak light and dribble the photons in over the period of a year, it will take you a year to finish.

L&O: Is speed versus intensity a linear relationship in barium titanate?

J.F.: No, it is a less than linear relationship because you waste photons. If every photon were used the same way, the relationship should be linear. If I double the rate at which I input photons, which is like doubling the number of steps per second I take going to the store, I should get to the store twice as quickly. But some of the photons are wasted, as though some of the steps didn't go in the right direction. More precisely, there are other levels in the crystal, which we call shallow traps. The charges get hung up in the shallow traps, and you have to free them. To go back to the walking-to-the-store analogy, it's like stepping into mud.

But that's not the entire story, either. It also gets muddier as you put light in. Instead of just having a single level of impurities, there is an extra level. As charges begin to populate the upper level, there are empty spaces below which can suck up the charges. Instead of taking a step forward, you just stay where you are.

It's a complicated relationship that took a long time to figure out. We have done some experiments recently to confirm our theories. One of my students, Daniel Mahgerefteh, did a series of experiments to show what the right dependence of speed on intensity is. The theory seems to work well in BaTiO₃.

L&O: How available are materials like BaTiO₃ and SBN?

J.F.: Well, how much money do you have? No, actually it's getting better now. It used to be that Sanders Associates was the world's only source of BaTiO₃. More recently, China has been supplying BaTiO₃ crystals to the world. Even so, supply cannot meet demand. I think there is at least a three-month wait for a good, big crystal.

That's unfortunate, because there are so many interesting things to try. People read about them and want to try them. They call me and say, "I've got a small company and would like to do this-and-so. Where can I get a BaTiO₃ crystal?" When I tell them it will cost them \$3,000 or so for the crystal, that's usually the end of the conversation.

As far as SBN is concerned, some is being grown in the Soviet Union and in China, and several research labs here are growing their own. CSK Co. in Los Angeles sells it.

Other crystals like BSO and LiNbO₃ are photorefractive and are for sale from various sources. But they lack the extraordinarily large Pockels coefficient of BaTiO₃ that enables you to do a whole new class of experiments using stimulated effects.

L&O: Was phase conjugation the first application of photorefraction?

J.F.: Phase conjugation was one of the first interesting effects demonstrated in a photorefractive crystal. Bob Hellwarth and I did that in 1980. Hellwarth had demonstrated phase conjugation in other nonlinear materials previously. What made doing phase conjugation interesting in BaTiO₃ was that the efficiency was huge. You got enormous por-

tions of light pouring back at you, as opposed to a tenth of a percent from other nonlinear materials.

L&O: How does stimulated phase conjugation in real time work?

J.F.: Let's look first at traditional phase conjugation with four-wave mixing in a nonlinear crystal. You put in a beam you want to conjugate, and you beat it with another beam which I will call a reference beam. In order to beat them together, they must be coherent with each other. So you make an intensity interference pattern in the material — a real-time hologram. Then you read out the hologram with another beam, a third, which is usually directed opposite to the reference beam. This beam is diffracted by the hologram and sends light back along the direction of your original input beam. That fourth beam is the phase conjugate of your original input beam. So, two beams write the hologram, a third reads the hologram, and the fourth beam is the signal beam. I think this used to be called three-wave mixing because you are only putting in three beams, but then the people involved decided four was more impressive than three so they changed the name.

Phase conjugation is really just holography in real time. In fact, phase conjugation was first demonstrated with holography almost 30 years ago, but not in real time. I believe it was demonstrated by Herwig Kogelnik at Bell Labs and also by Emmett Leith at the University of Michigan, although I don't know who was first.

In self-pumped phase conjugation in photorefractive materials, there are two mechanisms. The simpler one works as follows. [Representative results are shown in Figure 1.] You put in one beam and you get out a phase-conjugate beam. And you think that's magic, because you don't need to put in three beams, as in regular phase conjugation. But the answer is that those other two beams are really there, you just didn't put them in. They were derived from the original input beam — sucked away somewhere upstream and then rechanneled in the right direction to do just what you want.

What's especially remarkable is that it is so easy to do. It's not like you have to carefully design something, think about its structure for a long time, machine it

"The charges get hung up in shallow traps, and you have to free them. It's like walking in mud."

precisely and poke at the experiment for a year to get it going. You just direct a laser beam into the crystal and you get one out. The crystal takes care of the rest.

Even if you try to thwart the operation, you often cannot. For example, you look at the crystal, see the beam paths inside and say, "Okay, I see what's happening. I'll just block this beam from internally reflecting back into the crystal by putting a spot of paint on the crystal's surface to spoil the reflection." It turns out that the beams will usually outwit you; they will choose some other path. These materials like to phase-conjugate.

Loosely speaking, new paths form because it is easy for them to do so. In fact, you can show through a more rigorous analysis that the gain of the entire system increases when this happens. While we understand why new paths form, we don't yet know why these new paths are often filamentary.

L&O: What about the other type of self-pumped phase conjugation?

J.F.: The other kind of self-pumped phase conjugation is called stimulated backscattering. With stimulated backscattering, you put in one beam and you get back the phase conjugate. There are no other beams. This is like making a reflection hologram. If you could see the hologram in the crystal, it is formed by the beam you are putting in and the beam that is coming back. The grating planes of the hologram — the stripes — lie across the beam, slicing it as though you were cutting a carrot. The hologram backscatters the light you are putting in; the backscattered light interferes with the incoming beam and reinforces the hologram to backscatter some more light, until you finally reach a steady-state value.

This effect was first observed by the Soviets in methane gas, by Zel'dovich

and coworkers. Zel'dovich showed that not only was the ruby laser light backscattered, but that it was exactly backscattered. The beams would retrace whatever path they initially took into the gas. If you put in a picture, you would get back a picture. Zel'dovich showed that if the beam comes exactly back along its original path, it has a factor of two more gain than if it goes off in another direction or if it contains a non-phase-conjugate image. Later, Hellwarth showed why stimulated backscattering exhibited exactly a factor of two increase in gain.

Stimulated backscattering was observed in BaTiO₃ as well, although I'm not sure it has been observed in any of the other photorefractive crystals.

To me, the most interesting phenomenon of all the stimulated processes is called double phase conjugation, double-pumped phase conjugation, or mutually pumped phase conjugation. The third phrasing is probably best.

Send two beams into a photorefractive crystal. But this time they don't have to be coherent with each other. They can be from two different lasers. It is simplest to think in terms of the same type of laser, so picture two HeNe lasers, made by different companies, with slightly different cavity lengths so that the output frequencies will be somewhat different.

What the crystal does in this case is take the beam from laser number 1 and direct it back down the bore of laser number 2, and vice versa. At first, you might believe that to be impossible, because the beams are not coherent with each other. If they aren't coherent, how can they interfere? If they don't interfere, how can the crystal keep track of where they are coming from?

But it works, and that's understood now, too. This little gem was invented by a group in Israel — Baruch Fischer and his student Shmuel Sternklar. I think it was also shown independently by Smout and Eason in England.

L&O: Are there any obvious applications in the immediate future?

J.F.: The application that seems to have the most people excited is interconnection, especially using mutually pumped phase conjugation. If you can interconnect two lasers impinging from two different directions — not all angles work but wide angular ranges are possible —

Copy is subject to BSA's right to
permit fully legible reproduction

you have the beginnings of a telephone switch.

Picture an array of a thousand fibers on one side of the crystal and another array of a thousand fibers on the other side. If you want to connect fiber number 26 on one side with fiber number 92 on the other, you just turn on a little local laser from each one and the crystal connects the two.

The problem, so far, is that it is too easy to connect one fiber to another. When you try to connect two on the input side to two on the output side, each input tries to talk to *both* outputs. And so on with larger numbers of inputs and outputs. If you try to work around that, the connections begin to get weak. Phase conjugation works great if you want fan-out or fan-in; it doesn't work so well yet for an $N \times N$ switch.

The other exciting area of potential application lies in neural nets. The ability to store a lot of holograms on top of each other, encoded in some way, is quite enticing.

L&O: *It can't talk until this afternoon, but what is it doing to achieve the cause, what would it be?*

J.E: In an abstract sense, what I would like is to find something new that I had no idea would happen and no explanation for. The real fun is observing and then explaining things that you don't at first understand.

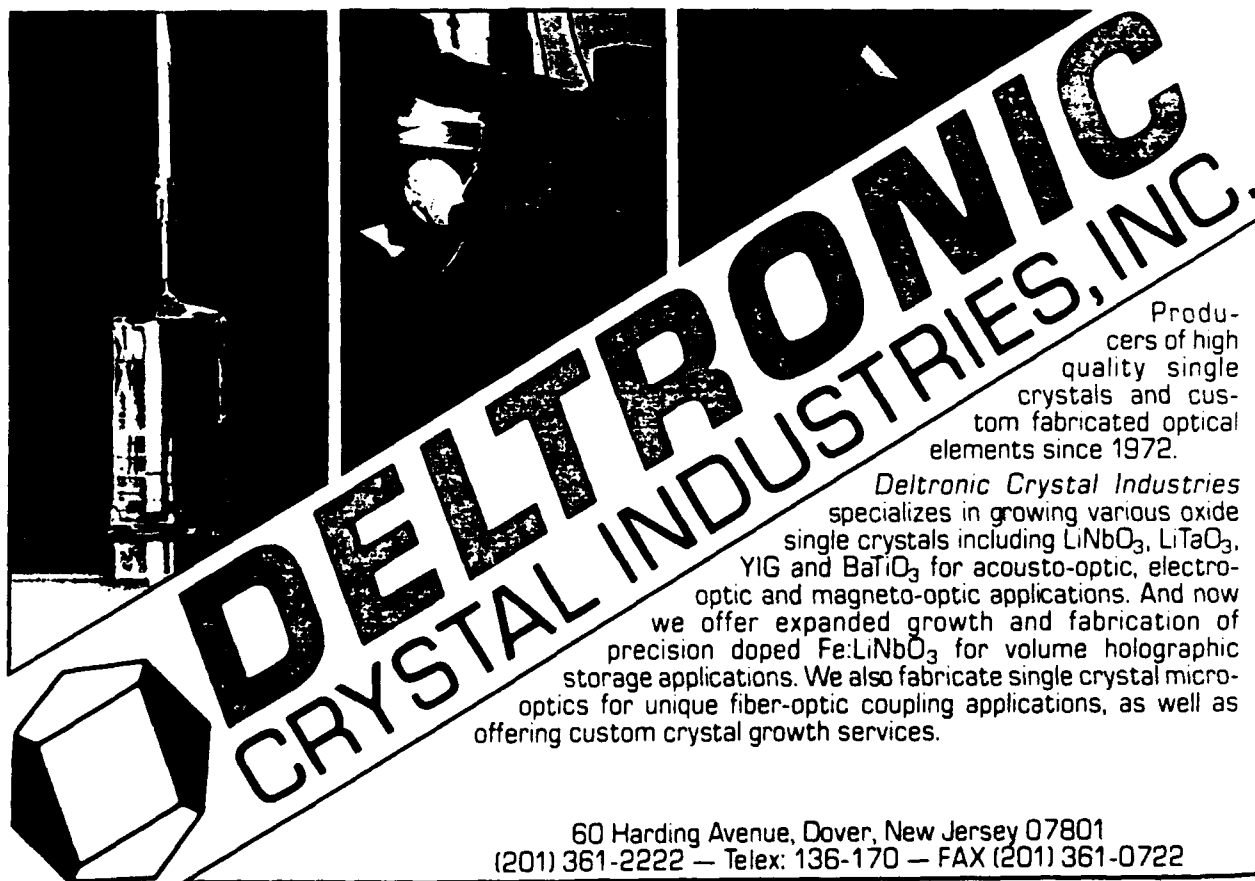
In a more practical sense, what would probably interest funding agencies the most is if we could find a way to make a material with a large optical nonlinearity that would also be fast. For just a few milliwatts per square centimeter of light intensity, the device would reach a very large nonlinearity very quickly. It could, say, reach that point within a microsecond or so.

People are starting to get smart about this. For BaTiO_3 , it takes many hops to get where you want to go. Conversely, in gallium arsenide the mobilities are much higher, but the Pockels coefficient is very small. So people are saying, "Let's forget about the Pockels coefficient and look for

some other way to change the index of refraction."

Very recently, Elsa Carmire and her student Arshin Partovi at USC, and two workers at Hughes — Marvin Klein and George Valley — collaborated in this area. They found that, if they used GaAs right near its bandgap, the electric field made by the charges after migrations would alter the absorption of the crystal. But you alter the absorption, you must also change the index of refraction, by the Kramers-Kronig relation. In their work, the change in the index of refraction was appreciable. So, they were able to see a relatively large beam-coupling effect in GaAs by ignoring the small Pockels coefficient and using another effect.

Other people are working with "designer" molecules, where charges can migrate very quickly and easily on conjugated polymer backbones. Once the charges have migrated, the electric fields may significantly alter properties of the material. This field is still in its infancy, but it looks very promising.



DELTRONIC
CRYSTAL INDUSTRIES, INC.

Producers of high quality single crystals and custom fabricated optical elements since 1972.

Deltronic Crystal Industries specializes in growing various oxide single crystals including LiNbO_3 , LiTaO_3 , YIG and BaTiO_3 for acousto-optic, electro-optic and magneto-optic applications. And now we offer expanded growth and fabrication of precision doped Fe:LiNbO_3 for volume holographic storage applications. We also fabricate single crystal micro-optics for unique fiber-optic coupling applications, as well as offering custom crystal growth services.

60 Harding Avenue, Dover, New Jersey 07801
(201) 361-2222 — Telex: 136-170 — FAX (201) 361-0722